Design and Development of Organic Photovoltaics Based on π-Conjugated Materials

A thesis submitted by

T Bhim Raju
Roll No. 11612233

to

Indian Institute of Technology Guwahati

for the award of the degree of

Doctor of Philosophy

Department of Chemistry
Indian Institute of Technology Guwahati
Guwahati - 781039
India

January, 2017

INDIAN INSTITUTE OF TECHNOLOGY GUWAHATI

Guwahati, Assam-781039, India

Department of Chemistry

STATEMENT

I do hereby declare that the work contained in the thesis entitled "**Design and Development of Organic Photovoltaics based on π-conjugated materials**" is the result of investigations carried out by me in the Department of Chemistry, Indian Institute of Technology Guwahati, Guwahati, Assam India under the supervision of Prof. Parameswar Krishnan Iyer, Department of Chemistry, Indian Institute of Technology Guwahati, Guwahati, Assam, India. This work has not been submitted elsewhere for the award of any degree.

Bheem Raju Telugu

Department of Chemistry,

Indian Institute of Technology Guwahati

Guwahati – 781039, India,

January, 2017

Prof. Parameswar Krishnan Iyer
Department of Chemistry
Indian Institute of Technology Guwahati
Guwahati-781039, Assam, India
Tel: +91-3612582314;
Email: pki@iitg.ernet.in

CERTIFICATE

This is to certify that **Mr. T Bhim Raju** has been working under my supervision since July 2011. I am forwarding his thesis entitled "**Design and Development of Organic Photovoltaics based on π-conjugated materials**" being submitted for the Ph.D. degree of this institute. I certify that he has fulfilled all the requirements according to the rules of this institute, and regarding the investigations embodied in his thesis and this work has not been submitted elsewhere for a degree.

Guwahati — Prof. Parameswar Krishnan Iyer

January, 2017 — Thesis Supervisor

Dedicated

To

My Family

ACKNOWLEDGEMENT

I express my unfathomable gratitude to my thesis supervisor Prof. Parameswar Krishnan Iyer for his incisive thinking, suggestions and cogent advice throughout whole research period. His constant encouragement, criticisms and painstaking planning have aided a long way for preparation of present thesis. His true scientific spirit, independence and self-reliance have helped me an immense to develop the quality of my research work. I shall remain indebted to him forever.

I would like to thank my doctoral committee members Prof. Bhisma Kumar Patel, Dr. Achal Kumar A. S and Dr. Vimal Katiyar for their valuable suggestions and comments during all assessments of the Ph. D. program.

I owe my sincere thanks to Prof. Saurabh S. Soni, Jayraj V. Vaghasiya and my Chemistry labmates Radha Krishna Ratha, Suresh Vasimalla, Sameer Hussain, Anamika Kalita, Akthar Hussain Malik, Arvin Sain Tanwar, Sayan Roy Chowdhury, P. Gopikrishna, Md. Adil Afroz, Niranjan Mehar, Laxmi Raman Adil, Subrato Mondol, Maimur Hossain, Debasish Barman, Nehal Zehra, Rabindranath Garai, Dr. Priyanka Dutta and device labmates Ashish Singh, Dipjyoti Das, Anamika Dey, Rahul Narasimhan, Ramesh Babu Yathirajula, Indrani Medhi, Ritesh Kant Gupta and Nystha Baishya for their help and suggestions during my research period.

I would like to express my profound gratitude to my seniors in Chemistry lab Dr. Prasanta J Goutam, Dr. Atul Kumar Dwivedi, Dr. Muthuraj Bala, Dr. Jupitara Das and from device lab Dr. Nimmakayala V. V. Subbarao, for their immense support, encouragement and help.

I would like to thank all the faculty members, research scholars, supporting staff of the Department of Chemistry and CIF, IIT Guwahati for their kind cooperation in all respects. I acknowledge DST and MHRD for fellowship for the entire period of the Ph.D. program.

Finally, I want to convey my sincere gratitude to my family members for their sustained help and encouragement in all my academic ventures. I feel deeply indebted to them for whatever I have achieved so far.

Bhim Raju Telugu

List of Figures

List of Tables

List of Symbols and Abbreviations

HOMO	Highest Occupied Molecular Orbital
LUMO	Lowest unoccupied Molecular Orbital
J_{sc}	Short-circuit current
V_{oc}	Open-circuit voltage
FF	Fill factor
PCE or η	Power conversion efficiency
IPCE	Incident photon to current conversion efficiency
AM	Air-mass
eV	Electron volt
J	Joule
µs	Micro second
µm	Micro meter
τ_e	electron lifetime
VB	Valence band
CB	Conduction band
D	Donor
A	Acceptor
Pc	Phthalocyanine
ICT	Intramolecular charge transfer
BODIPY	Boron-dipyrromethene
EIS	Electrochemical impedance spectroscopy
J-V	Photocurrent-voltage
OCVD	Open-circuit voltage decay
DFT	Density functional theory
DSSC	Dye sensitized solar cell
TRPL	Time-resolved photoluminescence
CDCA	Chenodeoxycholic acid
EtOH	Ethanol
DCA	Deoxycholic acid

TBAPF6	Tetrabutylammonium hexafluorophosphate
TBP	4-tert-butylpyridine
GSCN	Guanidium thiocyanate
R_{pt}	Charge transfer resistance
R_{rec}	Charge recombination resistance
J_0	Exchange-current density
HRMS	High-resolution mass spectrometry
BHJ	Bulk hetero junction
OLED	Organic light emitting diode
HRMS	High-resolution mass spectrometry
ACQ	Aggregation caused quenching
Hz	Hertz
MHz	Mega hertz
AIE	Aggregation induced emission
AIEE	Aggregation induced enhanced emission or Aggregation-induced emission enhancement (AIEE)
CPDT	4*H*-cyclopenta-[2,1-b:3,4-b']dithiophene
Br-CPDT	2,6-dibromo-4*H*-cyclopenta-[2,1-b:3,4-b']dithiophene
TBAI	Tetrabutylammonium iodide
TBAB	Tetrabutylammonium bromide
TBAC	Tetrabutylammonium chloride
TBAF	Tetrabutylammonium fluoride
W	Watt
mW	Milli watt
PL	Photoluminescence
UV-vis	Ultraviolet-visible
CV	Cyclic voltammetry
SEM	Scanning electron microscopy
FE-SEM	Field emission scanning electron microscopy
TBAP	Tetrabutyl ammonium perchlorate
E_g	Band gap
λ	Wavelength

s	Singlet
d	Doublet
dd	doublet of doublet
T	Triplet
Q	Quartet
M	Multiplet
Ω	Ohm
mA	Milli ampere
TCO	Transparent conductive metal oxide
DCM	Dichloromethane

Synopsis Report

Energy is one of the most important factors to influence human society in the 21st century. Scientists are now focusing on the development of renewable energy generated from natural resources such as sunlight, wind, rain, tides, and geothermal heat. Among these, solar cells are most promising and suitable for energy generation because the sunlight has the potential to make the largest energy contribution: only one hour of sunshine (3.8×10^{23} kW) is more than enough to satisfy the highest human demand for energy for an entire year.

Organic Photovoltaic devices have many advantages compared to inorganic semiconductors: Solar cells based on organic materials can be structurally flexible, and most of them are semi-transparent, low cost, and low weight. Organic solar cells, therefore, have a much larger application potential than conventional solar cells.

The whole thesis has been organized into six chapters. The first chapter is about the brief introduction of Organic Photovoltaic devices and some recent developments in the Dye sensitized solar cells (DSSC). The second chapter includes the synthesis of new dyes and fabrication of DSSC. The third chapter includes the synthesis of new dyes: effect of the various TiO_2 thickness on DSSC. The fourth chapter explains about the synthesis of new AIEE based materials and its application in DSSC. The fifth chapter describing about the synthesis of new thiophene 3,4-disubstituted dyes and effect of the electrolyte system on DSSC performance. Final chapter describes facile alkylation method of CPDT and brominated CPDT. The contents of the individual chapters are as follows

Chapter 1 describes necessary introduction to Photovoltaic devices; generations of solar cell, its performance parameters, feasibility and practicability. The chapter explains basic working principle of dye sensitized solar cell (DSSC), a detail explanation of components including in device. This chapter is concluded with the current state-of–the-art scenario and challenges related to design and synthesis of various wide band gap D-π-A, D-A-π-A dyes with a brief literature survey, including performance parameters and stability. The general procedures followed for fabrication of DSSC, basic instrumentation techniques/methods used for material characterization and device characterization also.

Finally, photovoltaic parameters and electrochemical impedance spectroscopy (EIS) measurements are being demonstrated.

Chapter 2 describes the design and synthesis of four new series of organic dyes based on meta-fluorine substituted phenyl moiety, used as a π-linker in various dyes, used for dye sensitized solar cell (DSSC) application. These dyes share same anchoring group (Cyano acrylic acid) with different donors such as carbazole, thiopene substituted carbazole, triphenylamine and phenothiazine moieties. For effective electron flow, the dyes were incorporated with novel D-π-A framework. The advantage of fluorine atom containing π-bridge/spacer is to generally obtain the electron-withdrawing ability and drastically tune the dye molecule properties, like changing the energy levels, governed by charge distribution, charge transfer from D to A and improving the electron mobility. We introduced linear octyl alkyl chains at the donor site to suppress the dye molecule aggregation and avoid close contact to the electrolyte on TiO_2 surface.

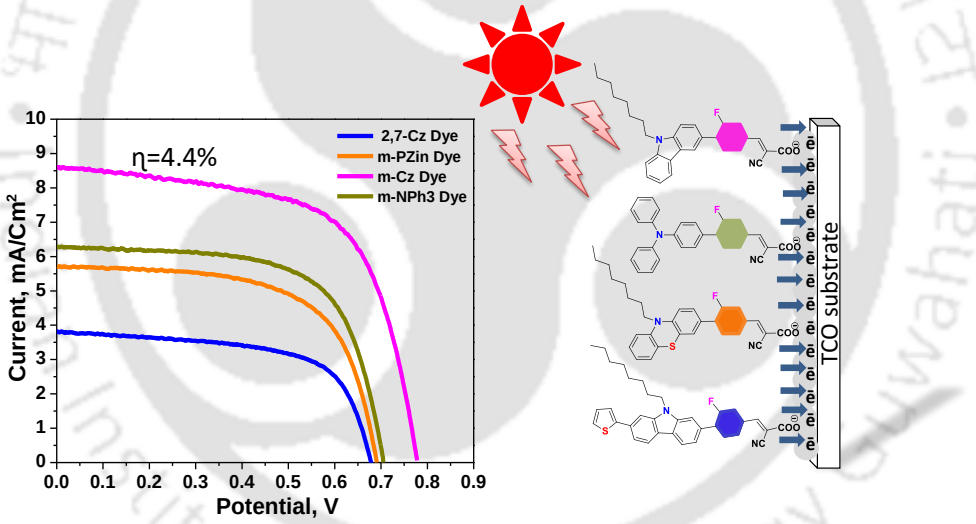

Without addition of any co-absorbent on TiO_2 layer we achieved highest efficiency (PCE) of 4.4% by using a simple Cz-dye due to the deep HOMO level, high molar absorption coefficient (13,126 $M^{-1}Cm^{-1}$), planarity of backbone and long excitation life time value (ns) = 1.25. These dye have high V_{oc} (0.778 V) and J_{sc} (8.65 mA/cm^2) and highest PCE of 4.2(± 0.2)%. The NPh3 and Pzin dyes have lower efficiency values (η=2.9% and 2.6%) while triphenylamine three dimensional, phenothiazine two dimensional (Butterfly) structure. In this chapter the efficiency of dyes was describe by optical, electrochemical

properties, planarity of dye molecules and charge transfer property by using Gaussian calculations

Chapter 3 demonstrates the effect of various TiO_2 thicknesses with new series of dyes having ortho-fluorine substituted phenyl spacers contain different donors like carbazole, triphenylamine and phenothiazine moieties. We introduced the linear hexyl chain to carbazole and phenothiazine moieties to suppress the dye aggregation on TiO_2 surface. The Optical, electrochemical, molecular orbital calculation and photovoltaic properties for different TiO_2 thicknesses (9-12µm) of the new dyes were investigated. Thicknesses of TiO_2 film have effects on open circuit voltage (V_{oc}), short circuit current (J_{sc}) and efficiency. We observed that the J_{sc} and V_{oc} of o-Cz dye with a TiO_2 film thickness of 12 µm (8.91 mA/cm^2 and 0.63 V) are larger than film thickness of 9 µm (8.40 mA/cm^2 and 0.57 V). It could be due to the increase in thickness of TiO_2 film. At optimum thickness of TiO_2 film (12 µm), o-Cz dye exhibits power conversion efficiency (η) of 3.63(± 0.4)%. This was improved efficiency of o-Cz dye from 3.3% to 4.0% without using any co-absorbents, while changing the thickness of TiO_2 film. The optimized geometry calculation of ortho fluoro phenyl π-spacer dyes was ascertained by DFT, using B3LYP/631G (d,p) basis set. The results reveal that o-Cz dye have high efficiency due to the deep HOMO level and it exhibit better charge transfer from donor to acceptor, compare to other dyes.

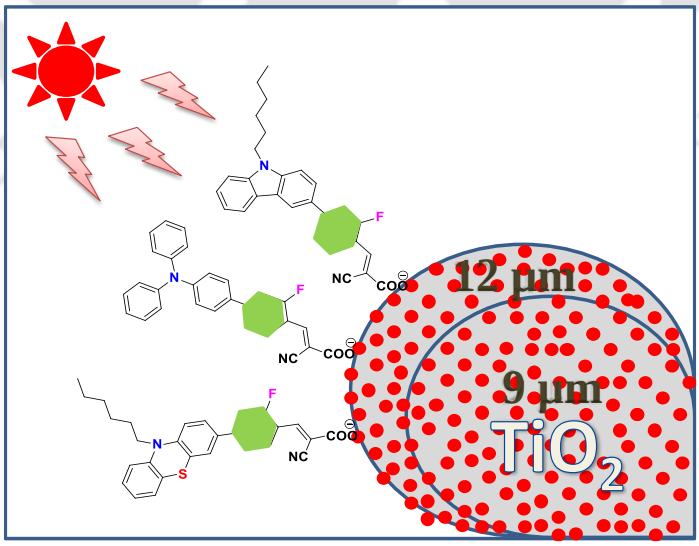

Chapter 4 explains Aggregation induced enhanced emission (AIEE) of new two sets of triphenylamine chromophores, and its application in DSSCs for the first time have been

demonstrated. The photoluminescence properties of three chromophores were well studied in solutions as well as in aggregated states. All three emit strong blue fluorescence in ethanol solution. However, two chromophores TPA-PHA, TPA-PFA exhibits AIEE property due to the formation of excimer in aggregation state. The results reveal that, the TPA-PFA had less quantum yield (Φ_{solid}=82.13) than TPA-PHA (Φ_{solid}=88.32) in aggregated state, the reason behind that m-fluorine substitution on phenyl contains chromophore makes "inductive effect", the substitution of fluorine atom has causes of more formation of ICT from Donor to Acceptor. From FESEM analysis we conclude that, both AIEE chromophores are exhibits two different kinds of nano aggregates in solid state.

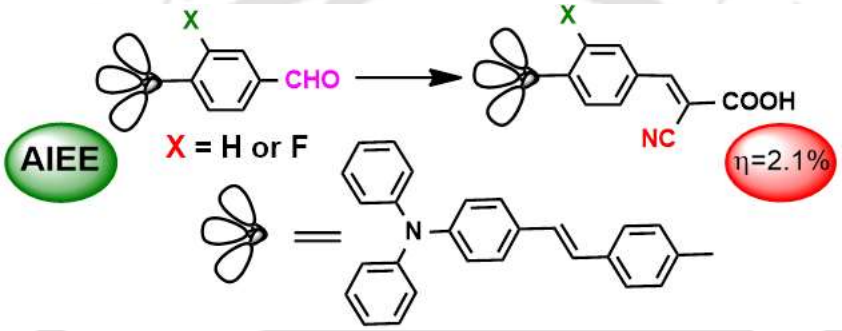

These AIEE chromophores were utilized and developed as new dyes i.e., Dye-1, Dye-2 for DSSC application. The dye-1, dye-2 exhibit a power conversion efficiency (PCE) of 2.1% (J_{sc}= 5.05 mA/cm^2, V_{oc}= 0.67 V and *FF*= 0.61) and 1.9% (J_{sc}= 4.68 mA/cm^2, V_{oc}= 0.70 V and *FF*= 0.59), respectively. The optimized geometry calculations of D-π-A chromophores, dyes were ascertained by DFT calculation by using CAM-B3LYP/631G (d,p) basis set.

Chapter 6 describes new π-spacer contains thiophene 3,4- di substituted organic dyes with double acceptor at 2,5-position frame work. Influence of triphenylaime and carbazole units substitution at 3,4-position of thiophene based dyes optical, electrochemical, theoretical and photovoltaic properties with various electrolytes (I^-/I_3^- and Co^{+2}/Co^{+3}) are studied. The 2Cz-Th-Dye and 2NPh3-Th-Dye does not exhibits broaden absorption in Visible region due to the blocking of electron delocalization at 2,5-positions by cyanoacrylic acid acceptor units. Substitution of two twisty donors at 3,4-position in 2Cz-Th-Dye, 2NPh3-Th-Dye retarded the dye aggregation and charge recombination on TiO_2 surface**.** Without using any additives, 2Cz-Th dye and NPh3-Th

dye in presence of cobalt (II/III) redox shuttle resulted in an overall power conversion efficiency (PCE) 3.3% and 3.1%, respectively. By replacing the one acceptor with any other donor, these thiophene moiety will effectively work as a new π-spacer in DSSC application.

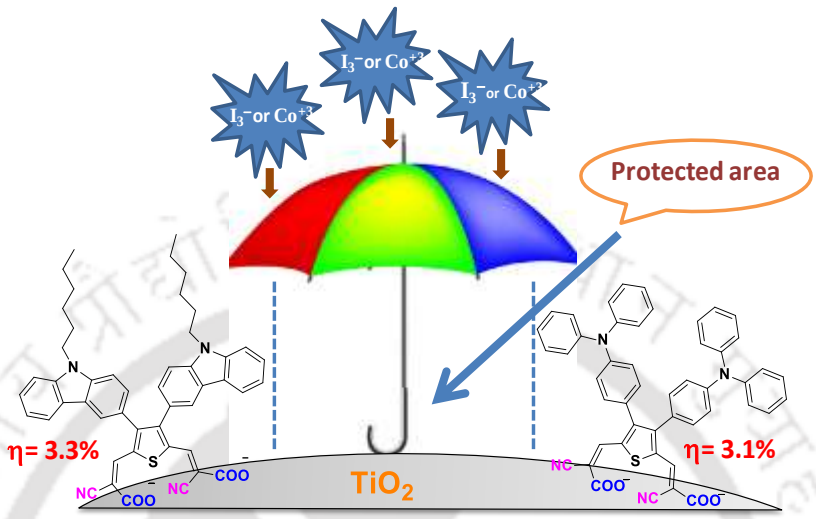

Chapter 5 describes efficient and facile alkylation of 4*H* Cyclopenta-[2,1-b:3,4-b']dithiophene in water. This method was also extended to successfully perform alkylation of 2,6-dibromo-4*H*-cyclopenta-[2,1-b:3,4-b']dithiophene for the first time. Our initial attempts 50% aq NaOH, TBAI, 1-bromo octane, CPDT were used for dialkylation in atmospheric conditions, but result, formation of a mixture of unwanted products in major amounts. The same reaction again started with careful degassing of the reaction mixture comprising three freeze–thaw cycles. Stirring the reaction at room temperature (35–40 °C) for extended time did not give desired dialkylated CPDT which prompted us to slowly raise the temperature. During the course of 5 minutes we observed that the colour of the reaction mixture changed into greenish black at 75 °C, however, no starting material was observed in the reaction mixture after 3h. This modification in the reaction conditions resulted in the development of highly successful dialkylation reaction of CPDT without the use of any organic solvents, metal catalyst, inert gases, strong acids, and high pressure/temperature, yet 82–96% isolated yield of the desired product 4,4'-dialkyl CPDT could be achieved with a variety of alkyl halides including chloro alkanes. This facile method has several advantages such as the exclusive use of water instead of high boiling toxic solvents, simple separation of the defect free dialkylated CPDT product and the use of mild reaction conditions.

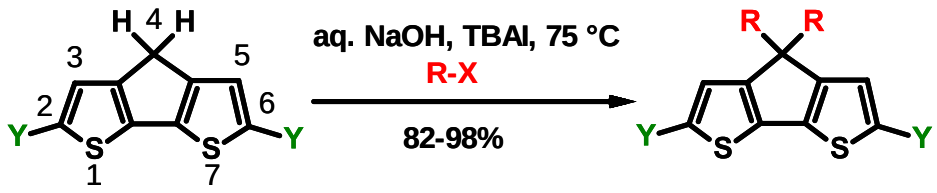

Y = H or Br R-X = Alkyl halide

Contents

Chapter 5: Influence of 3,4-di substituted Thiophene derivative π-extended dyes and its effect on dye-sensitized solar cells

Chapter 6: Highly efficient and facile alkylation of 4*H* Cyclopenta-[2,1-b:3,4-b']dithiophene in water

CHAPTER-1

Introduction

1.1 An Overview of Solar energy

The limited supply of today's main energy sources like oil, coal, and uranium will force us sooner than later to replace most of the currently used power plants, because they emit dangerous and hazardous gases. Reducing the "Greenhouse effect" and protect the environment is required presently.[1-3] The challenges in solving the energy and environmental issues at the global level, is to develop new technologies which can harvest clean renewable energy and minimize the rising environmental pollution. Sunlight, wind, rain, tides, waves, biomass *etc.*, are main renewable resources. Among them solar energy is the most abundant on earth and has the potential to satisfy future global needs of energy.[4,5] Each hour the earth's surface receives about 4.3 X 10^{20} J of energy from the sun, therefore, solar energy is considered as a potential "green energy" that can be exploited in the future.[6] However, the biggest challenge is the availability of earth abundant and highly efficient light harvesting materials, low manufacturing cost and simple devices architecture in order to convert solar energy to electrical energy or chemical fuels.[7,8] "Photovoltaics" is one of the promising technology for harvesting solar irradiation in which sunlight is converted into electrical energy. Scientific community has made great efforts toward the design and development of highly efficient solar cells and their commercial manufacturing.[9] However, most of the solar cells have disadvantages such as high cost, toxic substances involved in materials development or during processing etc., lack of long-term stability which limits their real world applications.[10] Figure **1.1** (A) illustrates the solar energy distribution curve with the major components, i.e., UV-Vis and infrared radiation in solar spectrum and (B) distribution of global energy potential (renewable and non-renewable) *vs* world consumption of energy.

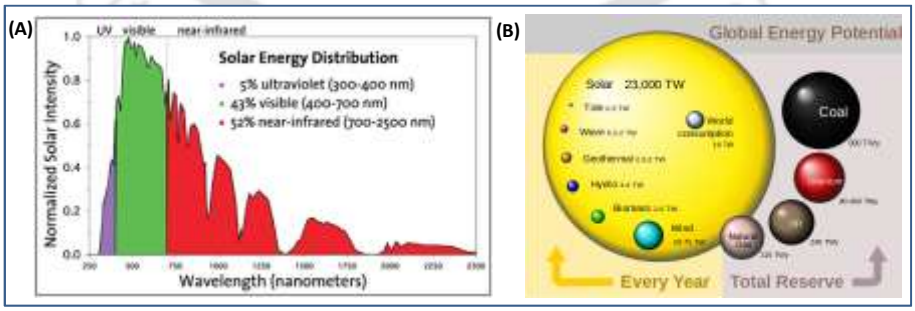

Figure 1.1 (A) Solar energy distribution graph illustrating UV-Vis and infrared radiation are the prime components of solar spectrum (Source: Lawrence Berkeley National Laboratory) (B) Energy potential of renewable energy sources per year and total estimated energy potential of fossil and nuclear fuels (Source: www.renewablegreenenergypower.com)

1.2 Solar Cell Generations

Photovoltaic devices (solar cells) have been categorized according to the generations of technologies.[11] These are categorized according to the time sequence they started playing big role in the solar cell field.

1.2.1 First Generation Solar cells (1G)

Solar cells are large scale, single junction devices made from single crystalline Si (c-Si) and multi-crystal silicon. About 90% of the current photovoltaic production in market is based on first generation technology. The ~25% efficiency of the single junction cells has been reported by Martin Green's group in 1998.[12,13] However, complicated manufacturing process, and high cost to produce 1 Watt of power by silicon solar cell is nearly 4 times higher than conventional energy (power plants) price due to the high cost of materials. Yet the price continuously goes down along with the progress of the technology, the 1G product will probably reach their price limit saturation before achieving the competitive edge in the market.

1.2.2 Second Generation Solar cells (2G)

Second generation solar cells are usually called thin-film solar cells because when compared to c-Si based cells they are made from layers of semiconductor materials only a few micrometers thick.[14,15] These are made from simple fabrication process with the combination of using lesser materials, which reduce the production cost. Basically three types of solar cells are considered in this category, amorphous silicon, cadmium telluried (CdTe) and copper indium gallium diselenide (CIGS). Although the second generation solar cells are economical, they are less efficient (η = ~16.8%) as compared to the first generation solar cells.

1.2.3 Third Generation Solar cells (3G)

Currently there is a lot of solar research ongoing across the world.[16] The objectives of the third generation of solar cells are (i) fabrication of low-cost, light weight, high efficiency, earth abundant and environment friendly materials, (ii) simple manufacturing process and (iii) large area production. 3G solar cells introduce the idea of multi junction solar cells, which can significantly increase the devise efficiency via improvement in harvesting of photons. This type of photovoltaic devices included dye-sensitized solar cells (DSSCs),[17-19] polymer solar cells (Bulk-hetero junction solar cells),[20] perovskite solar cells,[21-23] quantum dot sensitized solar cell[24] etc.

In DSSC, the use of organic dyes are advantageous due to their structural diversity and facile functionalization tunability of different components by chemical modification to fulfill the basic prerequisites for better device performance such as better light absorption, charge separation and charge transport.

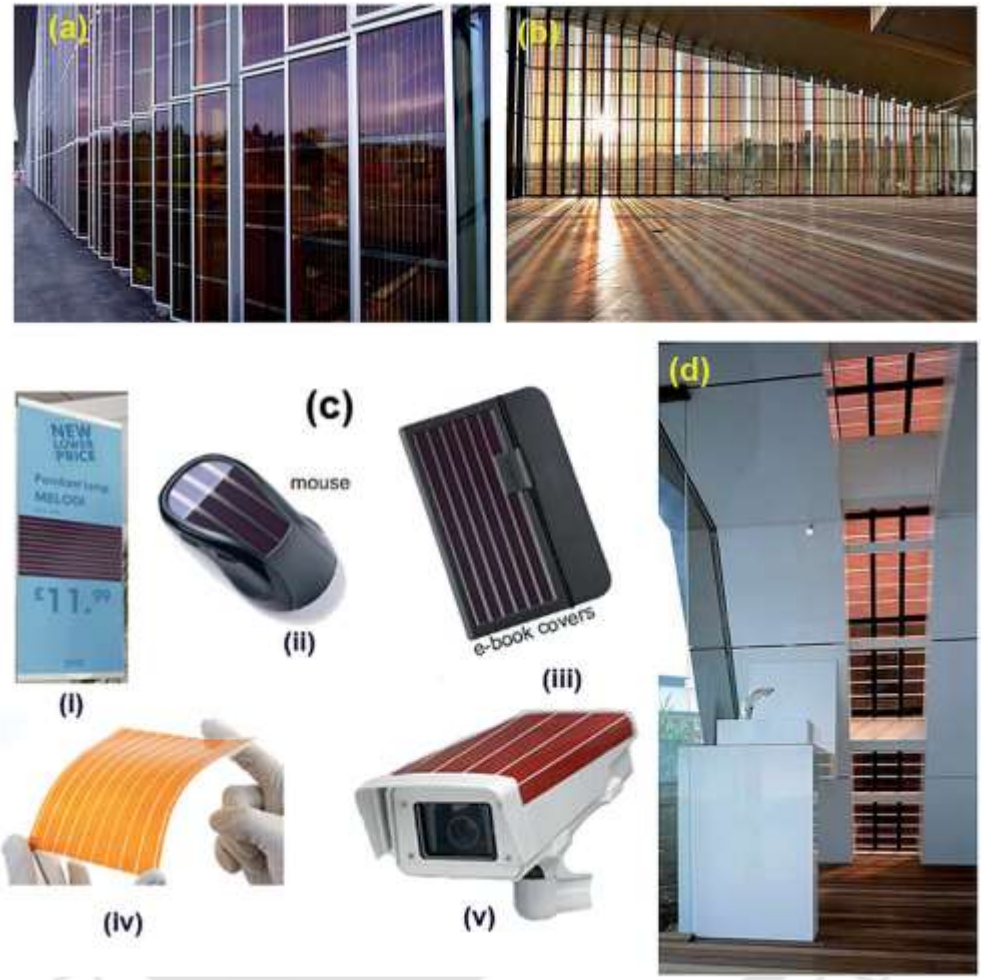

Figure 1.2 Examples of few flexible solar cell modules launched by different companies for the practical applications. Source: Figure taken from RSC.

Basically DSSCs are electrochemical cells, introduced by M. Grätzel and O'Regan in 1991.[25] They invented the DSSC based on a thin layer of TiO_2 nanoparticles impregnated on Ru dye in 1988, after they modified the device structure and published in 1991, with reported efficiency of 7-8%. Since this initial work, enormous efforts are being made and power conversion efficiency (PCE, η) up to ~14% has been achieved. A typical DSSC is constructed with a dye, which was absorbed by wide band gap semiconductor metal oxide (working electrode) such as TiO_2, ZnO or NiO, a liquid electrolyte containing I^-/I_3^- redox couples, and platinum-coated counter electrode.[18] The PCEs have exceeded over ~10%,

especially in the last decade, the field of DSSC and polymer solar cell has been growing fast and showing promising potential compared to the cheaper PV technology. For this reason, since last decade OPVs have become one of the most fascinating fields of research. This technology can withstand more than 20,000 h of continuous illumination, and stability of the device lifetime is beyond 20 years. Due to these advantages of OPV device, a number of companies such as G24 Innovations (G24i), solaronix, Dyesol, 3Gsolar, Aisin Seiki, Sharp, Toyota, and Sony etc. (Figure **1.2**) are involving themselves in development, manufacturing and commercialization of this technology.[26]

1.3 Components of DSSC

DSSC are the electrochemical device, comprising of two sandwiched electrodes, i.e., one photo anode and a passive cathode which acts as a counter electrode. A suitable redox couple electrolyte is introduced in between the two electrodes to complete the device. The schematic diagram of DSSC is shown in the Figure **1.3**. A typical DSSC consists of the following:

1. A transparent glass sheet covered with a conductive fluorine-doped tin oxide (FTO) or indium doped tin oxide (ITO) layer is used as anode which allows light to pass through and electron transport.

2. A wide band gap nano structured metal oxide (e.g., TiO_2, ZnO etc.) films are deposited over the FTO or ITO. In general, the optimum thickness of the layer is around 10-15 µm.

3. A monolayer of dye or photosensitizer such as metal complexes or organic molecules are anchored on the surface of the mesoporous oxide layer, which harvest the visible radiation of solar spectrum. After that, the sensitizer molecules are photoexcited and inject electrons into the metal oxide.

4. A suitable electrolyte (usually redox mediator such as iodide/tri-iodide (I^-/I_3^-) or Co^{+2}/Co^{+3} in an organic solvent) to regenerate the oxidized dye molecules itself during operation.

5. A counter electrode (cathode) which is most commonly fabricated by depositing a very thin layer of Platinum (Pt) on ITO or FTO to catalyze the redox couple regeneration reaction and collect the electrons from the external circuit. Metal sulfides, carbon based materials (graphene composites) etc. are also employed as an alternative to Pt electrode.

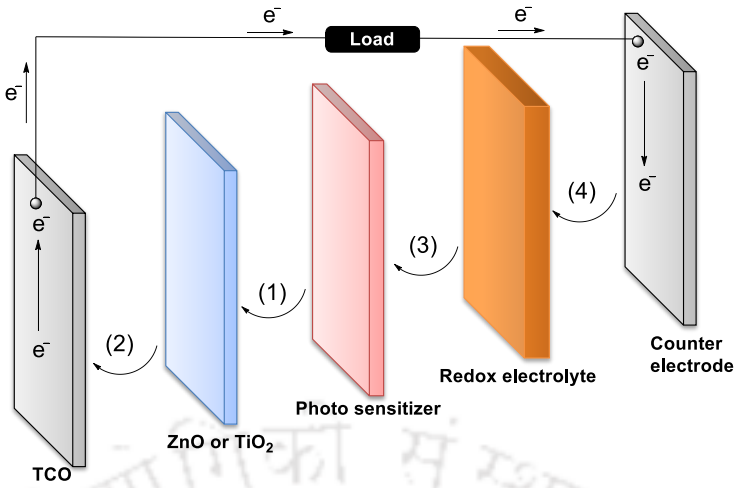

Figure 1.3 A Schematic representation of the components and electron transfer mechanism of a typical DSSC.

1.4 Working principle of DSSC

The generation of photocurrent in the DSSC takes place in steps as explained below. Equations (1) to (4) and Figure 1.4.

Initially the dye sensitizer absorbed on to semiconductor metal oxide (SMO), absorbs photon (sunlight) to generate the photoexcited state of the dye [Eq. (1); S*,], then the photoexcited dye (S*) quickly injects an electron in to the CB (LUMO) of SMO (~100 ps). At the same time, the photosensitizer generates its oxidized state (Eq. (2); S^+).

$$\mathbf{S + } h\nu \longrightarrow \mathbf{S^*} \qquad \mathbf{(1)}$$

$$\mathbf{S^*} \longrightarrow \mathbf{S^+ + e^-} \qquad \mathbf{(2)}$$

The resulting oxidized dye (S^+) is subsequently reduced back to its original natural state through the electron donation from the iodide/tri iodide redox mediator; this process is usually called dye regeneration or re-reduction (Eq. (3); ~1µs). The injected electrons move through the network of interconnected TiO_2 nanoparticles to reach at the FTO and then through the external circuit to the Pt-coated counter electrode.

$$2S^+ + 3\,I^- \longrightarrow 2S + I_3^- \qquad (3)$$

$$I_3^- + 2e^-(Pt) \longrightarrow 3\,I^- \qquad (4)$$

The I^- ion is regenerated by the reduction of I_3^- at the counter electrode through the donation of electrons from the external circuit Eq. (4), then the circuit is complete.

During this electron flow cycle, however, there are some undesirable side processes:

In DSSC during the photocurrent generation process the dye molecules are excited then electrons injected into the CB of the TiO_2 electrode. The undesired recombination processes are, (1) The electrons are recombining with oxidized dye molecule [Eq. (5)], (2) decay of excited state to the corresponding HOMO/VB of sensitizer itself [Eq. (7)] or (3) either recombines with I_3^- at the TiO_2 surface, resulting in lowering of photovoltaic performance of DSSC [Eq. (6)].

$$S^+ + e^-(TiO_2) \longrightarrow S \qquad (5)$$

$$I_3^- + 2e^-(TiO_2) \longrightarrow 3I^- \qquad (6)$$

$$S^* \longrightarrow S \qquad (7)$$

To achieve a higher photocurrent, the time scale of electron injection should be much faster than the radiative decay of sensitizer. In general, the relaxation process of photoexcited dye molecule in device is in the order of magnitude 10^{-7} s, while ultrafast electron injection from the dye molecule in femtosecond (10^{-15}) range is observed. Fortunately, the sensitizer regeneration process (through redox couple, 10^{-8} s) is much faster than the recombination kinetics in device. The necking process ($TiCl_4$ treatment) was used to suppress the back electron transfer recombination process [Eq. (5) & (6)] from the TiO_2 film.

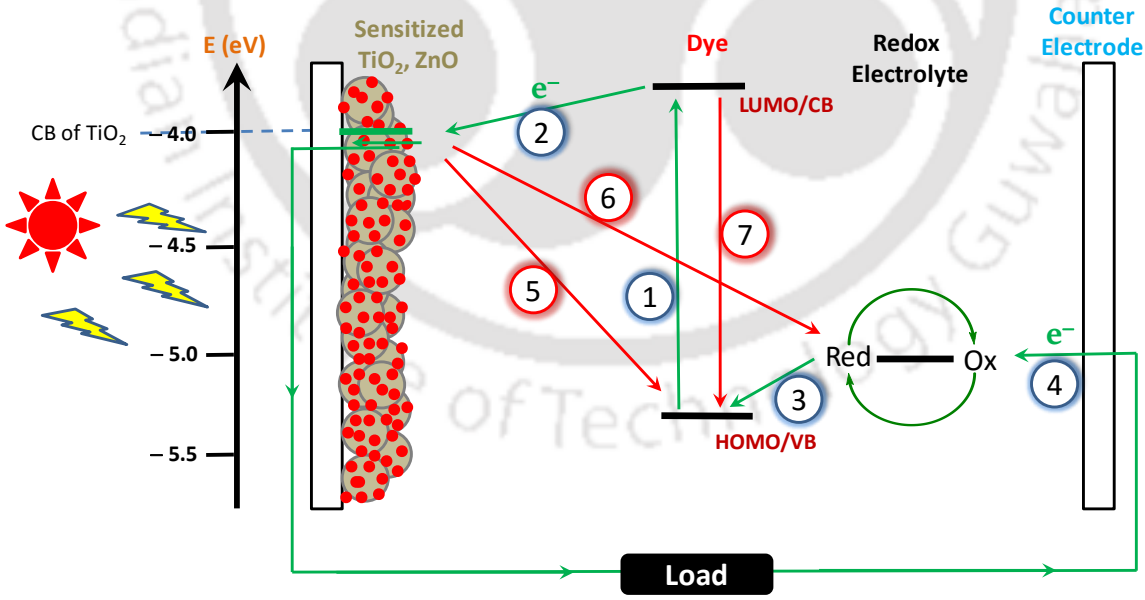

Figure 1.4 Schematic representation of prime components in DSSC and step-wise charge process taking pace in the device. Red and green colored arrows represent the basic forward and back electron transfer process taking place in the device.

1.5 Materials Development

1.5.1 Semiconductor Metal Oxide Electrode

Grätzel. M *et.al* reported the first DSSC in 1991, and in that device they had used mesoporous TiO_2 electrode, with high internal surface area, to support the monolayer of the sensitizer.[25] Researchers have developed many other metal oxide systems, such as ZnO, SnO_2, Nb_2O_5, $SrTiO_3$, and Zn_2SiO_4 etc. Since last decade researchers have focused on different types of nano structures such as spherical shape, nanotubes and single-crystalline nanorods *etc*., and optimize the thickness, morphology of the nanostructure electrode has been tested. [27-39]

TiO_2 have high refractive index (n= 2.4-2.5), stable and nontoxic metal oxide. Several crystal forms of TiO_2 occur naturally: anatase, rutile and brookite. Anatase is the most preferable structure in DSSC, due to the large band gap (3.2 eV) whereas, rutile is the most thermodynamically stable form (3.0 eV).[40] Researchers have developed new anatase nanostructures such as nanorods, nanowires, nanoparticals, nanobowls, nanosheet etc., by using hydrothermal, solvothermal, chemical vapor deposition, physical vapor deposition etc., techniques.[27-39]

The role of TiO_2 electrode is to provide sufficient area for dye absorption, light scattering, and suppression of charge recombination, charge transport, and improvement of the interfacial area. For typical dyes, the required optimized thickness of porous TiO_2 film is 10-20 µm, which depends on the absorption coefficient of the dye.[41-42] To produce high-performance of DSSC, colloidal TiO_2 is prepared by hydrolysis method, using Ti (IV) alkoxides. To get desired size of monodispersed particles, the hydrolysis and condensation kinetics must be controlled. The TiO_2 photoanode have been prepared by a very simple process. The TiO_2 colloidal solution is coated (by using doctoral blade technique or screen printing etc.,) on a TCO substrate and then sintered at 450-550 °C, producing a film of ~10-20 µm thickness. The porosity of the film is also important because the electrolyte, having redox ions must penetrate the film effectively to allow redox ions reaching all absorbed dyes and diffusing back to the counter electrode. The porosity (approximately 50-70%) is controlled by the sintering process by addition of a polymer such as ethyl cellulose (EC) and polyethylene glycol into the TiO_2 colloidal solution or paste.[43,44] The introduction of scattering layer on top of the transparent TiO_2 is also important, because scattering property of the film improves the light harvesting efficiency of the dye-sensitized film to increase the IPCE (incident photon to current

efficiency).[45-47] The $TiCl_4$ treatment of the TiO_2 film improves cell performance (especially increase J_{sc}). After coating TiO_2 film on the TCO, it was immersed in a 0.1-0.5 M $TiCl_4$ solution and then sintered at 450 °C for 30 min. It has been reported that it improves electron diffusion coefficients and lifetime, while the energy level of the CB of TiO_2 is positively shifted.[48]

Table 1.1 Semiconducting metal oxide electrodes structural and electronic properties generally used in solar cells.

Parameter	TiO_2	ZnO	SnO_2	Ref
Crystal structure	rutile, anatase	wurtzite	rutile	49-52
Band gap	3.0-3.2	3.2-3.4	3.6-3.8	49-53
Conduction band minimum (eV)	-4.41	-4.36	-4.48	54
Electron effective mass	9.0	0.26	0.275	55-57
Static dielectric constant ($\varepsilon_{\perp}$, $\varepsilon_{/\!/}$)	86, 170	9.26, 8.2	14.9	58
Electron mobility ($cm^2v^{-1}s^{-1}$)	0.1-4	130-200	200-250	49,57,59
Effective electron diffusion coefficient ($cm^2\ s^{-1}$)	4.3×10^{-4}	1.1×10^{-4}	7.3×10^{-5}	60

1.5.2 Molecular Design of organic dyes for DSSC

On the basis of the accumulated knowledge, organic dyes are synthesized since last two decades for DSSC, and the basic requirements to design the molecular dye for the DSSC are as follows:

(1) The organic dye must have at least one anchoring group (e.g., -COOH, $-SO_3H$, $-PO_3H_2$, Pyridine etc.,) for adsorption onto the TiO_2 surface.[61] Particularly carboxyl group containing dye can form an ester linkage, a chelating linkage, and strongly bidentate linking to TiO_2 surface to provide good electron interaction between the dye and surface of metal oxide.

(2) To achieve high photocurrent, efficient electron injection is necessary from the excited dye to CB of TiO_2. The LUMO level of dye must be higher (more negative) than the CB (-0.5 V vs NHE) of the TiO_2. On the other hand, to achieve high efficiency regeneration of dye from the I^-/I_3^- redox couple in the electrolyte, the HOMO energy level of the dye should be lower (more positive) than the I^-/I_3^- redox potential (0.4 V vs NHE).[62]

(3) Dye must have high molar absorption coefficients over the wide range of solar-spectrum.

(4) To achieve a durable DSSC, the dye must have chemical stability in its photoexcited state and in the redox reactions throughout the reaction cycle.

(5) Dye aggregation on the TiO_2 surface, leads to the low PCE (η) of the device, and should be avoided. D-π-A dyes are liable to undergo π-stacked aggregation on TiO_2 surface, which leads to reduced electron-injection yield from the dye to CB of TiO_2 owing to intermolecular energy transfer.

(6) Hydrophobic substituents on the dye skeleton acts as barriers to prevent the back electron transfer recombination [Eq. (6)]

In DSSCs, the key component is a sensitizer, due to its function of light harvesting and electron injection capacity. Generally, dyes are categorized into two types: (1) metal-organic dyes (2) pure organic dyes. Early research on metal-based sensitizers (N3, N719 and black dye etc.) are the most representative and most successful in DSSCs (Figure **1.5)** due to their long term stability and outstanding performances (PCE = >10% at AM 1.5G condition).[63-70]

However, these dyes have some disadvantages such as they are very expensive, challenging synthesis, tedious purification, lower molar extinction coefficient and environmental issues. On the other hand, organic dyes (metal-free) are gradually attracting researchers' attention due to the multiple advantages of relatively lower cost, high molar extinction coefficient, easy synthesis and excellent flexibility in structure modification, easily tunable functionalities and the photophysical as well as photochemical properties of dyes.

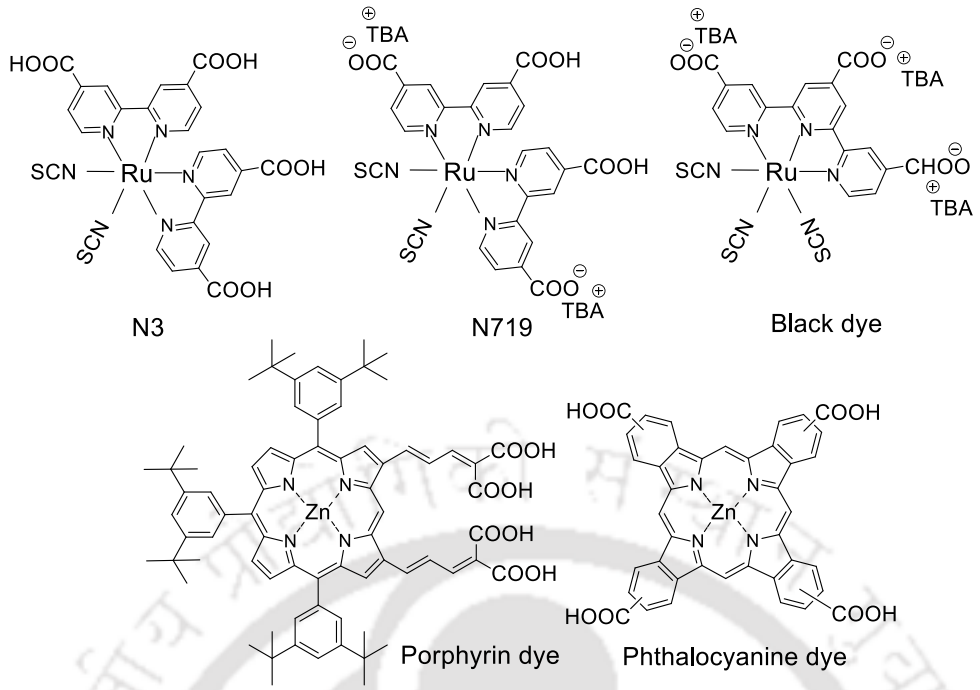

Figure 1.5 Commonly used metal- organic dyes for DSSC.

To achieve efficient electron injection, introduction of electron donating (D) and accepting (A) groups on the chromophore skeleton by expansion of π-conjugation in D-π-A organic dyes having more intramolecular charge transfer from D to A, results in efficient electron transfer from the excited dye LUMO level to CB of TiO_2. Generally, electron donors are "aromatic amines", and the electron acceptors are mostly "carboxyl acid derivatives". Increasing the electron-donating and accepting abilities of dye, respectively decreases the energy gaps between the HOMO and LUMO.[71-97] This results in redshift of the absorption peak. Introducing π-conjugation in D and A substituent also improves absorption spectra of dye. This is also one of the important consideration in the design of efficient dye, however, the LUMO levels of dye must match with the CB of TiO_2 (an energy gap of over 0.2 eV is necessary) and energy gap between 0.2-0.3 eV is necessary for the HOMO level of dye redox potential of the I^-/I_3^- electrolyte.[61]

Expansion of π-conjugated system through the introduction of thiophene, bithiophene, 3,4-ethylenedioxythiophene (EDOT), fused thiophene derivatives, furan, phenyl, methine (CH=CH), phenylenevinylene etc., units effectively causes a red shift of absorption spectra (ICT) due to destabilization of the HOMO level and (or) stabilization of the LUMO level, leading to a decrease in band gap.[71-88] The planar π-conjugated system could also contribute to enhance the absorption maxima of dyes, due to the enhancement of intramolecular charge transfer (ICT) between D to A.

Light absorption at the near IR (NIR, 600-1000 nm) region dyes are very hot topic nowadays. Unfortunately, very few reports on NIR region absorption dyes, such as squaraine dyes,[89,90] Pc dyes,[98] cyanine dyes and BODIPY dyes are available in literature.[99] But disadvantage of these cationic NIR dyes are lower LUMO levels and formation of dye aggregates.

In certain cases, the absorption maximum of the dye adsorbed on the TiO_2 layer is blue shifted compared with those in solution, due to the deprotonation of the carboxylic acid (formation of carboxylate) or in the "H-aggregation" of dyes on the TiO_2 surface. [73,100,101] Unfortunately, one of the main drawback of these D-π-A dyes are formation of strong π-stacked aggregates between the dye molecules on TiO_2 surface, causing reduced electron injection yields from the dyes to the CB of TiO_2, owing to intermolecular energy transfer between dyes. Addition of co-adsorbents such as deoxycholic acid (DCA) or chenodeoxycholic acid (CDCA) suppress the dye aggregation on the TiO_2 surface,[102] or introduction of sterically hindered substituents (bulky groups) such as long alkyl chains and aromatic units, into dye structure should effectively suppress dye aggregation, due to the disturbance in the π-π stacking.[81-85,97] Figure 1.6 schematically represents how to improve the better electron flow from donor to acceptor in dyes and different type of π-bridge, acceptors and star shape dyes, substitution of alkyl, alkoxy chains that inhibit the approach of I_3^- ions to TiO_2 surface.

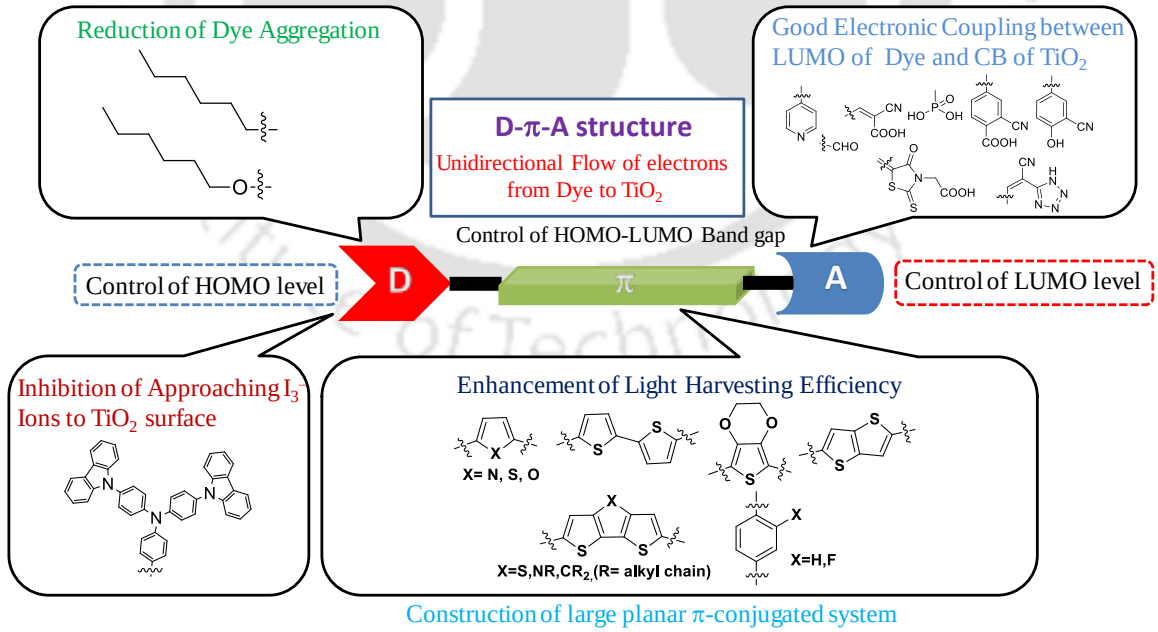

Figure 1.6 Schematic representation of molecular design of D-π-A organic dyes for improved photovoltaic performance.

Charge recombination between the injected electrons and I_3^- ions in the electrolyte can effectively reduce the V_{oc} of the device. Introducing long hydrophobic alkyl and alkoxy chains on the D moiety or π-bridge and introducing bulky aromatic units at donor side (D-D-π-A) effectively blocks the approach of hydrophilic I_3^- ions to the TiO_2 surface.[81-85] These results reveal that "starburst" shape sensitizers perform better V_{oc}, PCE than "rod" shape sensitizers.[84-87] Molecular orbital (MO) calculations revealed that, HOMO is delocalized over the donor-π-conjugated bridge and the LUMO is mostly localized on the acceptor moiety, thus indicating the photoexcitation of a D-π-A dye will result in migration of electron density towards the TiO_2 surface.

Dyes with cyanoacrylic acid as an acceptor have higher IPCE, J_{sc}, V_{oc} and η values than those with other acceptor, due to the strong binding ability and more effective electron injection from the excited state dye to CB of TiO_2. SO_3H, PO_3H_2 and $Si(OR)_3$ anchoring groups which have stronger binding properties than the –COOH group. However, SO_3H, PO_3H_2 groups have strong acidities, poor solubility in organic solvents and poor electron accepting abilities resulting in lower efficiency values. The binding ability, acceptor nature of $Si(OR)_3$ was low on TiO_2 surface.[61]

When nitro, cyano and fluorine groups containing phenyl π-spacer were located close to the metal oxide surface, it gives good electron communication between the dye and CB of metal oxide. Hence, researchers have focused to develop this new class of organic dyes.[103-105]

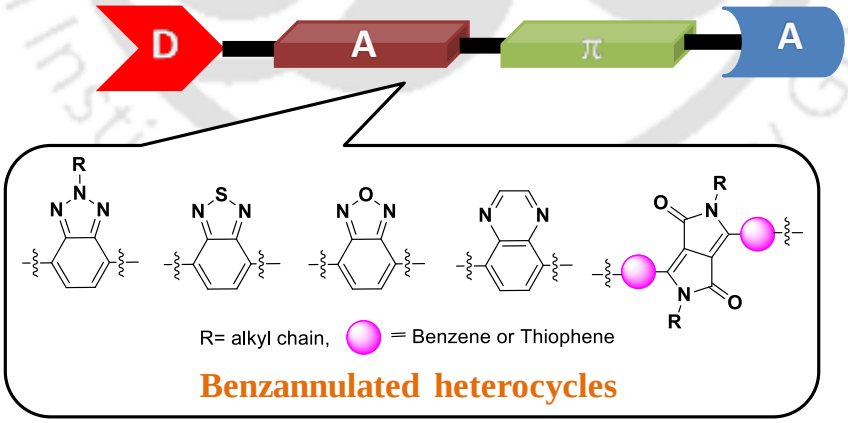

Figure 1.7 Schematic representations of auxiliary acceptors in D-A-π-A organic dyes for improved photovoltaic performance.

In 2011 research community developed new concept of D-A-π-A architecture dye and proposed this kind of dyes to be more stable and efficient.[93,106-115] Specifically, an

addition of auxiliary acceptor unit in between the D and π bridge, not only modulates the absorption spectra, energy levels, and photovoltaic performance, but also greatly improves the stability of devices. Several auxiliary acceptors or electron- withdrawing units such as Benzothiadiazole (BDT),[107,108] benzotriazole (BTZ),[109,110] quinoxaline (Qu),[111,112] Phthalimide,[113] and diketo-pyrrolopyrrole (DPP)[114] are introduced into D-A-π-A structure, and they demonstrated a significant increase in the PCE from 5%, to greater than 10%. Figure 1.7 represents different type of acceptors in D-A-π-A dyes. The electron withdrawing capacity increases in the sequence benzotriazole < quinoxaline < benzothiadiazole < benzoxadiazole. Theoretical and experimental evidence explains, larger electron withdrawing nature of auxiliary acceptor exhibit more spectral response and more photocurrent.[115,116] However, this kind of architecture has some disadvantages; electron-deficient benzannulated hetero cycles may cause partial charge-trapping and hamper electron injection in excited dye to CB of TiO_2.[117]

Researchers compare electron injection and recombination dynamics capacity of D-A-π-A and D-π-A-A dyes. They explain when the electron deficient unit is directly adjacent to the anchoring group (D-π-A-A), dyes exhibit large red shift in absorption band, but does not show any promising improvement in cell efficiency compare to D-π-A-A dyes. Because in D-π-A-A dyes have rapid recombination between the injected electrons and oxidized organic dyes was observed. This was, well explained by transient laser photolysis experiment technique. But, in D-A-π-A dyes (π-spacer between the acceptor and anchoring group) the back electron transfer was greatly retarded, resulting in vast improvement in PCE.[117] They conclude that D-A-π-A structure is more preferable with respect to D-π-A and D-π-A-A structures. Nevertheless choosing or designing optimal π-spacer in organic dyes remains a key issue.[118,119]

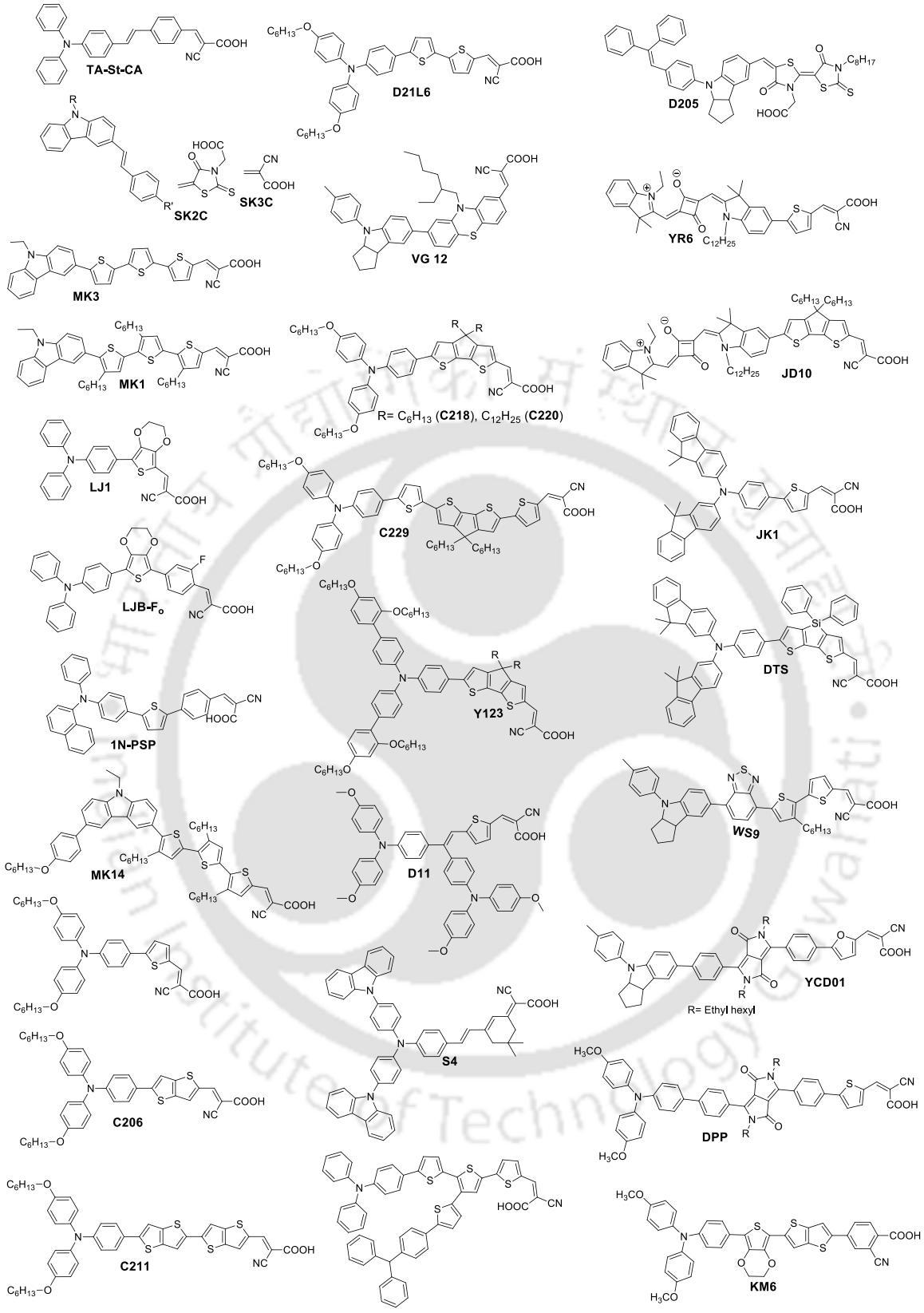

Figure 1.8 Chemical structure of various D-π-A and D-A-π-A dyes used in DSSC.

Table 1.2 Photovoltaic performances of various dyes

S.No	Dye	J_{sc} (mA.Cm^{-2})	V_{oc} (mV)	FF	PCE (η)	λ_{max}	Ref
1	TA-St-CA	18.1	743	0.675	**9.10**	386	71
2	SK2C	8.4	587	0.48	**2.4**	460	72
3	SK3C	18.3	725	0.67	**9.0**	435	72
4	MK2	15.22	730	0.75	**8.3**	485	73
5	MK5	10.16	670	0.64	**4.3**	480	73
6	LJ1	15.5	690	0.68	**7.30**	426	74
7	LJB-F_o	15.6	787	0.67	**8.22**	420	75
8	1N-PSP	16.8	740	0.57	**7.08**	422	77
9	MK14	16.0	710	0.71	**8.10**	483	78
10	-	118	775	0.74	**6.88**	514	76
11	C206	13.9	731	0.74	**7.54**	516	79
12	C211	15.2	720	0.73	**8.02**	524	80
13	D21L6	13.8	713.8	0.72	**7.11**	525	81
14	C218	15.8	769	0.73	**8.95**	555	81
15	C220	9.7	881	0.71	**6.08**	555	82
16	C229	15.3	850	0.73	**9.40**	600	83
17	Y123	15.9	910	0.71	**10.3**	472	84
18	D11	13.9	744	0.7	**7.23**	458	85
19	S4	13.8	630	0.69	**6.02**	480	86
20	-	15.6	650	0.6	**6.04**	465	87
21	D205	18.5	717	0.71	**9.52**	532	88
22	YR6	14.8	642	0.71	**6.74**	659	89
23	JD10	16.4	635	0.70	**7.3**	672	90
24	JK1	12.2	764	0.77	**7.20**	436	91

S.No	Dye	J_{sc} (mA.Cm^{-2})	V_{oc} (mV)	FF	PCE (η)	λ_{max}	Ref
25	DTS	13.9	739	0.73	**7.50**	459	92
26	WS9	18.0	696	0.72	**9.04**	536	93
27	YCD01	13.4	760	0.73	**7.43**	526	94
28	DPP	9.7	605	0.70	**4.14**	524	95
29	KM6	8.1	756	0.73	**4.50**	443	96
30	VG12	16.5	710	0.61	**7.2**	455	97

1.5.3 Redox Couples for Electrolyte

The electrolyte plays most crucial role in DSSC, the widely utilized component as a transport medium in DSSCs; it helps in continuous dye regeneration and transport of inner charge carriers during DSSC operation. All the device parameters such as J_{sc}, V_{oc}, FF and PCE will be significantly affected by the electrolyte and the electrolyte have interaction with the electrode interfaces. J_{sc} can be affected by the transport of the redox couple in the electrolyte, V_{oc} can affected by the redox potential of the electrolyte, and FF can be affected by the diffusion of charge carrier in electrolyte. The electrolyte can be classified into mainly 3 categories, (1) liquid electrolyte (2) quasi-solid electrolytes and (3) solid-state conductors. In general, liquid electrolyte consists of three main components: solvent, additive and ionic conductor.[120]

The liquid electrolytes are again classified into 2 types; (1) I^-/I_3^- redox couples (2) I^-/I_3^- free redox couples. In the I^-/I_3^- redox couple electrolyte, the mixture of iodides such as LiI, KI, NaI, tetra alkyl ammonium iodides (R_4NI) and imidazolium derivative iodides with concentration of 0.1-0.5 M and 0.05-0.1 M of I_2 dissolved in non-protonic organic solvents. Generally, nitrile solvents are used in DSSC, because they have relatively low viscosity, such as acetonitrile, methoxyacetonitrile, propionitrile, and 3-methoxypropionitrile etc. To improve J_{sc}, low-viscosity solvents are preferable due to the high ionic conductivity, but low-viscosity solvents have high vapor pressure, making it difficult to seal it for long term usage. Electrical additives (4-tert-butylpyridine (TBP), 1-methyl-benzimidazole, guanidium thiocyanate (GSCN) etc.) also have been added to electrolyte solution to improve the device performance. It changes (1) electrolyte potential value, (2) shifting the conduction band of semiconducting metal oxide, (3)

retarded recombination kinetics.[121,122] In order to improve the performance of the DSSC, research communities have been devoting their efforts to develop new electrolytes. The below Figure 1.9 explains redox potentials and structure of liquid electrolytes commonly used in DSSC.

(a) (b)

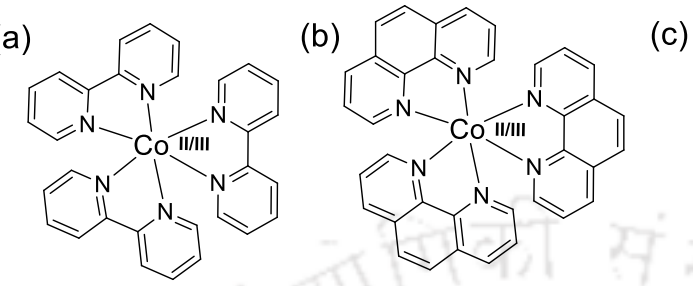

(c)

Electrolyte Syestem	Redox potential (in Volt)	(in eV)
I^-/I_3^-	0.35	-4.75
Co-bpy	0.56	-5.06
Co-phen	0.62	-5.12

Figure 1.9 Structure of liquid state electrolytes (a) $Co^{II/III}$-tris-(2,2'-bipyridine) (b) $Co^{II/III}$-tris-(1,10-phenanthroline) and (c) Redox potential of different electrolyte systems.

1.5.4 Counter electrode

Counter electrode, an integral part of DSSC, is vital to collect electrons from external load and to catalyze the reduction of redox couple in electrolyte. These electrons are conducted from the redox electrolyte to excited dye to bring them to ground state.[123] In I_3^-/I^- electrolyte medium DSSC, Pt is recognized as the most promising candidate for counter electrode.[124] Pt electrode has good intrinsic features like conductivity, high catalytic activity, and large effective surface area. Pt electrode itself has some disadvantages, like it is not suitable for other electrolytes such as Cobalt redox couple,[125] due to the large dispute in the electrochemical behavior of ligands that tends to decrease the catalytic activity of Pt electrode.[126] To overcome such practical and economic barriers, scientists have developed several noble metal-free and cost effective alternatives (carbon materials, transition metal compound, conducting polymers etc.,) as the efficient counter electrode.[125] The scientific community explains some ideal parameters for counter electrode, such as optical transparency of ~80% at 550 nm, charge transfer resistance of ~2-3 $\Omega.cm^2$, and sheet resistance of ~20 Ω sq^{-1}.[127] However, in most cases, it is difficult to incorporate all these parameters into one material to achieve optimum operation.

1.6 Experiment

1.6.1 Materials and Chemicals used

All reactions were performed under argon atmosphere and appropriate solvents were distilled from drying agents prior to use. The starting materials of dyes 3-bromo-9-alkyl-9H-carbazole, 4-bromo-N,N-diphenylaniline, 3-bromo-10-alkyl-10H-phenothiazine, 2-bromo-9-octyl-7-(thiophen-2-yl)-9H-carbazole were prepared according to the published references.[128-130] 2,7-dibromo carbazole, 2-Fluoro 4-formylphenyl boronic acid, 3-Fluoro 4-formylphenyl boronic, 1-bromo-4-(bromomethyl)benzene, 3,4-dibromothiophene-2,5-dicarbaldehyde acid, cyano aceticacid, Nano-crystalline TiO_2 semiconductor (<20 nm, 99.7%, anatase), ethyl cellulose (90.2%), 3-methoxy propionitrile (MNP), Guanidinium thiocyanate (GSCN), 4-tert butyl pyridine (TBP) and α-terpineol (90%) were purchased from Sigma-Aldrich and used as received. All other reagents were purchased from sigma Aldrich and used without purification. Compound was synthesized by Suzuki-coupling reaction, Witting-Horner and Knoevenagel condensation method according to the published journals. TCO (Transparent Conductive Oxide) glass (8-12 Ω/cm^2) and Meltonix tape were procured from Solaronix, Switzerland. Solvents like acetonitrile, ethanol and isopropanol, etc., was purchased from Merck and used without further purification.

1.6.2 Characterization of Materials and Devices

The synthesized compounds (dyes, photoanode etc.) and fabricated solar cells are characterized by using a number of techniques. The instrument methods / tools used in the present investigations include:

1. NMR spectroscopy using 400 MHz and 600 MHz Bruker Advance NMR instruments.
2. Mass spectroscopy using Agilent 6545 Q- TOF LC/MS instrument.
3. UV-Vis diffused reflectance absorption spectroscopy using spectrophotometer (Model JASCO V-650) equipped with 150 mm integrating sphere. For solution state PerkinElmer Lambda-35 spectrophotometer were used.
4. Cyclic voltammetry (CV) using CH instrument, Model CHI600E.
5. Photoluminescence using Horiba Jobin Vyon Fluoromax-4 spectrophotometer.
6. Time resolved Photoluminescence using LifeSpec II Edinburgh instrument having a lamp with frequency of 5 MHz and Nd:YAG laser of different excitation of wavelengths.

7. Spin coating using SPIN-150 spin coater.
8. Film/layer thickness measurement using a Veeco Dektak 150 surface profilometer.
9. Photocurrent-voltage (J-V) curves of solar cell using Keithley Sourcemeter 2420.
10. Standard solar spectrum using a Newport ORIEL Sol3A solar simulator fitted with a Xenon arc lamp, power 450W.
11. Electrochemical impedance spectroscopy (EIS) using CH instruments, Model CHI600E.

Cyclic Voltammetry experiments were performed on CH instruments 600E model with three standard electrochemical cells. Thin films of dyes were coated on glassy carbon electrode, and it was used as a working electrode, Ag/Ag^{+} electrode as the reference and Pt wire for counter electrode. 0.1 M tetrabutyl ammonium hexaflurophosphate (Bu_4NPF_6 or $TBAF_6$) for supporting electrolyte dissolve in acetonitrile solvent. CV curves were calibrated by using ferrocene as the standard. The *J–V* characteristics of the fabricated two different thickness based solar cell devices were measured using a Keithley-2420 digital source meter with a scan rate of 10 mV/s and sweeping the voltage in the range of -1 V to +1 V. Impedance Spectroscopy (EIS) measurements were carried out using CH instruments, Model CHI600E analyzer and recorded by sweeping frequency from 120 KHz to 0.1Hz in dark under -0.65V DC bias. A small AC perturbation (10mV) was imposed onto the system. Open-circuit voltage decay (OCVD) and Tafel polarization curves were obtained by using CH instruments, Model CHI600E electrochemical analyzer by sweeping potential ±0.65 in dark with 25mV/s scan rate.

Theoretical study

Electronic density distribution of frontier molecular orbital of metal-free organic dyes are estimated from density functional theory (DFT) calculations using the Gaussian 09 software at B3LYP level, 6-31 G(d,p), TD-DFT, CAM-B3LYP level, 6-31 G(d,p) basis sets for all dyes having fluorine atoms and doesn't have fluorine atom dyes frontier molecular orbital estimated by B3LYP level, 6-31 G basis set.[131]

1.6.3 Fabrication of photovoltaic devices

DSSC were fabricated using sandwich type configuration of photoelectrode and counter electrode. Photoelectrode was made from the commercial TiO_2 nanocrystaline semiconductor (P25, Degussa, Germany). Thin film of the TiO_2 particles was deposited

from the TiO_2 paste containing ethyl cellulose and α-terpeneol. The electrodes were calcinated in tubular furnace at 450 °C for 25 min. and then soaked into the 10 mM dye solution. Dye soaking of the photoelectrode was carried out in a glove box filled with nitrogen with very low light level for 18 h. Counter electrodes were fabricated by spin coating of 50mM H_2PtCl_6 solution in isopropanol onto predrilled FTO substrate followed by sintering at 450 °C for 15 min. Dye coated photoelectrode and Pt counter electrode were sealed together using hot melt sealing tape upon application of heat. Electrolyte solution comprises of the 0.5M LiI, 0.05M I_2, 0.5M TBP, 0.5M GSCN in 3-methoxy propionitrile, was inserted through the predrilled holes onto the counter electrode. Holes were sealed using epoxy adhesive and cover glass. DSSC were stored in dark at room temperature for 12 hours prior to measurements. Active area of the DSSC was set to 0.25 cm^2 and was maintained constant using the same screen for coating.

1.6.4 Photovoltaic parameters

The performance of solar cells are mainly characterized by five parameters: (1) short-circuit current (J_{sc}), (2) open-circuit voltage(V_{oc}), (3) fill factor (*FF*), (4) Power conversion efficiency (PCE, η) and (5) incident photon to current conversion efficiency (IPCE). The performances of a solar cell are evaluated from its corresponding photocurrent-voltage (*J-V*) curve. A schematic representation of *J-V* curve showing the effect of light is represented in Figure 1.10 (b) and explained below. When the sky is clear and sun is directly overhead creating the short path length through the atmosphere, solar radiation striking the earth's surface is maximum. This path length is known as the air mass (AM) and can be expressed as AM =1/Cos ϕ, where ϕ is called as the Zenith angle as shown in the Figure 1.10 (a). To compare solar cells characterized in different laboratories all over the world, a simulated solar spectrum of AM 1.5G (global) corresponding to a ϕ = 48.2° is used for standard and normal integrated irradiance of 1000 $W.m^{-2}$ is used to test their efficiency.

Short-circuit (J_{sc}) current is the current flowing through the solar cell, when the voltage across the cell is zero. This is obtained due to the collection of photon generated charge carries. J_{sc} increases with the light intensity because higher intensity (dye or donor of polymer) releases higher number of photons. J_{sc} strongly depends on the photophysical and electrochemical properties and molecular structure of the material. J_{sc} is expressed in $mA. cm^{-2}$ due to the generate photons in cell by unit area.

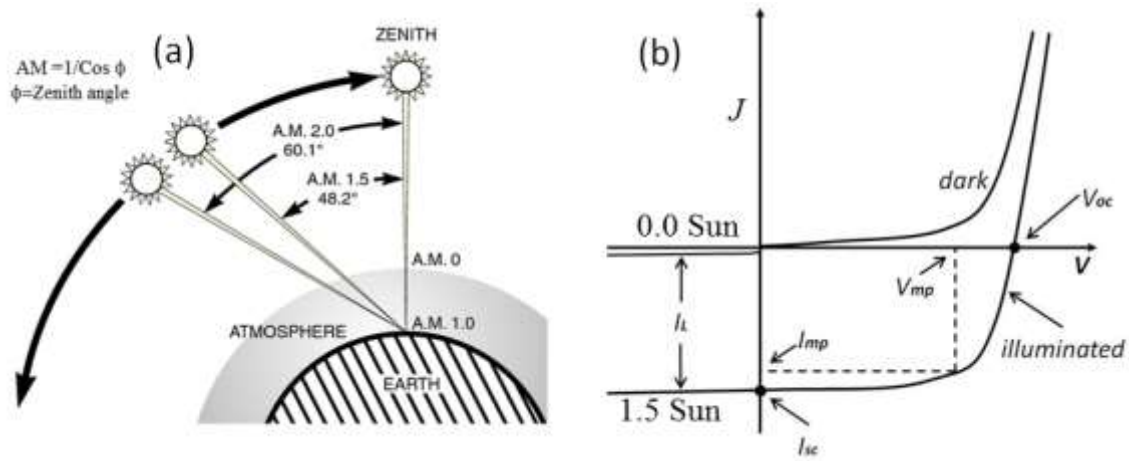

Figure 1.10 (a) Solar radiation path length in air mass (AM) unit and the zenith angle. (b) Schematic representation of photocurrent-voltage (J-V) curve of a solar cell under the dark condition and after illumination of sun light under AM 1.5G.

The open-circuit voltage (V_{oc}) of solar cell is the maximum obtainable voltage at zero current. In DSSC, the difference between the Fermi level of TiO_2 or ZnO coated on FTO/ITO and redox potential of electrolyte effects on the V_{oc}.

The fill factor (FF) is an important parameter for solar cell and is defined as the maximum power output ($P_{max} = J_{mp}.V_{mp}$) divided by the product of J_{sc} and V_{oc}. The rectangle area represents the FF, which is fit in the *J-V* curve as shown in the Figure 1.10 (b).

The FF can be expressed as:

$$FF= P_{max}/ J_{sc} V_{oc}$$

The η value of cell is defined as the ratio of the maximum output electrical power of the cell ($P_{out}= J_{sc.} V_{oc}$. FF) to the energy of the incident sunlight (P_{in}= 100 mW. Cm^{-2})

$$\eta= P_{out}/P_{in}$$

Another parameter related to the performance of a solar cell is (incident photon to current conversion efficiency) IPCE, which corresponds to the photocurrent density produced in external circuit under monochromatic illumination divided by the photon flux that strikes the cell.

$$IPCE= 1240. J_{sc} (\lambda)/ \lambda. P_{in}(\lambda)$$

Electrochemical Impedance Spectroscopy (EIS) measurement

Electrochemical impedance data of DSSC is represented in the form of either Bode plot or Nyquist plot.[132] A typical Nyquist plot of DSSC depicts three semicircles during the cell operation. (1) Charge transfer at the counter electrode, (2) charge transfer of the TiO_2/

dye/ electrolyte interface and (3) Nernst diffusion of the redox couple through the electrolyte and TiO_2 film. Figure 1.11 shows the typical Nyquist plots recorded under dark condition in a sweeping frequency from 120 KHz to 0.1Hz. For better understanding the three semi circles in the Nyquist plot, the value of Rs represent the sheet resistant of the FTO substrate in the device, while R_k and R_D represent the diameter of the respective semicircle. The middle semicircle (f_{max}) is correlated to the rate of recombination resistance of electrons (k_{eff}) at the working electrode/electrolyte interfaces. The electron life time (τ_e) in the photovoltaic device was estimated by the below equation.

$$\tau_e = 1/2\pi . f_{max}$$

Higher life time values represent the maximum photo induced electron density availability in the photovoltaic device.

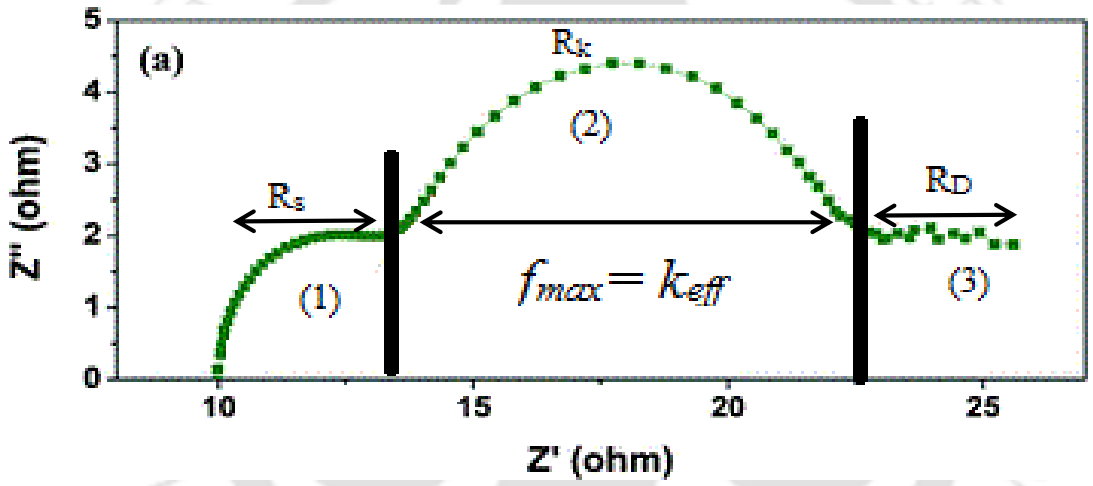

Figure 1.11 Schematic representation of Nyquist plot with all the three semicircles.

1.7 Conclusion

For the last two decades DSSCs have received increased attention because they convert solar energy to electrical energy with low cost and easy fabrication process. With major efforts in design and synthesis of different dyes, large improvements in the performance of DSSC > 13% have been achieved. However, further development of design and synthesis of D-π-A/D-A-A/D-π-A-A/D-A-π-A based dyes is necessary to meet the requirement for their practical application. In the brief discussion on DSSC, we have focused on the role of semiconductor oxide materials, design and development of photosensitizers, electrolytes and counter electrode materials to enhance the device performance. In this content we have discussed mainly the advantages of metal-free

organic dyes, its molecular design and synthetic strategies to improve the photovoltaic performance and chemical and environmental stabilities of various types of dyes discussed here. But there is still a need to design the efficient dye to cover the complete solar spectrum with suitable energy levels to produce high electric current, electrolyte and counter electrode to optimize the chemical and physical properties to improve the solar cell efficiency.

1.8 References

1. Kerr, R. A.; Service, R. F. *Science* **2005**, *309*, 101.
2. Ringpfeil, M. *Nature Biotechnol*, **2004**, *22*, 1077.
3. Goldmberg, J. *Science* **2007**, *315*, 808.
4. Gross, R.; Leach, M.; Bauen, A. *Environ. Int*. **2003**, *29*, 105.
5. Hedberg, D.; Kullander, S.; Frank, H. *Ambio*. **2010**, *39*, 1.
6. Lewis, N. S.; Nocera, D. G. *Proc. Natl. Acad. Sci. U.S.A* **2006**, *103*, 15729.
7. Butler, D. *Nature*, **2008**, *454*, 558.
8. Schiermeier, Q.; Tollefson, J.; Scully, T.; Witze, A.; Morton, O. *Nature* **2008**, *454*, 816.
9. Tyagi, V. V.; Rahim, N. A. A.; Rahim, N. A.; Selvaraj, J. A. L. *Renew. Sust. Energ. Rev*. **2013**, *20*, 443.
10. Chaar, L. El.; Lamonata, L. A.; Zein, N. El. *Renew. Sust. Energ. Rev*. **2011**, *15*, 2165.
11. Bagnall, D. M.; Boreland, M. *Energy Policy*, **2008**, *36*, 4390.
12. Zhao, J.; Wang, A.; Green, M. A.; Ferrazza, F. *Appl. Phys. Lett*. **1998**, 73, 1991.
13. Green, M. A.; Emery, K.; Hishikawa, Y., Warta, W.; Dunlop, E. D. *Prog. Photovolt. Res. Appl*. **2012**, *20*, 12.
14. Shah, A.; Torres, P.; Tscharner, R.; Wyrsch, N.; Keppner, H. *Science* **1999**, *285*, 692.
15. Bloss, W. H.; Pfisterer, F.; Schubert, M.; Walter, T. *Prog. Photovoltaics* **1995**, *3*, 3.
16. Kim, M. R.; Ma, D. *J. Phys. Chem. Lett*. **2015**, *6*, 85.
17. Wu, Y. Z.; Zhu, W. H.; Zakeeruddin, S. M.; Grätzel, M. *ACS Appl. Mater. Inter.* **2015**, *7*, 9307-9318.

18. Hagfeldt, A.; Boschloo, G.; Sun, L. C.; Kloo, L.; Pettersson, H. *Chem. Rev.* **2010**, *110*, 6595-6663.
19. Mishra, A.; Fischer, M. K. R.; Bauerle, P. *Angew Chem. Int. Edit.* **2009**, *48*, 2474-2499.
20. Dou, L. T.; You, J. B.; Hong, Z. R.; Xu, Z.; Li, G.; Street, R. A.; Yang, Y. *Adv. Mater.* **2013**, *25*, 6642-6671.
21. Stranks, S. D.; Snaith, H. J. *Nat. Nanotechnol.* **2015**, *10*, 391-402.
22. Park, N. G. *Mater. Today* **2015**, *18*, 65-72.
23. Niu, G. D.; Guo, X. D.; Wang, L. D. *J. Mater. Chem. A* **2015**, *3*, 8970-8980.
24. Duan, J. L.; Zhang, H. H.; Tang, Q. W.; He, B. L.; Yu, L. M. *J. Mater. Chem. A* **2015**, *3*, 17497-17510.
25. O'Regan, B., Grätzel, M. *Nature* **1991**, *353*, 737-740.
26. Azhar. F.; Rajan. J.; Thomas M. B.; Francisco. F. S.; Juan. B. *Energy. Environ. Sci*. **2014**, *7*, 3952–3981.
27. Ozgur, U.; Alivov, Y. I.; Liu, C.; Teke, A.; Reshchikov, M. A.; Dogan, S.; Avrutin, V.; Cho, S. J.; Morkoc, H. *J. Appl. Phys.* **2005**, 98, 041301.
28. Saito, M.; Fujihara, S. *Energ. Environ. Sci.* **2008**, *1*, 280-283.
29. Lin, C. Y.; Lai, Y. H.; Chen, H. W.; Chen, J. G.; Kung, C. W.; Vittal, R.; Ho, K. C. *Energ. Environ. Sci.* **2011**, *4*, 3448-3455.
30. Cheng, H. M.; Hsieh, W. F. *Energ. Environ. Sci.* **2010**, *3*, 442-447.
31. Chiu, W. H.; Lee, C. H.; Cheng, H. M.; Lin, H. F.; Liao, S. C.; Wu, J. M.; Hsieh, W. F. *Energ. Environ. Sci.* **2009**, *2*, 694-698.
32. Chen, W.; Qiu, Y. C.; Zhong, Y. C.; Wong, K. S.; Yang, S. H. *J. Phys. Chem. A* **2010**, *114*, 3127-3138.
33. Park, K.; Zhang, Q. F.; Garcia, B. B.; Zhou, X. Y.; Jeong, Y. H.; Cao, G. Z. *Adv. Mater.* **2010**, *22*, 2329-2332.
34. Gindri, I. M.; Frizzo, C. P.; Bender, C. R.; Tier, A. Z.; Martins, M. A. P.; Villetti, M. A.; Machado, G.; Rodriguez, L. C.; Rodrigues, D. C. *ACS Appl. Mater. Inter.* **2014**, *6*, 11536-11543.
35. Ren, L.; Li, Y. Z.; Hou, J. T.; Zhao, X. J.; Pan, C. X. *ACS Appl. Mater. Inter.* **2014**, *6*, 1608-1615.
36. Deepak, T. G.; Subash, D.; Anjusree, G. S.; Pai, K. R. N.; Nair, S. V.; Nair, A. S. *ACS Sustain. Chem. Eng.* **2014**, *2*, 2772-2780.

37. Xu, M.; Da, P. M.; Wu, H. Y.; Zhao, D. Y.; Zheng, G. F. *Nano Lett.* **2012**, *12*, 1503-1508.
38. Li, H. L.; Yu, Q. J.; Huang, Y. W.; Yu, C. L.; Li, R. Z.; Wang, J. Z.; Guo, F. Y.; Jiao, S. J.; Gao, S. Y.; Zhang, Y.; Zhang, X. T.; Wang, P.; Zhao, L. C. *ACS Appl. Mater. Inter.* **2016**, *8*, 13384-13391.
39. Li, W.; Wu, Z. X.; Wang, J. X.; Elzatahry, A. A.; Zhao, D. Y. *Chem. Mater.* **2014**, *26*, 287-298.
40. Park, N. G.; van de Lagemaat, J.; Frank, A. J. *J. Phys. Chem. B* **2000**, *104*, 8989-8994.
41. Barbe, C. J.; Arendse, F.; Comte, P.; Jirousek, M.; Lenzmann, F.; Shklover, V.; Gratzel, M. *J. Am. Ceram. Soc.* **1997**, *80*, 3157-3171.
42. Kalyanasundaram. K.; Grätzel. M. *Coord. Chem. Rev.* **1998**, *177*, 347–414.
43. Bai, Y.; Mora-Sero, I.; De Angelis, F.; Bisquert, J.; Wang, P. *Chem. Rev.* **2014**, *114*, 10095-10130.
44. Saito, Y.; Kambe, S.; Kitamura, T.; Wada, Y.; Yanagida, S. *Sol. Energ. Mat. Sol. C.* **2004**, *83 (1)*, 1-13.
45. Usami, A. *Chem. Phys. Lett.* **1997**, *277*, 105-108.
46. Ferber, J.; Luther, J. *Sol. Energ. Mat. Sol. C* **1998**, *54*, 265-275.
47. Rothenberger, G.; Comte, P.; Gratzel, M. *Sol. Energ. Mat. Sol. C* **1999**, *58*, 321-336.
48. Lee, S. W.; Ahn, K. S.; Zhu, K.; Neale, N. R.; Frank, A. J. *J. Phys. Chem. C* **2012**, *116*, 21285-21290.
49. Özgür, Ü.; Alivov, Ya. I.; Liu, C.; Teke, A.; Reshchikov, M. A.; Dôgan, S.; Avrutin, V.; Cho, S.-J.; Morkoc, H. *J. Appl. phy.* **2005**, *98*, 041301
50. Diebold, U. *Surf. Sci. Rep*. **2003**, *48*, 53-229.
51. Scanlon, D. O.; Dunnill, C. W.; Buckeridge, J.; Shevlin, S.A.; Logsdail, A. J.; Woodley, S.M.; Catlow,C. R. A.; Powell, M. J.; Palgrave, R. G.; Parkin, I. P.; Watson, G. W.; Keal, T. W.; Sherwood, P.; Walsh, A.; Sokol, A. A. *Nat. Mater.* **2013**, *12*, 798-801.
52. Batzill, M.; Diebold, U. *Prog. Surf. Sci*. **2005**, *79*, 47-154.
53. Matar, S. F.; Campet, G.; Subramanian, M. A. *Prog. Solid State Chem*. **2011**, *39*, 70-95.
54. Tvrdy, K.; Frantsuzov, P. A.; Kamat, P. V. *Proc. Natl. Acad. Sci. USA* **2011**, *108*, 29-34.

55. Oskam, G.; Hu, Z.; Penn, R. L.; Pesika, N.; Searson, P. C. *Phys. Rev. E* **2002**, *66*, 011403.
56. Button, K. J.; Fonstad, C. G.; Dreybrodt. W. *Phys. Rev. B* **1971**, *4*, 4539.
57. Jarzebski, Z. M.; Marton, J. P. J. *Electrochem. Soc*. **1976**, *123*, 299C-310C.
58. Young, K. F.; Frederikse, H. P. R. *J. Phys. Chem. Ref. Data* **1973**, *2*, 313-409.
59. Tang, H.; Prasad, K.; Sanjinès, R.; Schmid, P. E.; Lèvy, F. *J. Appl. Phys*. **1994**, *75*, 2042-2047.
60. Tiwana, P.; Docampo, P.; Johnston, M. B.; Snaith, H. J.; Herz, L. M. *ACS Nano* **2011**, *5*, 5158-5166.
61. Zhang, L.; Cole, J. M. *ACS Appl. Mater. Inter*. **2015**, 7, 3427-3455.
62. Ooyama, Y.; Harima, Y. *Chem. Phys. chem.* **2012**, *13*, 4032-4080.
63. Barea, E. M.; Gonzalez-Pedro, V.; Ripolles-Sanchis, T.; Wu, H. P.; Li, L. L.; Yeh, C. Y.; Diau, E. W. G.; Bisquert, J. *J. Phys. Chem. C* **2011**, *115*, 10898-10902.
64. Luo, J.; Xu, M. F.; Li, R. Z.; Huang, K. W.; Jiang, C. Y.; Qi, Q. B.; Zeng, W. D.; Zhang, J.; Chi, C. Y.; Wang, P.; Wu, J. S. *J. Am. Chem. Soc.* **2014**, *136*, 265-272.
65. Shi, Y. B.; Liang, M.; Wang, L. N.; Han, H. Y.; You, L. S.; Sun, Z.; Xue, S. *ACS Appl. Mater. Inter.* **2013**, *5*, 144-153.
66. Nazeeruddin, M. K.; Kay, A.; Rodicio, I.; Humphrybaker, R.; Muller, E.; Liska, P.; Vlachopoulos, N.; Grätzel, M. *J. Am. Chem. Soc.* **1993**, *115*, 6382-6390.
67. Nazeeruddin, M. K.; Splivallo, R.; Liska, P.; Comte, P.; Grätzel, M. *Chem. Commun.* **2003**, *(12)*, 1456-1457.
68. Nazeeruddin, M. K.; Pechy, P.; Grätzel, M. *Chem. Commun.* **1997**, *(18)*, 1705-1706.
69. Nazeeruddin, M. K.; Pechy, P.; Renouard, T.; Zakeeruddin, S. M.; Humphry-Baker, R.; Comte, P.; Liska, P.; Cevey, L.; Costa, E.; Shklover, V.; Spiccia, L.; Deacon, G. B.; Bignozzi, C. A.; Gratzel, M. *J. Am. Chem. Soc.* **2001**, *123*, 1613-1624.
70. Mathew, S.; Yella, A.; Gao, P.; Humphry-Baker, R.; Curchod, B. F. E.; Ashari-Astani, N.; Tavernelli, I.; Rothlisberger, U.; Nazeeruddin, M. K.; Gratzel, M. *Nat. Chem.* **2014**, *6*, 242-247.
71. Hwang, S.; Lee, J. H.; Park, C.; Lee, H.; Kim, C.; Park, C.; Lee, M. H.; Lee, W.; Park, J.; Kim, K.; Park, N. G.; Kim, C. *Chem. Commun.* **2007**, *(46)*, 4887-4889.
72. Soni, S. S.; Fadadu, K. B.; Vaghasiya, J. V.; Solanki, B. G.; Sonigara, K. K.; Singh, A.; Das, D.; Iyer, P. K. *J. Mater. Chem. A* **2015**, *3*, 21664-21671.

73. Wang, Z. S.; Koumura, N.; Cui, Y.; Takahashi, M.; Sekiguchi, H.; Mori, A.; Kubo, T.; Furube, A.; Hara, K. *Chem. Mater.* **2008**, *20*, 3993-4003.
74. Liu, W. H.; Wu, I. C.; Lai, C. H.; Lai, C. H.; Chou, P. T.; Li, Y. T.; Chen, C. L.; Hsu, Y. Y.; Chi, Y. *Chem. Commun.* **2008**, *41*, 5152-5154.
75. Chen, B. S.; Chen, D. Y.; Chen, C. L.; Hsu, C. W.; Hsu, H. C.; Wu, K. L.; Liu, S. H.; Chou, P. T.; Chi, Y. *J. Mater. Chem.* **2011**, *21*, 1937-1945.
76. Li, R. Z.; Lv, X. J.; Shi, D.; Zhou, D. F.; Cheng, Y. M.; Zhang, G. L.; Wang, P. *J. Phys. Chem. C* **2009**, *113*, 7469-7479.
77. Chang, Y. J.; Chow, T. J. *Tetrahedron* **2009**, *65*, 4726-4734.
78. Koumura, N.; Wang, Z. S.; Miyashita, M.; Uemura, Y.; Sekiguchi, H.; Cui, Y.; Mori, A.; Mori, S.; Hara, K. *J. Mater. Chem.* **2009**, *19*, 4829-4836.
79. Zhang, G. L.; Bai, Y.; Li, R. Z.; Shi, D.; Wenger, S.; Zakeeruddin, S. M.; Gratzel, M.; Wang, P. *Energ. Environ. Sci.* **2009**, *2*, 92-95.
80. Zhang, G. L.; Bala, H.; Cheng, Y. M.; Shi, D.; Lv, X. J.; Yu, Q. J.; Wang, P. *Chem. Commun*. **2009**, *(16)*, 2198-2200.
81. Li, R. Z.; Liu, J. Y.; Cai, N.; Zhang, M.; Wang, P. *J. Phys. Chem. B* **2010**, *114*, 4461-4464.
82. Cai, N.; Moon, S. J.; Cevey-Ha, L.; Moehl, T.; Humphry-Baker, R.; Wang, P.; Zakeeruddin, S. M.; Gratzel, M. *Nano Lett.* **2011**, *11*, 1452-1456.
83. Bai, Y.; Zhang, J.; Zhou, D. F.; Wang, Y. H.; Zhang, M.; Wang, P. *J. Am. Chem. Soc.* **2011**, *133*, 11442-11445.
84. Tsao, H. N.; Burschka, J.; Yi, C. Y.; Kessler, F.; Nazeeruddin, M. K.; Grätzel, M. *Energ. Environ. Sci.* **2011**, *4*, 4921-4924.
85. Hagberg, D. P.; Yum, J. H.; Lee, H.; De Angelis, F.; Marinado, T.; Karlsson, K. M.; Humphry-Baker, R.; Sun, L. C.; Hagfeldt, A.; Grätzel, M.; Nazeeruddin, M. K. *J. Am. Chem. Soc.* **2008**, *130*, 6259-6266.
86. Ning, Z. J.; Zhang, Q.; Wu, W. J.; Pei, H. C.; Liu, B.; Tian, H. *J. Org. Chem.* **2008**, *73*, 3791-3797.
87. Thomas, K. R. J.; Hsu, Y. C.; Lin, J. T.; Lee, K. M.; Ho, K. C.; Lai, C. H.; Cheng, Y. M.; Chou, P. T. *Chem. Mater.* **2008**, *20*, 1830-1840.
88. Ito, S.; Miura, H.; Uchida, S.; Takata, M.; Sumioka, K.; Liska, P.; Comte, P.; Pechy, P.; Grätzel, M. *Chem. Commun.* **2008**, *(41)*, 5194-5196.
89. Shi, Y. R.; Hill, R. B. M.; Yum, J. H.; Dualeh, A.; Barlow, S.; Grätzel, M.; Marder, S. R.; Nazeeruddin, M. K. *Angew. Chem. Int. Edit.* **2011**, *50*, 6619-6621.

90. Delcamp, J. H.; Shi, Y. R.; Yum, J. H.; Sajoto, T.; Dell'Orto, E.; Barlow, S.; Nazeeruddin, M. K.; Marder, S. R.; Grätzel, M. *Chem. –Eur. J.* **2013**, *19*, 1819-1827.
91. Kim, S.; Lee, J. K.; Kang, S. O.; Ko, J.; Yum, J. H.; Fantacci, S.; De Angelis, F.; Di Censo, D.; Nazeeruddin, M. K.; Grätzel, M. *J. Am. Chem. Soc.* **2006**, *128*, 16701-16707.
92. Ko, S.; Choi, H.; Kang, M. S.; Hwang, H.; Ji, H.; Kim, J.; Ko, J.; Kang, Y. *J. Mater. Chem.* **2010**, *20*, 2391-2399.
93. Wu, Y. Z.; Marszalek, M.; Zakeeruddin, S. M.; Zhang, Q.; Tian, H.; Grätzel, M.; Zhu, W. H. *Energ. Environ. Sci.* **2012**, *5*, 8261-8272.
94. Qu, S. Y.; Qin, C. J.; Islam, A.; Wu, Y. Z.; Zhu, W. H.; Hua, J. L.; Tian, H.; Han, L. Y. *Chem. Commun.* **2012**, *48*, 6972-6974.
95. Qu. S.; Wu. W.; Hua. J.; Kong. C.; Long.Y.; Tian.H. *J. Phys. Chem. C* **2010**, *114*, 1343–1349.
96. Katono, M.; Bessho, T.; Wielopolski, M.; Marszalek, M.; Moser, J. E.; Humphry-Baker, R.; Zakeeruddin, S. M.; Gratzel, M. *J. Phys. Chem. C* **2012**, *116*, 16876-16884.
97. Kumar, C. V.; Raptis, D.; Koukaras, E. N.; Sygellou, L.; Lianos, P. *Org. Electron.* **2015**, *25*, 66-73.
98. Yella, A.; Mai, C.; Zakeeruddin, S. M.; Chang, S.; Hsieh, C.; Yeh, C.; Grätzel, M. *Angew. Chem., Int. Edit.* **2014**, *53*, 2973−2977.
99. Singh, S. P.; Gayathri, T. *Eur. J. Org. Chem.* **2014**, *22*, 4689-4707.
100. Pastore, M.; De Angelis, F. *ACS Nano* **2010**, *4*, 556-562.
101. Feng, S.; Li, Q. S.; Sun, P. P.; Niehaus, T. A.; Li, Z. S. *ACS Appl. Mater. Inter.* **2015**, *7*, 22504-22514.
102. Xie, Y. S.; Tang, Y. Y.; Wu, W. J.; Wang, Y. Q.; Liu, J. C.; Li, X.; Tian, H.; Zhu, W. H. *J. Am. Chem. Soc.* **2015**, *137*, 14055-14058.
103. Chen, D. Y.; Hsu, Y. Y.; Hsu, H. C.; Chen, B. S.; Lee, Y. T.; Fu, H.; Chung, M. W.; Liu, S. H.; Chen, H. C.; Chi, Y.; Chou, P. T. *Chem. Commun.* **2010**, *46*, 5256-5258.
104. Chen, B. S.; Chen, D. Y.; Chen, C. L.; Hsu, C. W.; Hsu, H. C.; Wu, K. L.; Liu, S. H.; Chou, P. T.; Chi, Y. *J. Mater. Chem*. **2011**, *21*, 1937-1945.
105. Wei, T. T.; Sun, X.; Li, X.; Agren, H.; Xie, Y. S. *ACS Appl. Mater. Inter*. **2015**, *7*, 21956-21965.

106. Zhu, W. H.; Wu, Y. Z.; Wang, S. T.; Li, W. Q.; Li, X.; Chen, J. A.; Wang, Z. S.; Tian, H. *Adv. Funct. Mater*. **2011**, *21*, 756-763.
107. Wu, Y. Z.; Zhang, X.; Li, W. Q.; Wang, Z. S.; Tian, H.; Zhu, W. H. *Adv. Energy Mater*. **2012**, *2*, 149-156.
108. Zhu, H. B.; Li, W. Q.; Wu, Y. Z.; Liu, B.; Zhu, S. Q.; Li, X.; Ågren, H.; Zhu, W. H. *ACS Sustainable Chem. Eng*. **2014**, *2*, 1026−1034.
109. Cui, Y.; Wu, Y. Z.; Lu, X. F.; Zhang, X.; Zhou, G.; Miapeh, F. B.; Zhu, W. H.; Wang, Z. S. *Chem. Mater*. *2011*, **23**, 4394−4401.
110. Yen, Y.; Lee, C.; Hsu, C.; Chou, H.; Chen, Y.; Lin, J. T. *Chem. -Asian J*. **2013**, *8*, 809−816.
111. Pei, K.; Wu, Y. Z.; Islam, A.; Zhu, S. Q.; Han, L. Y.; Geng, Z. Y.; Zhu, W. H. *J. Phys. Chem. C* **2014**, *118*, 16552−16561.
112. Pei, K.; Wu, Y. Z.; Li, H.; Geng, Z. Y.; Tian, H.; Zhu, W. H. *ACS Appl. Mater. Inter*. **2015**, *7*, 5296−5304.
113. Li, W. Q.; Wu, Y. Z.; Zhang, Q.; Tian, H.; Zhu, W. H. *ACS Appl. Mater. Inter*. **2012**, *4*, 1822−1830.
114. Qu, S. Y.; Wu, W. J.; Hua, J. L.; Kong, C.; Long, Y. T.; Tian, H. *J. Phys. Chem. C* **2010**, *114*, 1343−1349.
115. Patel, D. G. D.; Feng, F.; Ohnishi, Y.; Abboud, K. A.; Hirata, S.; Schanze, K. S.; Reynolds, J. R. *J. Am. Chem. Soc.* **2012**, *134*, 2599−2612.
116. Blouin, N.; Michaud, A.; Gendron, D.; Wakim, S.; Blair, E.; Neagu-Plesu, R.; Belletete, M.; Durocher, G.; Tao, Y.; Leclerc, M. *J. Am. Chem. Soc*. **2007**, *130*, 732−742.
117. Yen, Y.; Chou, H.; Chen, Y.; Hsu, C.; Lin, J. T. *J. Mater. Chem*. **2012**, *22*, 8734−8747.
118. Zhang, J.; Kan, Y.; Li, H.; Geng, Y.; Wu, Y.; Su, Z. *Dyes Pigm*. **2012**, *95*, 313−321.
119. Yan, C. C.; Ma, W. T.; Ren, Y. M.; Zhang, M.; Wang, P. *ACS Appl. Mater. Inter*. **2015**, *7*, 801−809.
120. Wu, J.; Lan, Z.; Lin, J.; Huang, M.; Huang, Y.; Fan, L.; Luo, G. *Chem. Rev*. **2015**, *115*, 2136-2173.
121. Kambe, S.; Nakade, S.; Kitamura, T.; Wada, Y.; Yanagida, S. *J. Phys. Chem. B* **2002**, *106*, 2967-2972.

122. Nakade, S.; Saito, Y.; Kubo, W.; Kanzaki, T.; Kitamura, T.; Wada, Y.; Yanagida, S. *Electrochem. Commun*. **2003**, *5*, 804-808.
123. Reddy, K. G.; Deepak, T. G.; Anjusree, G. S.; Thomas, S.; Vadukumpully, S.; Subramanian, K. R. V.; Nair, S. V.; Nair, A. S. *Phys. Chem. Chem. Phys*. **2014**, *16*, 6838-6858.
124. Hsieh, T.-L.; Chen, H.-W.; Kung, C.-W.; Wang, C.-C.; Vittal, R.; Ho, K.-C. *J. Mater. Chem*. **2012**, *22*, 5550-5559
125. Yun, S.; Hagfeldt, A.; Ma, T.; *Adv. Mater*. **2014**, *26*, 6210-6237.
126. Sapp, S. A.; Elliott, C. M.; Contado, C.; Caramori, S.; Bignozzi, C. A. *J. Am. Chem. Soc*. **2002**, *124*, 11215-11222.
127. Trancik, J. E.; Barton, S. C.; Hone, J. *Nano Lett*. **2008**, *8*, 982-987.
128. Marotta, G.; Kumar, C. P.; Lobello, M. G.; Cavazzini, F.; Salvatori, P.; Ganesh, K.; Nazeeruddin, M. K.; Chandrasekharam, M.; De Angelis, F. *Dalton T*. **2015**, *44*, 5369-5378.
129. Gudeika, D.; Grazulevicius, J. V.; Volyniuk, D.; Juska, G.; Jankauskas, V.; Sini, G. *J. Phys. Chem. C* **2015**, *119*, 28335-28346.
130. Yang, Y. S.; Do Kim, H.; Ryu, J. H.; Kim, K. K.; Park, S. S.; Ahn, K. S.; Kim, J. H. *Synthetic Met.* **2011**, *161*, 850-855.
131. Frisch, M. J.; Trucks, G. W.; Schlegel, H. B.; Scuseria, G. E.; Robb, M. A.; Cheeseman, J. R.; Scalmani, G.; Barone, V.; Mennucci, B.; Petersson, G. A.; *et al*. Gaussian 09, Revision D. 01; Gaussian, Inc.: Wallingford, CT, **2013**.
132. Phadke, S.; Du Pasquier, A.; Brinie, D. P. *J. Phys. Chem. C* **2011**, *115*, 18342-18347

CHAPTER-2

Influence of *m*-fluorine substituted phenylene spacer dyes in dye-sensitized solar cells

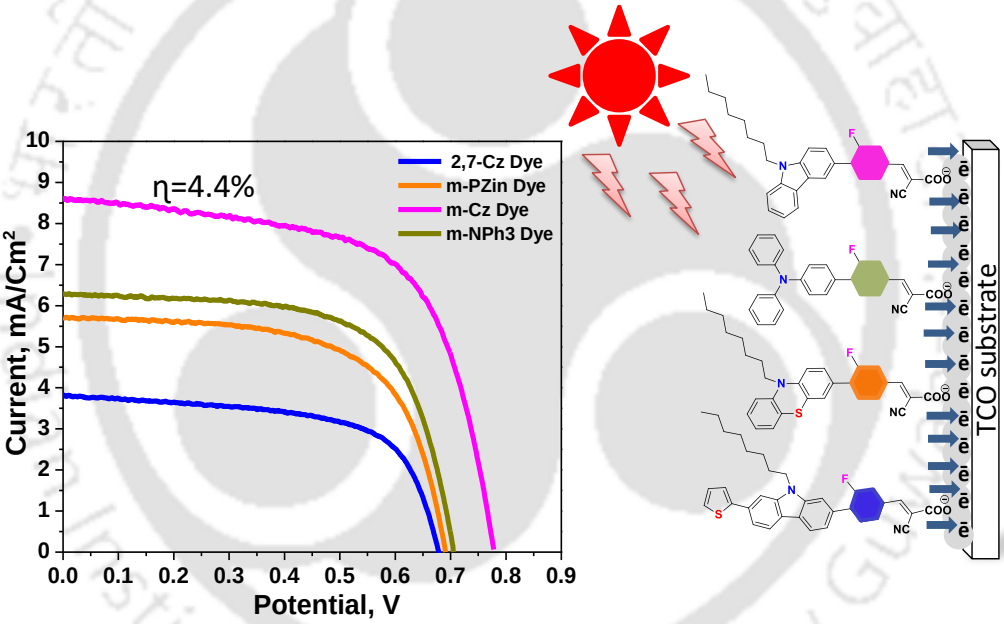

Org. Electron., **2016**, *39*, 371-379.

Abstract

A series of new organic dyes based on fluorine substituted phenyl moiety, used as a π-linker in various dyes, were designed and synthesized for dye sensitized solar cell (DSSC) application. These dyes share same anchoring group (Cyano acrylic acid) with different donors such as carbazole, thiopene substituted carbazole, triphenylamine and phenothiazine moieties. For effective electron flow, the dyes were incorporated with novel D-π-A framework. The optical, electrochemical, time-resolved photoluminescence (TRPL) spectra and photovoltaic properties of the dyes were carefully studied. The results reveal that without addition of any co-adsorbent, among all fluoro-phenyl spacer dyes, the Cz-dye showed highest open circuit voltage (V_{oc}) of 0.77 V, short circuit current (J_{sc}) of 8.65 mA.cm^{-2} and exhibited enhanced PCE value of 4.2 (± 0.2) %, due to deeper HOMO level of the dye and planarity of the backbone with better charge transfer occurring form D to A. The optimized calculation of geometries of all the dyes were ascertained by Density functional theory (DFT) using B3LYP/631G(d,p) basis set.

2.1 Introduction

Due to the growing demand for green energy, researchers have been attracted towards sustainable energy resources and thereby a great deal of attention on efficient solar cells development is under investigation. DSSCs with remarkable performance initially developed by Grätzel and O'Regan have generated immense hope in harvesting solar energy.[1] Ruthenium-based sensitizers (N3, N719 and black dye) are representative and most successful in DSSCs due to their long term stability and outstanding performances (PCE = >10% at AM 1.5 condition).[2,3] However, these dyes are inconvenient for commercial applications as they are very expensive, challenging synthesis, tedious purification, lower molar extinction coefficient and environmental issues. On the other hand, organic dyes (metal-free) are gradually attracting researchers attention due to the multiple advantages of relatively lower cost, high molar extinction coefficient, easy synthesis and excellent flexibility in structure modification, easily tunable functionalities and the photophysical as well as photochemical properties of dyes.[4-7] In the recent past, donor–π–acceptor (D-π-A) structures based on organic sensitizers were constructed to harvest solar energy efficiently. For efficient dye material development, different donor moieties such as carbazole, thiopene substituted carbazole, triphenylamine and phenothiazine are incorporated with cyanoacrylic acid as acceptor / anchoring group (Figure 2.1). Because these donors have good electron donating ability and cyanoacrylic acid has efficient electron injection ability, it is believed that both can improve the overall performances of the dye molecules. Spacer/π–linker in between the D and A also plays a crucial role for the superior performance of the cell.[8-11]

Recently, several groups have made tremendous efforts to design organic sensitizers to obtain higher PCE and have incorporated fluorine atom into the π-bridge of organic dyes. The advantage of fluorine atom containing π-bridge/spacer is to generally obtain the electron-withdrawing ability and drastically tune the dye molecule properties, like changing the energy levels, governed by charge distribution, charge transfer from D to A and improving the electron mobility. In addition, fluorine atom substituted π-bridge also has strong influence on the intra and inter molecular interaction through hydrogen-bonding and decrease the LUMO energy level of the dye.[12] Several organic dyes possessing fluorine substituents have been reported. Ortho substituted fluorine phenyl spacer with 4,4'-dialkyl Cyclopenta[2,1-b:3,4-b']dithiophene (CPDT) were reported for efficient DSSCs.[13] Similarly, few other reports appeared where comparative study with

and without fluorine substituted phenyl spacer for tuning electron flow in DSSC were studied, thereby explaining that ortho-fluorinated phenyl plays a very important role for improving the cell performance (especially improve open-circuit voltage).[14,15] On the contrary, ortho-fluorinated phenyl that does not play any significant role for improving the device performance has also been reported.[16]

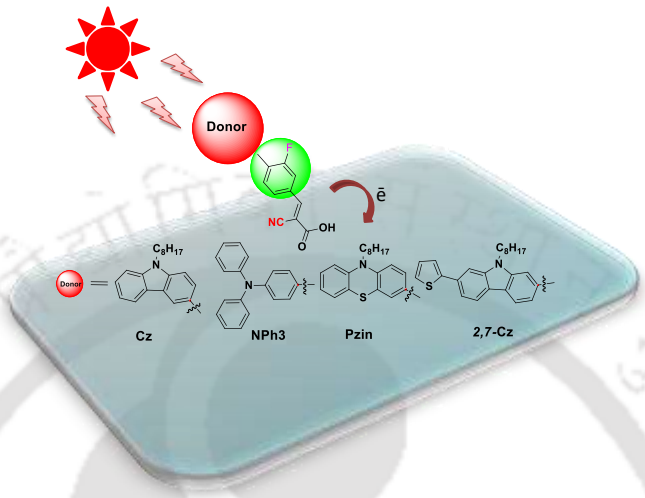

Figure 2.1 Chemical structure of organic dyes

For achieving optimized structure, meta-substituted fluoro phenyl (*m*-PhF) group was introduced as a π-linker, four different polycyclic aromatic moieties were employed as electron-donating groups and cyanoacrylic acid moiety acts as anchoring group (Scheme 2.1). Linear octyl alkyl chains were introduced at the donor site to suppress the dye molecule aggregation and avoid close contact to the electrolyte on TiO_2 surface. Fluorine substituted phenyl as a spacer containing dye improves the intra and inter molecular interactions, but without addition of any co-absorbent (CDCA or DCA) on TiO_2 layer highest efficiency (PCE) of 4.4% was achieved by using a simple Cz-dye. These novel dyes have high open-circuit voltage (0.778 V) and short-circuit current (8.65 mA/cm^2) and highest PCE of 4.2(± 0.2) %, corresponding to the simple D-π-A architecture of CZ-dye. This dye has a deep HOMO level, high molar absorption coefficient (13,126 $M^{-1}cm^{-1}$), planarity of backbone and long excitation life time value τ(ns) = 1.25, 2.80 (Table 2.1) compared to other dyes. Comparatively, 2,7-Cz dye (molar absorption coefficient= 19,752 $M^{-1}cm^{-1}$) has a similar architecture to Cz-dye, but due to blue shift in the absorption spectral values, weak charge transfer from D to A was observed which affected the cell efficiency with this dye. The NPh3 and Pzin dyes have lower efficiency values (η=2.9% and 2.6%) while triphenylamine had three dimensional and

phenothiazine two dimensional (Butterfly) structure. These novel dyes are characterized by NMR (^{1}H NMR, ^{13}C NMR, ^{19}F NMR), mass spectrometry (ESI) and the corresponding optical, electrochemical and photovoltaic properties are also presented and discussed elaborately.

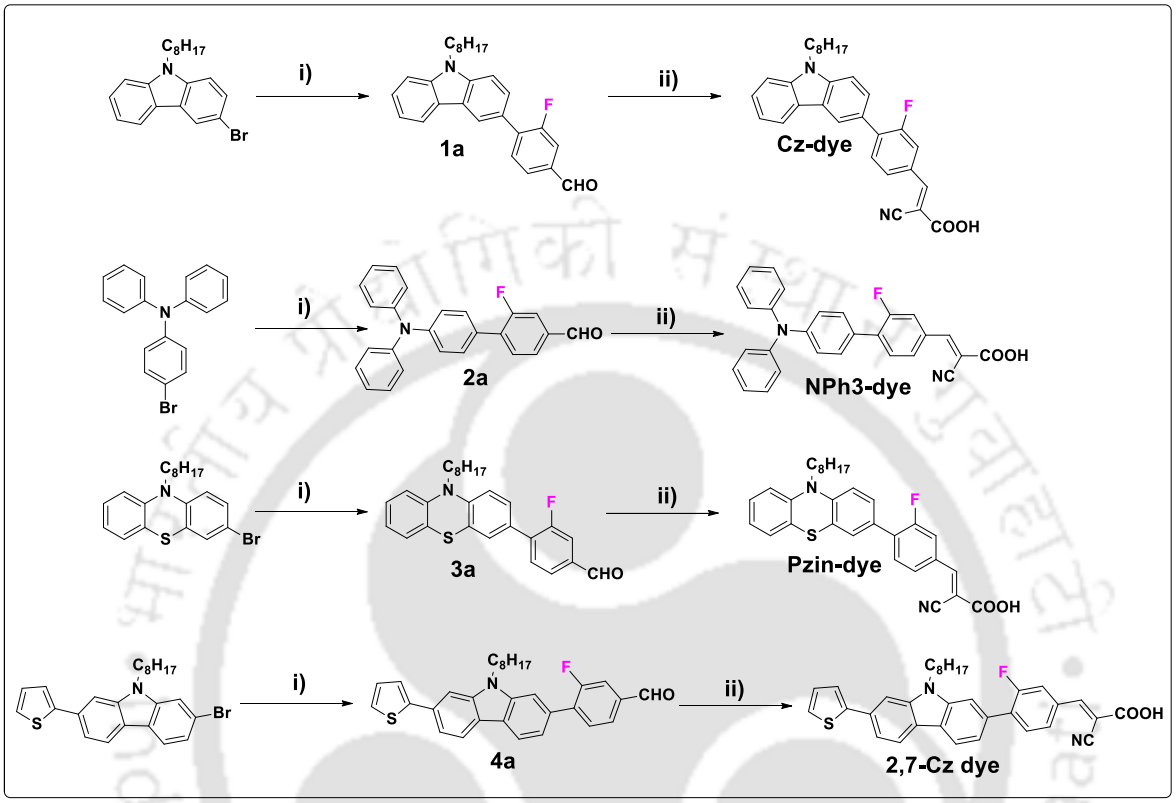

Scheme 2.1 Synthetic route of organic sensitizers (i) 2-fluoro-4-formyl phenyl boronic acid, THF:H_2O=2:1, Aliquat, K_2CO_3, $Pd(PPh_3)_4$, 85 °C, 12 h. (ii) Cyanoacetic acid, Piperidine, CH_3CN, 85 °C, 8 h.

2.2 Results and discussion

2.2.1. Optical properties

The absorption spectra of organic sensitizers in dichloromethane solution are shown in Fig. 2.2 (a) and corresponding data in Table 2.1. Each of these organic dyes exhibit two or three major absorption bands in the UV-Vis region in the range of 244-356 nm which are assigned to the localized aromatic π-π* transition of conjugated system and peaks in visible region are attributed to the intramolecular charge transfer (ICT) between the donor and acceptor. All dyes in 259-400 nm range exhibits two or three major peaks, due to the π-π* transition of conjugated system.

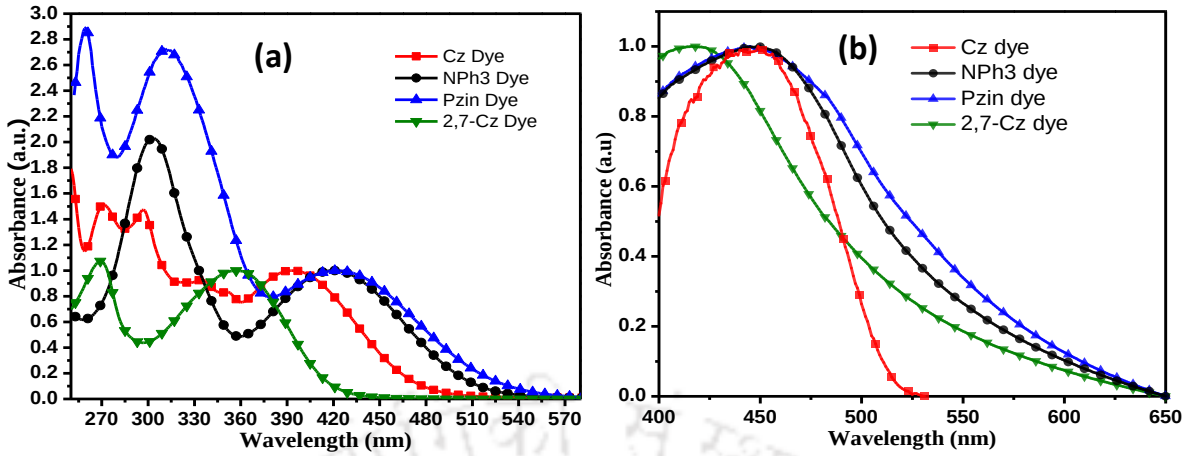

Figure 2.2 (a) Normalized UV-vis absorption spectra of organic dyes in dichloro methane solution. (b) Normalized UV-vis absorption of organic dyes absorbed on TiO_2 films.

The absorption maximum wavelength of Cz-dye, NPh3-dye, Pzin-dye and 2,7-Cz dyes were found to be 393, 420, 423 and 357 nm with the corresponding molar extinction coefficients 13126, 10656, 3850 and 19752 $M^{-1}cm^{-1}$ respectively. Incorporation of an electron rich conjugated heteroaromatic/aromatic segment is beneficial to increase the molar extinction coefficient that were observed in 2,7-Cz dye.[17] The absorption maxima of NPh3-dye are very similar to Pzin-dye (in visible region). Comparatively phenyl spacer dyes and fluorine substituted phenyl spacer dyes showed blue-shift in absorption spectra due to the meta-fluorine inductive effect.[14]

2,7-Cz dye showed remarkable blue shift in absorption spectra relative to other dyes, due to the poor charge transfer from donor to acceptor. Fig. 2.2(b) shows the broadened absorption spectra of dyes compared to those dyes in solution state due to corresponding dye absorbed on TiO_2 film.

2.2.2 Electrochemical characterization

The first oxidation potential peaks corresponding to HOMO level of the dyes were measured from cyclic voltammetry, which indicates the removal of an electron from donor moiety. HOMO energy levels were estimated by using E_{HOMO} = [-(E_{onset} - $E_{onset(FC/FC^+ vs. Ag/AgCl)}$) - 4.8] eV equation. LUMO levels were determined by the onset of the absorption spectra (E_g =1240/λ), E_g= E_{HOMO}-E_{LUMO}. Experimentally evaluated redox potentials of the dyes are shown in **Figure 2.3**, and its corresponding data summarized in Table 2.1. The order of donor strength matches the oxidation potential of dye series, Pzin-

dye < Cz-dye < 2,7 Cz-dye < NPh3 dye. Cz-dye and 2,7 Cz dyes HOMO levels are -5.55 and -5.63 eV, NPh3 and Pzin-dyes HOMO levels -6.02 and -5.35 eV.

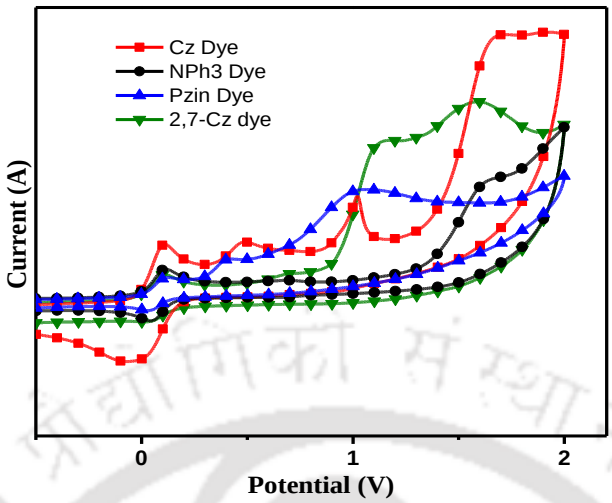

Figure 2.3 Cyclic voltammograms corresponding to the oxidation of organic dyes in 0.1M $TBAPF_6/CH_3CN$.

Table 2.1 Optical, electrochemical and lifetime characterization of dyes

Dye	Solution λ_{max} [nm][a)]	Film λ_{max} [nm][b)]	$\varepsilon_{max}/M^{-1}cm^{-1}$	HOMO [eV][c)]	LUMO [eV][c)]	τ(ns)
Cz-dye	393	526	13,126	-5.55	-3.20	1.25, 2.80
NPh3-dye	420	544	10,656	-6.02	-3.75	1.35, 3.35
Pzin-dye	423	561	3580	-5.35	-3.14	0.89, 2.71
2,7-Cz dye	357	522	19,752	-5.63	-3.26	2.66, 4.33

[a)]Maximum absorption wavelength of dyes in chloroform solution; [b)]Maximum absorption wavelength of dyes that were absorbed onto the TiO_2 films; [c)]onset potentials from CV measurements of thin films in 0.1 M Bu_4NPF_6 / CH_3CN solution, estimated from E_{HOMO} = -{(E^{on}_{ox}-$E_{1/2(ferrocene)}$) + 4.8} eV and E_{LUMO} = Estimated band gap by using onset of UV (TiO_2 film) – E_{HOMO}.

2.2.3 Theoretical molecular orbital calculation

The electronic distributions of the frontier molecular orbitals of D-π-A based dyes were studied using density functional theory (DFT) calculations at B3LYP/6-31G(d,p) level basis set and shown in Figure 2.4. The HOMO levels of the dyes are mainly located on the donor segment, having carbazole, triphenylamine, phenothiazine and thiophene substituted carbazole. In Cz-dye, the HOMO level is strongly diffused into carbazole unit as well as into fluoro phenyl spacer resulting in better intramolecular charge transfer (ICT) through the D to A therefore giving maximum PCE. However, in Pzin and NPh3

dyes the HOMO level is located on the phenothiazine and triphenyl amine and slightly diffused into fluoro phenyl π-bridge, but in the case of 2,7-Cz dye the HOMO level was strongly located on carbazole unit and not on the substituted thiophene unit (Figure 2.4).

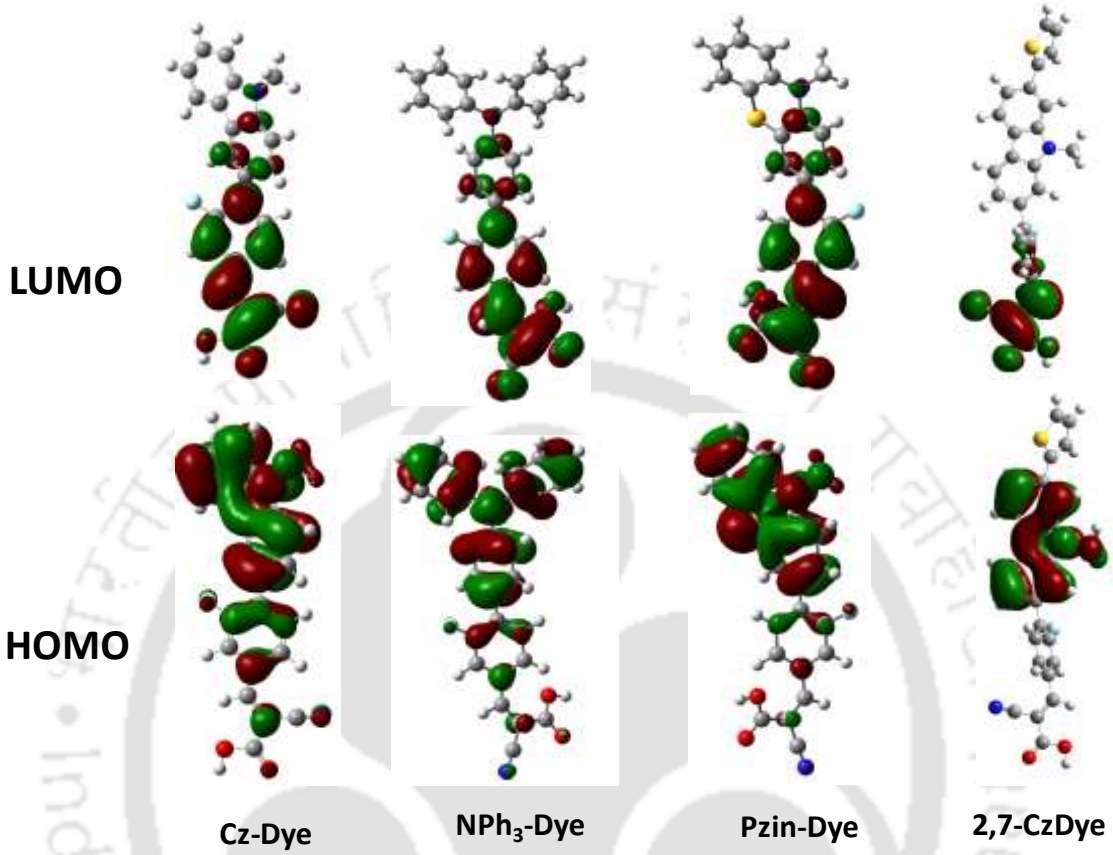

Figure 2.4 Electronic distributions of frontier molecular orbitals in various dye molecules.

The LUMO level electron density is mainly located on the cyanoacrylic acid acceptor and slightly diffused into fluorine substituted phenyl unit in Cz-dye, NPh3-dye and Pzin-dyes, but in 2,7-Cz dye the LUMO energy level was mainly located on the cyanoacrylic acid. In the fluoro phenyl spacer containing D-π-A conjugated dyes the HOMO and LUMO levels are well separated, which is an advantage for charge migration from donor to acceptor in photo excitation state of dyes.

2.2.4 Time-Resolved Photoluminescence (TRPL) studies:

Time-resolved photoluminescence (TRPL) measurements were performed on dye solution in chloroform applying a pulsed 375 nm excitation (Fig. 2.5) and corresponding data are shown in Table 2.1.

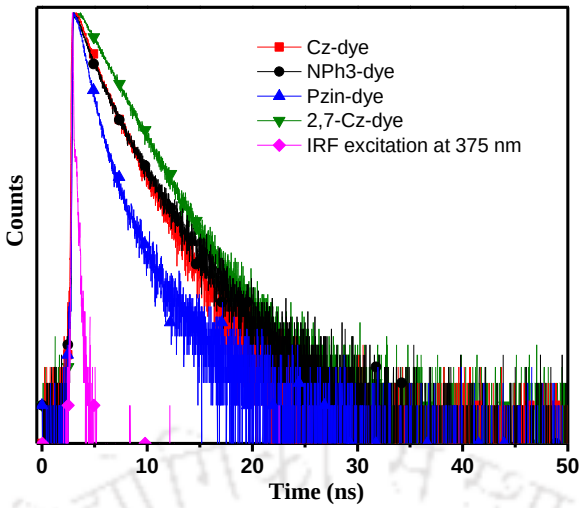

Figure 2.5 Time-resolved photoluminescence (TRPL) spectra of dyes recorded in $CHCl_3$ solution, with respect to their fitting curves at excitation wavelength of 375 nm.

2.3 Fabrication of photovoltaic devices

DSSCs were fabricated using sandwich type configuration of photoelectrode and counter electrode. Photoelectrode was made from the commercial TiO_2 nanocrystalline semiconductor (P25, Degussa, Germany). Thin film of the TiO_2 particles were deposited from the TiO_2 paste containing ethyl cellulose and α-terpineol. The electrodes were calcined in tubular furnace at 450 °C for 25 minute and then soaked into the 10 mM dye solution. Photoelectrode soaked in dye was kept in a glove box filled with argon with very low light level for 18 h. Counter electrodes were fabricated by spin coating of 50 mM H_2PtCl_6 solution in isopropanol onto predrilled FTO substrate followed by sintering at 450 ºC for 15 min. Dye coated photoelectrode and Pt counter electrode were sealed together using hot melt sealing tape upon application of heat. Electrolyte solution comprises of the 0.5M LiI, 0.05M I_2, 0.5M TBP, 0.5M GSCN in 3-methoxy propionitrile, inserted through the predrilled holes onto the counter electrode. Holes were sealed using epoxy adhesive and cover glass. DSSC were stored in dark at room temperature for 12 hours prior to measurements. Active area of the DSSC was set to 0.25 cm^2 and was maintained constant using the same screen for coating.

2.4 Photovoltaic performance of DSSCs

2.4.1 Photocurrent-voltage (*J-V*) properties

The parameters of DSSCs fabricated with these dyes, i.e., short circuit current (J_{sc}), open-circuit voltage (V_{oc}), fill factor (*FF*), and total power conversion efficiency (η), measured

under AM 1.5 solar light (100 mW cm^{-2}) are summarized in **Table 2.2,** and the photocurrent - voltage (*J-V*) plots are shown in **Figure 2.6**. The major structural factor is the effect of inserting a different donor group and substituent at the *m*-substituted fluro phenyl π-bridge in dye skeleton.

The presence of substituted or un-substituted carbazole moiety as a donor in dyes, Cz and 2,7-Cz exhibited two opposite effect i.e. thiophene free carbazole (Cz) showed good efficiency (4.2%) compared to thiophene substituted carbazole (2,7-Cz). The most apparent difference was observed in the J_{sc} values of 2,7-Cz (3.81mA cm^{-2}) and Cz (8.65 mA cm^{-2}). This observed difference might be due to loss in planarity upon introduction of thiophene which ultimately hampered the intra molecular charge transfer. Similar observation was noticed in the computation study (Figure 2.4). From the figure, it is revealed that Cz have most effective charge transfer compared to 2,7-Cz molecule, as a result of this electron injection in titania surface becomes slow. Moreover, effective charge transfer enhancing V_{oc} in case of Cz was due to two reasons; (i) shifting of Fermi energy level of titania to upper side and (ii) reduced dark current by decreasing the rate of charge recombination. Overall, these effects enhance the efficiency of the devices.

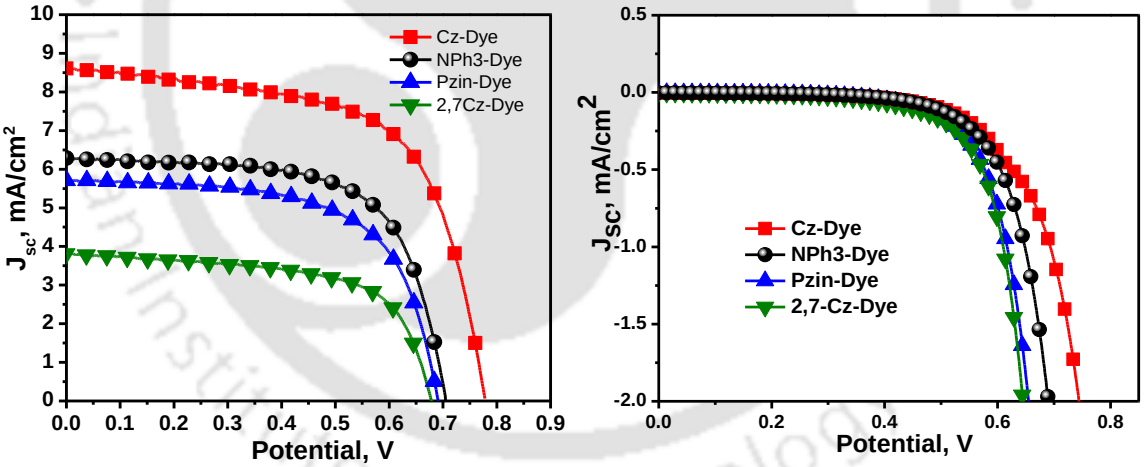

Figure 2.6 *J*−*V* curves of the DSSCs employing the dyes with donor moieties of carbazole (Cz), N-arylamine (NPh3), phenothiazine (Pzin) and thiophene substituted carbazole (2,7-Cz) with 1 sun illumination (left side) and without illumination (right side).

In addition, loss of planarity in 2,7-Cz reduces the dye loading as the molecule occupies larger surface area than un-substituted linear molecules. Cz with long octyl chain have been known to be capable of high efficiency probably due to the strong electron-donating ability of the carbazole unit when electrons transfer from the carbazole donor moiety to

the cyanoacrylic acceptor group.[18] The effect of donor moiety is explicitly displayed by the following order of efficiency, 2,7Cz < Pzin < NPh3 < Cz. The values of *FF* of all devices ranged from 0.60–0.65, yet did not show much difference among each other.

Table 2.2 Performances of the DSSCs Shown in Figure 2.6.

Abbreviation of Dye	Donor type	J_{sc}(mA/cm^2)	V_{oc} (V)	*FF*	η (%)
Cz	Carbazole	8.65 ± 0.10	0.778 ± 0.02	0.62 ± 0.05	4.2 ± 0.2
Pzin	Phenothiazine	5.74 ± 0.09	0.691 ± 0.01	0.65 ± 0.05	2.6 ± 0.1
NPh3	N-arylamine	6.25 ± 0.12	0.705± 0.01	0.65 ± 0.02	2.9 ± 0.1
2,7Cz	Thiophene substituted carbazole	3.81 ± 0.08	0.678± 0.02	0.60 ± 0.04	1.5 ± 0.1

2.4.2 Electrochemical Impedance Spectroscopy (EIS)

Electrochemical impedance spectroscopy (EIS) was employed to study the electron recombination in DSSCs based on these dyes under -0.65V bias applied voltages in the dark and analyzed by the software Z-view. The values of electron life time as well as capacitance values of various devices were calculated from impedance measurements, and are listed in Table 2.3. A typical Nyquist plot is shown in Figure 2.7, and the evaluated parameters are listed in Table 2.4.

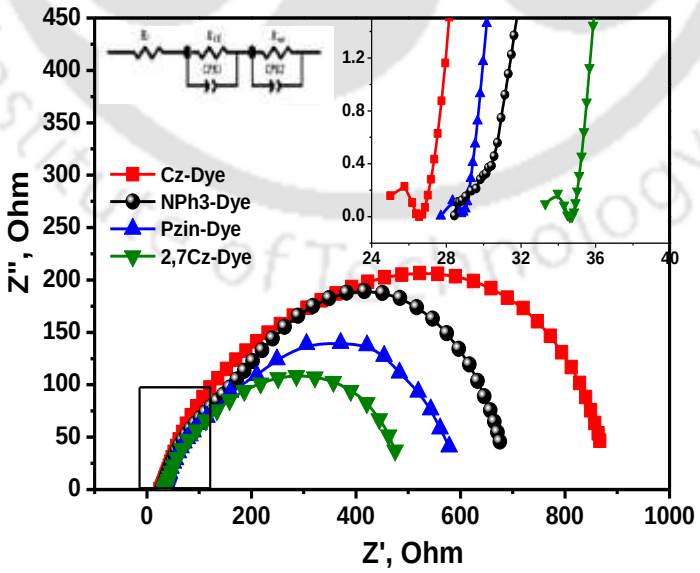

Figure 2.7 Electrochemical impedance measurements of DSSC based on dyes Cz, NPh3, Pzin and 2,7-Cz recorded in dark at -0.65 V DC bias. [(Inset shows magnification of the first arc of original curves and shows equivalent circuit model used for fitting).]

Table 2.3 The values of electron life time as well as capacitance values of various devices calculated from impedence measurements.

Dyes	τ_e (mS)[a]	C (F cm^{-2})
Cz-Dye	0.246	0.00147
NPh3-Dye	0.174	0.00153
Pzin-Dye	0.158	0.00158
2,7 Cz-Dye	0.112	0.00163

[a]Lifetime of injected electrons, estimated by fitting the middle-frequency of the Nyquist plots (ESI) into the expression $\tau_e = 1/(2\pi f)$, where f is the frequency.

The impedance response was fitted by using widely accepted transmission line model in order to estimate the electron transfer parameters such as charge transfer resistance (R_{pt}) and charge recombination resistance at the TiO_2 surface (R_{rec}) and can be deduced by fitting the curves using equivalent circuit. (Inset of Figure 2.7).

It should be noted that in this figure, the first arc which is attributed to the R_{pt} at Pt/electrolyte interface is a depressed semicircle so cannot be visible perfectly. Fitting of the second arc yields the R_{rec} and CPE-P (a component of CPE). Magnitude of CPE-P is associated with surface roughness and porosity of the photoelectrode. EIS results revealed that the electron transport property of Cz device is quite enhanced which has been reflected by middle arc (lower frequency shift) and give R_{rec} as higher than other devices. The radius of the middle semicircles increases in the order 2,7-Cz < NPh3 < Pzin < Cz. The R_{pt} at counter electrode is comparable in all the devices but a subtle difference has been observed in the R_{rec}. Recombination resistance of the Cz device is higher than that of remaining devices suggesting that the Cz device is performing with higher PCE. The electron lifetime can also be increased from 2,7-Cz to Cz, while a shift of low-frequency corresponds to a longer electron lifetime and it is subjected to larger value of V_{oc}. Here, Cz device shows higher electron lifetime in TiO_2 matrix with higher f_{max} in ESI spectra which is responsible for overall performance of the device.

Table 2.4 Charge transfer parameters of the dye sensitized solar cells

Dye	R_{pt} (Ohm)[a]	R_{rec} (Ohm) [a]	CPE-P [a]	f_{max} (Hz)	J_o(μA/cm^2)[b]
Cz-Dye	25.0	750	0.65	517	0.55
Pzin-Dye	27.7	320	0.64	397	0.43
NPh3- Dye	28.4	430	0.54	360	0.45
2,7 Cz- Dye	33.3	180	0.51	278	0.40

[a]*Values estimated by fitting nyquist plot* [b]*estimated from tafel polarization curves*

2.4.3 Electron lifetime (τ_e)

The open-circuit voltage decay technique was used as a method for monitoring the successive decay of photovoltaic V_{oc} after turning off the illumination in a steady state and the suppressed charge recombination at the FTO-electrolytes interface also can be confirmed by this technique. Figure 2.8 (a) shows V_{oc} decay curves of DSSCs with different donor moiety based photosensitizers and was recorded during relaxation from illuminated equilibrium state to the dark state. The decay response of different sensitizers based devices fabricated with I^-/I_3^- electrolyte, show that the recombination is significantly reduced by the TiO_2 photoanode. Figure 2.8 (b) shows electron life time (τ) calculated from the OCVD curves, from following equation.[19]

$$\tau_n = \frac{K_B T}{e}\left(\frac{dV_{oc}}{dt}\right)^{-1}$$

Where, '*e'* is the positive elementary charge, (dV_{oc}/dt) the derivation of V_{oc} and K_BT is the thermal energy. The photovoltaic decay rate is directly related to electron τ_e, because as the illumination of the photovoltaic devices at the OCP is interrupted, excess electrons are diminished through recombination. The Cz device showed much longer electron lifetimes compared to the other devices. These results conclude that donor moiety in dye and electrolyte significantly suppressed the recombination rate, resulting in the longer lifetime.

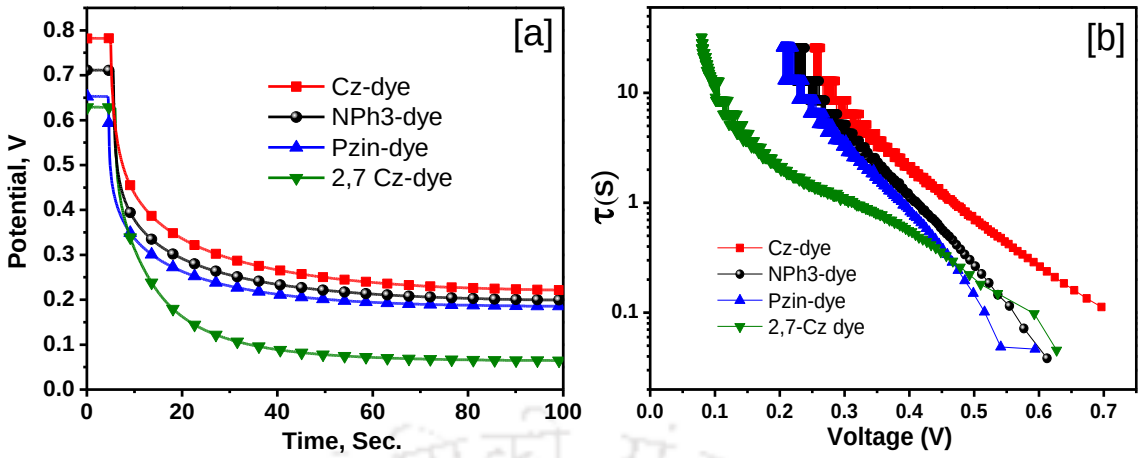

Figure 2.8 OCVD spectra for different donor moiety based sensitizers in DSSCs (a) decay curves after illumination is turned off, and (b) plots of photovoltaic devices electron lifetime (τ_n) as a function of open circuit voltage, $V_{oc.}$

2.4.4 Tafel Polarization

Tafel polarization technique is used to obtain better insight into the recombination dynamic of the solar cells there by getting exact idea about the increase in photo-voltage (Figure 2.9).[20] Tafel analysis provides information on the interfacial charge transfer of electrolyte redox couple on the photoanode electrode and cathodic/anodic reaction occurring at the semiconductor electrolyte interface which can be understood by Buttler-Volmer equation. Tafel measurement data was fitted using corr-view software and exchange current density was estimated for all devices.

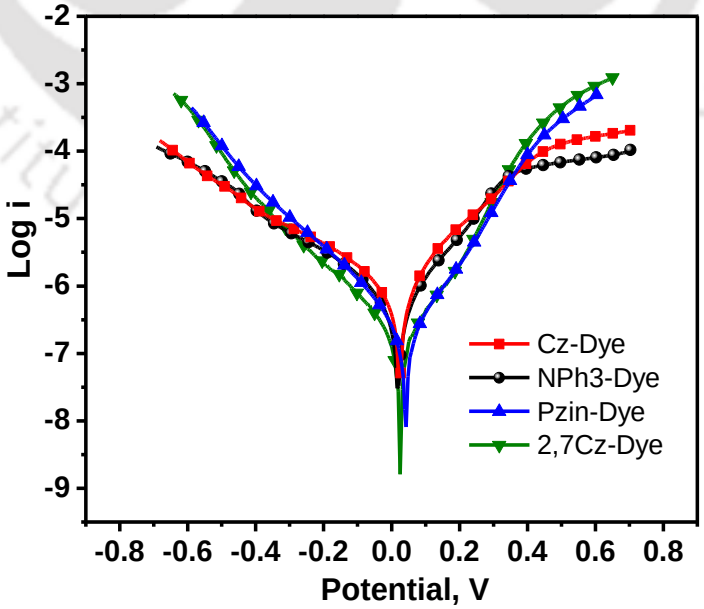

Figure 2.9 Tafel polarization curves for DSSC's showing the intensities of dark current (Tafel data were recorded in dark and fitted using corr-view software)

In Table 2.4, conclusion about the slope of this region represents the R_{pt}, which is inversely proportional to the exchange-current density (J_0). Thus, the steep slope of the Tafel zone has a large J_0 and a small R_{pt} value.

2.5 Experimental section

The chemical structures of dyes are shown in Figure 2.1 and the synthetic route is depicted in **scheme 2.1**. All reactions were performed under argon atmosphere and appropriate solvents were distilled from drying agents prior to use. The starting materials of dyes 3-bromo-9-octyl-9*H*-carbazole, 4-bromo-*N*,*N*-diphenylaniline, 3-bromo-10-octyl-10*H*-phenothiazine, 2-bromo-9-octyl-7-(thiophen-2-yl)-9*H*-carbazole were prepared according to the literature. [21-23]

2.5.1 General synthetic procedure of compound "1a-4a"

In a clean 50 mL round bottom flask, bromo containing starting material (0.2 mmol) and 2-Fluoro 4-formylphenyl boronic acid (0.25 mmol) was dissolved in THF (12 mL), 2M K_2CO_3 aqueous solution (6 mL) and degassed. Finally, $Pd(PPh_3)_4$ (20 mol%) catalyst was added to the reaction mixture under inert atmosphere. Then the reaction mixture was refluxed overnight. The mixture was cooled to RT, filtered through celite and extracted with chloroform solution. The extracted solvent was washed with brine solution thrice and dried over $MgSO_4$. The liquid residue was purified by column chromatography (silica gel, ethyl acetate-hexane 1:1 as eluent).

2.5.2 General synthetic procedure of organic sensitizers

In a clean 50 mL round bottom flask, the mixture of compound '1a-4a' (0.2 mmol) and cyanoacetic acid (0.3 mmol) were dissolved in acetonitrile and chloroform (1:1) solution. Finally piperidine (0.02 mmol) was added to the solution and refluxed for 10 h. After cooling, the solution was removed by rotavapor under reduced pressure. Extracted compound was washed with chloroform and 0.1 M aqueous solution of HCl. Then the organic layer was dried over $MgSO_4$. The solid was finally washed with hexane and 3% ethyl acetate in hexane to get a pure compound.

3-fluoro-4-(9-octyl-9H-carbazol-3-yl) benzaldehyde (1a)

Yield= 65%, ^{1}H NMR (400 MHz, $CDCl_3$): δ (ppm) 10.01 (s, 1H), 8.33 (s, 1H), 8.14 (d, 1H), 7.74 (d, 2H), 7.72-7.68 (m, 2H), 7.49-7.47 (m, 2H), 7.25 (d, 1H), 4.31 (t, 2H), 1.90 (t, 2H), 1.43-1.24 (m, 10H), 0.85 (t, 3H). ^{13}C NMR (100 MHz, $CDCl_3$): δ (ppm) 190.90, 161.11, 159.46, 141.01, 140.69,136.60, 136.51, 131.74, 131.72, 126.89, 126.86, 126.31, 125.13123.35, 122.97, 121.40, 120.68, 119.47, 116.67, 116.51, 109.19, 109.02,43.43,

31.98, 29.91, 29.56, 29.37, 29.18, 27.50, 22.80, 14.26. ^{19}F NMR (282 MHz, $CDCl_3$): δ (ppm) -116.39. HRMS (ESI) m/z: $[M+H]^+$ calcd for $C_{27}H_{29}FNO$ 402.2233, found 402.2231.

4'-(diphenylamino)-2-fluoro-[1,1'-biphenyl]-4-carbaldehyde (2a)

Yield= 66%, ^{1}H NMR (400 MHz, $CDCl_3$): δ (ppm) 9.99 (s, 1H), 7.72 (d, 1H), 7.66-7.61 (m, 2H), 7.48 (d, 2H), 7.30 (t, 4H), 7.17 (d, 4H), 7.15 (d, 2H), 7.08 (t, 2H). ^{13}C NMR (100 MHz, $CDCl_3$): δ (ppm) 190.73, 161.43, 158.93, 148.65, 147.42, 136.65, 136.59, 135.16, 135.03, 131.02, 130.98, 130.06, 130.03, 129.62, 125.24, 123.80, 122.57, 116.71, 116.47. ^{19}F NMR (282 MHz, $CDCl_3$): δ (ppm) -116.24. HRMS (ESI) m/z: $[M+H]^+$ calcd for $C_{25}H_{19}FNO$ 368.1451, found 368.1451.

3-fluoro-4-(10-octyl-10H-phenothiazin-3-yl) benzaldehyde (3a)

Yield= 65%, ^{1}H NMR (400 MHz, $CDCl_3$): δ (ppm) 9.97 (s, 1H), 7.69 (d, 1H), 7.63 (d, 1H), 7.56 (t, 1H), 7.43 (d, 1H), 7.35 (s, 1H), 7.18-7.12 (m, 2H), 6.94-6.91 (m, 2H), 6.88 (t, 1H), 3.87 (t, 2H), 1.83 (t, 2H), 1.47-1.27 (br m, 10H), 0.88 (t, 3H). ^{13}C NMR (100 MHz, $CDCl_3$): δ (ppm) 190.70, 160.87, 159.20, 144.95, 144.76, 130.83, 128.28, 128.26, 127.78, 127.65, 127.56, 126.27, 124.29, 122.89, 116.61, 116.45, 115.67, 115.33, 47.71, 31.90,29.91, 29.37, 27.10, 26.98, 22.79, 14.27. ^{19}F NMR (282 MHz, $CDCl_3$): δ (ppm) HRMS -115.64. (ESI) m/z: $[M+H]^+$ calcd for $C_{27}H_{29}FNOS$ 434.1954, found 434.1956.

3-fluoro-4-(9-octyl-7-(thiophen-2-yl)-9H-carbazol-2-yl) benzaldehyde (4a)

Yield= 60%, ^{1}H NMR (400 MHz, $CDCl_3$): δ (ppm) 10.04 (s, 1H), 8.16 (d, 1H), 8.11 (d, 1H), 7.77 (t, 2H), 7.73 (d, 1H), 7.62(m, 2H), 7.55 (d, 2H), 7.45-7.43 (m, 3H), 7.40-7.38(m, 3H), 7.37-7.35 (m, 2H), 7.34-7.33 (d, 2H), 7.15-7.10 (m, 3H), 4.36 (t, 2H), 1.92 (t, 2H), 1.63-1.26 (m, 10H), 0.89-0.849 (m, 3H). ^{13}C NMR (100 MHz, $CDCl_3$): δ (ppm) 190.96, 163.20, 161.59,145.65, 137.34, 132.90, 131.96, 130.22, 129.29, 128.49, 128.32, 126.29, 125.35, 124.85, 123.46, 121.42, 119.36, 116.54, 109.89, 106.26, 102.79, 84.01,43.30, 32.02, 31.64, 29.91, 29.37, 27.00, 22.80, 13.76. ^{19}F NMR (282 MHz, $CDCl_3$): δ (ppm) -112.89. HRMS (ESI) m/z: $[M+H]^+$ calcd for $C_{31}H_{31}FNOS$ 484.2110, found 484.2107.

(*E*)-2-cyano-3-(3-fluoro-4-(9-octyl-9H-carbazol-3-yl) phenyl) acrylic acid (Cz dye):

Yield= 62%, ^{1}H NMR (400 MHz, $CDCl_3$): δ (ppm) 7.62 (s, 2H), 7.45 (s, 2H), 7.16 (d, 2H), 7.00 (m, 2H), 6.91(s, 1H), 6.73 (m, 1H), 6.43 (s, 1H), 3.46 (t, 2H), 1.29-0.79 (m, 15H). ^{13}C NMR (100 MHz, $CDCl_3$): δ (ppm) 160.14, 158.45, 154.56, 154.47, 152.12, 140.43, 139.93, 133.62, 132.64, 130.94, 126.75, 126.11, 125.35, 124.81, 122.90, 122.59, 121.08, 120.80, 120.58, 118.83, 108.18,42.80, 32.01, 29.90, 29.45, 28.74, 27.12, 22.63,

13.99. ^{19}F NMR (282 MHz, $CDCl_3$): δ (ppm) -115.96. HRMS (ESI) m/z: $[M+H]^+$ calcd for $C_{30}H_{30}FN_2O_2$ 469.2291, found 469.2269.

(*E*)-2-cyano-3-(4'-(diphenylamino)-2-fluoro-[1,1'-biphenyl]-4-yl) acrylic acid (NPh3 dye):

Yield= 71%, ^{1}H NMR (400MHz, $CDCl_3$): δ (ppm) 7.10-6.80 (br, m, 15H). ^{13}C NMR (100 MHz, $CDCl_3$): δ (ppm) 160.02, 158.35, 148.06, 147.29, 139.46, 132.58, 131.71, 130.26, 129.78, 129.50, 127.31, 125.14, 123.56, 122.10, 117.90, 117.79, 114.28. ^{19}F NMR (400MHz, $CDCl_3$): δ (ppm) -115.95. HRMS (ESI) m/z: $[M+H]^+$ calcd for $C_{28}H_{20}FN_2O_2$ 435.1509, found 435.1524.

(*E*)-2-cyano-3-(3-fluoro-4-(10-octyl-10H-phenothiazin-3-yl) phenyl) acrylic acid (Pzin dye): Yield= 75%, ^{1}H NMR (400MHz, $CDCl_3$): δ (ppm) 8.25 (s, 1H), 7.82 (d, 2H), 7.76-7.72 (m, 1H), 7.53 (d, 1H), 7.41 (d, 2H), 7.16-7.12 (m, 2H), 6.91-6.86 (m, 4H), 3.86 (t, 2H), 1.82 (t, 2H), 1.42-1.26 (br m, 10H), 0.88 (t, 3H). ^{13}C NMR (100 MHz, $CDCl_3$): δ (ppm) 163.70, 162.02, 160.47, 158.91, 154.99, 154.60, 139.39, 133.54, 133.27, 131.40, 131.12, 130.76, 128.31, 128.03, 127.57, 127.51, 124.16, 122.91, 120.82, 118.70, 118.53, 117.63, 117.48, 115.67, 115.36, 115.05, 114.24, 102.81, 32.10, 29.87, 29.37, 29.33, 27.01, 22.72, 14.29. ^{19}F NMR (282 MHz, $CDCl_3$): δ (ppm) -115.02. HRMS (ESI) m/z: $[M+2]^+$ calcd for $C_{30}H_{30}FN_2O_2S$ 501.2012, found 501.2015.

(*E*)-2-cyano-3-(3-fluoro-4-(9-octyl-7-(thiophen-2-yl)-9H-carbazol-2-yl)phenyl) acrylic acid (2,7-Cz dye):

Yield= 73%, ^{1}H NMR (400 MHz, $CDCl_3$): δ (ppm) 8.12-8.04 (m, 3H), 7.80 (d, 2H), 7.62 (s, 2H), 7.58 (br d, 3H), 7.49 (t, 2H), 7.41(d, 2H), 7.31 (t, 2H), 7.12 (d, 1H), 4.30 (t, 2H), 2.04 (d, 2H) 1.88-1.68 (m, 4H), 1.39-1.23 (m, 6H), 0.84-0.82 (m, 3H). ^{13}C NMR (100 MHz, $CDCl_3$): δ (ppm) 171.32, 160.69, 159.18, 148.84, 145.72, 141.60, 141.20, 133.61, 133.12, 132.61, 132.18, 131.62, 128.75, 128.25, 126.61, 124.86, 123.33, 122.05, 121.08, 120.53, 120.28, 118.90, 118.04, 111.31, 109.60, 106.21, 60.39,53.72, 44.60, 32.24, 29.12, 27.33, 22.75, 13.91. ^{19}F NMR (282 MHz, $CDCl_3$): δ (ppm) -116.25. HRMS (ESI) m/z: $[M+Na]^+$ calcd for $C_{34}H_{30}FN_2NaO_2S$ 572.1910, found 572.2277.

2.6 Summary

In summary, fluorine substituted phenyl moiety, used as a π-linker in various dyes, were designed and synthesized for dye sensitized solar cell (DSSC) application. These dyes have different donors such as carbazole, thiopene substituted carbazole, triphenylamines

and phenothiazine moieties and same anchoring group (cyanoacrylic acid). This difference obviously affected their photoelectric and optical properties. We observed that in the presence of substituted or un-substituted carbazole moiety as a donor in dyes, Cz and 2,7-Cz exhibited two opposite effects i.e. thiophene free carbazole (Cz) shows good efficiency (4.2 %) compared to thiophene substituted carbazole (2,7-Cz). Due to the loss of planarity the dyes occupy larger surface area than un-substituted linear molecules resulting in weak charge transfer from donor to acceptor. The order of efficiency and charge transfer was 2,7-Cz < Pzin < NPh3 < Cz and were concluded from photocurrent - voltage (*J-V*) plots, electrochemical impedance spectroscopy (EIS) study, Tafel polarization technique, electron lifetime (τ_e) and DFT calculation. These fluorine substituted phenyl spacer dyes improve the intra and inter molecular interactions, without addition of any co-absorbent on TiO_2 layer to provide highest PCE of 4.2% using this very simple Cz-dye and presents opportunities to be applicable further in solid state DSSCs.

2.7 References

1. Oregan, B.; Gratzel, M. *Nature* **1991**, *353*, 737-740.
2. Gratzel, M. *J. Photoch. Photobio. A* **2004**, *168*, 235-235.
3. Nazeeruddin, M. K.; Baranoff, E.; Gratzel, M. *Sol. Energy* **2011**, *85*, 1172-1178.
4. Ahmad, S.; Guillen, E.; Kavan, L.; Gratzel, M.; Nazeeruddin, M. K. *Energ. Environ. Sci.* **2013**, *6*, 3439-3466.
5. Yao, Z. Y.; Zhang, M.; Wu, H.; Yang, L.; Li, R. Z.; Wang, P. *J. Am. Chem. Soc.* **2015**, *137*, 3799-3802.
6. Mishra, A.; Fischer, M. K. R.; Bauerle, P. *Angew. Chem. Int. Ed.* **2009**, *48*, 2474-2499.
7. Joly, D.; Pelleja, L.; Narbey, S.; Oswald, F.; Meyer, T.; Kervella, Y.; Maldivi, P.; Clifford, J. N.; Palomares, E.; Demadrille, R. *Energ. Environ. Sci.* **2015**, *8*, 2010-2018.
8. Soni, S. S.; Fadadu, K. B.; Vaghasiya, J. V.; Solanki, B. G.; Sonigara, K. K.; Singh, A.; Das, D.; Iyer, P. K. *J. Mater. Chem. A* **2015**, *3*, 21664-21671.
9. Kang, X. W.; Zhang, J. X.; O'Neil, D.; Rojas, A. J.; Chen, W.; Szymanski, P.; Marder, S. R.; El-Sayed, M. A. *Chem. Mater.* **2014**, *26*, 4486-4493.

10. Zhu, H. B.; Liu, B.; Liu, J. C.; Zhang, W. W.; Zhu, W. H. *J. Mater. Chem. C* **2015**, *3*, 6882-6890.
11. Koumura, N.; Wang, Z. S.; Mori, S.; Miyashita, M.; Suzuki, E.; Hara, K. *J. Am. Chem. Soc*. **2006**, *128*, 14256-14257.
12. Cho, N.; Han, J.; Song, K.; Kang, M. S.; Jun, M. J.; Kang, Y.; Ko, J. *Tetrahedron* **2014**, *70*, 427-433.
13. Chen, D. Y.; Hsu, Y. Y.; Hsu, H. C.; Chen, B. S.; Lee, Y. T.; Fu, H.; Chung, M. W.; Liu, S. H.; Chen, H. C.; Chi, Y.; Chou, P. T. *Chem. Commun*. **2010**, *46*, 5256-5258.
14. Chen, B. S.; Chen, D. Y.; Chen, C. L.; Hsu, C. W.; Hsu, H. C.; Wu, K. L.; Liu, S. H.; Chou, P. T.; Chi, Y. *J. Mater. Chem.* **2011**, *21*, 1937-1945.
15. Scrascia, A.; De Marco, L.; Laricchia, S.; Picca, R. A.; Carlucci, C.; Fabiano, E.; Capodilupo, A. L.; Della Sala, F.; Gigli, G.; Ciccarella, G. *J. Mater. Chem. A* **2013**, *1*, 11909-11921.
16. Tamilavan, V.; Kim, A. Y.; Kim, H. B.; Kang, M.; Hyun, M. H. *Tetrahedron* **2014**, *70*, 371-379.
17. Venkateswararao, A.; Thomas, K. R. J.; Lee, C. P.; Ho, K. C. *Asian J. Org. Chem.* **2015**, *4*, 69-80.
18. Fadadu, K. B.; Soni, S. S. *Electrochim. Acta*. **2013**, *88*, 270-277.
19. Zaban, A.; Greenshtein, M.; Bisquert, J. *Chemphyschem*. **2003**, *4*, 859-864.
20. Cameron, P. J.; Peter, L. M.; Hore, S., *J. Phys. Chem. B* **2005**, *109*, 930-936.
21. Wu, J. F.; Lai, G. Q.; Li, Z. F.; Lu, Y. X.; Leng, T. H.; Shen, Y. J.; Wang, C. Y. *Dyes Pigments* **2016**, *124*, 268-276.
22. Kato, S.; Shimizu, S.; Kobayashi, A.; Yoshihara, T.; Tobita, S.; Nakamura, Y. *J. Org. Chem*. **2014**, *79*, 618-629.
23. Dincalp, H.; Saltan, G. M.; Aykut, D.; Zafer, C. *Spectrochim. Acta A* **2015**, *149*, 157-165.

Appendix

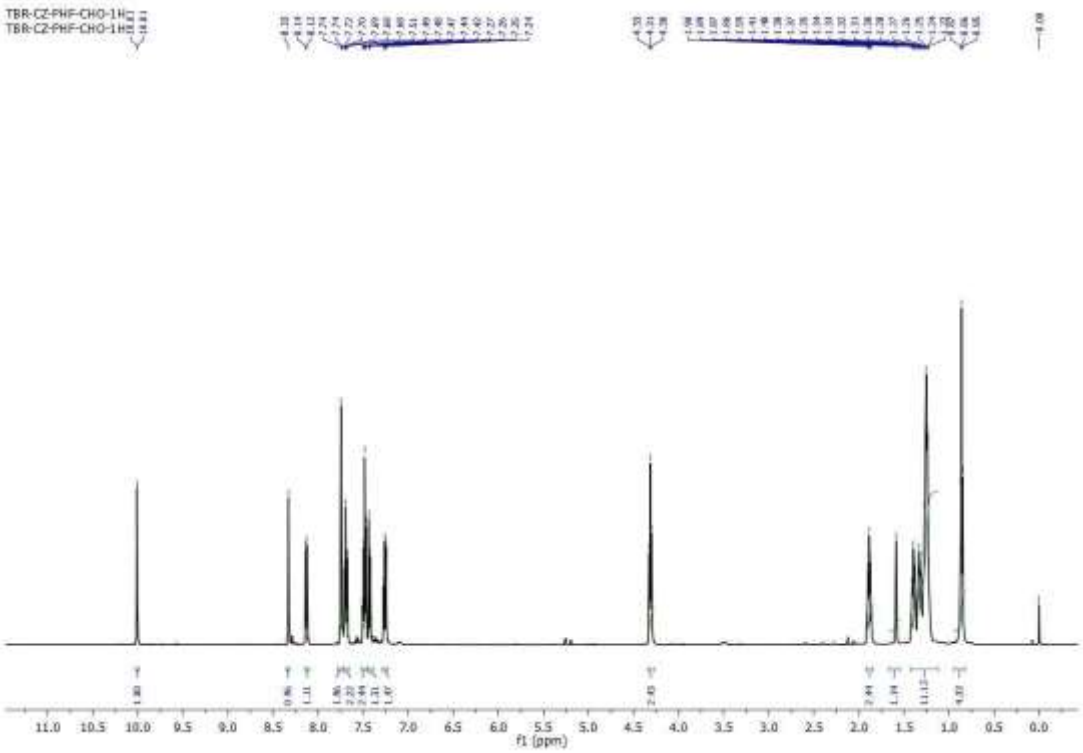

^{1}H NMR spectrum of 3-fluoro-4-(9-octyl-9*H*-carbazol-3-yl) benzaldehyde (1a) in $CDCl_3$.

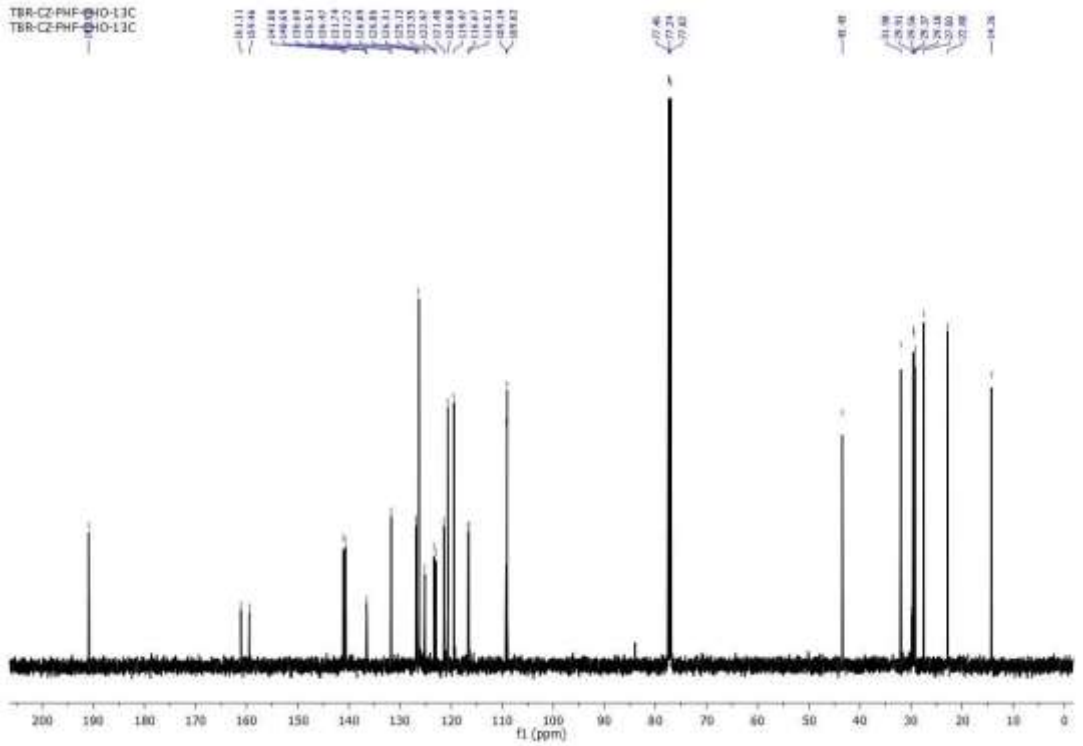

^{13}C NMR spectrum of 3-fluoro-4-(9-octyl-9*H*-carbazol-3-yl) benzaldehyde (1a) in $CDCl_3$.

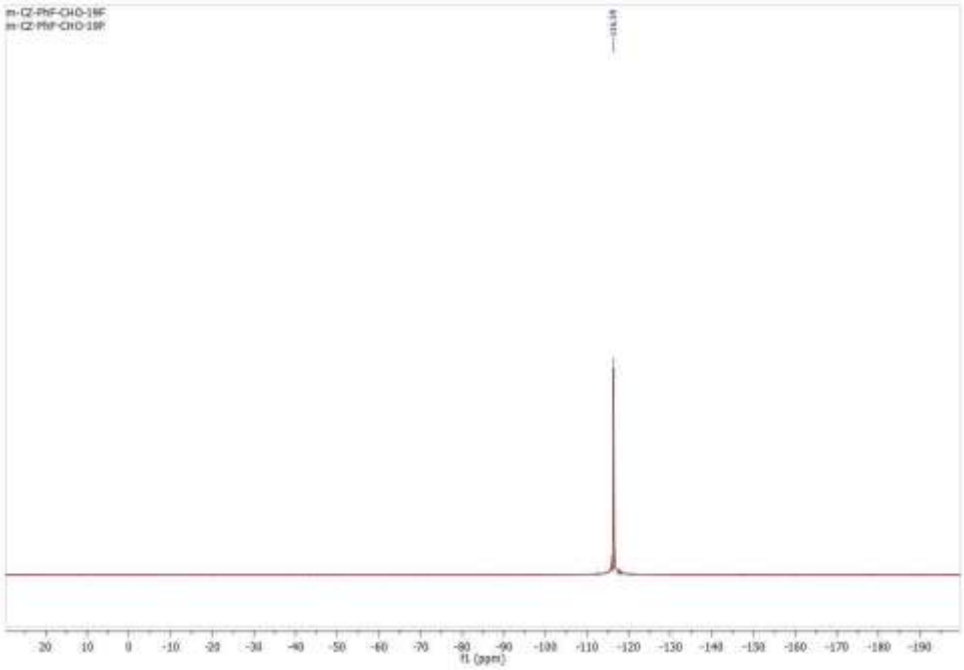

^{19}F NMR spectrum of 3-fluoro-4-(9-octyl-9*H*-carbazol-3-yl) benzaldehyde (1a) in $CDCl_3$.

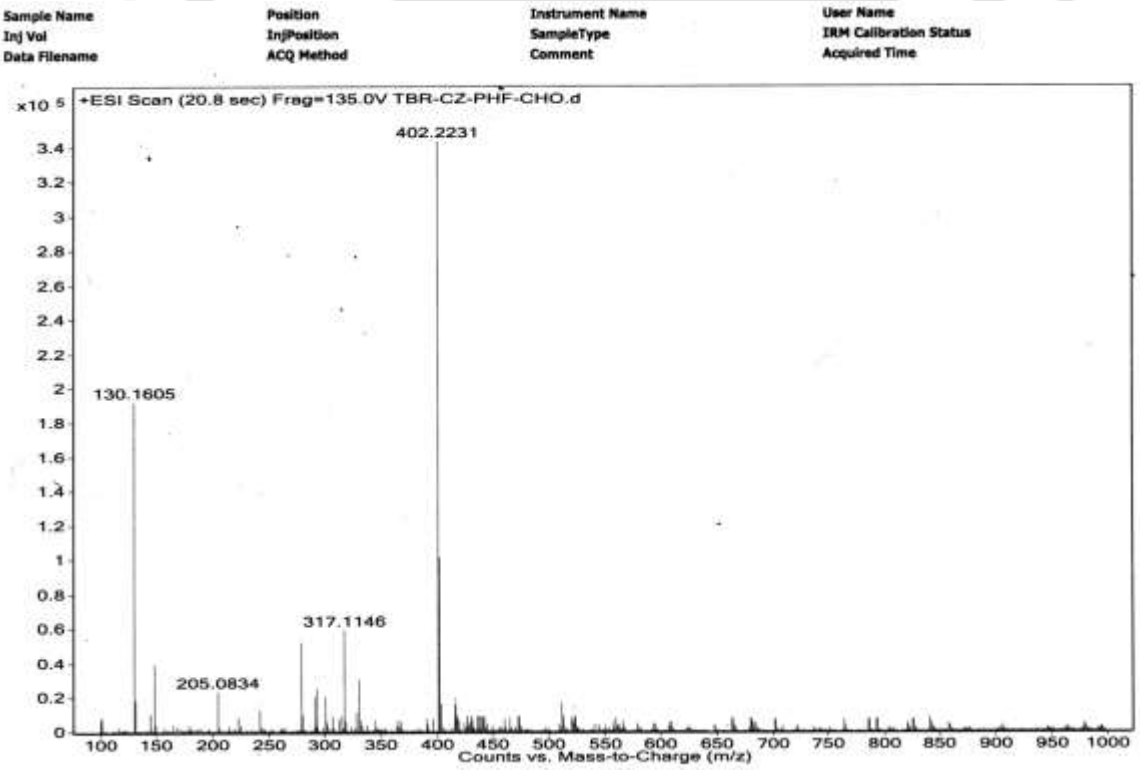

HRMS (ESI) spectrum of 3-fluoro-4-(9-octyl-9*H*-carbazol-3-yl) benzaldehyde (1a).

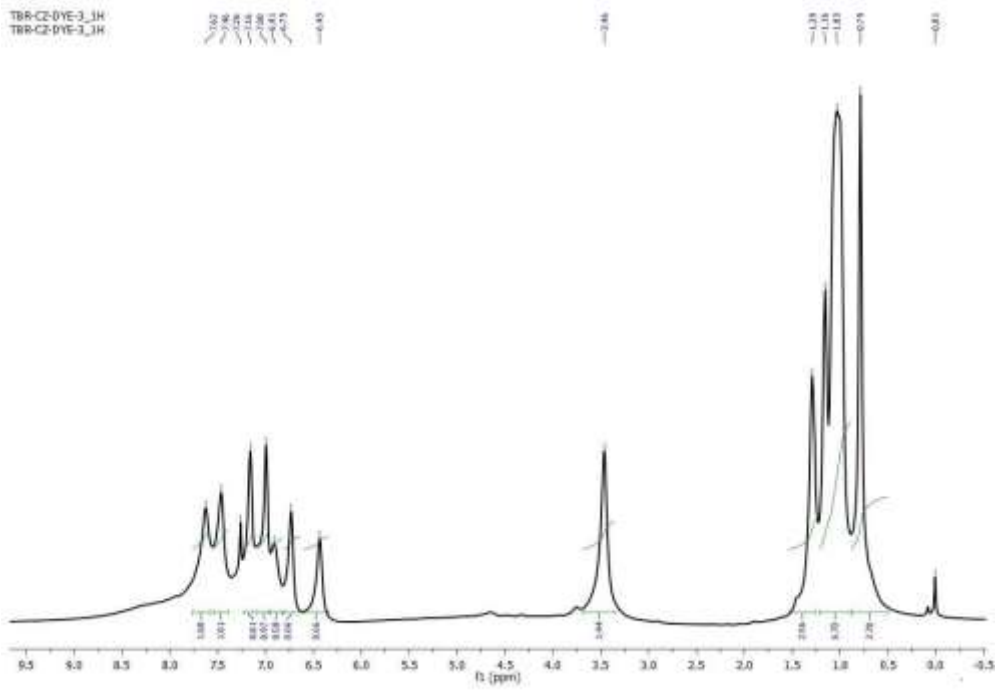

^{1}H NMR spectrum of (*E*)-2-cyano-3-(3-fluoro-4-(9-octyl-9H-carbazol-3-yl) phenyl) acrylic acid (Cz-dye) in $CDCl_3$.

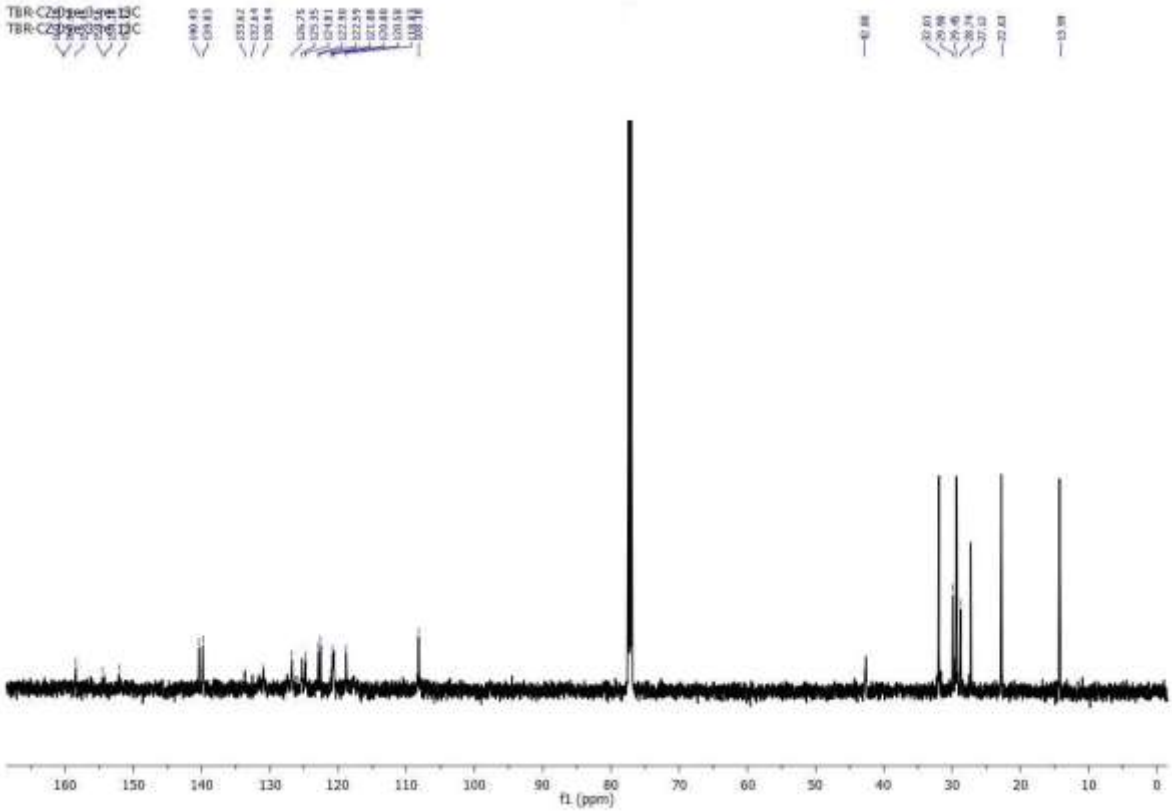

^{13}C NMR spectrum of (*E*)-2-cyano-3-(3-fluoro-4-(9-octyl-9H-carbazol-3-yl) phenyl) acrylic acid (Cz-dye) in $CDCl_3$.

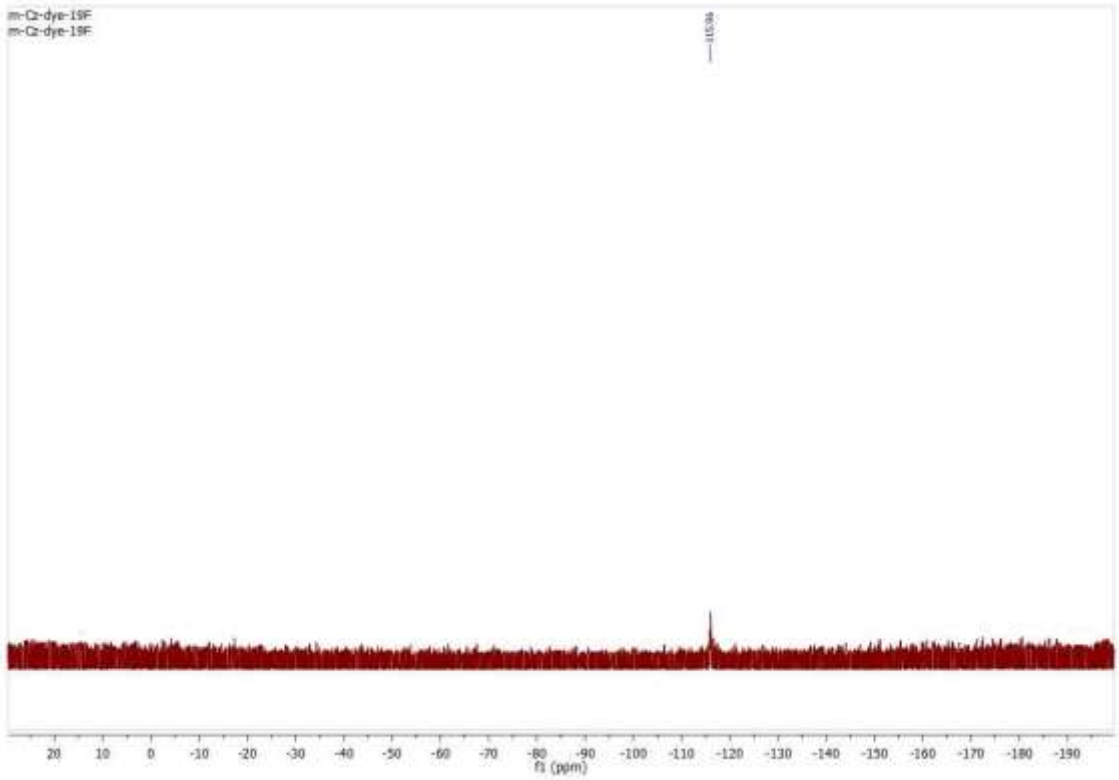

^{19}F NMR spectrum of (*E*)-2-cyano-3-(3-fluoro-4-(9-octyl-9H-carbazol-3-yl) phenyl) acrylic acid (Cz-dye) in $CDCl_3$.

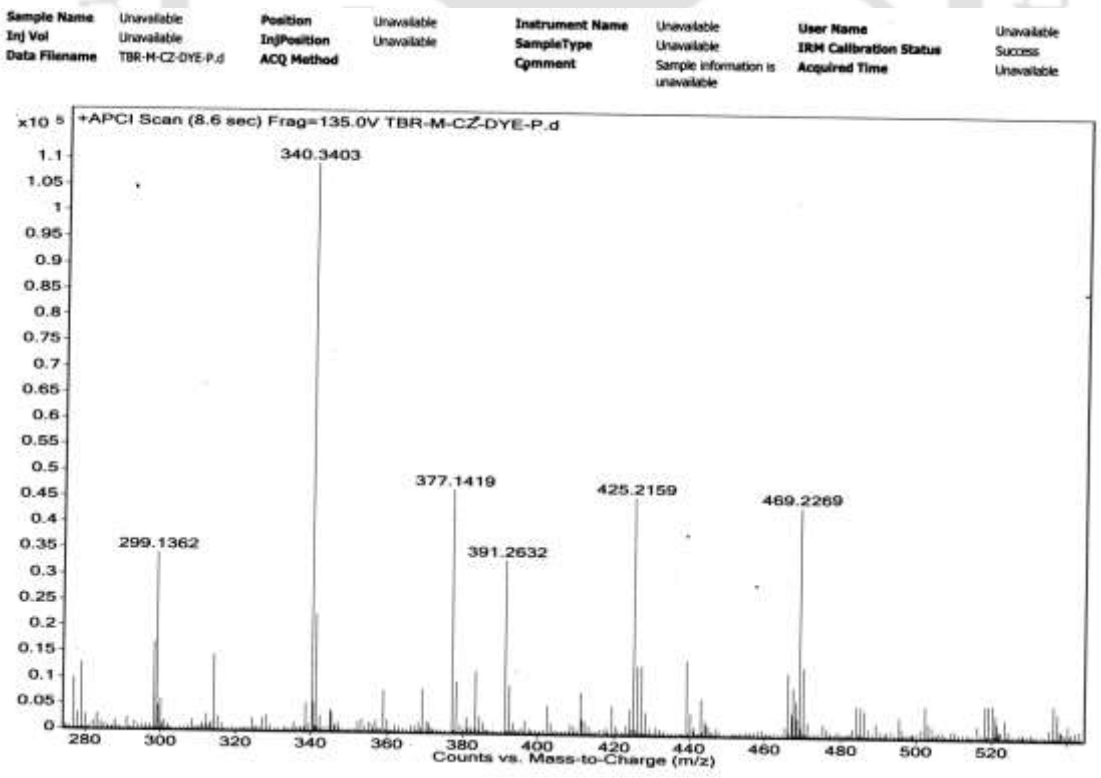

HRMS (ESI) spectrum of of (*E*)-2-cyano-3-(3-fluoro-4-(9-octyl-9H-carbazol-3-yl) phenyl) acrylic acid (Cz-dye).

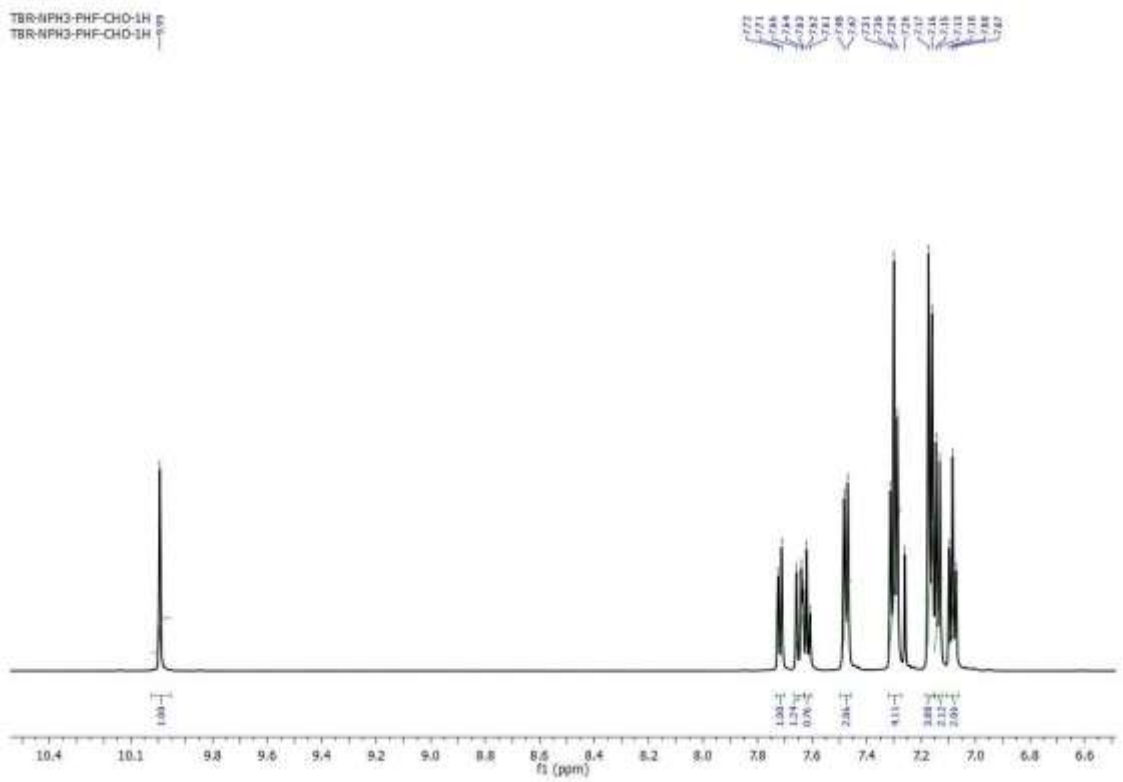

^{1}H NMR spectrum of 4'-(diphenylamino)-2-fluoro-[1,1'-biphenyl]-4-carbaldehyde (2a) in $CDCl_3$.

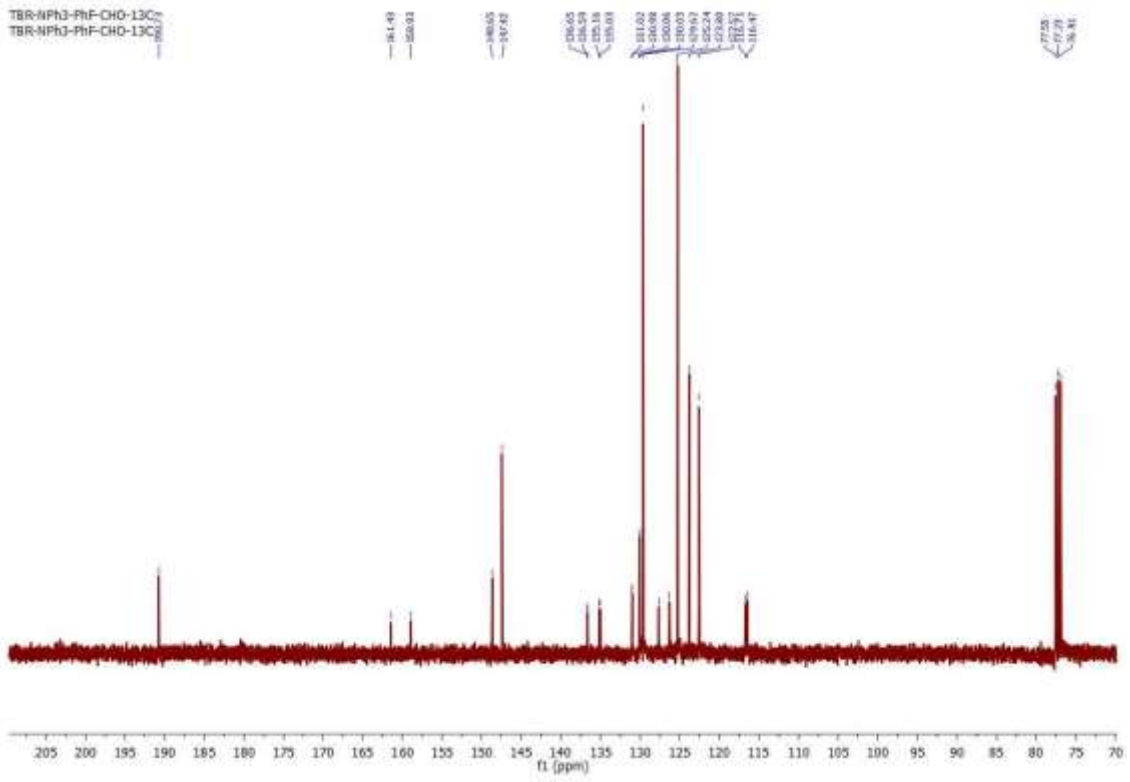

^{13}C NMR spectrum of 4'-(diphenylamino)-2-fluoro-[1,1'-biphenyl]-4 carbaldehyde (2a) in $CDCl_3$.

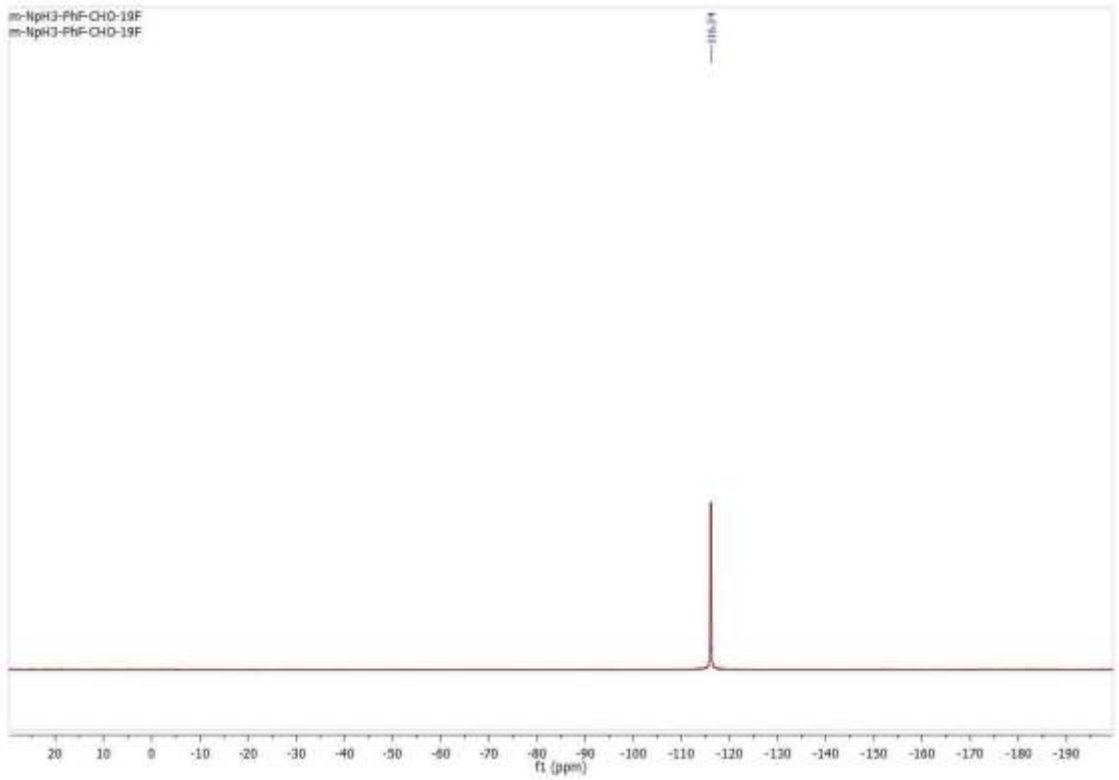

^{19}F NMR spectrum of 4'-(diphenylamino)-2-fluoro-[1,1'-biphenyl]-4 carbaldehyde (2a) in $CDCl_3$.

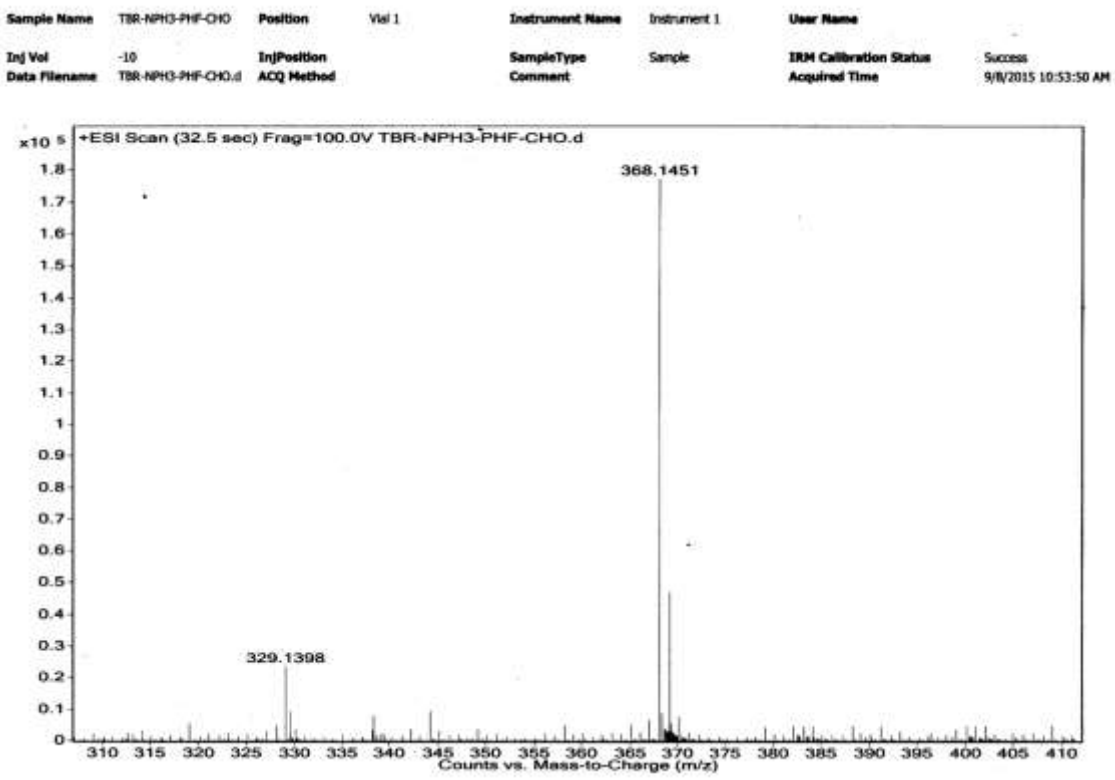

HRMS (ESI) spectrum of 4'-(diphenylamino)-2-fluoro-[1,1'-biphenyl]-4-carbaldehyde (2a).

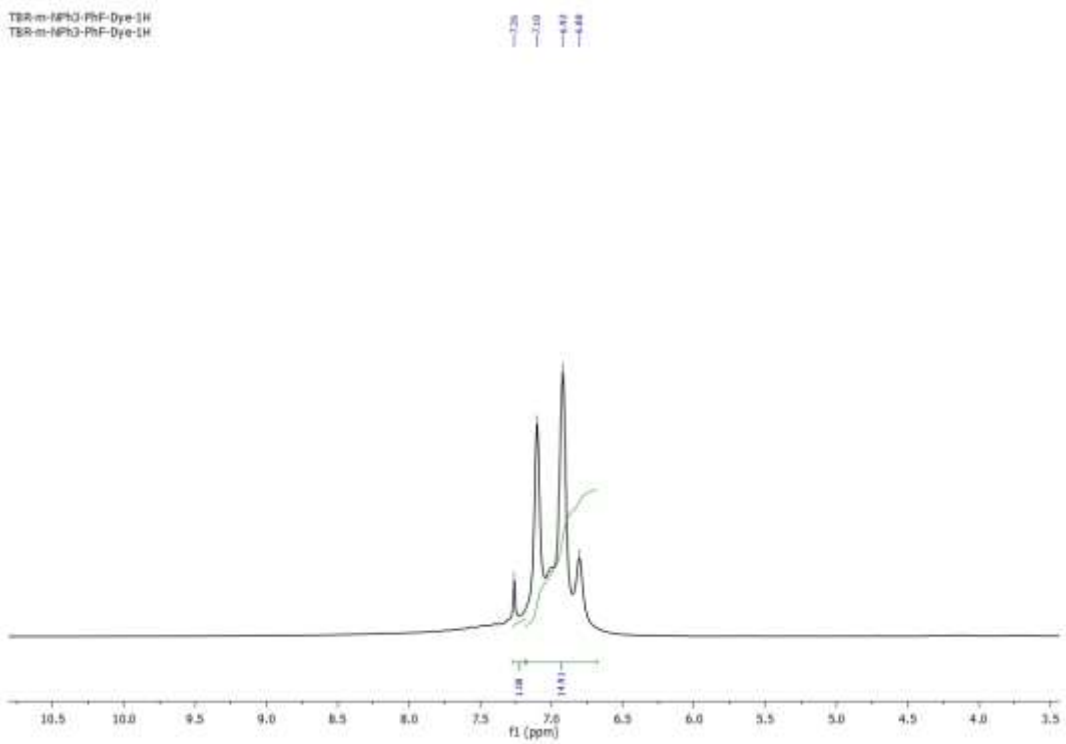

^{1}H NMR spectrum of (*E*)-2-cyano-3-(4'-(diphenylamino)-2-fluoro-[1,1'-biphenyl]-4-yl) acrylic acid (NPh3 dye) in $CDCl_3$.

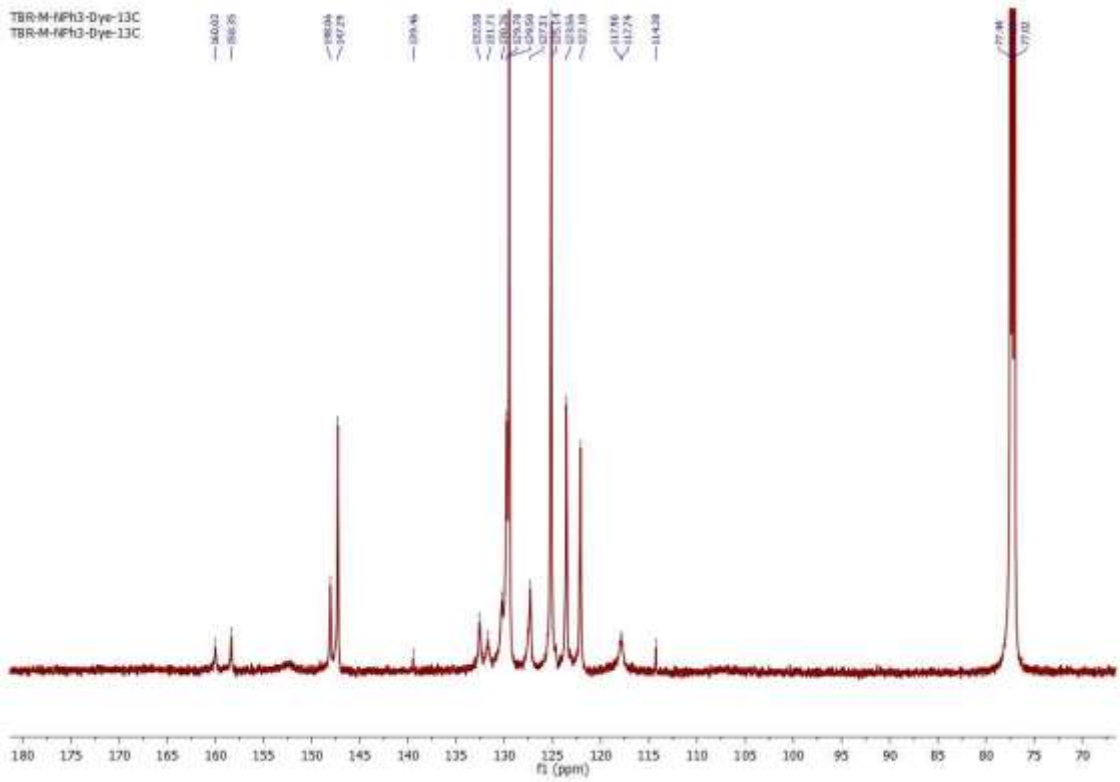

^{13}C NMR spectrum of (*E*)-2-cyano-3-(4'-(diphenylamino)-2-fluoro-[1,1'-biphenyl]-4-yl) acrylic acid (NPh3 dye) in $CDCl_3$.

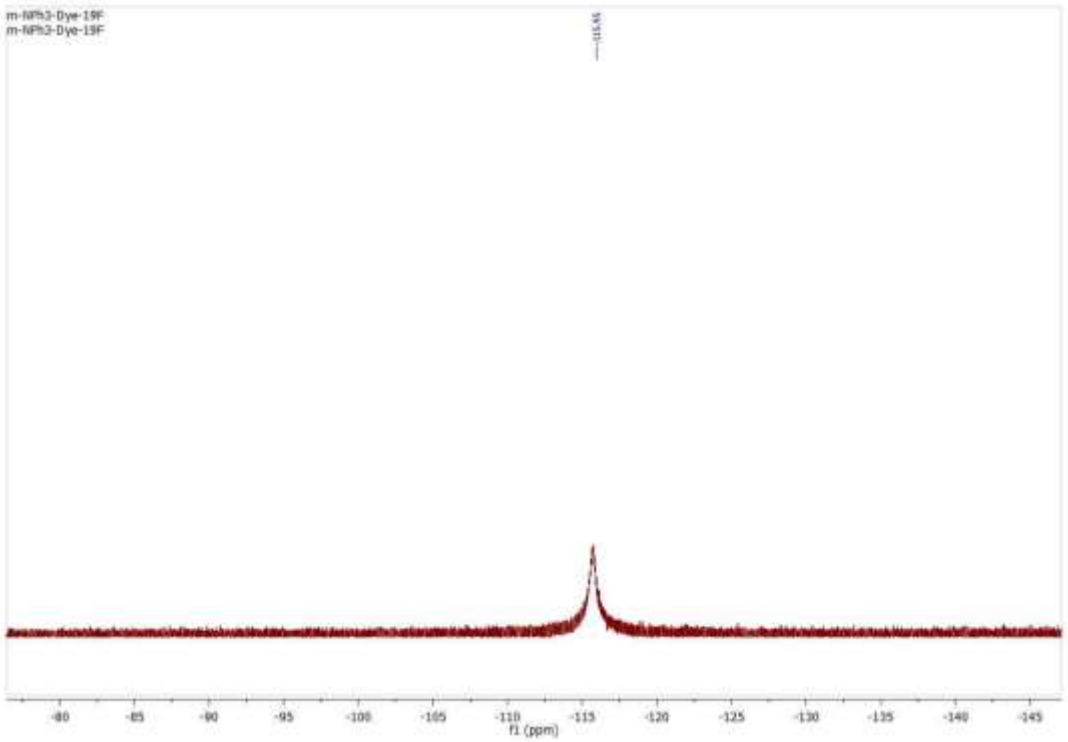

^{19}F NMR spectrum of (*E*)-2-cyano-3-(4'-(diphenylamino)-2-fluoro-[1,1'-biphenyl]-4-yl) acrylic acid (NPh3 dye) in $CDCl_3$.

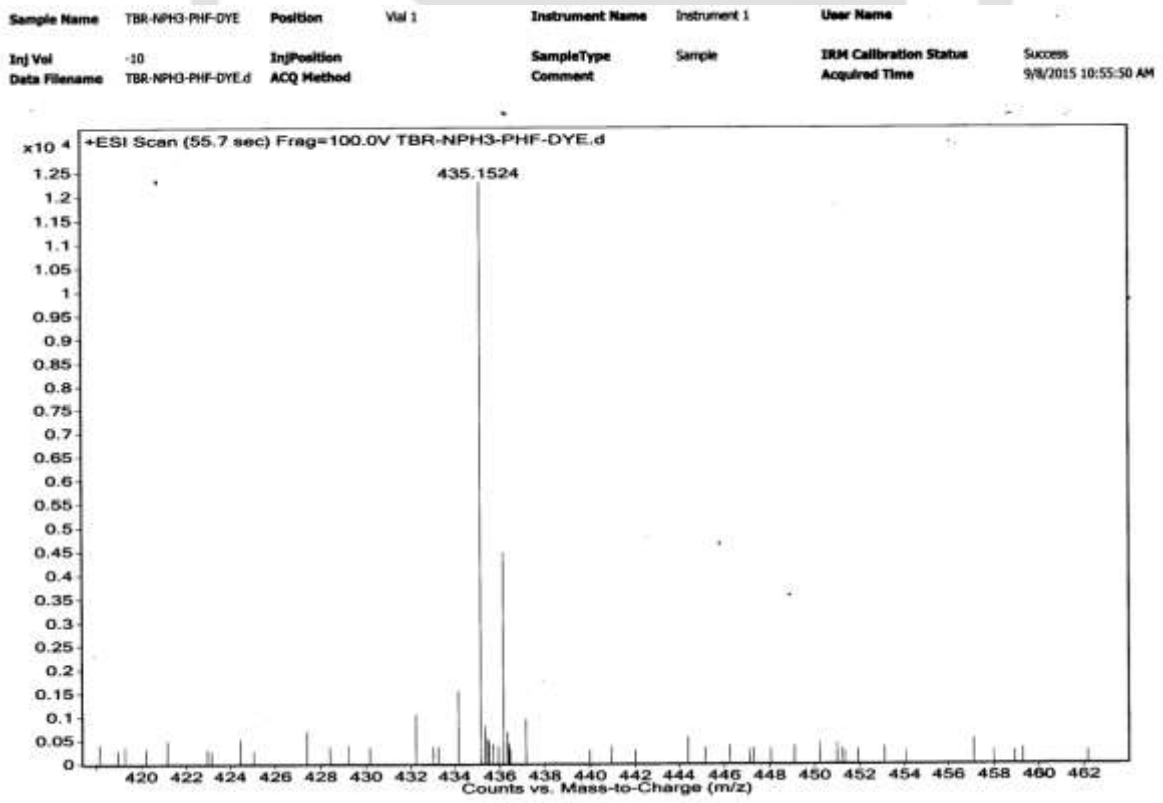

HRMS (ESI) spectrum of (*E*)-2-cyano-3-(4'-(diphenylamino)-2-fluoro-[1,1'-biphenyl]-4-yl) acrylic acid (NPh3 dye).

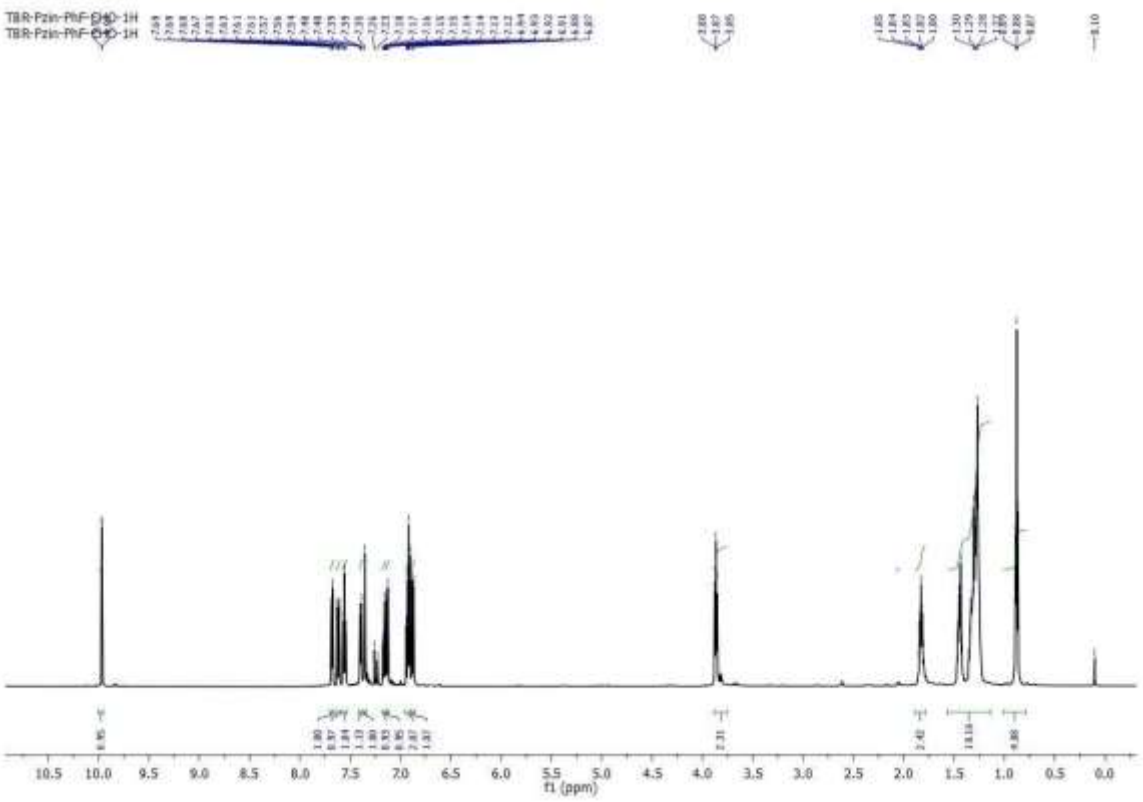

^{1}H NMR spectrum of 3-fluoro-4-(10-octyl-10*H*-phenothiazin-3-yl) benzaldehyde (3a) in $CDCl_3$.

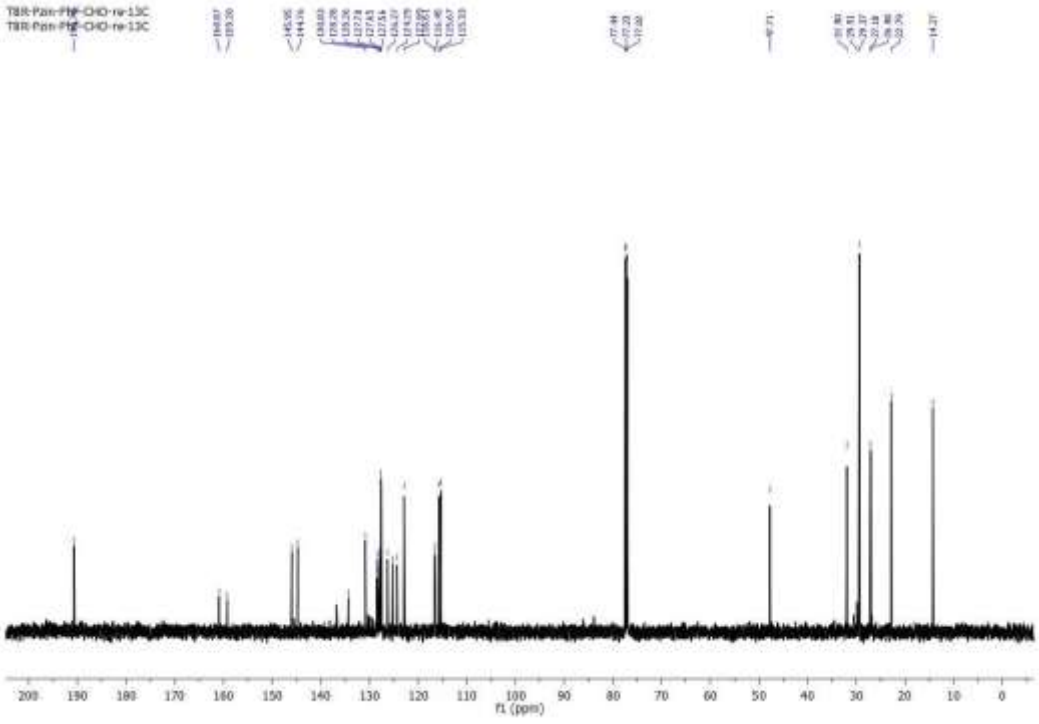

^{13}C NMR spectrum of 3-fluoro-4-(10-octyl-10*H*-phenothiazin-3-yl) benzaldehyde (3a) in $CDCl_3$.

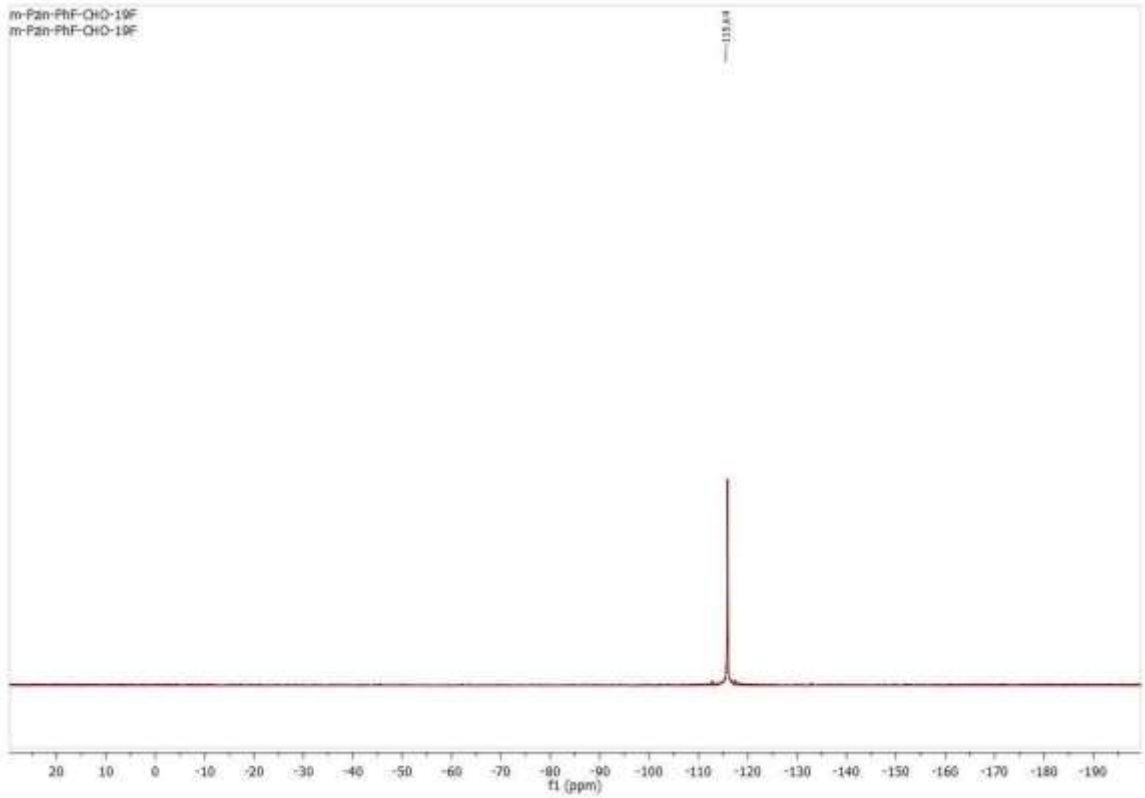

^{19}F NMR spectrum of 3-fluoro-4-(10-octyl-10*H*-phenothiazin-3-yl) benzaldehyde (3a) in $CDCl_3$.

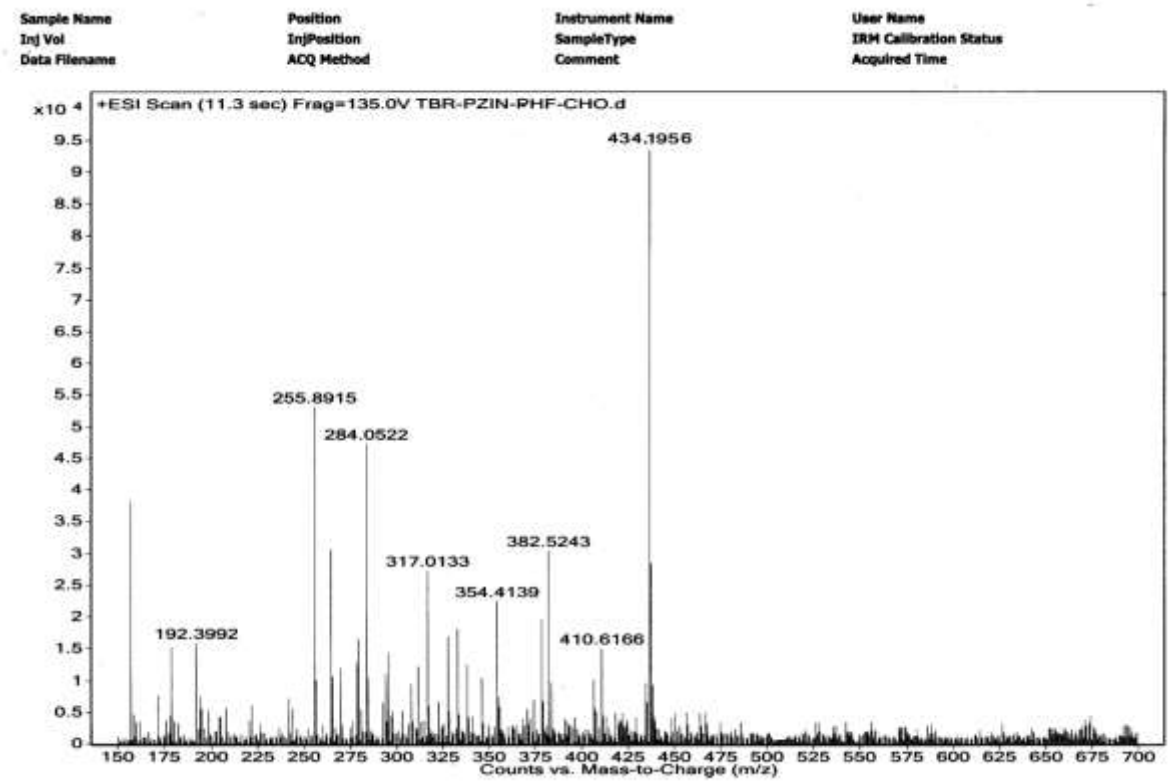

HRMS (ESI) spectrum of 3-fluoro-4-(10-octyl-10*H*-phenothiazin-3-yl) benzaldehyde (3a).

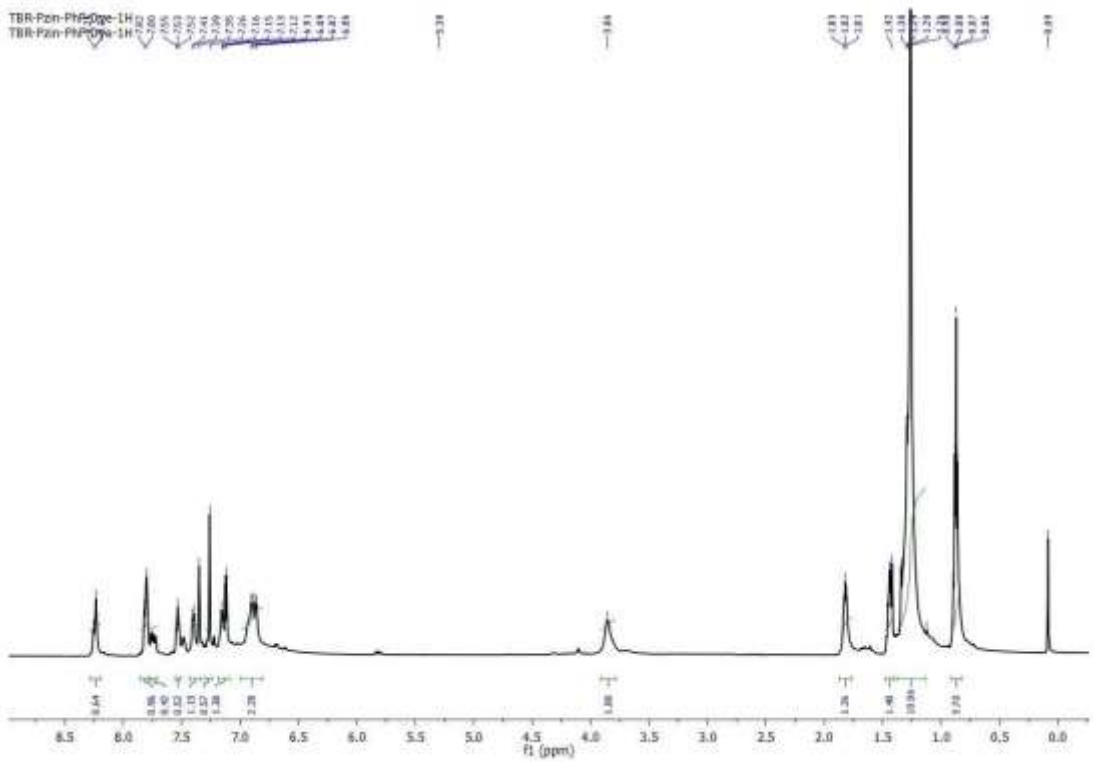

^{1}H NMR spectrum of (*E*)-2-cyano-3-(3-fluoro-4-(10-octyl-10*H*-phenothiazin-3-yl) phenyl) acrylic acid (Pzin dye) in $CDCl_3$.

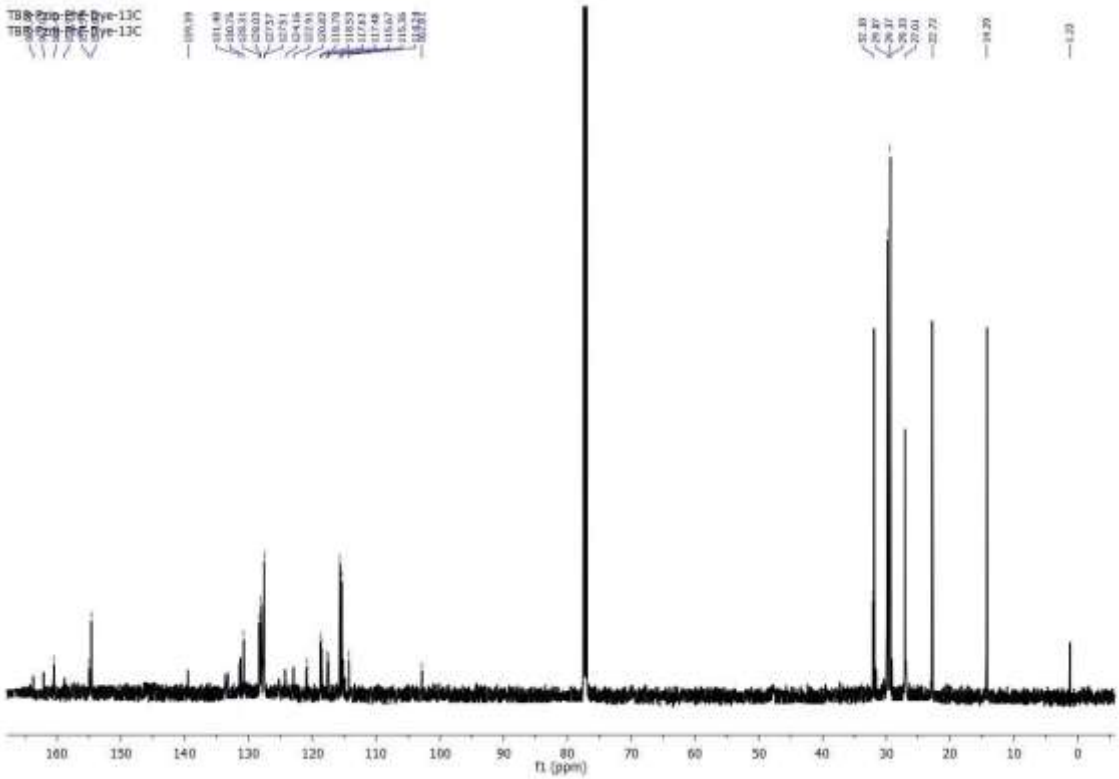

^{13}C NMR spectrum of (*E*)-2-cyano-3-(3-fluoro-4-(10-octyl-10*H*-phenothiazin-3-yl) phenyl) acrylic acid (Pzin dye) in $CDCl_3$.

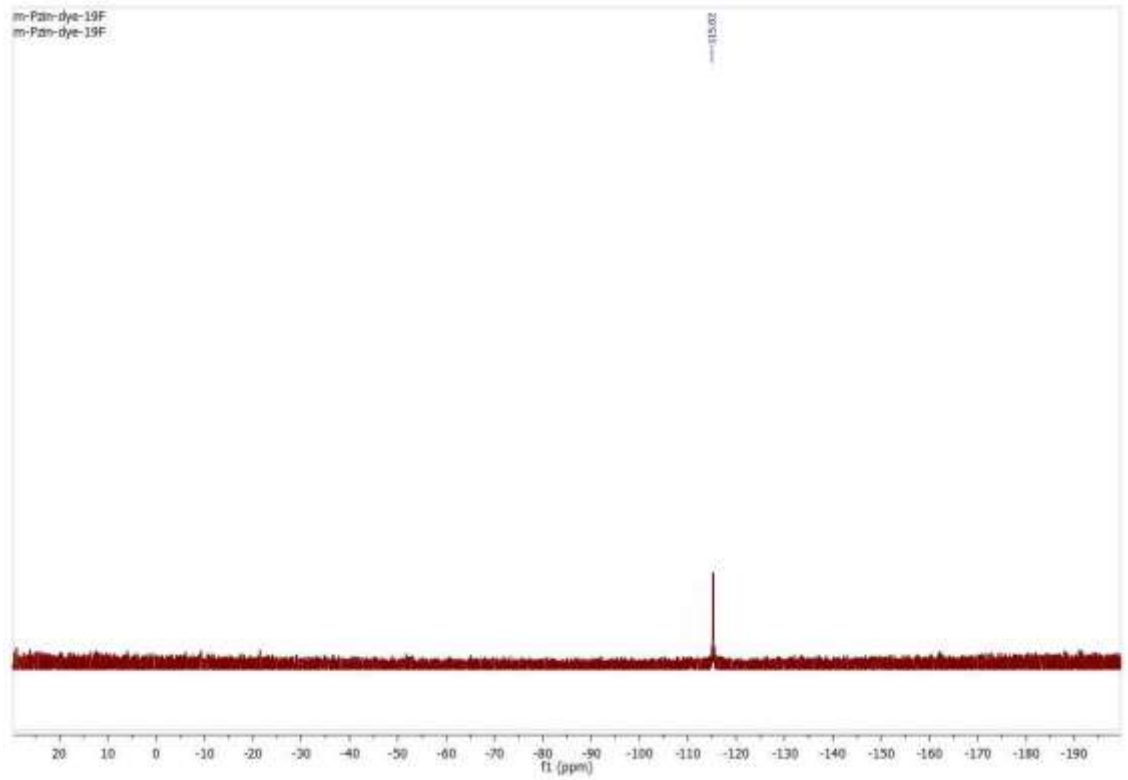

^{19}F NMR spectrum of (*E*)-2-cyano-3-(3-fluoro-4-(10-octyl-10*H*-phenothiazin-3-yl) phenyl) acrylic acid (Pzin dye) in $CDCl_3$.

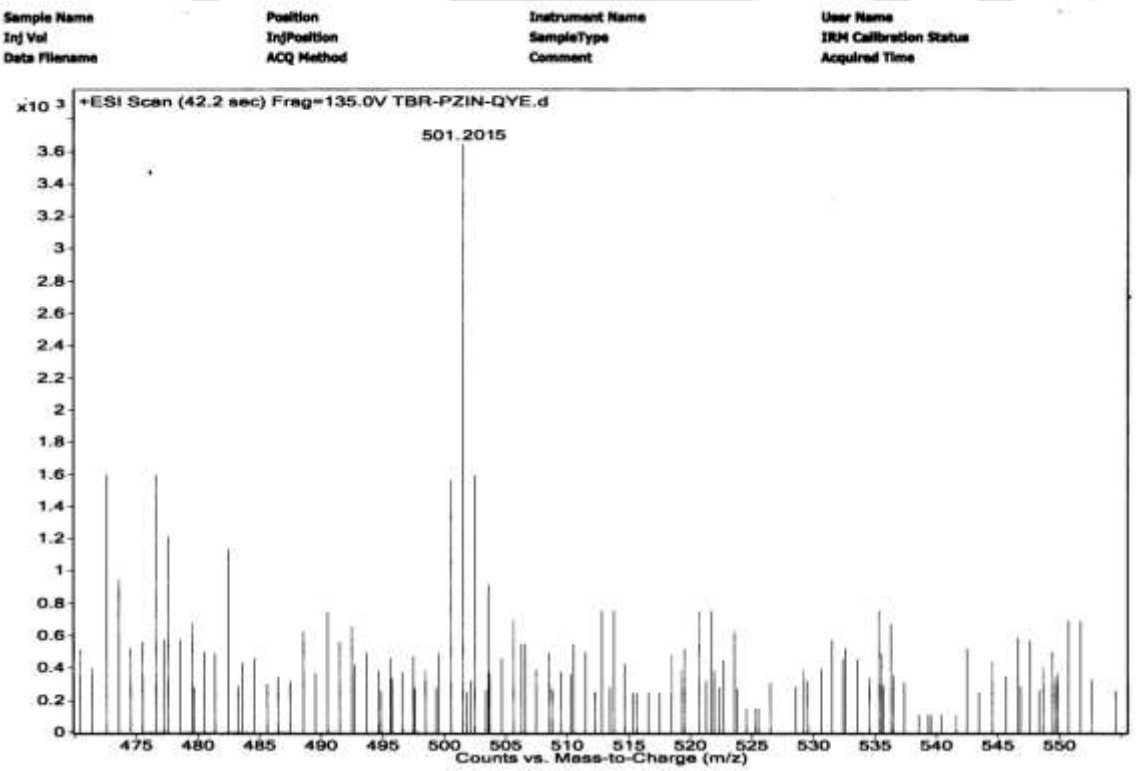

HRMS (ESI) spectrum of (*E*)-2-cyano-3-(3-fluoro-4-(10-octyl-10*H*-phenothiazin-3-yl) phenyl) acrylic acid (Pzin dye).

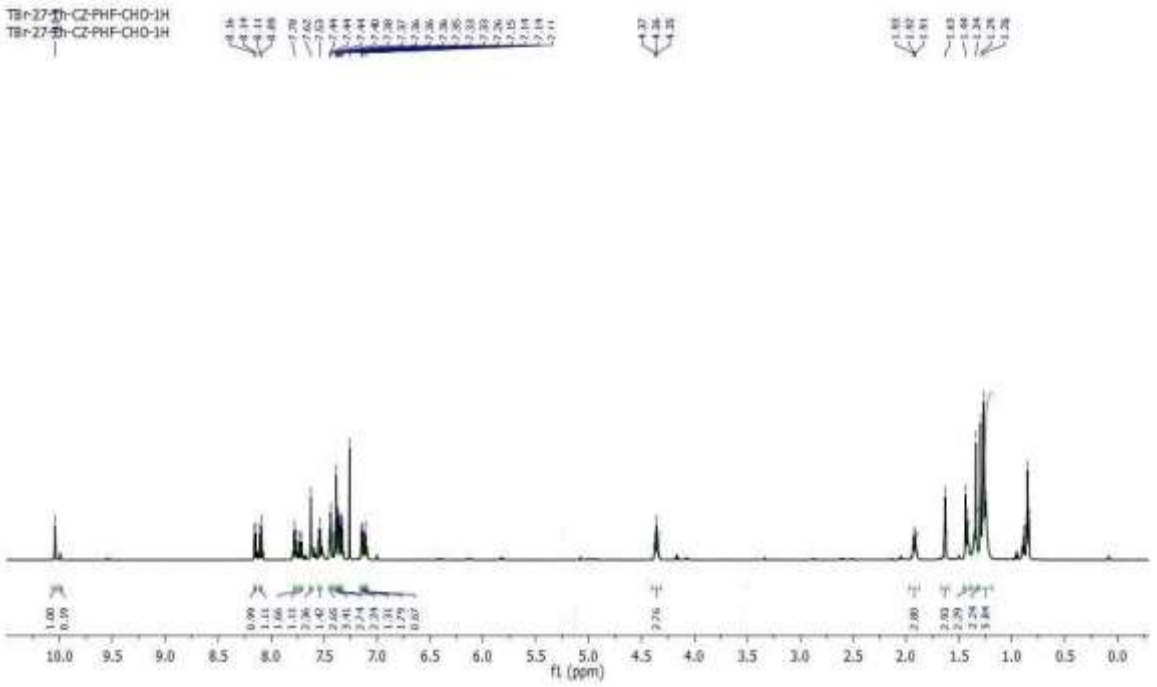

^{1}H NMR spectrum 3-fluoro-4-(9-octyl-7-(thiophen-2-yl)-9*H*-carbazol-2-yl) benzaldehyde (4a) in $CDCl_3$.

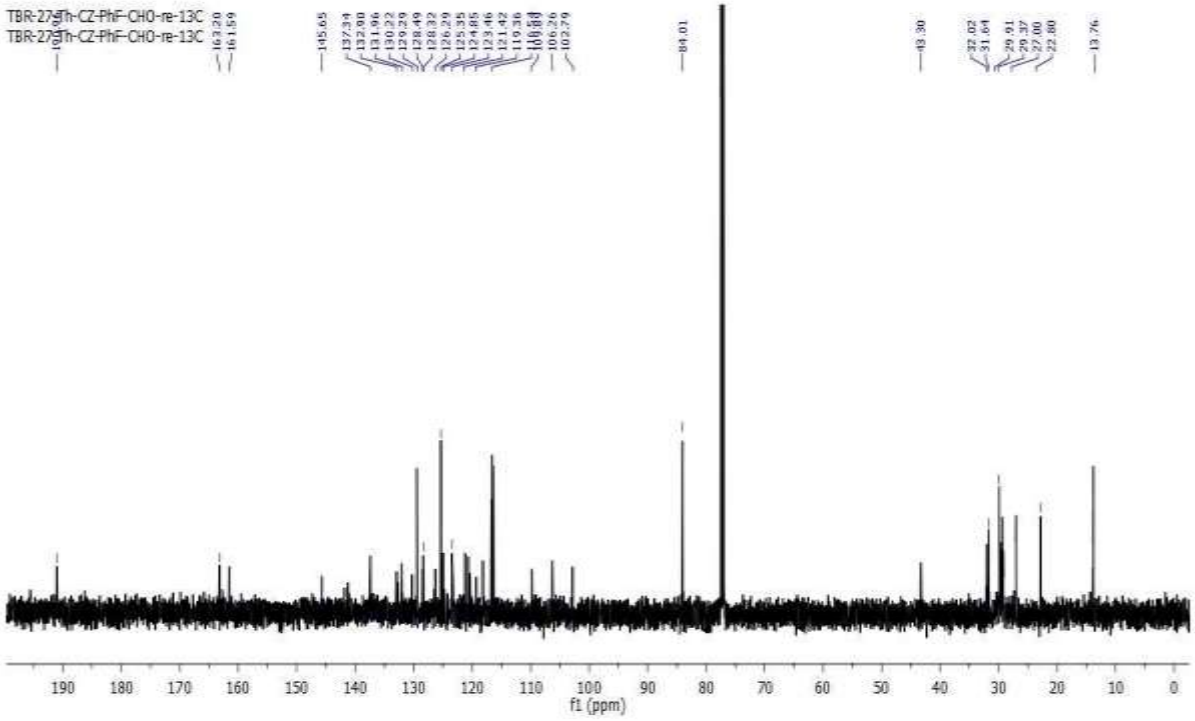

^{13}C NMR spectrum 3-fluoro-4-(9-octyl-7-(thiophen-2-yl)-9*H*-carbazol-yl) benzaldehyde (4a) in $CDCl_3$.

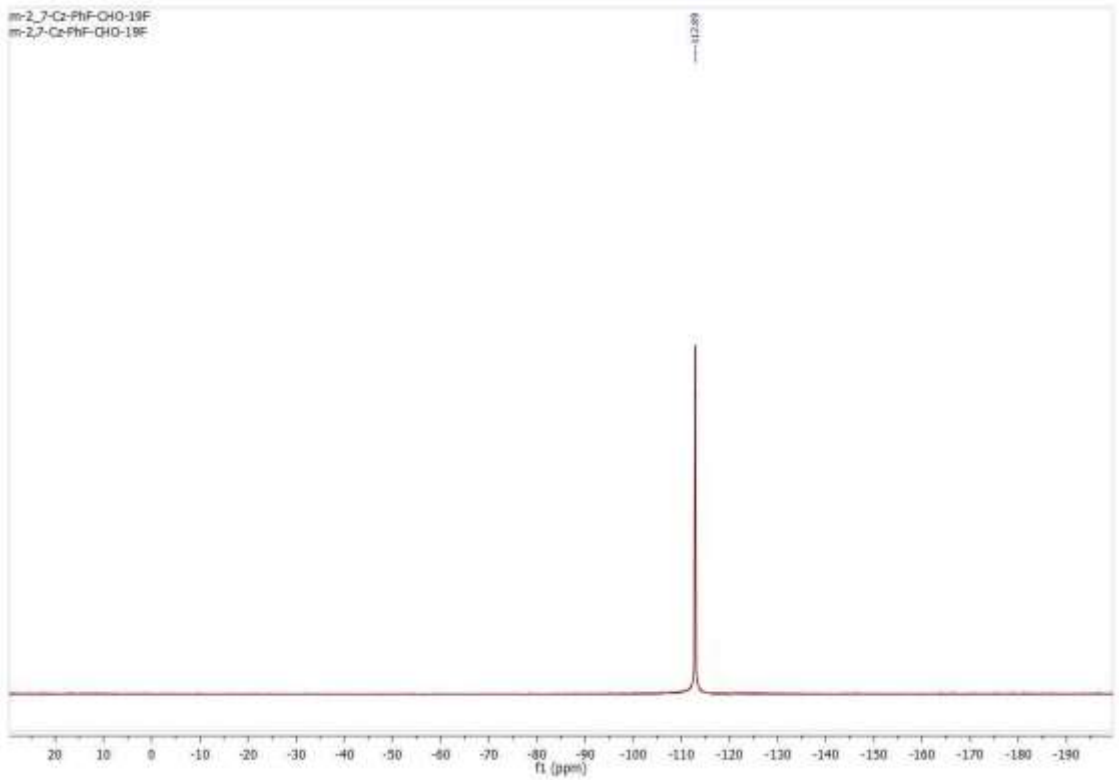

^{19}F NMR spectum 3-fluoro-4-(9-octyl-7-(thiophen-2-yl)-9*H*-carbazol-yl) benzaldehyde (4a) in $CDCl_3$.

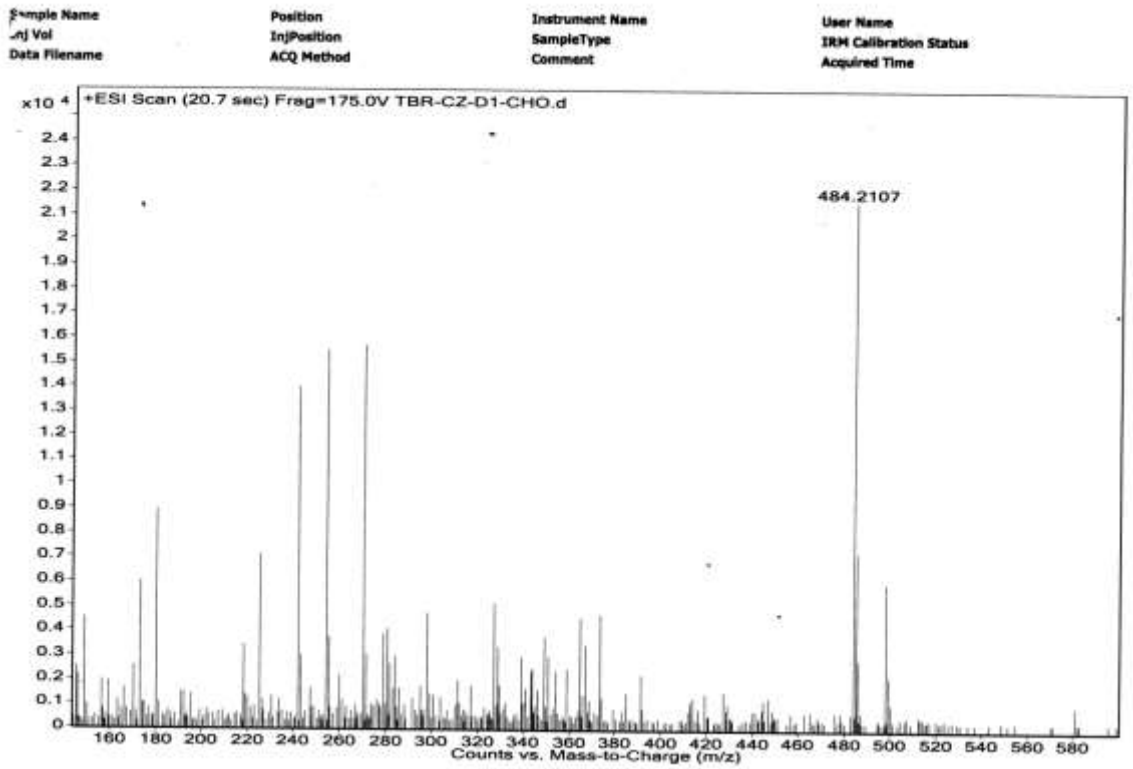

HRMS (ESI) spectrum of 3-fluoro-4-(9-octyl-7-(thiophen-2-yl)-9*H*-carbazol-2-yl) benzaldehyde (4a).

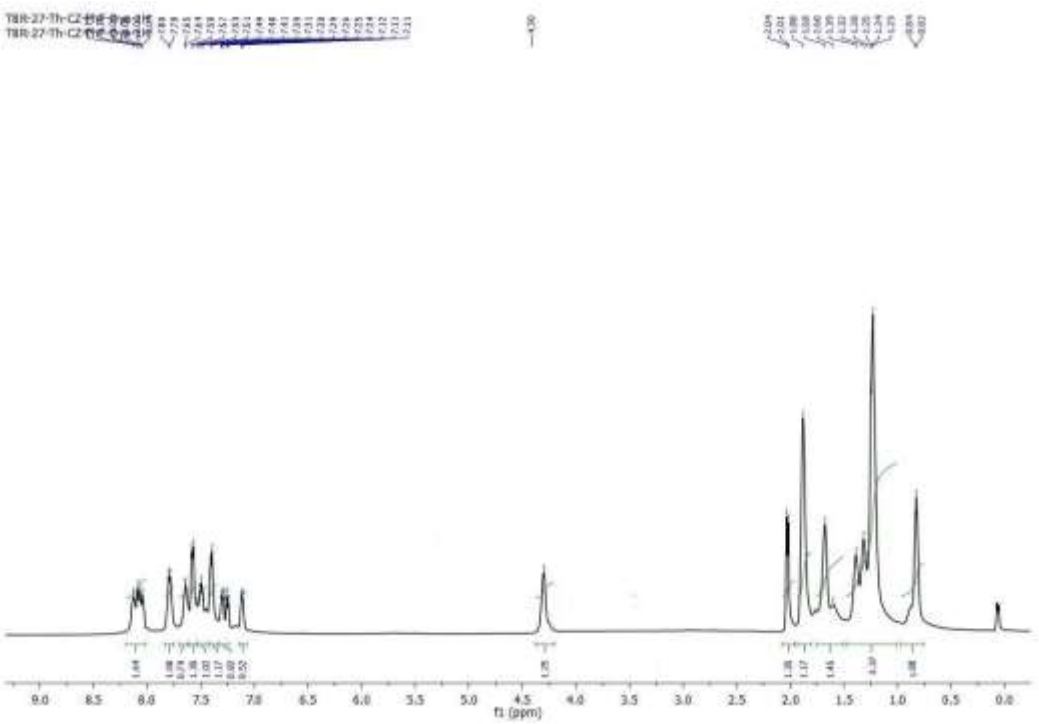

^{1}H NMR Spectrum of (*E*)-2-cyano-3-(3-fluoro-4-(9-octyl-7-(thiophen-2-yl)-9*H*-carbazol-2-yl)phenyl) acrylic acid (2,7-Cz dye) in $CDCl_3$.

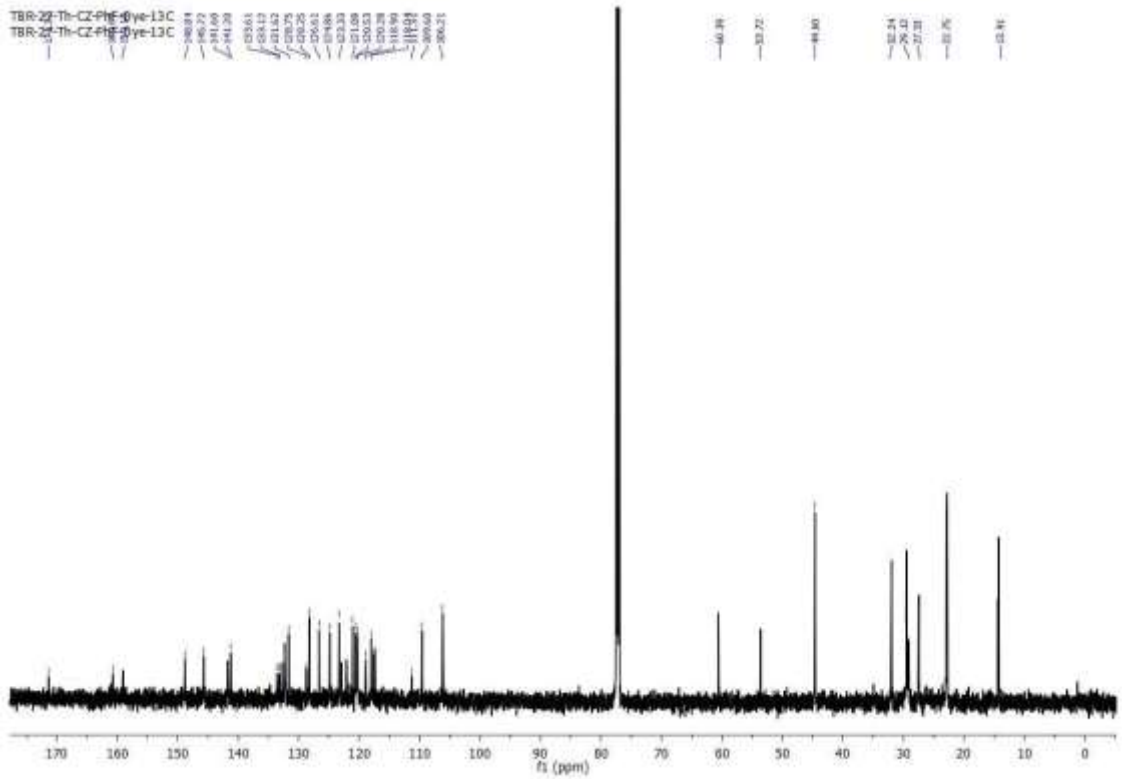

^{13}C NMR Spectrum of (*E*)-2-cyano-3-(3-fluoro-4-(9-octyl-7-(thiophen-2-yl)-9*H*-carbazol-2-yl)phenyl) acrylic acid (2,7-Cz dye) in $CDCl_3$.

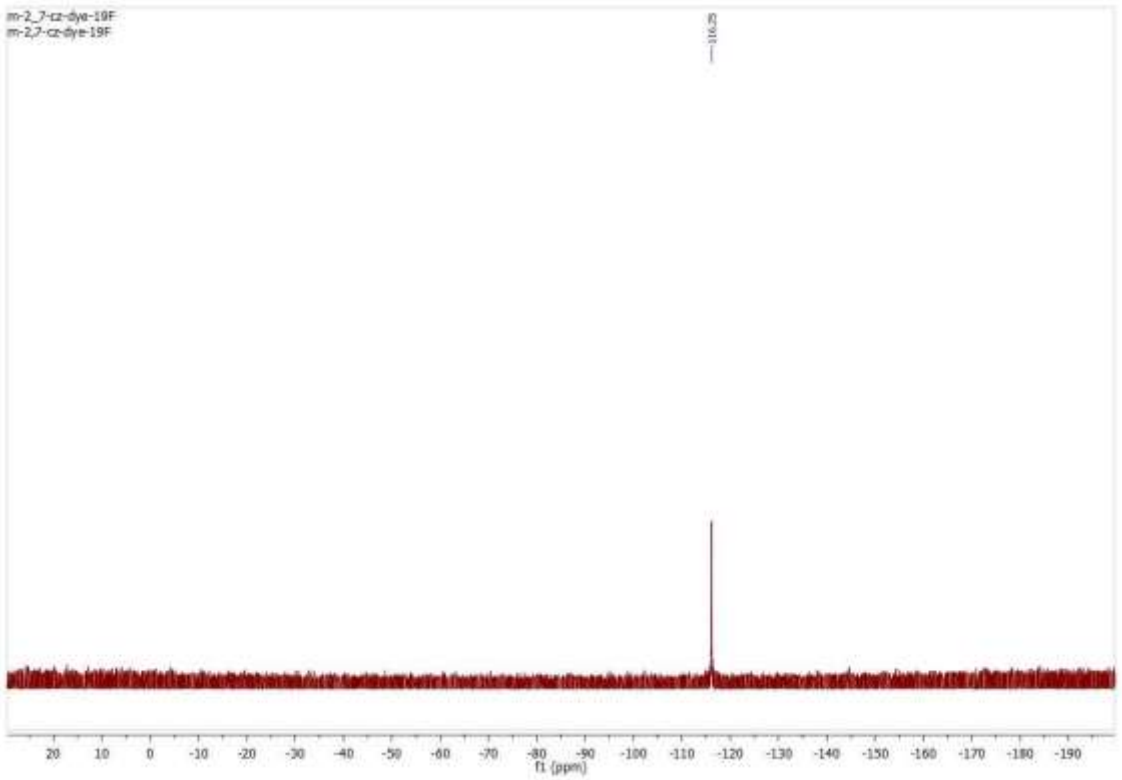

^{19}F NMR spectrum of (*E*)-2-cyano-3-(3-fluoro-4-(9-octyl-7-(thiophen-2-yl)-9H-carbazol-2-yl)phenyl) acrylic acid (2,7-Cz dye) in $CDCl_3$.

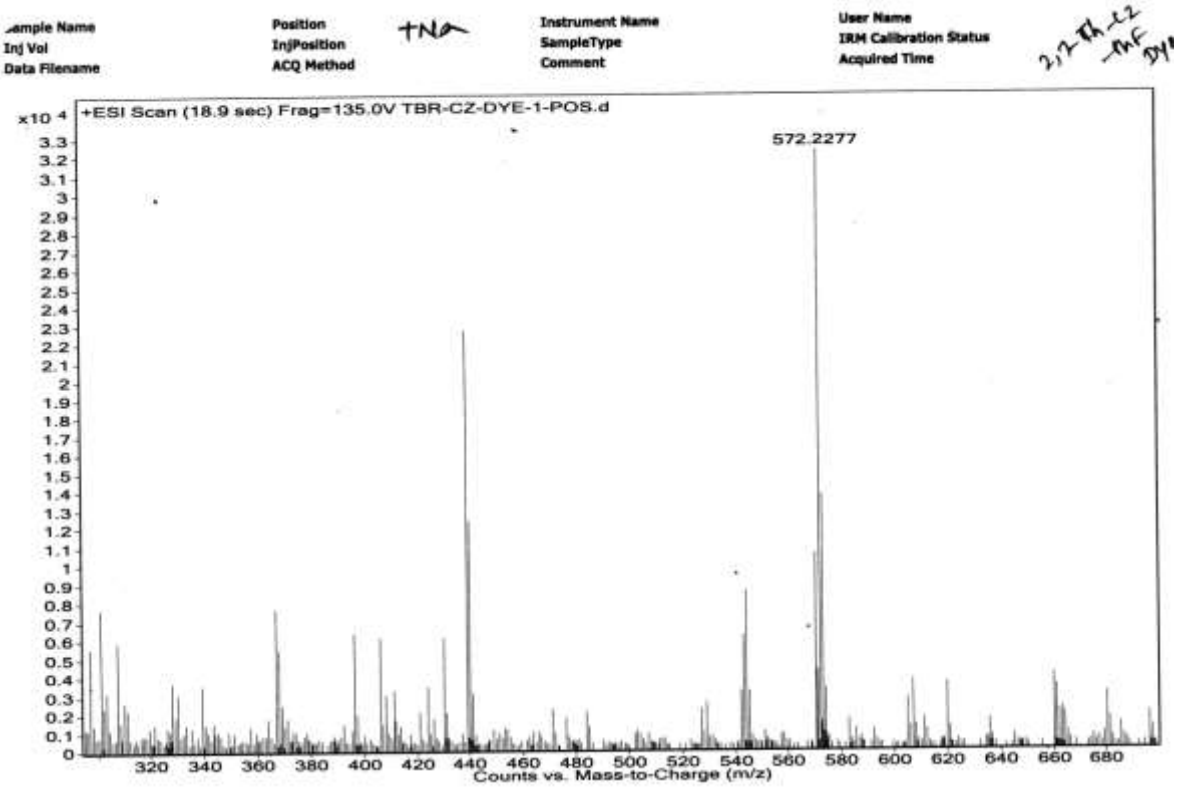

HRMS (ESI) spectrum of (*E*)-2-cyano-3-(3-fluoro-4-(9-octyl-7-(thiophen-2-yl)-9*H*-carbazol-2-yl)phenyl) acrylic acid (2,7-Cz dye).

CHAPTER-3

Design, synthesis and DSSC performance of *o*-fluorine substituted phenylene spacer sensitizers: Effect of TiO_2 thickness variation

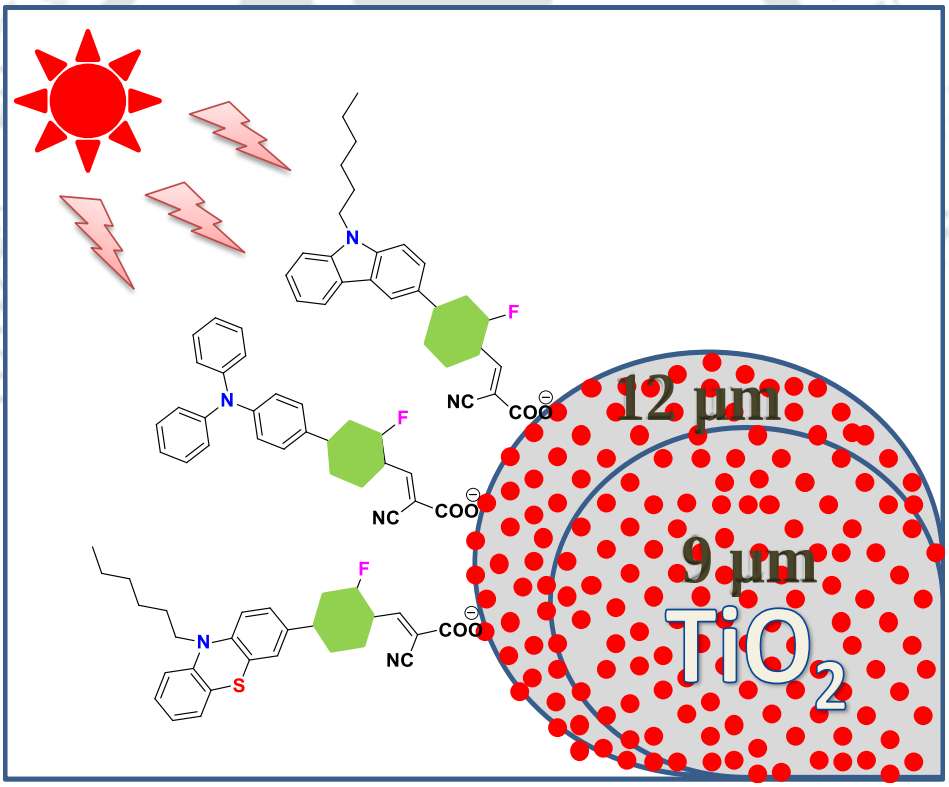

Phys. Chem. Chem. Phys., **2016**, *18*, 28485-2849.

Abstract

The design and development of a new series of dyes with ortho-fluorine substituted phenyl spacers having different donors is presented. Optical, electrochemical, molecular orbital calculation and photovoltaic properties for different TiO_2 thicknesses (9-12 µm) of the new dyes were investigated. Thicknesses of TiO_2 film have effects on the open circuit voltage (V_{oc}), short circuit current (J_{sc}) and efficiency. We observed that the J_{sc} and V_{oc} of o-Cz dye with a TiO_2 film thickness of 12µm (8.91 mA/cm^2 and 0.63 V) are larger than film thickness of 9µm (8.40 mA/cm^2 and 0.57 V). It could be due to the increase in thickness of TiO_2 film. At optimum thickness of TiO_2 film (12µm), o-Cz dye exhibits power conversion efficiency (η) of 3.63 (± 0.4)%. This was an improved efficiency of o-Cz dye from 3.3% to 4.0% without using any co-absorbents, while changing the thickness of TiO_2 film. However, the o-Cz dye has planar structure, whereas the remaining o-NPh3 and o-Pzin dyes have three and two dimensional structures. The optimized geometry calculation of ortho fluoro phenyl π-spacer dyes were ascertained by Density functional theory (DFT) by using B3LYP/631G(d,p) basis set. The results reveal that o-Cz dye have high efficiency due to the deep HOMO level and it exhibits better charge transfer from donor to acceptor, compared to other dyes.

3.1 Introduction

Dye-sensitized solar cells (DSSCs) are an attractive alternative to conventional solar cell, because of their reasonable solar to electricity conversion efficiency, low cost of materials, low manufacturing cost, and simple fabrication on rigid and flexible substrates.[1,2] In DSSCs, dye harvesting the light generate free charge carriers after electron inject into conduction band of TiO_2. The electron is transferred to the TiO_2/Dye/electrolyte interface.[3] In the last decade ruthenium and porphyrin based sensitizers were mostly considered for high performance DSSC applications, due to the high light to electric power conversion efficiency and long term stability, while these dyes have some drawbacks for commercial application due to the low abundance of this metal, modest extinction coefficients, tedious purification, challenging synthesis and environment issues.[4-6] For this reason, huge efforts have been made on the development of the new and efficient metal-free organic sensitizers that could improve the device performance and potentially low cost production. These DSSC are gradually attracting attention due to the easy synthesis and excellent flexibility in structure modification, high molar extinction coefficient and easy tunable functionalities. Also, the photochemical as well as photophysical properties of dyes are compared to porphyrin and ruthenium sensitizers.[7-9] Herein, we report the effect of fluorine substitution on phenyl unit at ortho position (used as a π-linker) to cyanoacrylate, and its effect on dyes having carbazole, triphenyl amine and phenothiazine donor moieties sharing same acceptor (cyanoacetic acid).[10,11] We introduced the linear hexyl chain on carbazole and phenothiazine moieties to suppress the dye aggregation on TiO_2 surface. On the other hand, carbazole dye shows highest life time values and better charge transfer from donor to acceptor (due to the planar structure). The cell with carbazole donor moiety shows highest open circuit voltage (V_{oc}) and short circuit current (J_{sc}) at 12µm TiO_2 thickness.

Generally, fluorine has electron-withdrawing ability. When fluorine atom is incorporated in to π-bridge in organic sensitizers the dye molecule properties drastically changes, like changing the molecular energy levels, improving the electron mobility, governed by charge distribution and charge transfer from D to A. When fluorine atom is substituted on π-spacer, the LUMO level of the sensitizer decreases and influences intra and inters molecular interaction through H-bonding. The earlier reports reveal that, an ortho fluorine substituent on phenyl unit to cyanoacrylic acid can enhance the light absorption property and improves the efficiency than unsubstituted and meta fluorine substituent to

cyanoacetic acid. In phenyl spacer having two fluorine atoms substituent at ortho position to cyanoacrylate the performance of cell efficiency was drastically decreased. The main reason was that the planarity of dye backbone was disturbed due to steric hindrance. The results explain that single fluorine substituent is better than double substituent at ortho position to cyanoacrylic acid dyes.[12-16]

The power conversion efficiency was impeded by recombination, slow electron percolation and electron trap states on the surface of TiO_2, light harvesting and dye aggregation.[17,18] Recent studies show that increasing the thickness of TiO_2 film increases internal surface area and the absorption amount of dye also increases (Table 3.1, Figure 3.1). In our experiments three different new dyes were studied for their optical, electrochemical, life time and theoretical (DFT calculations) properties (scheme 3.1, Figure 3.2-3.5) and its corresponding data are shown in Table 3.2. The photovoltaic properties were also studied with different (9-12 µm) thickness of TiO_2 with same redox electrolyte and equivalent active area. The variation of current–voltage characteristics of dyes with different thickness of TiO_2 films are shown in Table 3.[19,20] The statistical performance shows that, the open circuit voltage (V_{oc}) and fill factor (*FF*) of all dyes are improved. o-Cz dye exhibits best performance with overall power conversion efficiency of 2.9% in 9µm thickness and 3.6% in 12µm thickness. On increasing the thickness of TiO_2 film the transmittance decreased, reducing the incident light intensity on the dye absorbed on top surface of TiO_2. This shows lower injection of electrons from excited state of dye to conduction band of TiO_2 and more recombination occurs which results in poor production of current. Thus increasing the thickness of TiO_2 does not contribute significantly in improvement of photovoltaic performance. If we decrease the thickness of TiO_2 the dye loading capacity will obviously decrease, thereby the injections capacity of excited state dye to conduction band of TiO_2 also decrease, resulting in the lower photovoltaic performance. Looking carefully at the literature, in majority cases, TiO_2 photoanode having thickness between 8-12 µm was used. We have tried 8, 9, 12 and 14µm. In case of 8µm thickness, loading of metal free sensitizers is lower compared to other higher thickness. However, for extremely high thickness i.e. 14µm, we observed poor adhesion towards TCO substrate and as a consequence cracking was observed (after calcination) in SEM image (Please see following SEM images Fig. 3.1).

Table 3.1 Dye loading capacities on different thickness (9-12 µm) of TiO_2 films.

Dyes	Dye loading on 9µm TiO_2 thickness ($mol^{-1}.cm^{-1}$)	Dye loading on 12µm TiO_2 thickness ($mol^{-1}.cm^{-1}$)
o-Cz	1.1×10^{-6}	2.3×10^{-6}
o-NPh3	0.5×10^{-6}	0.8×10^{-6}
o-Pzin	0.8×10^{-6}	0.9×10^{-6}

Figure 3.1 The SEM images of various thickness TiO_2 photoanode (a) 9µm, (b) 12µm and (c) 14µm.

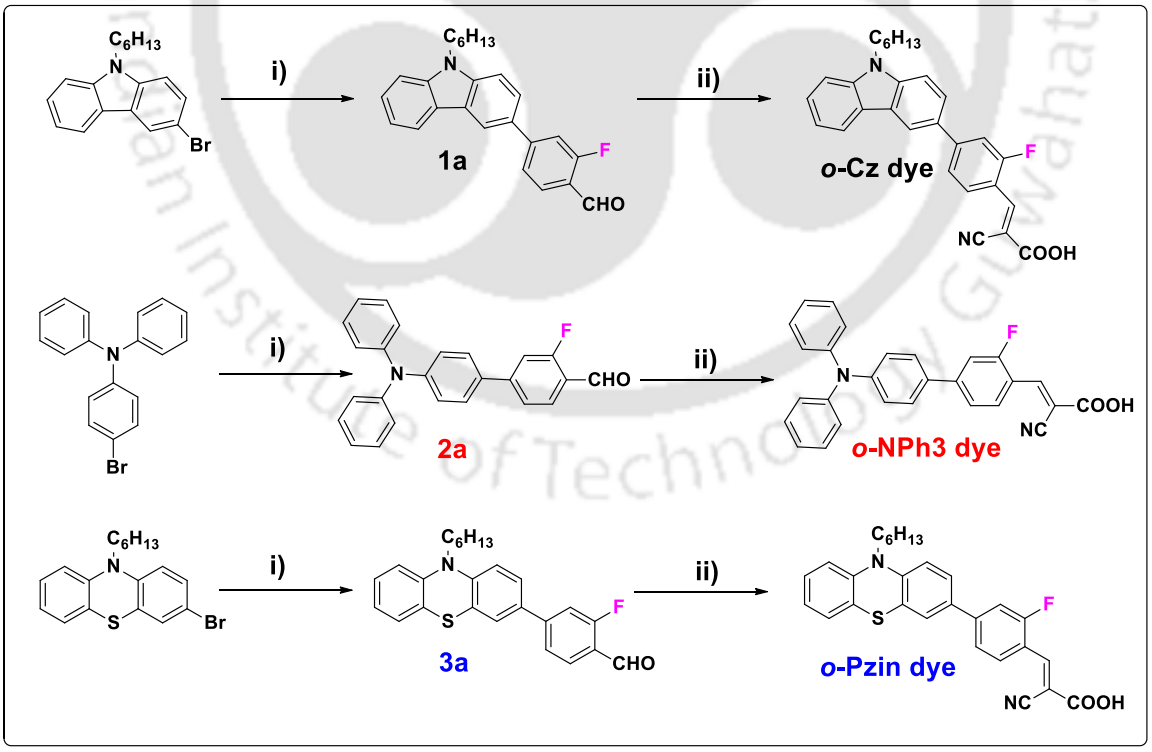

Scheme 3.1 Synthetic route of organic sensitizers (i) 3-fluoro-4-formyl phenyl boronic acid, THF: H_2O=2:1, Aliquat, K_2CO_3, $Pd(PPh_3)_4$, 85 °C, 12h. (ii) Cyanoacetic acid, Piperidine, CH_3CN, 85 °C, 8h.

3.2 Results and Discussion

3.2.1Optical Properties

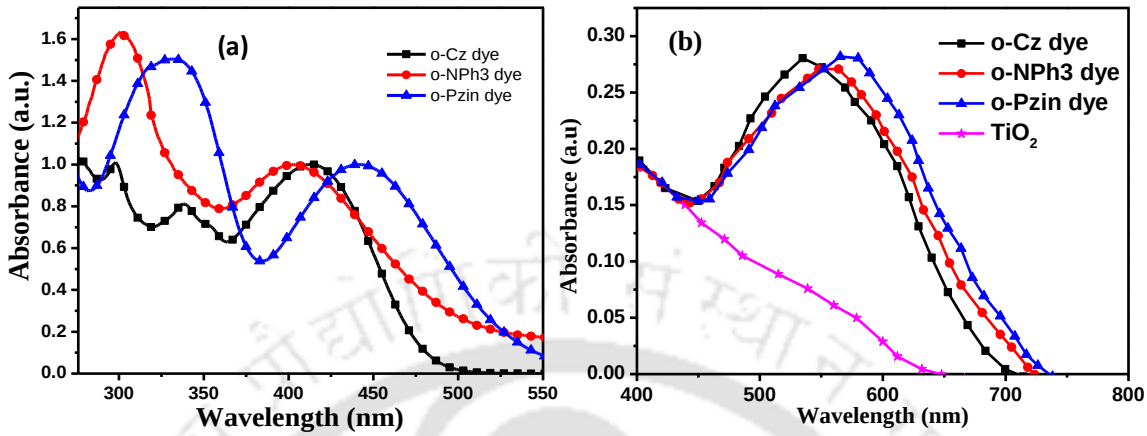

Figure 3.2 (a) Normalized UV-Vis absorption spectra of organic dyes in chloroform solution. (b) UV-Vis absorption of organic dyes absorbed on TiO_2 films.

The UV-Vis absorption spectra of all dyes in chloroform solution and absorbed on TiO_2 films are depicted in Figure 3.2 and the detailed parameters are summarized in Table 3.2. o-NPh3 and o-Pzin dyes exhibit two major distinct broad absorption peaks in the range of 300-570 nm. Similarly, o-Cz dye exhibit two minor and one major broad absorption bands in the range of 300-500 nm in chloroform solution (Figure 3.2(a)). We ascribed shorter wavelength peaks in the range of 300-380 nm, due to the localized aromatic π-π* electronic transition of the chromophores, while the longer wavelength band located at 380-570 nm are attributed to the intramolecular charge transfer (ICT) from the donor to acceptor. The simplest o-Pzin dye exhibit maximum absorption wavelength (λ_{max}) at 441 nm with a molar extinction coefficient ε= 16,230 $M^{-1}cm^{-1}$ due to charge transfer transitions of conjugated molecule. The dyes o-Cz and o-NPh3 exhibit similar spectral properties at λ_{max} of 412(ε= 25,002 $M^{-1}cm^{-1}$) and 402 nm (ε= 15,829 $M^{-1}cm^{-1}$), respectively. Comparatively o-NPh3 dye exhibit broad absorption band in visible region than o-Cz dye in solution as well as dyes absorbed on TiO_2 surface. The decreasing order of the maximum absorption wavelength was o-Pzin dye> o-NPh3 dye> o-Cz dye. This order of absorption is due to donating ability of the donor moiety in the organic dyes shown in Fig. 3.2 and corresponding data in Table 3.2.

Figure 3.2 (b) shows the absorption spectra of dyes on TiO_2 films, the maximum absorption peak of o-Cz, o-NPh3 and o-Pzin are located at 536, 557 and 571 nm,

respectively. The higher molar absorption coefficient of o-CZ dye compared to o-Pzin and o-NPh3 dyes is due to the better planarity and strong π-π* transition.

3.2.2 Electrochemical Characterization

Cyclic voltammetry was carried out in argon atmosphere to investigate HOMO-LUMO levels and band gap of the sensitizers. The cyclic voltammograms of the dyes are shown in Figure 3.3, and relevant data are summarized in Table 3.2. HOMO levels of all dyes are calculated from onset oxidation potential of dyes, according to E_{HOMO} =-(E_{ox} - $E_{1/2(ferrocene))}$ + 4.8) eV formula. Except for o-Pzin dye, remaining two dyes exhibit a quasi-reversible oxidation peak, i.e. one electron oxidation couple which can be attributed to the oxidation of the triphenyl amine and carbazole.

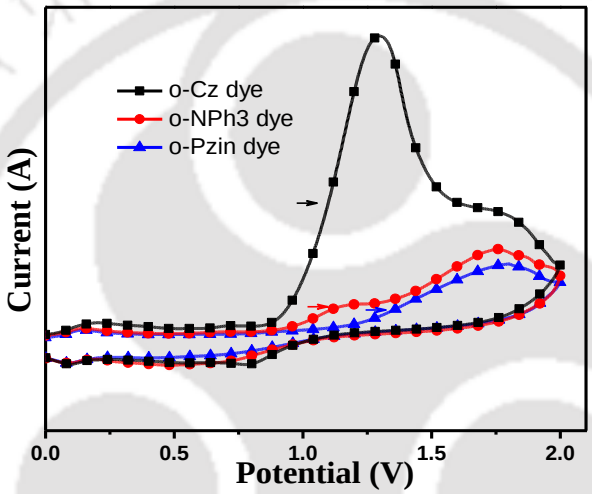

Figure 3.3 Cyclic voltammograms corresponding to the oxidation of organic dyes in 0.1M TBAF/CH_3CN. Colored arrows represent the first oxidation peak of dyes.

All dyes show an oxidation potential peak (V vs NHE) in the range of 0.97 V-1.2 V (5.47-5.70 eV). The HOMO level of o-Pzin, o-NPh3 and o-Cz dyes are 0.97 V (5.47 eV), 1.13 V (5.63 eV) and 1.2 V (5.70 eV) respectively. The oxidation potential of all dyes versus normal hydrogen electrode (V vs NHE) values is more positive or lower than the redox potential of I^-/I_3^- (0.4 V vs NHE or -5.1 eV), which indicates oxidized dyes can regenerate effectively. i.e. o-Cz dye have effective regeneration ability.

The LUMO level of dyes were calculated from the onset thin film absorption spectra of dyes (E_{LUMO} = Estimated band gap by using onset of $UV_{(film)}$ – E_{HOMO}), which are 2.58, 2.60 and 2.63 eV of the o-Cz, o-NPh3 and o-Pzin dyes respectively. These energy levels are higher than the Conduction band (CB) of the TiO_2 electrode (-0.5 V vs NHE or -4.0

eV), which predicts sufficient driving force for electron injection from oxidized dye to CB of nanocrystaline TiO_2 surface.

Table 3.2 Optical, electrochemical and life time characterization of dyes

Dye	Solution λ_{max} [nm][a)]	Film λ_{max} [nm][b)]	$\varepsilon_{max}/M^{-1}cm^{-1}$	HOMO [eV][c)]	LUMO [eV][c)]	τ(ns)
***o*-Cz-dye**	412	536	25,002	-5.70	-2.56	1.70
***o*-NPh3-dye**	402	557	15,829	-5.63	-2.61	1.37, 4.01
***o*-Pzin-dye**	441	571	16,230	-5.47	-2.65	0.19

[a)]Maximum absorption wavelength of dyes in chloroform solution; [b)]Maximum absorption wavelength of dyes that were absorbed onto the TiO_2 films; [c)]onset potentials from CV measurements of thin films in 0.1 M Bu_4NPF_6 / CH_3CN solution, estimated from E_{HOMO} = -{(E^{on}_{ox}-$E_{1/2(ferrocene)}$) + 4.8} eV and E_{LUMO} = Estimated band gap by using onset of UV (film) – E_{HOMO}.

3.2.3 Theoretical molecular orbital calculations

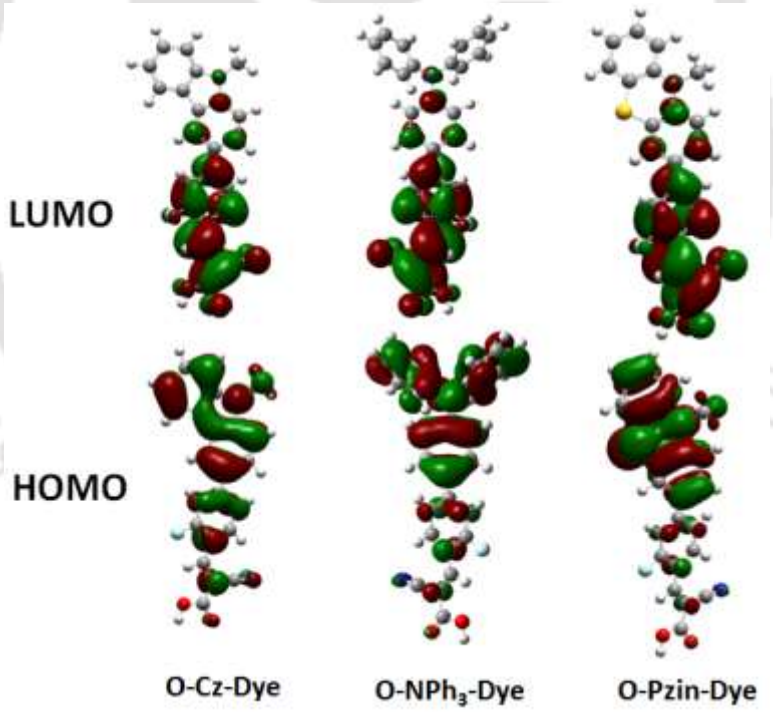

Figure 3.4 Electronic distributions of optimized frontier molecular orbitals in various dye molecules.

To understand the optimized structure of dyes and its geometries, electronic structures were ascertained by using Density functional theory (DFT) calculations in Gaussian 09 program at B3LYP/631G(d,p) basis sets and optimized geometries are shown in Figure 3.4. Carbazole, triphenylamine and phenothiazine donors share same ortho fluorine

substituted phenyl spacer and cyanoacrylic acid as anchoring group in D-π-A architecture. The optimized geometry of o-Cz dye clearly shows that planar structure and HOMO level are located on carbazole unit and strongly diffused into π-spacer. In o-NPh3, o-Pzin dyes have three dimensional, butterfly (two dimensional) structures respectively, but HOMO levels are mainly located on donor moiety and slightly diffused into fluorine substituted phenyl spacer. The LUMO levels should be located on the anchoring group, π-linker and slightly diffused into donor moieties. In all these dyes representative HOMO and LUMO levels are well separated, this is an advantage for charge migration from donor to acceptor in photo excitation state

3.2.4 Time-Resolved Photoluminescence (TRPL) studies:

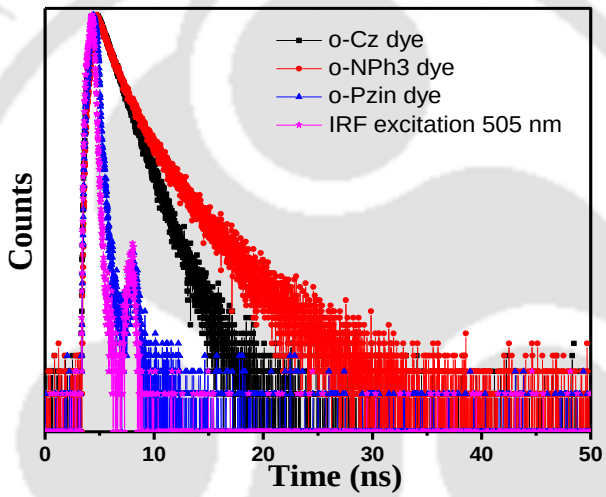

Figure 3.5 Time-resolved photoluminescence (TRPL) spectra of dyes recorded in $CHCl_3$ solution, with respect to their fitting curves at excitation wavelength of 505 nm.

Time-resolved photoluminescence (TRPL) measurements of dyes were carried out in chloroform solution. All the dyes were applied with a pulse excitation at 505 nm (Fig. 3.5) and corresponding data are summarized in Table 2. o-Cz dye exhibits higher lifetime value than o-NPh3 and o-Pzin dye. The order of lifetime of dyes are o-Cz dye > o-NPh3 dye > o-Pzin dye. The reason for higher lifetime of o-Cz dye may be due to the planar structure and more intra molecular charge transfer from donor to acceptor with respect to other dyes.

3.3 Fabrication of solar cell

TiO_2 photoelectrodes were prepared by following the previous reported process.[21] A transparent layer of TiO_2, with thickness 9µm and 12µm, was used as a photoelectrode. A TCO glass substrate on deposition of TiO_2 blocking (ethanolic titanium tetra isopropoxide) layer and calcined in tubular furnace at 450 °C for 10 min. Then, on the prepared TiO_2 thin film, the paste containing ethyl cellulose and α-terpineol was dispersed and the film was prepared by the doctor blade method, paste containing ethyl cellulose and α-terpineol to make disperse paste and the film was prepared by the same doctor blade method. The thickness of prepared TiO_2 film was 9 and 12µm. The electrode was cooled to 60 °C and soaked into the various sensitizer solutions (10^{-5} M in dicholoromethane and ethanol) for 24 h. Then counter electrode was prepared by spin coating method using Pt salt (50 mM H_2PtCl_6 solution in IPA) and electrode was calcined at 450 °C for 10 min. DSSC was assembled in a sandwich type configuration and sealed. The electrolyte consists of 0.5M LiI, 0.055M Iodine and 0.5M 4-tert-butyl pyridine in 3-methoxy propionitrile was inserted through the predrilled holes onto counter electrodes. Devices were stored in dark for 24 h prior to photovoltaic measurements.

3.4 Photovoltaic characterization

3.4.1 Photocurrent-Voltage properties measurements of 9 and 12 µm thickness devices

Figure 3.6 and 3.7 shows the *J-V* curves of DSSCs with 9µm, 12µm thickness of TiO_2 photoanode measured under light and dark condition. The results show that the energy conversion efficient (PCE) of the DSSCs changes dramatically with the thickness. The various photovoltaic parameters of DSSC with different film thicknesses are depicted in Table 3.3. From these results, the J_{sc}, V_{oc} and PCE of DSSC were seen to increase with the increase of the TiO_2 film thickness from 9µm to 12µm. This might be due to higher amount of dye loading in case of 12µm compare to 9µm thick film. From these results it can be assumed, 12µm thick TiO_2 film exhibits good performance compared to 9µm TiO_2 film. However, the J_{sc}, V_{oc} and PCE of o-Cz sensitized device are 8.91 mA/cm^2, 0.632 V and 3.6%, respectively which are higher than other two sensitizers. The higher PCE of o-Cz devices might be due to planar structural geometry and location of HOMO level located on donor moiety which strongly diffused in to the π-bridge.

The V_{oc} in 12µm TiO_2 film increases compared to 9µm TiO_2 thin film. The result indicates that the recombination rate increases with the increase of photoanode thickness.

It is due to the long diffusion distance for the photoelectron to transport to the electrode that enhances the probability of recombination.[22] The optimized thickness of TiO_2 film is 12µm, which enhance ~20% PCE compared to 9µm thick titania film.

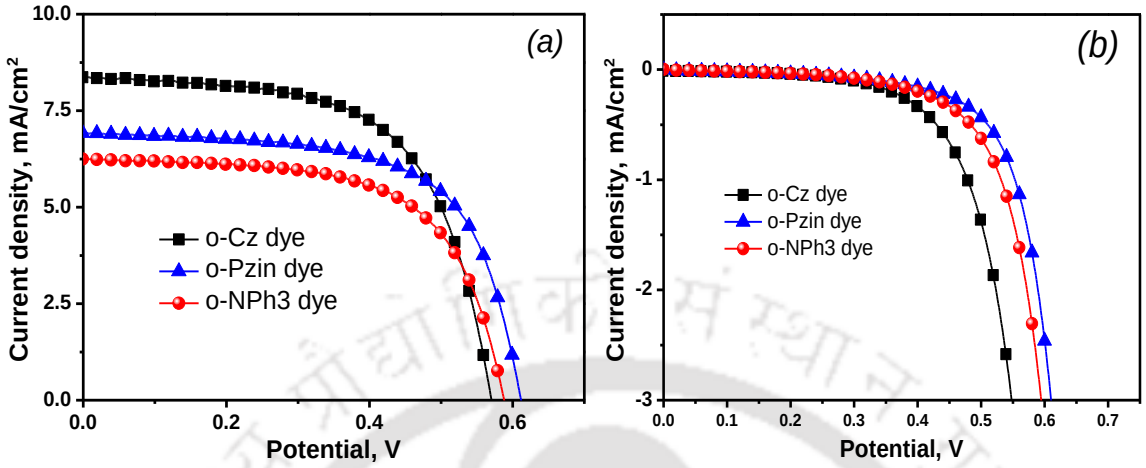

Figure 3.6 (a) 9µm TiO_2 thin film photoanode *J-V* measurements in light (left) and (b) dark condition.

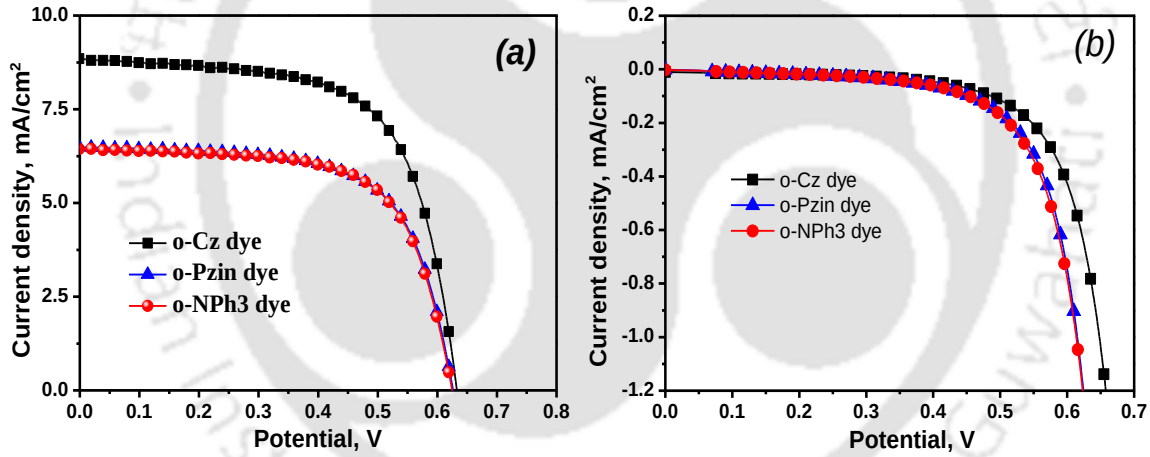

Figure 3.7 (a) 12 µm TiO_2 thin film photoanode *J-V* measurement in light. (b) dark condition.

For DSSCs, V_{oc} is determined by the difference between the Fermi level of TiO_2 and the redox potential of the electrolyte. The Fermi level can be shifted by changing the electron density in TiO_2. Since a higher electron density is obtained by longer electron lifetime, the higher V_{oc} of the o-Cz device could be related with longer electron lifetime if the conduction band edge potential is the same among the cells. This is because the presence of long alkyl chain onto both moieties (o-Cz and o-Pzin) suppresses the dye aggregation on TiO_2 photoanode surface, hence they show higher V_{oc} compared to o-NPh_3.

3.4.2 Electrochemical Impedance Spectroscopy (EIS) measurements of 9 and 12 µm thickness of DSSC devices

To get further insight into variation of V_{oc} among the DSSCs based on different thickness and sensitizers, the interfacial charge transfer process within DSSCs using EIS technique were investigated. As shown in Figure 3.8, two semicircles were observed in the Nyquist plots.

Table 3.3 Photovoltaic parameters of different thickness dyes

Devices	*Thickness*	J_{sc} *(mA/cm²)*	V_{oc} *(V)*	P_{max}	*FF (%)*	*η (%)*
o-Cz	**9 (µm)**	8.40 ± 0.4	0.570 ± 0.03	2.94	61.4	2.9 ± 0.4
o-Pzin		6.96 ± 0.3	0.611 ± 0.06	2.72	63.9	2.7 ± 0.2
o-NPh3		6.28 ± 0.2	0.587 ± 0.05	2.31	62.6	2.3 ± 0.1
o-Cz	**12 (µm)**	8.91 ± 0.5	0.632 ± 0.04	3.60	63.9	3.6 ± 0.4
o-Pzin		6.53 ± 0.3	0.625 ± 0.05	2.67	65.4	2.7 ± 0.1
o-NPh3		6.46 ± 0.2	0.624 ± 0.06	2.68	66.5	2.7 ± 0.3

The smaller (higher frequency from 10^3 to 10^5 Hz) and larger semicircles (lower frequency from 1 to 10^2 Hz) in the Nyquist plots were attributed to the charge transfer at the counter electrode/electrolyte interface and the TiO_2/dye/electrolyte interface respectively. Small circles were almost similar in all the dyes due to the use of same counter electrode and electrolyte. In the EIS measurement curves Figure 3.8 [fitted using equivalent circuit (Figure 3.8 (b))] and obtained parameters are shown in Table 3.4 and Table 3.5.

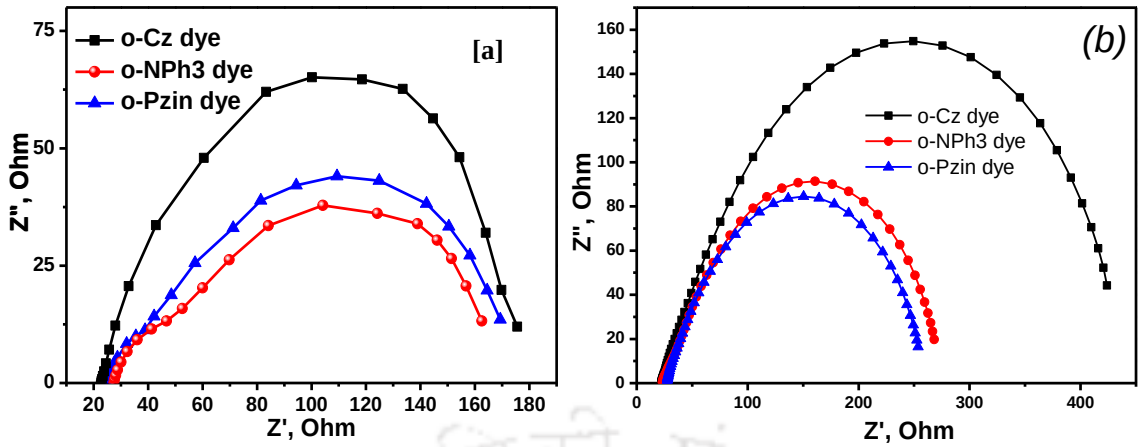

Figure 3.8 Electrochemical Impedance measurements of 9µm thickness device (a), 12µm thickness device recorded in dark at -0.65 V DC bias (b) and equivalent circuit model used for fitting (c) (insert the Fig. 8).

3.4.3 Electron lifetime (τ_e) measurements of 9 and 12 µm thickness devices

The recombination resistance of the o-Cz device was larger than those of other devices according to the value derived from curve fitting in Z-view software. Electron lifetime (τ_n) calculated for all three devices are of the following order; o-NPh3 (100ms) < o-PZin (106 ms) < o-Cz (230 ms).

Table 3.4 DSSC parameters R_{pt}, R_{rec}, τ_n and J_o extracted from EIS measurements and Tafel polarization study of 9µm thickness device

Dye	R_{pt} (Ohm)[a]	R_{rec} (Ohm) [a]	CPE-P [a]	τ_n (ms)[a]	J_o ($\mu A/cm^2$)[b]
o-Cz	22.5	150	0.68	0.159	0.52
o-Pzin	27.0	105	0.67	0.138	0.40
o-NPh3	25.5	132	0.63	0.140	0.39

Table 3.5 DSSC parameters R_{pt}, R_{rec}, τ_n and J_o extracted from EIS measurements and Tafel polarization study of 12 µm thickness device

Dye	R_{pt} (Ohm)[a]	R_{rec} (Ohm) [a]	CPE-P [a]	τ_n (ms)[a]	J_o ($\mu A/cm^2$)[b]
o-Cz	19.9	440	0.66	0.230	0.61
o-Pzin	24.8	384	0.65	0.106	0.48
o-NPh3	22.3	246	0.56	0.100	0.43

[a]Values estimated by fitting nyquist plot [b]estimated from tafel polarization curves

This trend is in good agreement with the variation tendency of V_{oc} (o-NPh3 (0.624V) < o-Pzin (0.625V) < o-Cz (0.632V)) observed in the *J-V* curves. The o-NPh3 dye has slightly lower τ_n and recombination resistance as compared to the o-Cz and o-Pzin dyes having long alkyl chain, indicating that the presence of an alkyl chain can act as charge suppressor, resulting into lower recombination resistance.[23]

Open-circuit voltage decay (OCVD) method is a powerful technique to study electron lifetime and electron recombination velocity in DSSCs.[24] In order to conduct the OCVD measurement, the simulated solar light is illuminated at device and a steady-state voltage was obtained. This indicated that equilibrium between electron injection and electron recombination is attained at the TCO surface. A potentiostat then monitors the decay of V_{oc}, after interrupting the illumination.

Figure 3.9 shows the OCVD decay curves of the 12µm TiO_2 thick photoanode with different sensitizer based devices. It was observed that the OCVD curve of the o-Cz device was much slower than that o-Pzin and o-NPh3. It was proposed to quantify the extent of electron recombination with the redox electrolyte and has been proven effective.

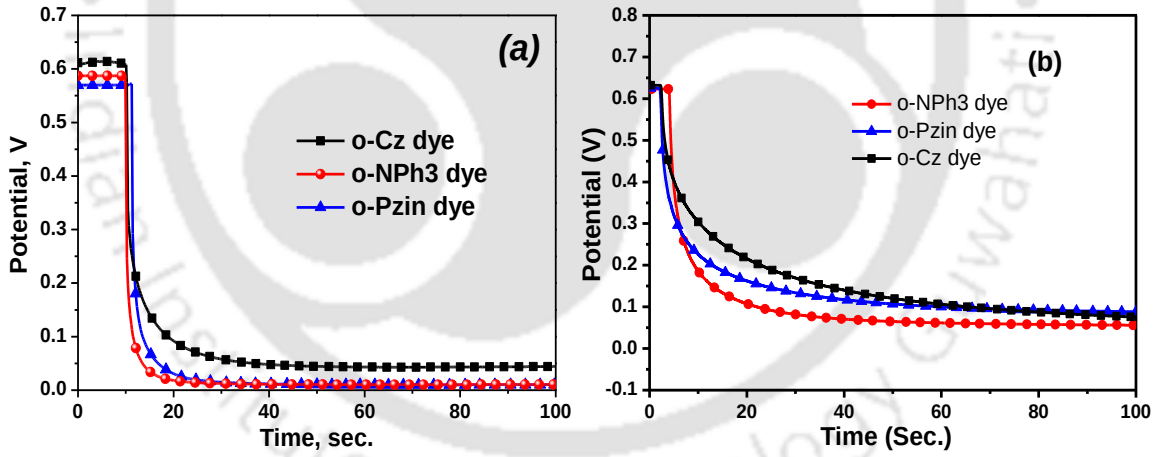

Figure 3.9 OCVD spectra of (a) 9 µm thickness device, (b) 12 µm thickness device, decay curves after illumination are turned off.

3.4.4 Tafel Polarization measurements of 9 and 12 µm thickness devices

Tafel polarization technique used to back electron transfer reaction study in DSSCs device has been show in Figure 3.10. This technique is used to analyze the interface charge transfer of iodine/triiodide redox mediator on the photoanode surface. The kinetics of the anodic reactions occurring at the electrolyte and TiO_2 photanode interface can be represented using the Buttler-Volmer equation,

$$j = -j\left(exp^{\alpha_c nF}/_{RT}\,(E - E_{eq}) - exp^{\alpha_a nF}/_{RT}\,(E - E_{eq})\right)$$

J_0 is the exchange current density, E_{eq} is the equilibrium potential of iodide/triiodide redox system, E is the applied voltage; α_a and α_c are the anodic and cathodic transfer coefficients respectively. It is clear from this equation that $j = j_o$ as $E = E_{eq}$ in dark. Tafel measurement data was fitted using corr-view software and J_o was estimated for all devices shown in Table 3.4 and 3.5. From the above technique, it is concluded that DSSC device with o-Cz sensitizer possess higher J_o (6.1×10^{-5} cm^2) compared to other sensitizer based devices. As this, J_o value is inversely proportional to sheet resistance, R_{pt}, (19.9 Ω), confirm smooth electron transport between Pt/electrolyte interface.

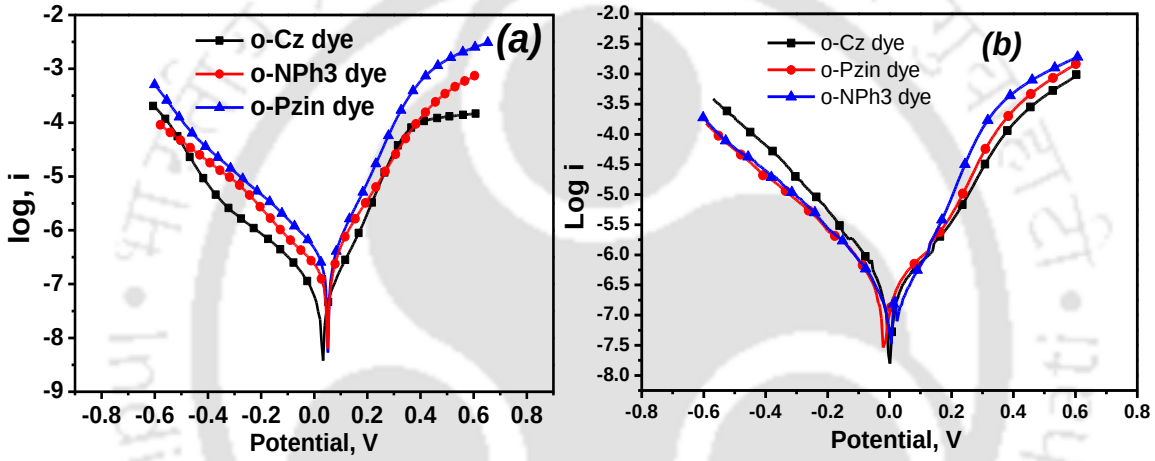

Figure 3.10 Tafel polarization study of (a) 9 µm thickness devices, (b) 12 µm thickness devices.

3.4.5 IPCE spectra of 9 and 12 µm thickness devices

Figure 3.11 shows the IPCE of solar cells sensitized by dyes with 9µm, 12µm thickness photoanode. Compared to the DSSC cell sensitized by the dyes with 9 mm thickness, the DSSC cell sensitized by the dyes with 12µm thickness have higher PCE, IPCE spectra because of their higher J_{sc} and V_{oc}. The devices at 12µm thickness reduce the charge recombination, leading to improvement in the J_{sc}. However, the V_{oc} related to the electron density is obtained by longer electron life time, as explained by the above analysis (Tafel, OCVD and EIS). The onset wavelength of the IPCE spectra was 700-750 nm for all the three dyes. The dye, o-CZ at 12µm photoanode thickness exhibits highest IPCE value ~40-45% in the range of 420-620 nm, showing highly efficient performance of the solar cell performance as compared to o-NPh3 and o-Pzin dyes.

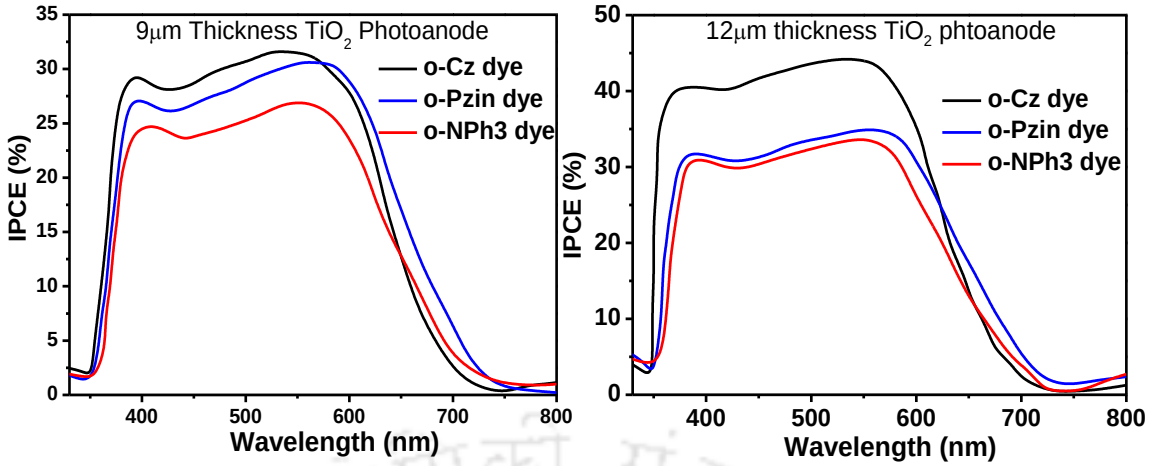

Figure 3.11 IPCE characteristics of the sensitizers 9μm TiO_2 photoanode thickness (left side) 12μm TiO_2 photoanode thickness (right side).

3.5 Experimental section

3.5.1 General synthetic procedure of compound 1a-3a:

In a clean round bottom flask, a mixture of bromo contain starting material (0.2 mmol) and 3-Fluoro 4-formylphenyl boronic acid (0.25 mmol) and 2M K_2CO_3 aqueous solutions (6 ml) to add THF (12 ml) solution and degassed with argon. Finally, $Pd(PPh_3)_4$ (20 mol%) catalyst added to the reaction mixture under inert atmosphere. Then the reaction was carried out by 12 h reflux. After cooling the reaction down to RT, evaporate the THF solution under reduced pressure. The extracted compound was wash with chloroform and brine solution. Finally, extracted chloroform was dried with anhydrous $NaSO_4$. The liquid yellow residue was purified by column chromatography (silica gel, ethyl acetate-hexane 1:2 as eluent).

3.5.2 General synthetic procedure of organic sensitizers

In a clean RB, the mixture of compound '1a-3a' (0.2 mmol) and cyanoacetic acid (0.3 mmol) dissolve in acetonitrile and chloroform (1:1) solution. Finally, piperidine (0.02 mmol) was added to the solution, and then the solution was refluxed for 10 h. After cooling, the solution was removed by rotavapour in reduced pressure. Extracted compound was wash with chloroform and 0.1 M aqueous solution of HCl. Then the organic layer was dried with $NaSO_4$. The solid was finally washed with hexane and 2% ethyl acetate in hexane to get a pure compound.

2-fluoro-4-(9-hexyl-9*H*-carbazol-3-yl)benzaldehyde (1a):

Yield-80%, ^{1}H NMR (400 MHz, $CDCl_3$): δ (ppm) 10.37 (s, 1H), 8.33 (d, 1H), 8.16 (d, 1H), 7.93 (t, 2H), 7.72 (d, 1H), 7.61 (m, 2H), 7.53-7.50 (m, 2H), 7.47-7.43 (m, 4H), 7.30

(t, 2H), 4.30 (t, 2H), 1.88 (t, 2H), 1.45-1.28 (m, 6H), 0.92-0.87 (m, 3H). ^{13}C NMR (100 MHz, $CDCl_3$): δ (ppm) 187.15, 166.73, 164.08, 150.70, 141.04, 129.34, 129.19, 127.32, 126.39, 125.01, 123.73, 123.15, 122.86, 120.63, 119.54, 119.34, 114.23, 109.40, 109.24, 43.39, 31.73, 29.11, 27.12, 22.72, 14.20. ^{19}F NMR (376 MHz, $CDCl_3$): δ (ppm) -121.75. HRMS (ESI) m/z: $[M+H]^+$ calcd for $C_{25}H_{25}FNO$ 374.1920, found 374.1928.

4'-(diphenylamino)-3-fluoro-[1,1'-biphenyl]-4-carbaldehyde (2a):

Yield-75%, ^{1}H NMR (400 MHz, $CDCl_3$): δ (ppm) 10.33 (s, 1H), 7.88 (t, 1H), 7.48-7.44 (m, 2H), 7.31-7.25 (m, 6H), 7.14-7.05 (m, 8H). ^{13}C NMR (100 MHz, $CDCl_3$): δ (ppm) 190.71, 160.98, 159.32, 148.63, 147.40, 136.61, 135.09, 130.98, 130.04, 129.60, 127.60, 126.28, 125.21, 123.78, 122.54, 116.64, 116.48. ^{19}F NMR (376 MHz, $CDCl_3$): δ (ppm) -121.74. HRMS (ESI) m/z: $[M+H]^+$ calcd for $C_{25}H_{19}FNO$ 368.1451, found 368.1451.

2-fluoro-4-(10-hexyl-10*H*-phenothiazin-3-yl)benzaldehyde (3a):

Yield-70%, ^{1}H NMR (400 MHz, $CDCl_3$): δ (ppm) 10.41 (s, 1H), 7.93 (t, 1H), 7.45(t, 3H), 7.43 (s, 1H), 7.36(d, 1H), 7.24-7.19 (m, 3H), 7.01(t, 1H), 6.96-6.93 (m, 3H), 3.92 (t, 2H), 1.90 (t, 2H), 1.40-1.38 (m, 6H), 0.96-0.95 (m, 3H). ^{13}C NMR (100 MHz, $CDCl_3$): δ (ppm) 186.88, 166.40, 163.87, 148.38, 146.11, 144.52, 132.25, 129.20, 127.59, 126.22, 125.81, 125.63, 124.05, 122.84, 122.31, 115.70, 115.59, 113.78, 113.56, 47.81, 31.57, 26.87, 26.65, 22.91, 14.17. ^{19}F NMR (376 MHz, $CDCl_3$): δ (ppm) -121.46. HRMS (ESI) m/z: $[M+H]^+$ calcd for $C_{25}H_{25}FNOS$ 406.1640, found 406.1641.

(*E*)-2-cyano-3-(2-fluoro-4-(9-hexyl-9H-carbazol-3-yl)phenyl)acrylic acid (o-Cz dye):

Yield-85%, ^{1}H NMR (400 MHz, $CDCl_3$): δ (ppm) 8.35 (s, 2H), 8.05 (s, 2H), 7.94 (s, 1H), 7.42 (m, 5H), 7.36 (d, 1H), 4.02 (t, 2H), 1.85 (t, 2H), 1.39-1.24 (m, 6H), 0.82 (m, 3H). ^{13}C NMR (100 MHz, $CDCl_3$): δ (ppm) 163.04, 161.33, 148.43, 140.87, 140.67, 129.16, 128.93, 126.95, 126.13, 124.70, 123.34, 122.76, 120.51, 119.30, 118.78, 117.99, 116.61, 114.16, 113.51, 113.36, 109.10, 108.97, 43.08, 31.59, 28.92, 26.96, 22.60, 14.08. ^{19}F NMR (376 MHz, $CDCl_3$): δ (ppm) -121.15. HRMS (ESI) m/z: $[M+H]^+$ calcd for $C_{28}H_{26}FN_2O_2$ 441.1978, found 441.1974.

(*E*)-2-cyano-3-(4'-(diphenylamino)-3-fluoro-[1,1'-biphenyl]-4-yl)acrylic acid (o-NPh3 dye):

Yield-80%, ^{1}H NMR (400 MHz, $CDCl_3$): δ (ppm) 8.27 (s, 1H), 8.05 (s, 1H), 7.23 (s, 1H), 7.20 (m, 4H), 7.13 (m, 3H), 6.95 (m, 8H), 6.84 (m, 2H). ^{13}C NMR (100 MHz, $CDCl_3$): δ (ppm) 162.55, 160.83, 148.30, 147.63, 147.40, 145.46, 142.01, 139.50, 131.78, 129.55, 129.36, 129.09, 127.71, 125.06, 124.77, 123.60, 122.77, 122.03, 119.10, 114.28, 112.93,

112.87. ^{19}F NMR (376 MHz, $CDCl_3$): δ (ppm) 113.09. HRMS (ESI) m/z: $[M+H]^+$ calcd for $C_{28}H_{20}FN_2O_2$ 435.1509, found 435.1500.

(*E*)-2-cyano-3-(2-fluoro-4-(10-hexyl-10*H*-phenothiazin-3-yl)phenyl)acrylic acid (o-Pzin dye):

Yield-85%, ^{1}H NMR (400 MHz, $CDCl_3$): δ (ppm) 8.56 (s, 1H), 8.45 (s, 1H), 7.43(d, 1H), 7.38 (d, 1H), 7.32 (s, 1H), 7.28 (d, 1H), 7.15 (t, 1H), 6.93 (t, 1H), 6.85 (m, 3H), 3.83 (t, 2H), 1.80 (t, 2H), 1.31-1.26 (m, 6H), 0.89 (m, 3H). ^{13}C NMR (100 MHz, $CDCl_3$): δ (ppm) 167.24, 163.51, 161.79, 147.80, 146.86, 146.45, 144.43, 131.92, 129.66, 129.24, 127.63, 126.25, 125.66, 125.60, 123.89, 123.02, 122.59, 118.01, 115.65, 115.50, 113.27, 113.12, 102.70, 47.83, 31.71, 29.88, 26.78, 22.78, 14.18. ^{19}F NMR (376 MHz, $CDCl_3$): δ (ppm) -111.83. HRMS (ESI) m/z: $[M+H]^+$ calcd for $C_{28}H_{26}FN_2O_2S$ 406.1640, found 406.1641.

3.6 Summary

A series of new DSSC devices have been fabricated containing newly developed organic sensitizers with varying donor moieties such as carbazole, phenothiazine and triphenylamine. The influence of varying the donor moiety in the sensitizers as well as the effect of the TiO_2 thickness (9 and 12 mm) resulted in interesting optical and photovoltaic characteristics. The o-Cz dye device with 12 mm thickness displayed a reduced charge recombination compared to the other devices reported herein, which led to an improvement in J_{sc}. As a result of these variations, the solar cell based on o-Cz dye showed superior photovoltaic performance with a J_{sc} of 8.91 mA/cm^2, a V_{oc} of 0.632 V, and an *FF* of 63.9, corresponding to an overall conversion efficiency of 3.6% (±0.4) under standard AM 1.5G irradiation. Overall these results confirm that single ortho fluorine substitution in cyanoacrylic acid dyes is better than double substitution at the ortho position, whereas the planar structures in o-Cz dyes are better than the three and two dimensional structures for improved PCE and other device parameters without using any additional co-absorbents.

3.7 References:

1. O'regan, B.; Grätzel, M. *Nature* **1991**, *353*, 737-740.
2. Hardin, B. E.; Snaith, H. J.; McGehee, M. D. *Nat. Photonics*, **2012**, *6*, 162-169.
3. Hagfeldt, A.; Boschloo, G.; Sun, L. C.; Kloo, L.; Pettersson, H. *Chem. Rev*. **2010**, *110*, 6595-6663.
4. Gao, F.; Wang, Y.; Shi, D.; Zhang, J.; Wang, M. K.; Jing, X. Y.; Humphry-Baker, R.; Wang, P.; Zakeeruddin, S. M.; Grätzel, M. *J. Am. Chem. Soc*. **2008**, *130*, 10720-10728.
5. Mathew, S.; Yella, A.; Gao, P.; Humphry-Baker, R.; Curchod, B. F. E.; Ashari-Astani, N.; Tavernelli, I.; Rothlisberger, U.; Nazeeruddin, M. K.; Grätzel, M. *Nat. Chem*. **2014**, *6*, 242-247.
6. Bessho, T.; Zakeeruddin, S. M.; Yeh, C. Y.; Diau, E. W. G.; Grätzel, M. *Angew. Chem. Int. Ed*. **2010**, *49*, 6646-6649.
7. Zeng, W. D.; Cao, Y. M.; Bai, Y.; Wang, Y. H.; Shi, Y. S.; Zhang, M.; Wang, F. F.; Pan, C. Y.; Wang, P. *Chem. Mater*. **2010**, *22*, 1915-1925.
8. Cao, Y. M.; Cai, N.; Wang, Y. L.; Li, R. Z.; Yuan, Y.; Wang, P. *Phys. Chem. Chem. Phys*. **2012**, *14*, 8282-8286.
9. Yao, Z. Y.; Zhang, M.; Wu, H.; Yang, L.; Li, R. Z.; Wang, P. *J. Am. Chem. Soc*. **2015**, *137*, 3799-3802.
10. Ogawa, J.; Agrawal, S.; Koumura, N.; Mori, S. *J. Phys. Chem. C* **2016**, *120*, 3612-3618.
11. Murakami, T. N.; Koumura, N.; Kimura, M.; Mori, S. *Langmuir* **2014**, *30*, 2274-2279.
12. Cho, N.; Han, J.; Song, K.; Kang, M. S.; Jun, M. J.; Kang, Y.; Ko, J. *Tetrahedron* **2014**, *70*, 427-433.
13. Chen, D. Y.; Hsu, Y. Y.; Hsu, H. C.; Chen, B. S.; Lee, Y. T.; Fu, H.; Chung, M. W.; Liu, S. H.; Chen, H. C.; Chi, Y.; Chou, P. T. *Chem. Commun*. **2010**, *46*, 5256-5258.
14. Chen, B. S.; Chen, D. Y.; Chen, C. L.; Hsu, C. W.; Hsu, H. C.; Wu, K. L.; Liu, S. H.; Chou, P. T.; Chi, Y. *J. Mater. Chem*. **2011**, *21*, 1937-1945.
15. Scrascia, A.; De Marco, L.; Laricchia, S.; Picca, R. A.; Carlucci, C.; Fabiano, E.; Capodilupo, A. L.; Della Sala, F.; Gigli, G.; Ciccarella, G. *J. Mater. Chem. A* **2013**, *1*, 11909-11921.

16. Lin, Y. D.; Chow, T. J. *J. Photoch. Photobio. A* **2012**, *230*, 47-54.
17. Listorti, A.; O'Regan, B.; Durrant, J. R. *Chem. Mater*. **2011**, *23*, 3381-3399.
18. Reynal, A.; Forneli, A.; Martinez-Ferrero, E.; Sanchez-Diaz, A.; Vidal-Ferran, A.; O'Regan, B. C.; Palomares, E. *J. Am. Chem. Soc*. **2008**, *130*, 13558-13567.
19. Zhou, Z. J.; Fan, J. Q.; Wang, X.; Zhou, W. H.; Du, Z. L.; Wu, S. X. *ACS Appl. Mater. Inter*. **2011**, *3*, 4349-4353.
20. Baglio, V.; Girolamo, M.; Antonucci, V.; Arico, A. S. *Int. J. Electrochem. Sc*. **2011**, *6*, 3375-3384.
21. Soni, S. S.; Fadadu, K. B.; Vaghasiya, J. V.; Solanki, B. G.; Sonigara, K. K.; Singh, A.; Das, D.; Iyer, P. K. *J. Mater. Chem. A* **2015**, *3*, 21664-21671.
22. Tsai, J. K.; Hsu, W. D.; Wu, T. C.; Meen, T. H.; Chong, W. J. *Nanoscale Res. Lett*. **2013**, *8*, 459.
23. Babel, A.; Jenekhe, S. A. *Synthetic Met*. **2005**, *148*, 169-173.
24. Bisquert, J.; Zaban, A.; Greenshtein, M.; Mora-Sero, I. *J. Am. Chem. Soc*. **2004**, *126*, 13550-13559.

Appendix

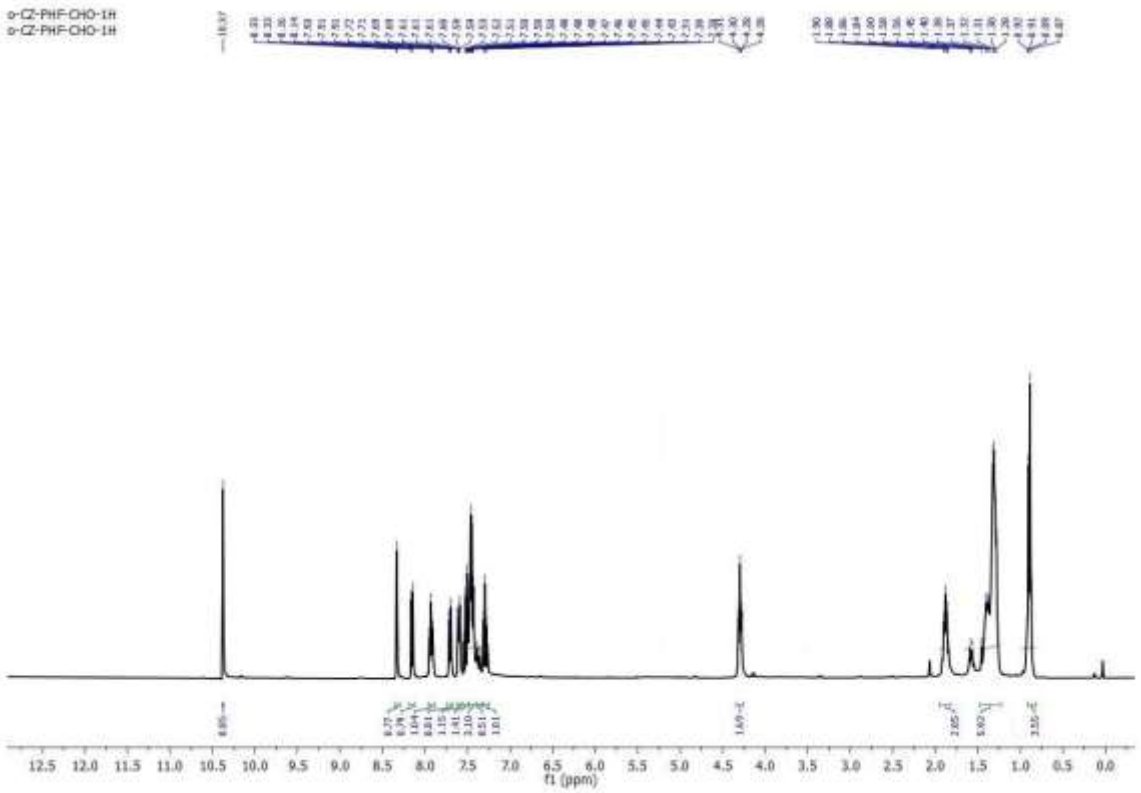

^{1}H NMR spectrum of 2-fluoro-4-(9-hexyl-9*H*-carbazol-3-yl)benzaldehyde (1a) in $CDCl_3$.

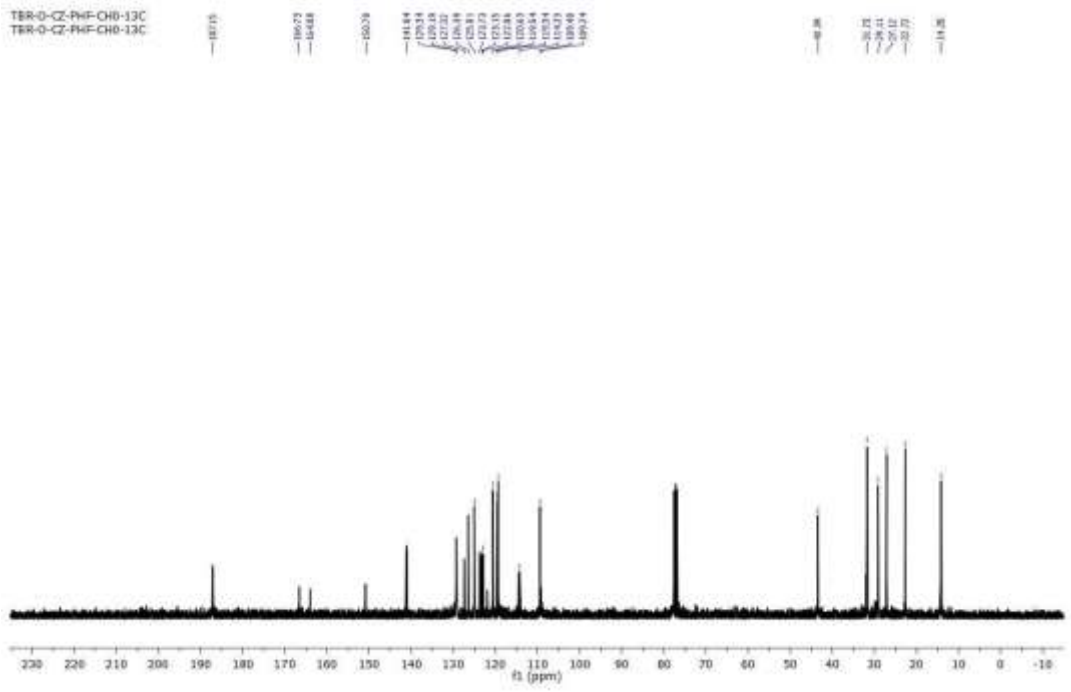

^{13}C NMR spectrum of 2-fluoro-4-(9-hexyl-9*H*-carbazol-3-yl)benzaldehyde (1a) in $CDCl_3$.

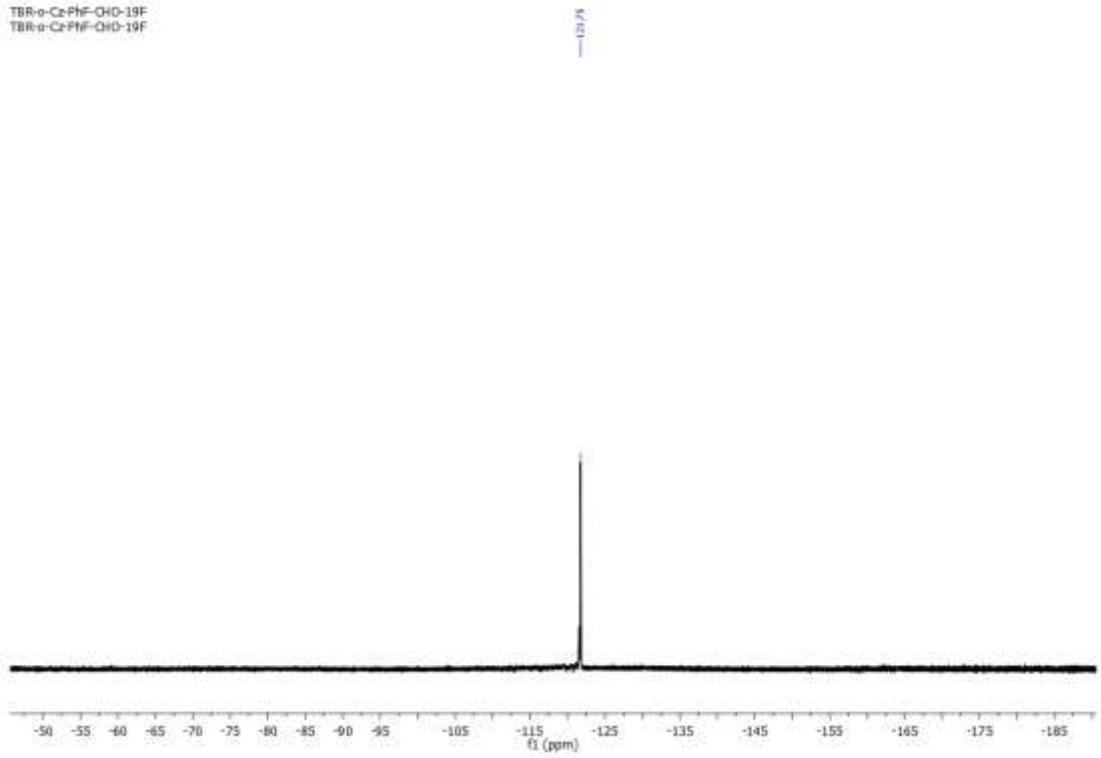

^{19}F NMR spectrum of 2-fluoro-4-(9-hexyl-9*H*-carbazol-3-yl)benzaldehyde (1a) in $CDCl_3$.

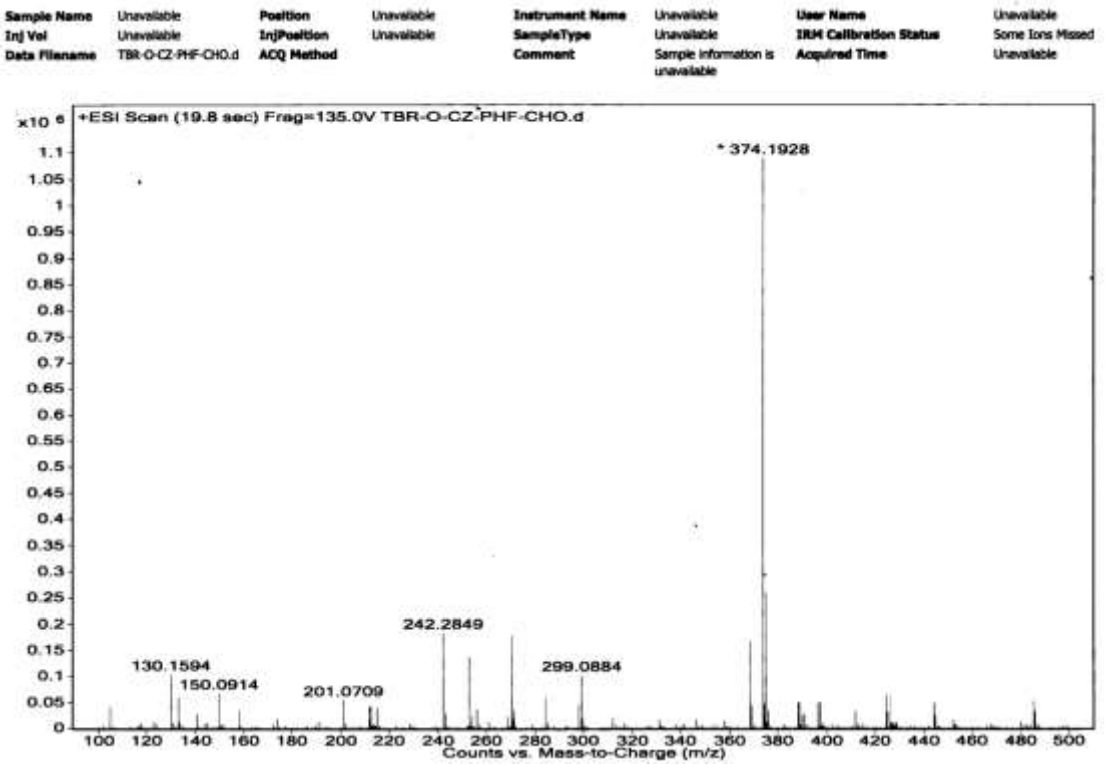

HRMS (ESI) spectrum of 2-fluoro-4-(9-hexyl-9*H*-carbazol-3-yl)benzaldehyde. (1a).

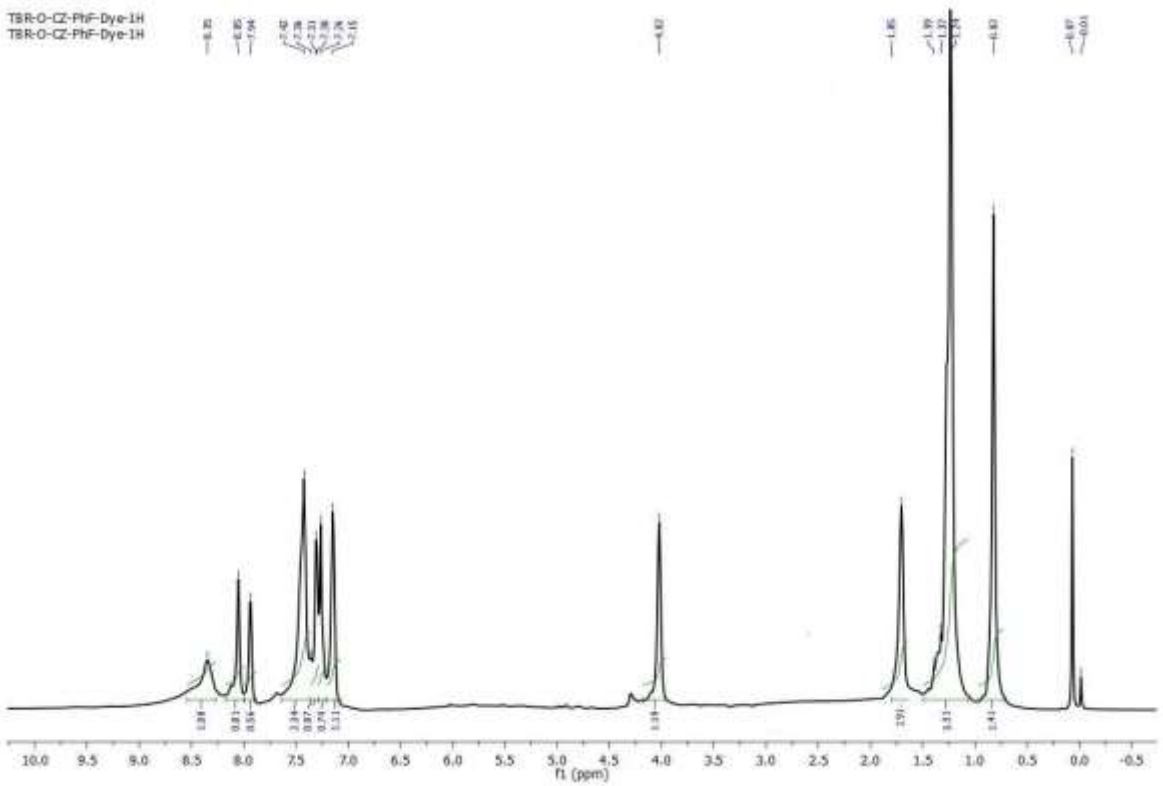

^{1}H NMR spectrum of (*E*)-2-cyano-3-(2-fluoro-4-(9-hexyl-9*H*-carbazol-3-yl)phenyl)-acrylic acid (o-Cz dye) in $CDCl_3$.

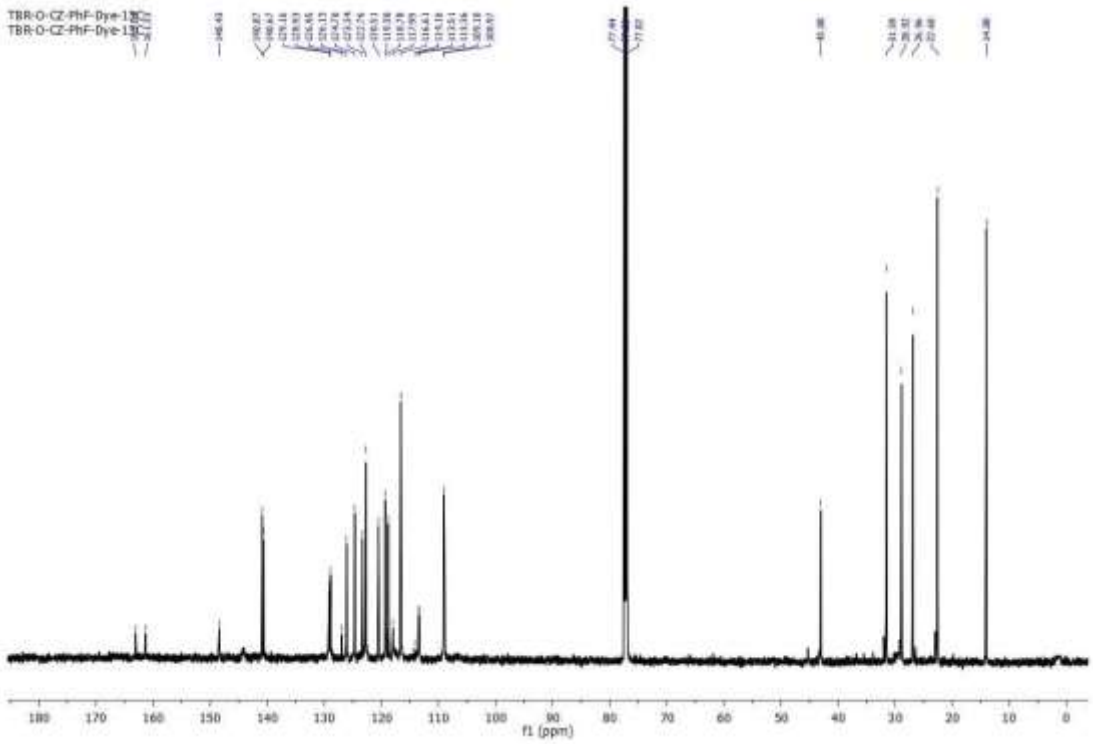

^{13}C NMR spectrum of (*E*)-2-cyano-3-(2-fluoro-4-(9-hexyl-9*H*-carbazol-3-yl)phenyl)-acrylic acid (o-Cz dye) in $CDCl_3$.

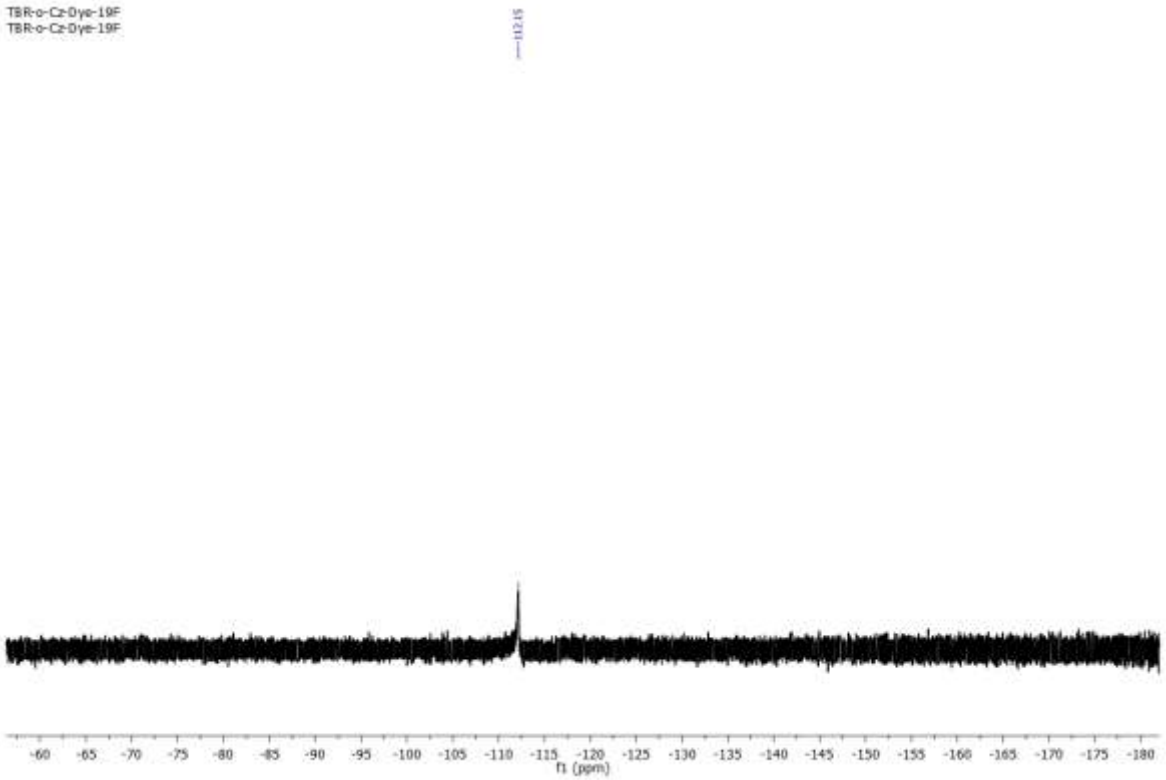

^{13}C NMR spectrum of (*E*)-2-cyano-3-(2-fluoro-4-(9-hexyl-9*H*-carbazol-3-yl)phenyl)-acrylic acid (o-Cz dye) in $CDCl_3$.

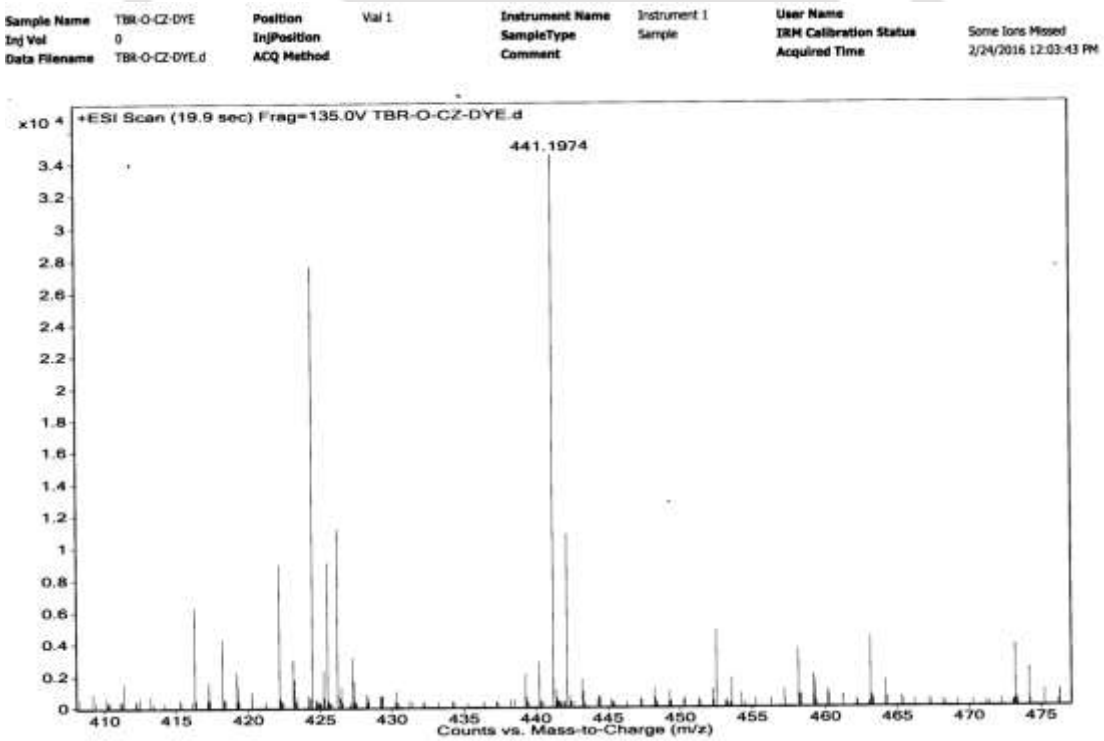

HRMS spectrum of (*E*)-2-cyano-3-(2-fluoro-4-(9-hexyl-9*H*-carbazol-3-yl) phenyl)-acrylic acid (o-Cz dye).

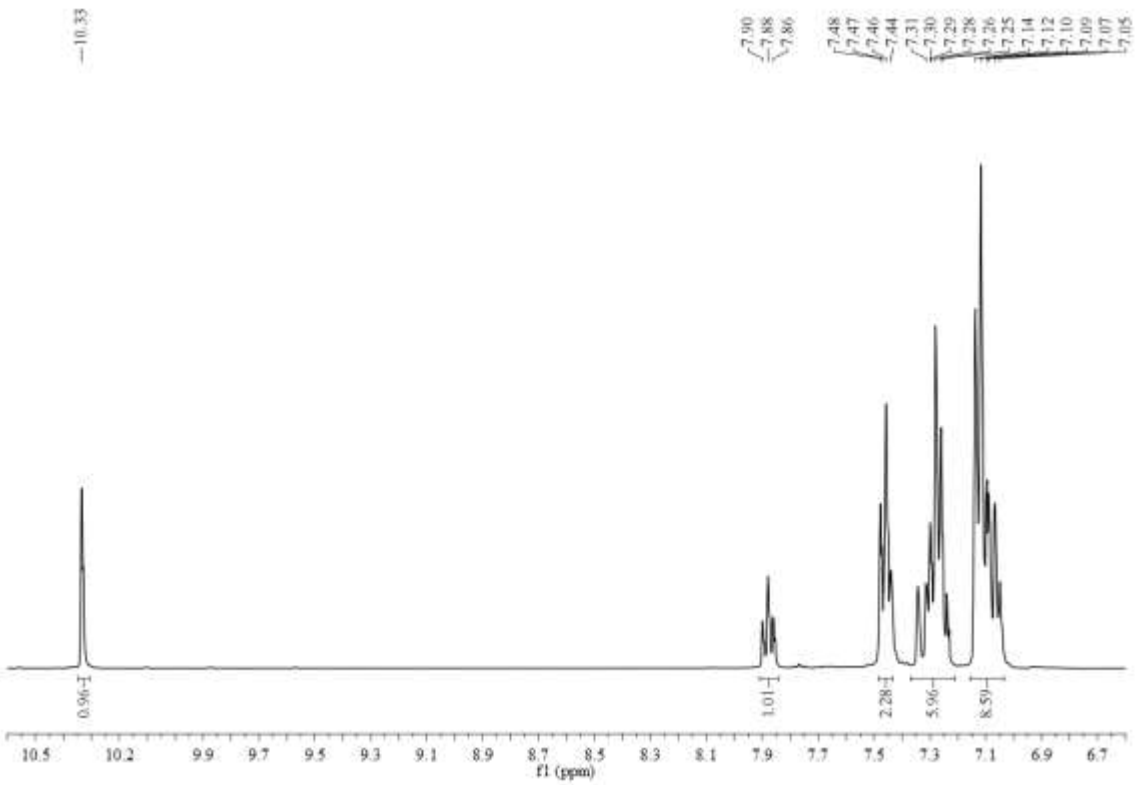

^{1}H NMR spectrum of 4'-(diphenylamino)-3-fluoro-[1,1'-biphenyl]-4-carbaldehyde (2a) in $CDCl_3$.

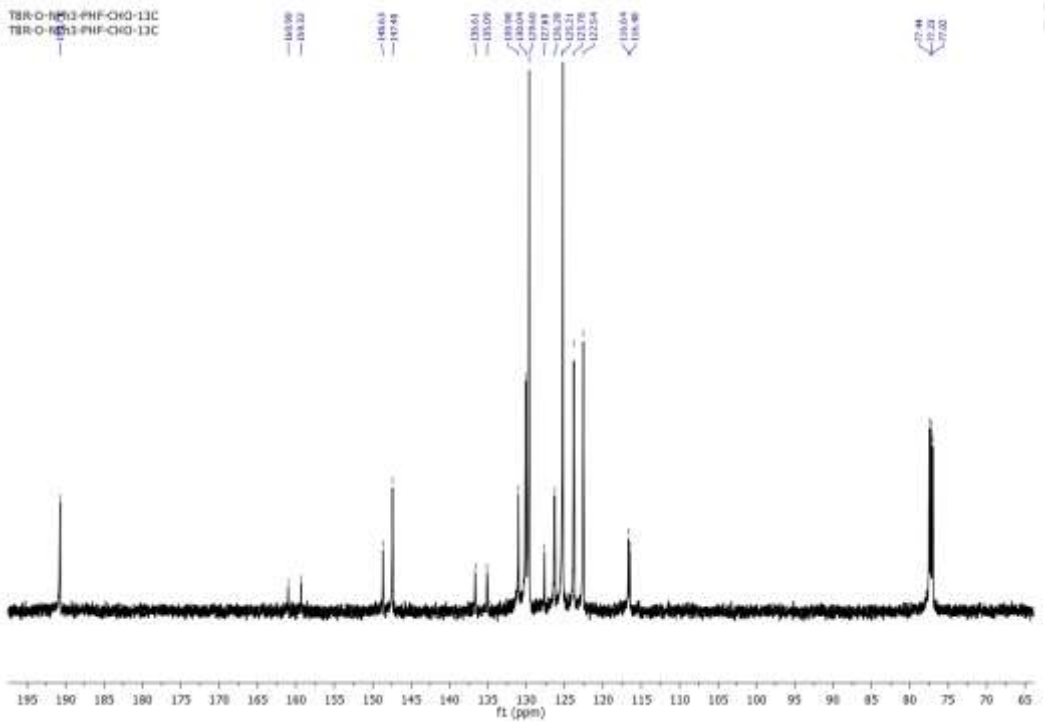

^{13}C NMR spectrum of 4'-(diphenylamino)-3-fluoro-[1,1'-biphenyl]-4-carbaldehyde (2a) in $CDCl_3$.

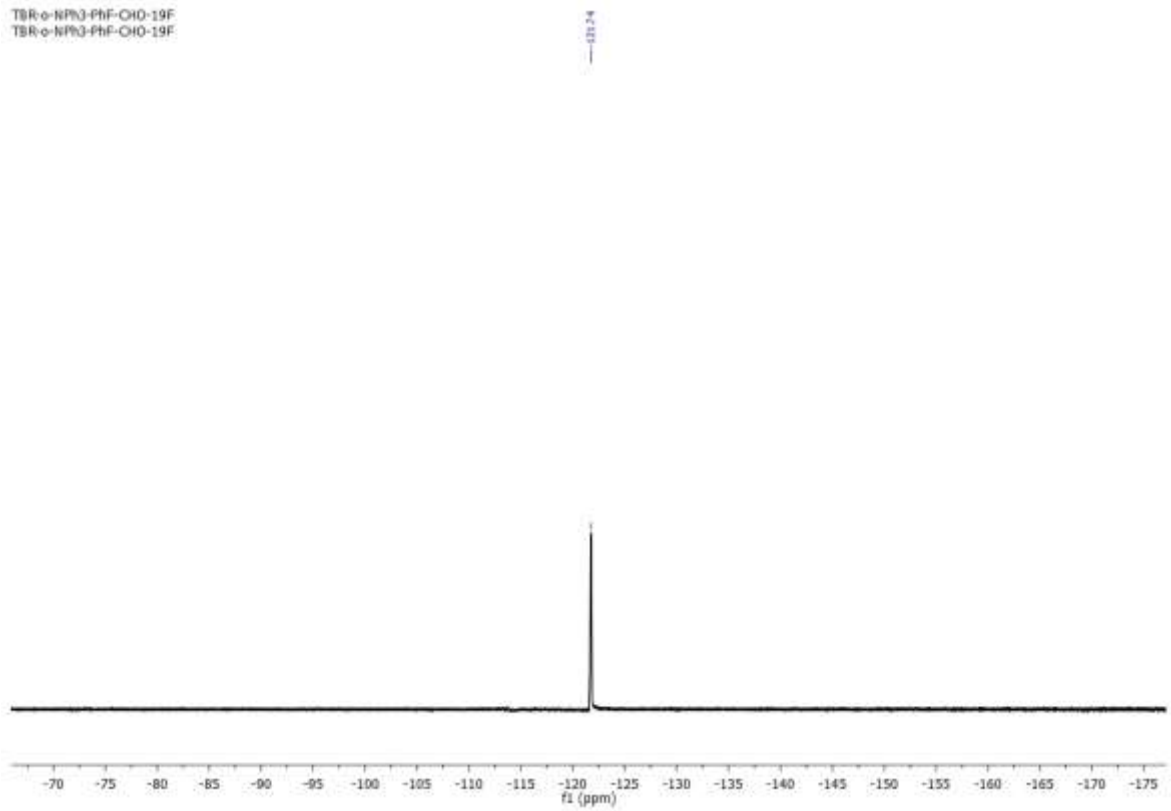

^{19}F NMR spectrum of 4'-(diphenylamino)-3-fluoro-[1,1'-biphenyl]-4-carbaldehyde (2a) in $CDCl_3$.

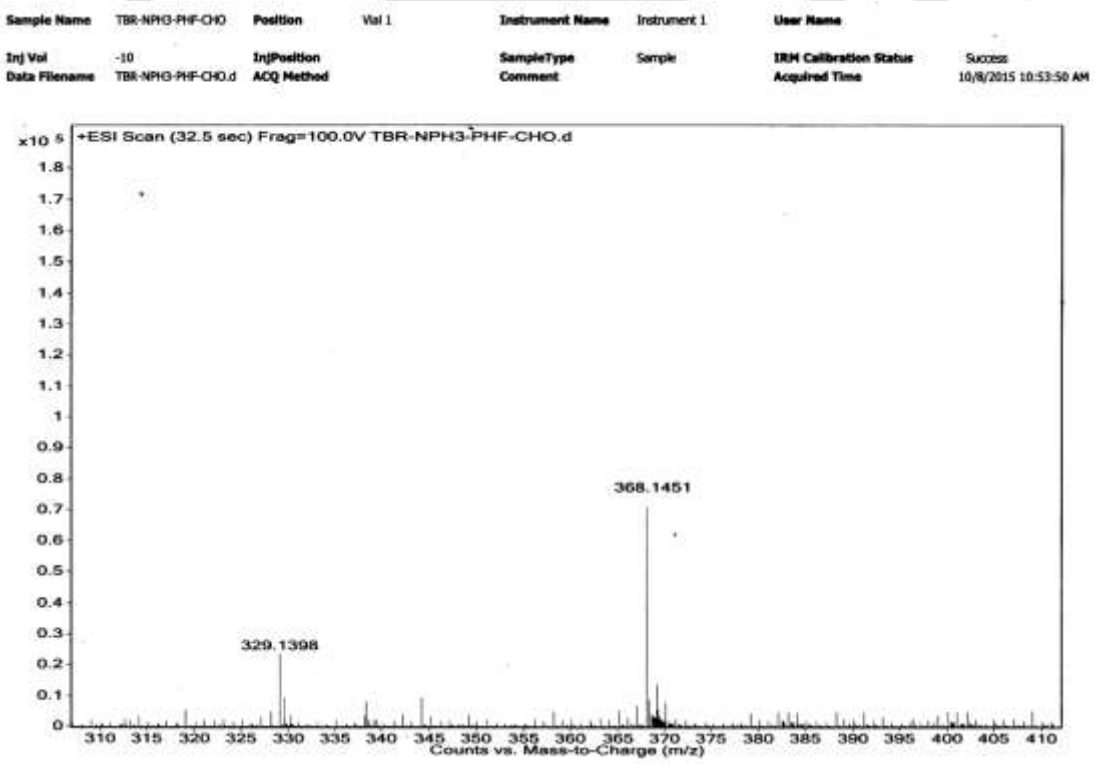

HRMS (ESI) spectrum of 4'-(diphenylamino)-3-fluoro-[1,1'-biphenyl]-4-carbaldehyde (2a).

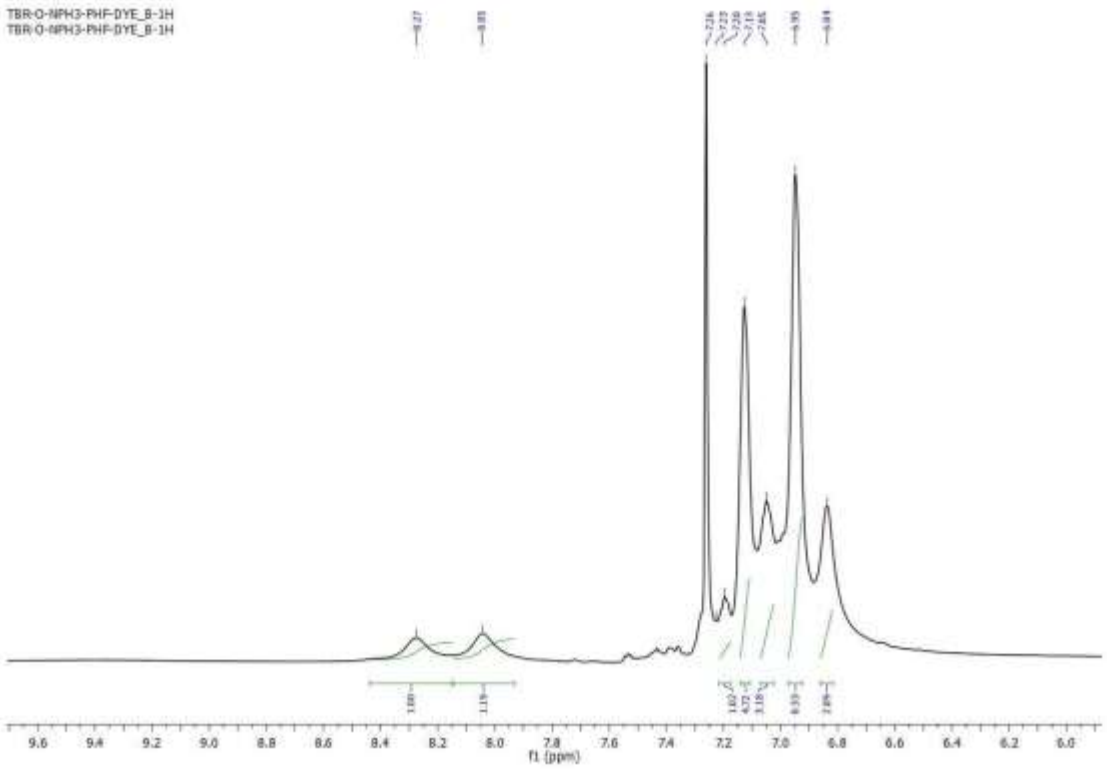

^{1}H NMR spectrum of (*E*)-2-cyano-3-(4'-(diphenylamino)-3-fluoro-[1,1'-biphenyl]-4-yl)acrylic acid (o-NPh3 dye) in $CDCl_3$.

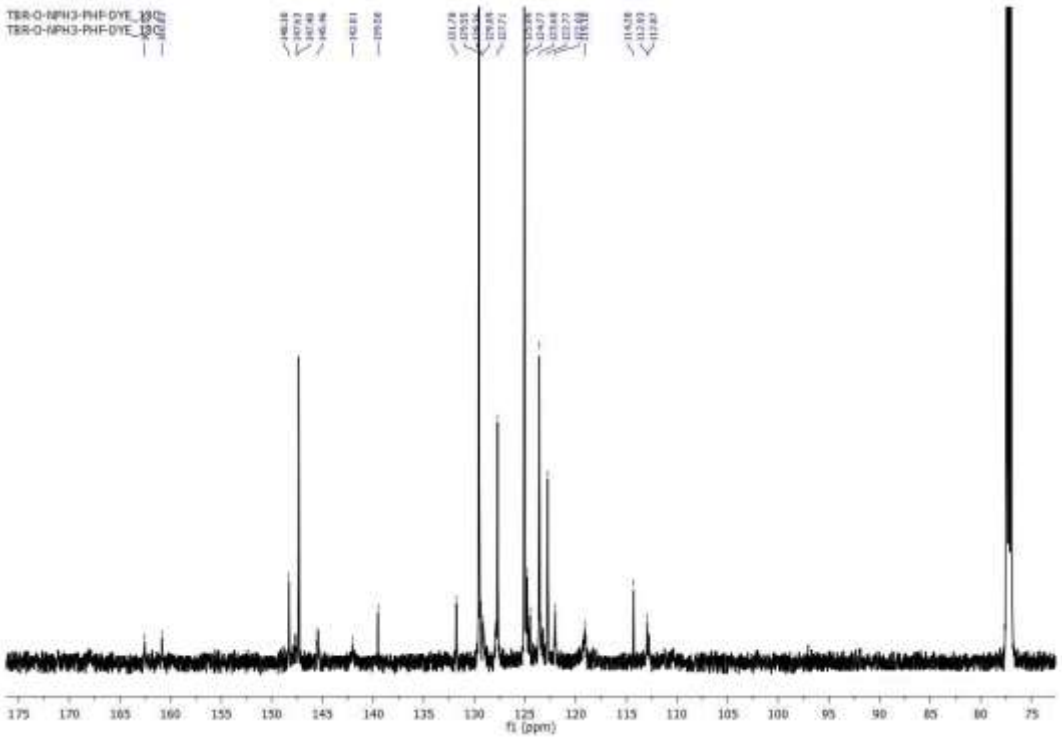

^{13}C NMR spectrum of (*E*)-2-cyano-3-(4'-(diphenylamino)-3-fluoro-[1,1'-biphenyl]-4-yl)acrylic acid (o-NPh3 dye) in $CDCl_3$.

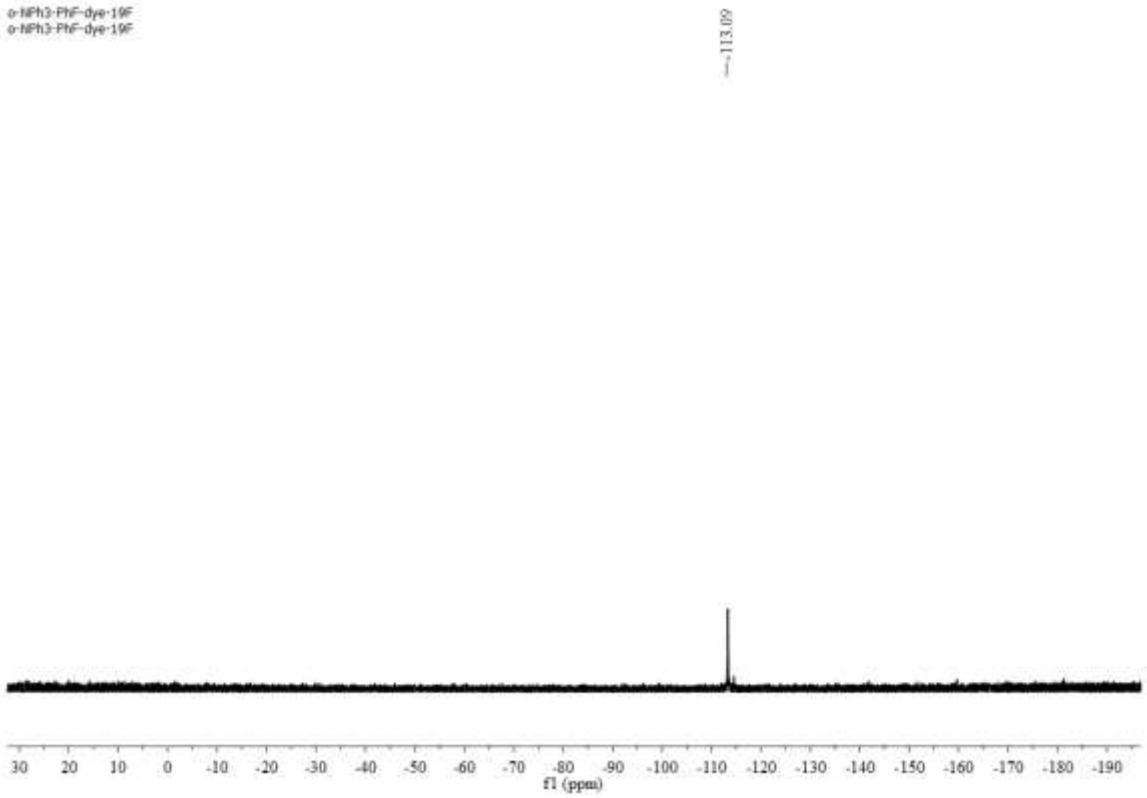

^{19}F NMR spectrum of (*E*)-2-cyano-3-(4'-(diphenylamino)-3-fluoro-[1,1'-biphenyl]-4-yl)acrylic acid (o-NPh3 dye) in $CDCl_3$.

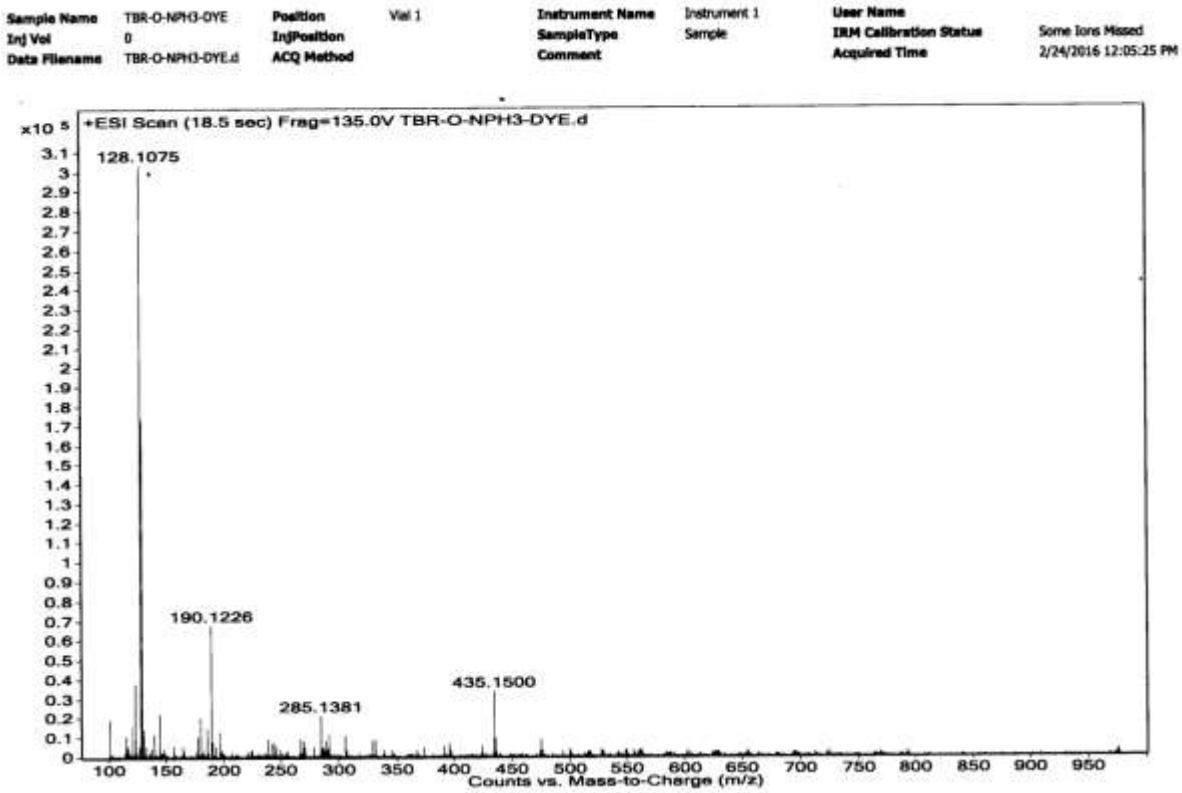

HRMS spectrum of (*E*)-2-cyano-3-(4'-(diphenylamino)-3-fluoro-[1,1'-biphenyl]-4-yl)acrylic acid (o-NPh3 dye).

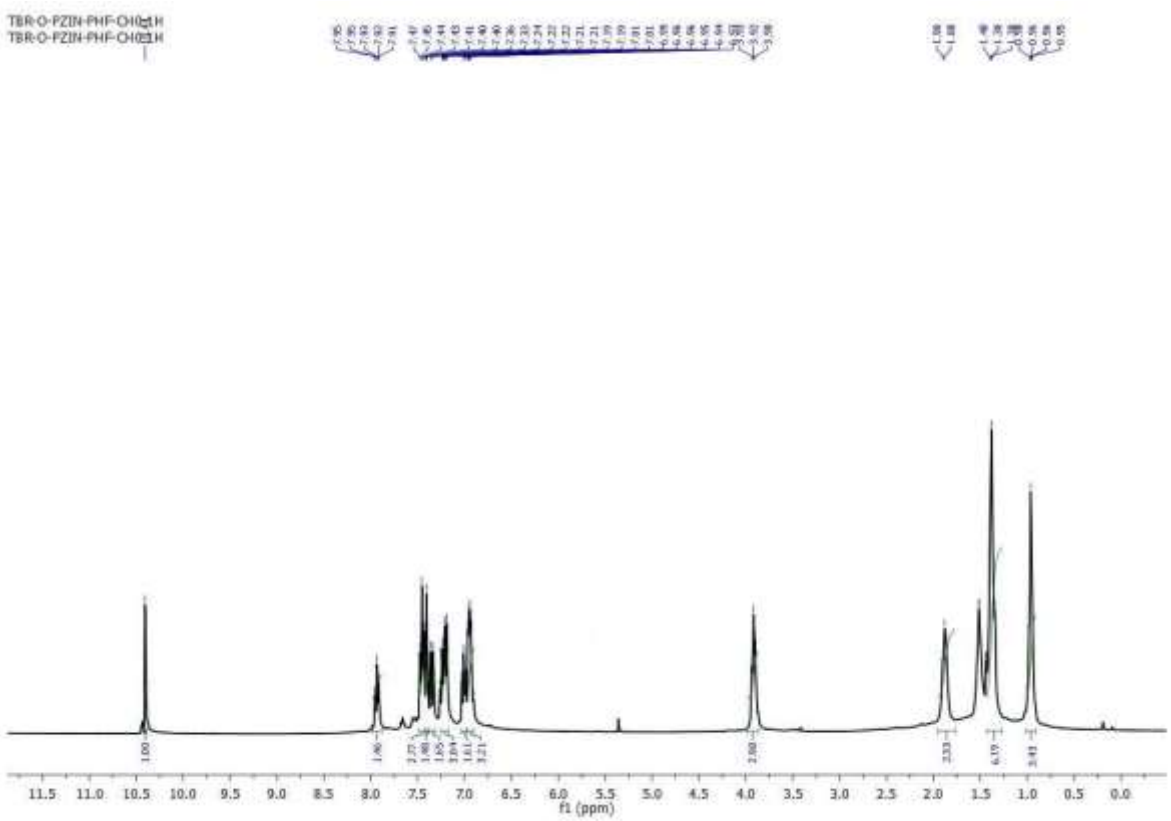

^{1}H NMR spectrum of 2-fluoro-4-(10-hexyl-10*H*-phenothiazin-3-yl)benzaldehyde (3a) in $CDCl_3$.

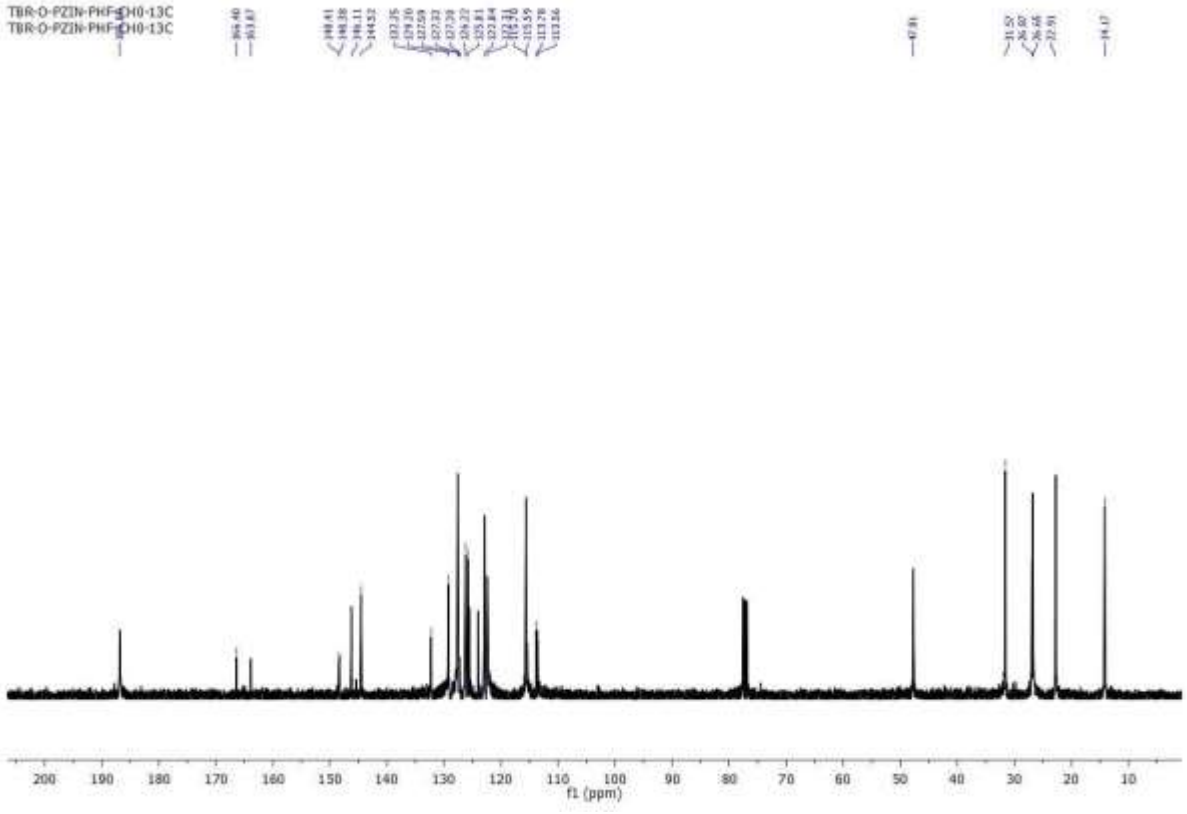

^{13}C NMR spectrum of 2-fluoro-4-(10-hexyl-10*H*-phenothiazin-3-yl)benzaldehyde (3a) in $CDCl_3$.

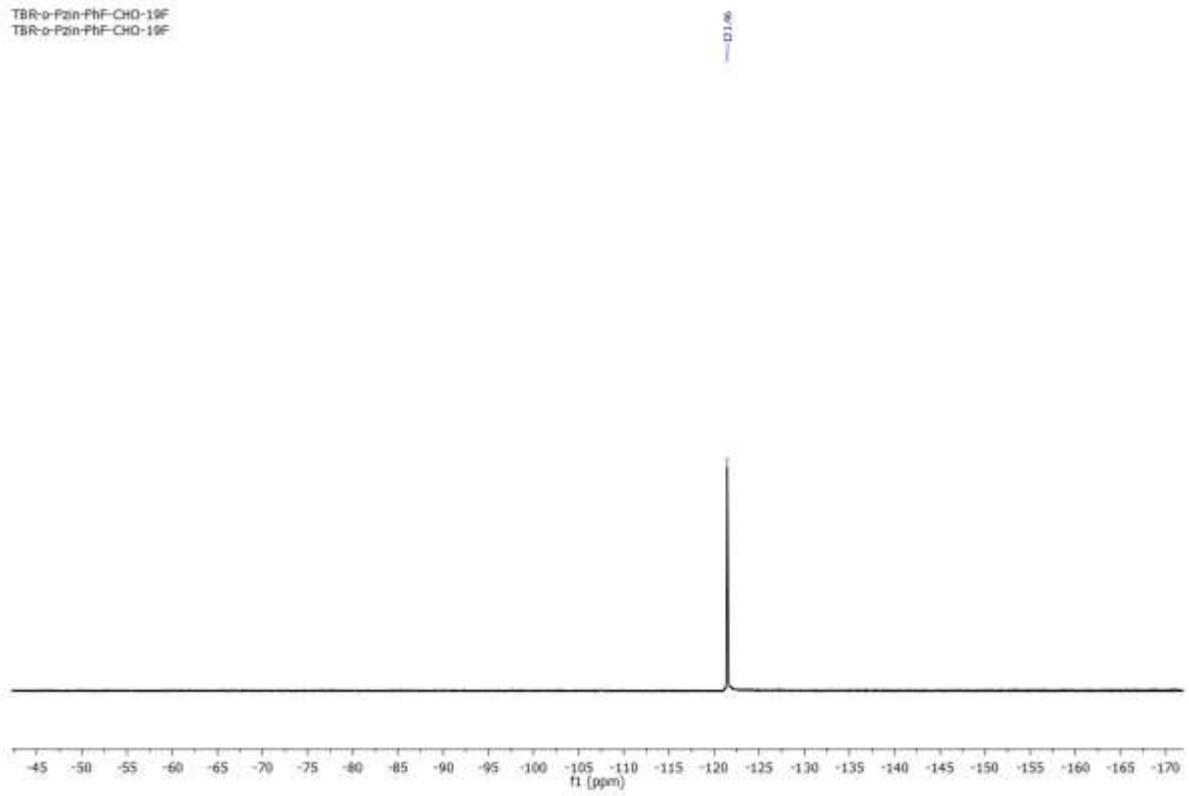

^{19}F NMR spectrum of 2-fluoro-4-(10-hexyl-10*H*-phenothiazin-3-yl)benzaldehyde (3a) in $CDCl_3$.

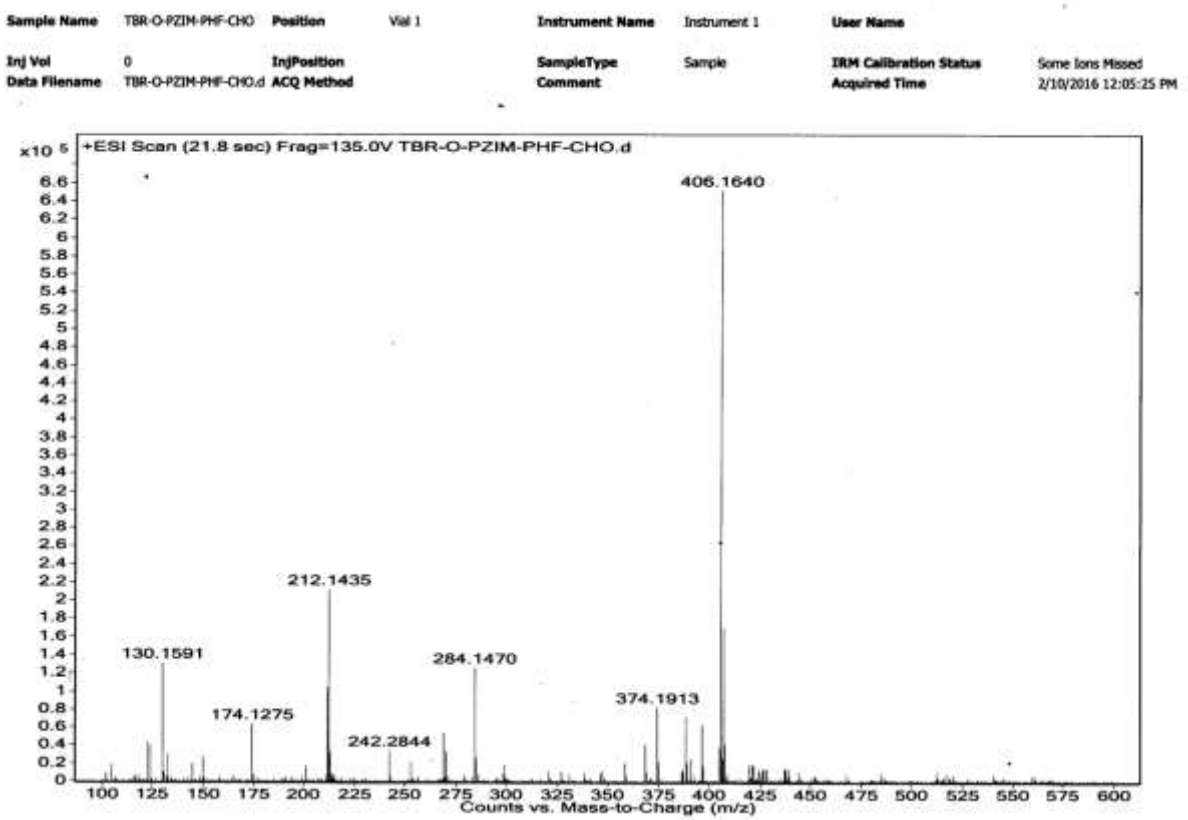

HRMS spectrum of 2-fluoro-4-(10-hexyl-10*H*-phenothiazin-3-yl)benzaldehyde (3a).

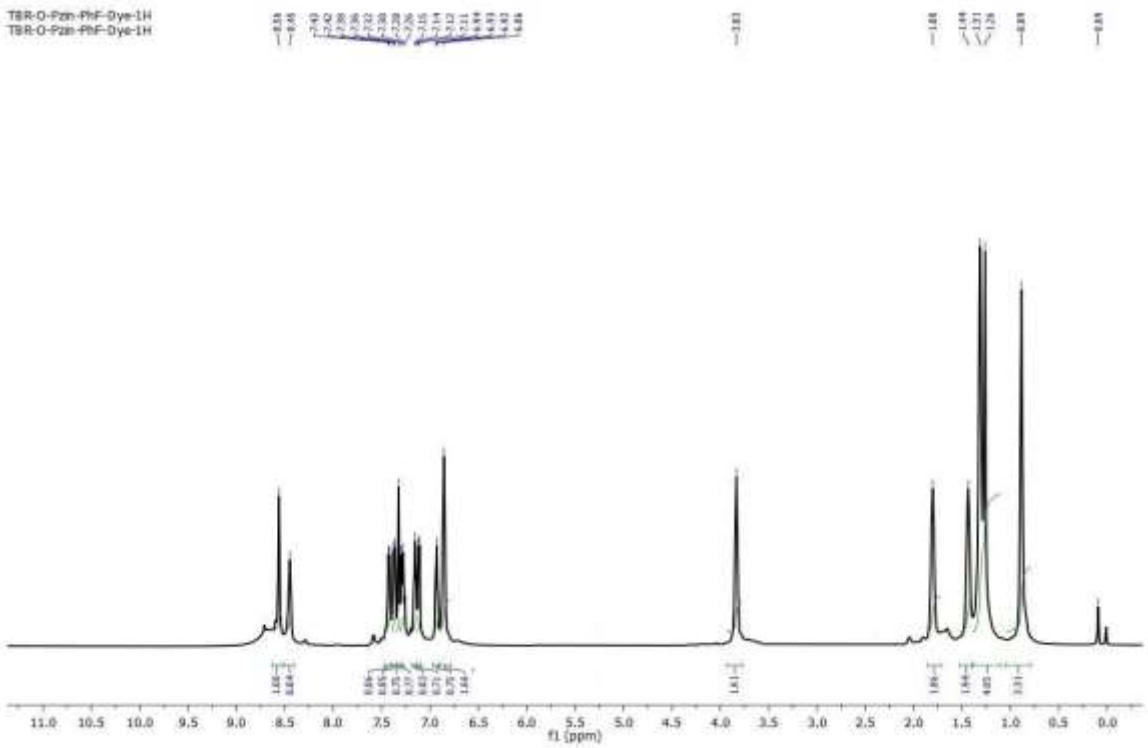

^{1}H NMR spectrum of (*E*)-2-cyano-3-(2-fluoro-4-(10-hexyl-10*H*-phenothiazin-3-yl)phenyl)acrylic acid (o-Pzin dye) in $CDCl_3$.

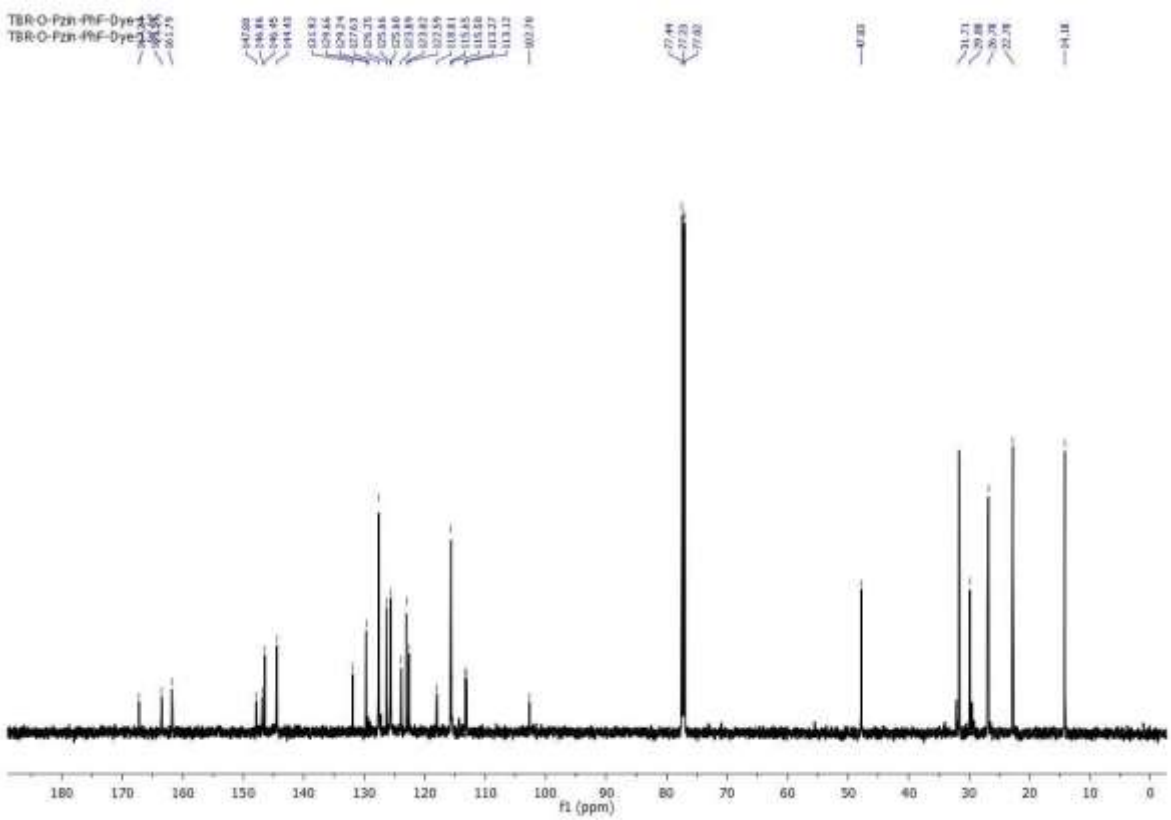

^{13}C NMR spectrum of (*E*)-2-cyano-3-(2-fluoro-4-(10-hexyl-10*H*-phenothiazin-3-yl)phenyl)acrylic acid (o-Pzin dye) in $CDCl_3$.

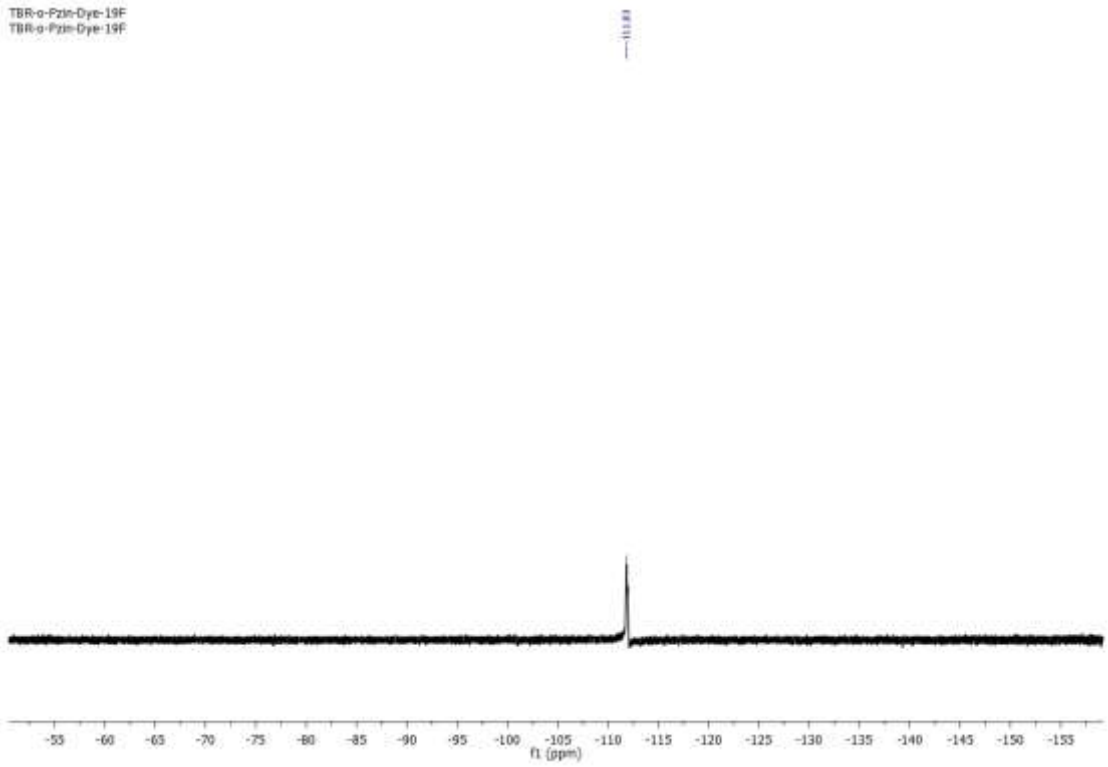

^{19}F NMR spectrum of (*E*)-2-cyano-3-(2-fluoro-4-(10-hexyl-10*H*-phenothiazin-3-yl)phenyl)acrylic acid (o-Pzin dye) in $CDCl_3$.

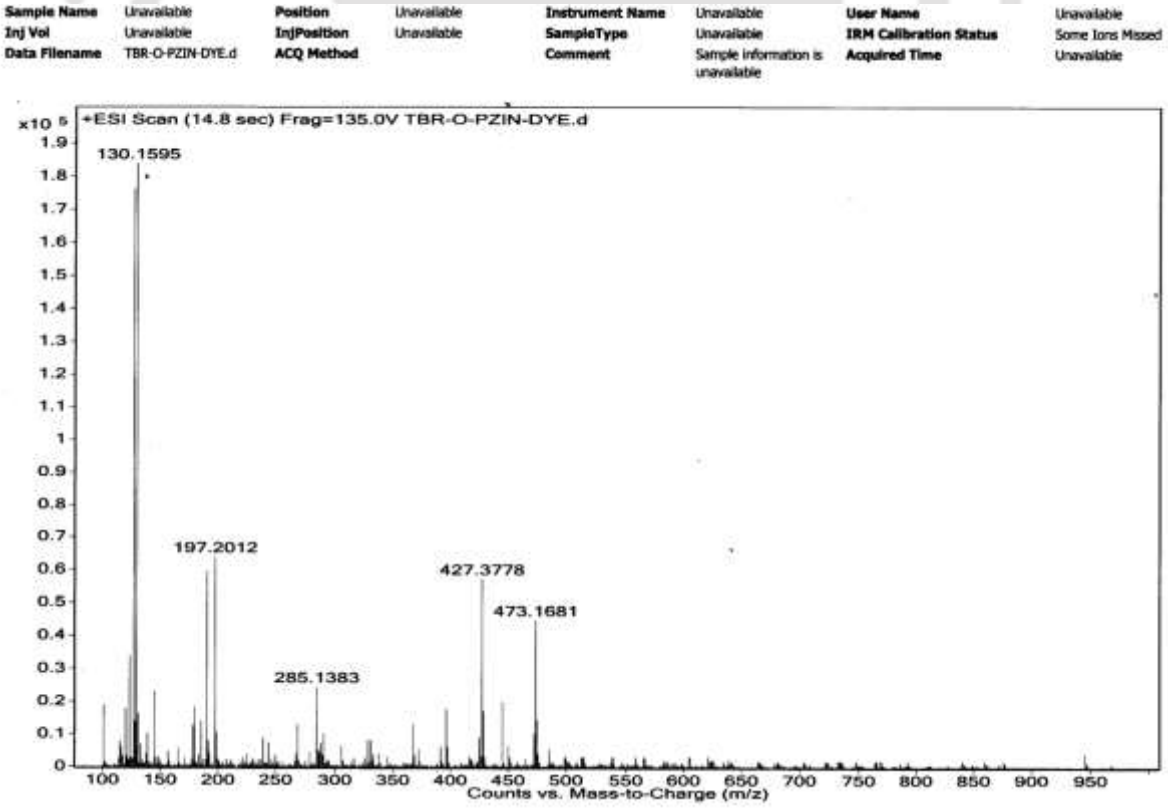

HRMS spectrum of (*E*)-2-cyano-3-(2-fluoro-4-(10-hexyl-10*H*-phenothiazin-3-yl)phenyl)acrylic acid (o-Pzin dye).

CHAPTER-4

The solvatochromism and aggregation-induced enhanced emission of triphenylamine substituted styrene derivatives and its application in dye sensitized solar cells

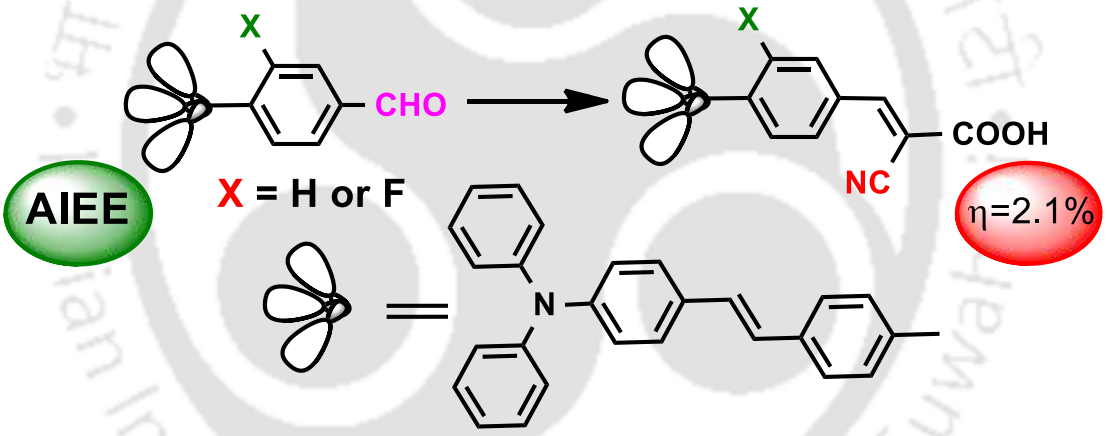

(*manuscript communicated*)

Abstract:

New five triphenylamine (TPA) based D-π-A structural motifs were designed and synthesized. The photoluminescence properties of all three chromophores were studied in solutions as well as in aggregated states. All three chromophores emit strong blue fluorescence in ethanol solution. However, two chromophores TPA-PHA ((*E*)-4'-(4-(diphenylamino)styryl)-[1,1'-biphenyl]-4-carbaldehyde), TPA-PFA ((*E*)-4'-(4-(diphenylamino)styryl)-2-fluoro-[1,1'-biphenyl]-4-carbaldehyde) exhibit AIEE effect in aggregation state. The results reveal that, due to the formation of excimer in excited state. The TPA-PFA had lesser quantum yield than TPA-PHA in aggregated state, since the *m*-fluorine substitution on phenyl containing chromophore makes an "inductive effect", and the substitution of fluorine atom causes formation of ICT from Donor to Acceptor. From FESEM analysis we concluded that, both AIEE chromophores exhibit two different kinds of "Nano aggregates" in solid state. These AIEE chromophores were utilized to develop new dyes i.e., Dye-1, Dye-2 for DSSC application for first time. The dye-1, dye-2 exhibit a power conversion efficiency (PCE) of 2.1% (J_{sc}= 5.05 mA/cm^2, V_{oc}= 0.67 V and *FF*= 0.61) and 1.9% (J_{sc}= 4.68 mA/cm^2, V_{oc}= 0.70 V and *FF*= 0.59), respectively. The optimized geometry calculations of D-π-A chromophores, dyes were ascertained by DFT calculation by using CAM-B3LYP/631G(d,p) basis set.

4.1 Introduction

Great efforts have been made to investigate various number of organic chromophore with strong fluorescence.[1-6] Unfortunately, many of them suffer from abrupt fluorescence quenching upon aggregation in aqueous media. This phenomenon is known as ACQ (aggregation caused quenching), mainly due to the strong inter molecular π-π stacking and other non-radiative pathways, which seriously limits their application (Fig. 4.1 and 4.2).[7-8] Fortunately to overcome this problem, Tang *et al*. designed and synthesized materials showing AIE or AIEE properties.[9] These materials, show weak emission in solution state, but exhibit strong fluorescence upon aggregation in aqueous media. Various mechanistic pathways such as restriction of intramolecular rotation (RIR), restriction of intramolecular motion (RIM), restriction of intramolecular vibration (RIV), conformational planarization, E/Z isomerization, J-aggregate formation and twisted intramolecular charge transfer (TICT) have been explored to achieve AIE/AIEE by hampering the intramolecular π-π stacking. The design and development of AIE/AIEE or solid state emission materials has gained immense attention due to their application in various fields, such as organic light emitting devices (OLEDs), organic solid-state lasers,

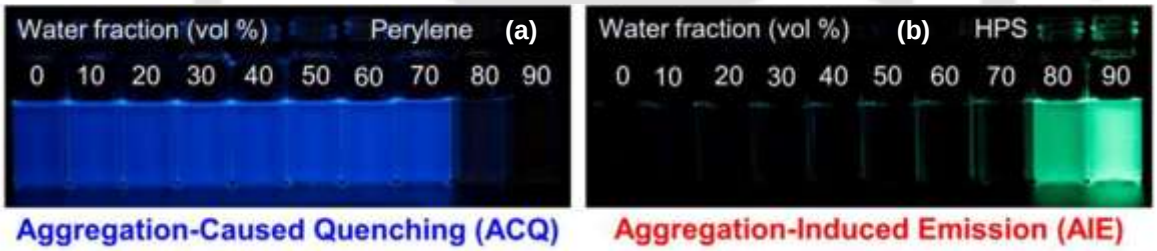

Figure 4.1 Fluorescence photographs (a) a chromophore with aggregation-caused quenching (ACQ) effect (Example: *N*,*N*-dicyclohexyl-1,7-dibromo-3,4,9,10-perylenetetracarboxylic diimide) (b) a chromophore with aggregation-induced emission (AIE) effect (Example: hexaphenylsilole) in THF/water mixtures with different water contents and (c) a chromophore with aggregation-induced enhance emission (AIEE) effect (Example: (*E*)-4-(2-([1,1'-biphenyl]-4-yl)vinyl)-*N*,*N*-diphenylaniline)

flat panel displays, bio imaging and fluorescent sensors etc., but the development of AIE/AIEE materials is still challenging due to the ACQ and other non-radiative pathways occurring in excited state.[10]

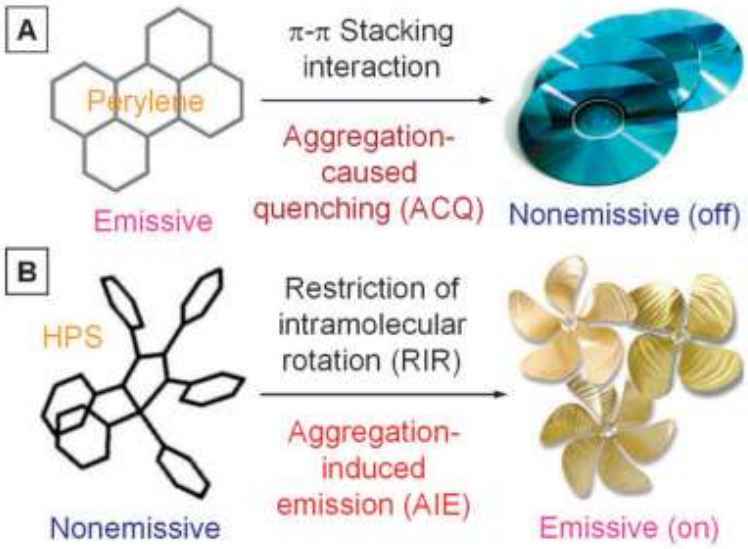

Figure 4.2 Planar chrmophore such as pyrene tend to aggregate just as discs pile up due to strong π-π stacking interactions, which commonly turn ‘‘off’’ light emission (a), whereas nonplanar propeller-shaped chrmophore such as hexaphenylsilole (HPS) behave oppositely, with their light emissions turned ‘‘on’’ by aggregate formation, due to the restricted intramolecular rotation in the aggregates (b). (Figure taken from RSC)

In recent decades, researchers have devoted much attention towards triphenylamine based materials. However, triphenylamine is widely used as donor in electroactive materials such as OLED, DSSC and BHJ-solar cell etc., due to its good electron donating and transporting properties, as well as its non-planar or starburst (3-D) molecular structure suppress the intramolecular π-π stacking resulting in high fluorescence and high quantum yield in aggregated or solid state.[11-20] With the above consideration, we have designed and developed three chromophores (one AIEE-inactive, two AIEE-actives), showing D-π-A configuration. In this work, two AIEE molecules containing both donating and accepting groups connect to a special π-conjugated frame work. TPA was used as a donor, styrene was used as a π-bridge, phenyl aldehyde (TPA-PHA) and *m*-fluorine substitution of phenyl aldehyde (TPA-PFA) acts as an acceptor in D-π-A system (**Scheme 4.1**). These compounds often exhibit AIE or AIEE property which are believed to be a promising candidates for use in various organic devices. TPA-PFA exhibits more “extinction coefficient” than TPA-PHA in chloroform as shown in **Table. 4.1**, but the

"quantum yield" of TPA-PFA (solution state, solid state) is less than TPA-PHA, due to the "meta fluorine inductive effect" and formation of nanoparticles.[20] The fluorine substitution on phenyl containing chromophore (TPA-PFA) shows good optical and electrical properties due to their high electron affinity, that causes formation of charge transfer from D to A and it additionally forms "H-bonding" to the neighboring unit, showing AIEE thereby emitting yellow fluorescence in aggregated state. However, TPA-PHA exhibits more quantum yield than TPA-PFA due to the formation of Nano rods in aggregated states which were confirmed by FE-SEM analysis and PL intensity (8.0 X 10^5).

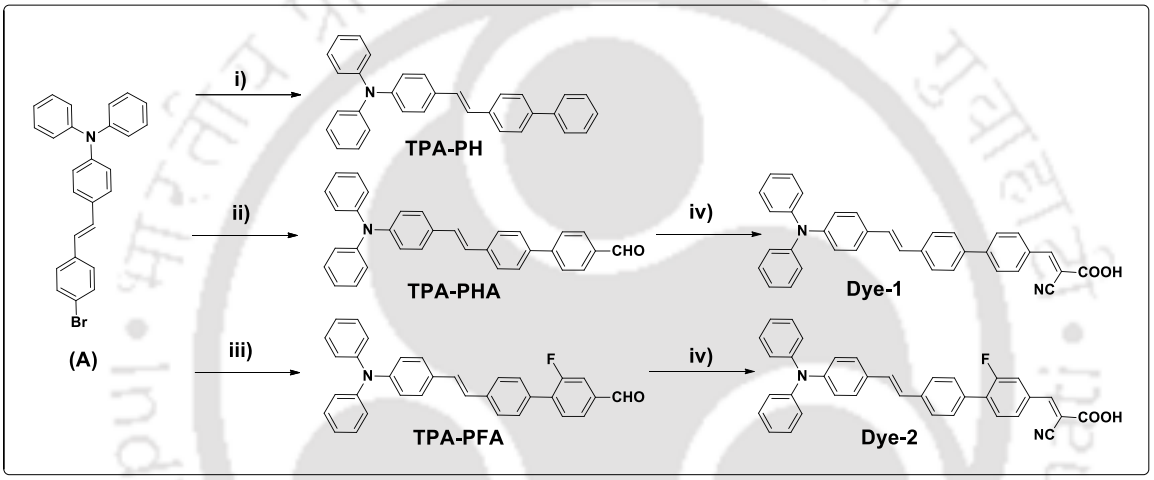

Scheme 4.1 i) Phenyl boronic acid, $Pd(PPh_3)_4$, K_2CO_3, THF:H_2O= 2:1, 85 °C, 12h, ii) 4-Formyl phenyl boronic acid, $Pd(PPh_3)_4$, K_2CO_3, THF:H_2O= 2:1, 85 °C, 12h, iii) 2-Floro,4-Formyl phenyl boronic acid, $Pd(PPh_3)_4$, K_2CO_3, THF:H_2O= 2:1, 85 °C, 12h, iv) CH_3CN:$CHCl_3$ (1:1), cayano acetic acid, Piperidine, 80 °C, 8h.

Many groups have reported organic chromophores that exhibit AIE/AIEE property due to restriction of intramolecular interactions in solid state like HPS, TPE etc., due to the free motion of the phenyl units in the solid state.[10] Based on these observations we synthesized "TPA-PH" ((*E*)-4-(2-([1,1'-biphenyl]-4-yl)vinyl)-*N*,*N*-diphenylaniline) chromophore. Unfortunately, "TPA-PH" does not show AIE/AIEE property due to strong π-π stacking thereby exhibiting ACQ property of the molecule (Crystal data Figure 4.15). When the substitution of aldehyde functional group at para position on Phenyl unit chromophores (TPA-PHA and TPA-PFA) exhibit strong AIEE property in solid state, due molecular conformations have been rigidified by the multiple intermolecular interactions

to aldehyde group such as C-H···π and C-H···O, and also the aldehyde group acts as an electron acceptor that increases the dipole moment in D-π-A molecule, endowing TPA-PHA, TPA-PFA with strong intra molecular charge transfer (ICT) feature and AIEE behavior.

When, especially the structural aspects of electron withdrawing/acceptor nature of aldehyde group was introduced into the novel chromophores they work as dyes in DSSCs, a feature that has been introduced carefully for the first time. However, the strong aggregation ability, weak electron injection capacity and modest binding ability of these chromophores were utilized and further modified successfully to be used in DSSC application.[21] The optical, electrochemical, theoretical and photovoltaic properties of the dyes were carefully studied. Without using any co-absorbents and additives the power conversion efficiency (PCE, η) of Dye-1, Dye-2 exhibits 2.1%, 1.9%. Comparatively, dye-2 exhibits 0.2% less efficiency than dye-1, due to the inductive effect of *m*-fluorine substitution on dye-2. These novel chromophores, and dyes have strong acceptor or anchoring groups i.e., aldehyde and cyanoacrylic acid unit, respectively. To the best of our knowledge this is the first report to utilize these AIE chromophores in DSSCs application.

4.2 Results and discussion

4.2.1 Optical Properties

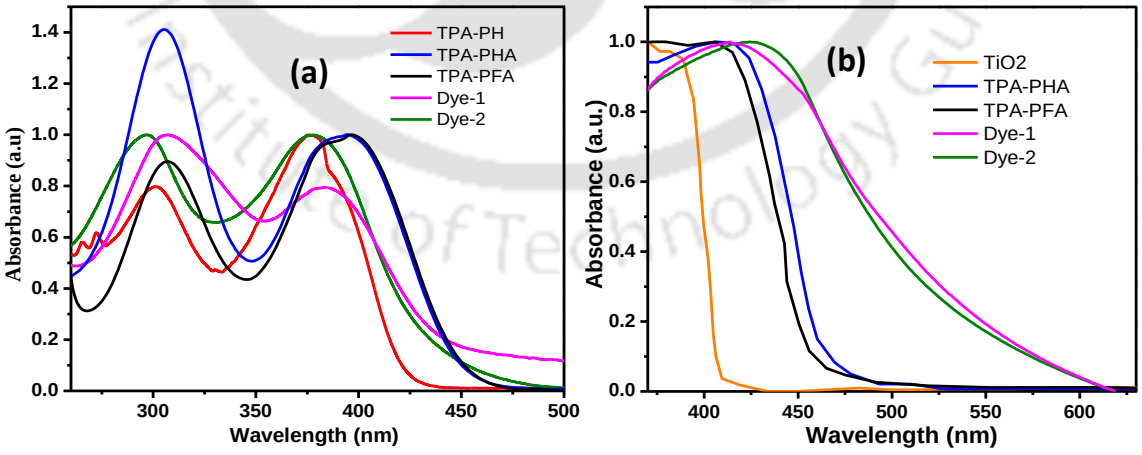

Figure 4.3 (a) Normalized absorption spectra of chromophores and dyes in $CHCl_3$ solution. (b) Normalized absorption spectra of TiO_2 electrode sensitized by chromophores and dyes after absorption of 24 h.

The UV-Vis absorption spectra of triphenylamine substituted styrene derivative chromophores and dyes in chloroform solution are shown in Fig. 4.3 and corresponding photophysical data are presented in Table 4.1. Each of these molecules exhibits two major absorption bands in the UV-Vis region in the range of 250-470 nm. Peak at 250-350 nm, are assigned to the localized aromatic π-π* transitions of conjugated (triphenylamine) system and the latter one in visible region is due to intramolecular charge transfer from donor to acceptor. The absorption maximum of TPA-PHA is very similar to TPA-PFA dye. In detail, the absorption bands of TPA-PH are located at 300 nm and 370 nm, which are red-shifted to 305, 390 nm in TPA-PHA and 307, 392 nm in TPA-PFA after substitution of aldehyde acceptor due to the intramolecular charge transfer (ICT) occurring from donor of triphenylamine to acceptor of aldehyde in D-π-A system. However, in TPA-PH both peaks are attributed to the π-π* transitions of triphenylamine and para phenyl substituted styrene unit. TPA-PH, TPA-PHA and TPA-PFA show an emission maximum in liquid state at 455 nm, 474 nm, and 483 nm, whereas at 462 nm, 530 nm, and 545 nm in aggregated state, respectively. All the above information suggests that both UV-Vis and PL spectra of three chromophores exhibit increase in the wavelength with electron-accepting ability of the acceptor: PhF-CHO > Ph-CHO > Ph.

4.2.2 Solvatochromism of chromophores

To get a clear insight of ICT, the optical properties of TPA-PH, TPA-PHA and TPA-PFA in the solvents of different polarity were investigated. When the solvent polarity changes from hexane to water, significant changes in the absorption spectra was not observed (Figure 4.4). However, monotonically increasing tendency in PL spectrum (Fig. 4.5), with increasing solvent polarity was observed moreover for each compound. is progressively shifted from 30 to 150 nm longer wavelength. TPA-PH, TPA-PFA and TPA-PHA chromophores exhibited solvatochromism with increasing solvent polarity. In $CHCl_3$ solution TPA-PFA exhibit maximum emission intensity at 556 nm, due to the *m*-

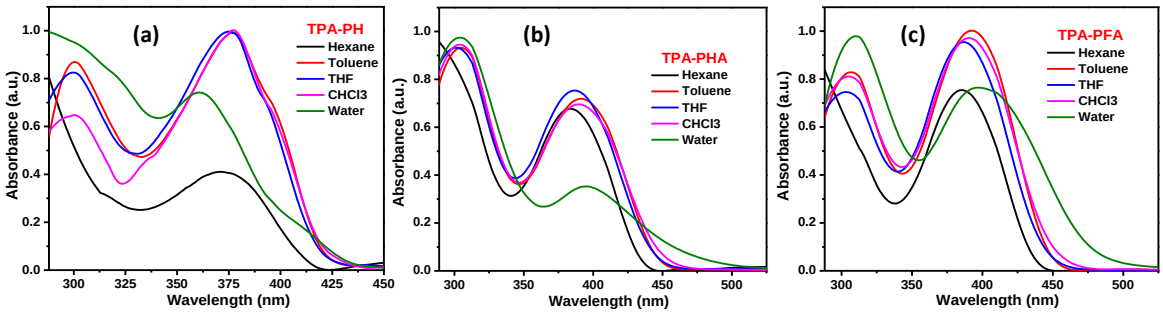

Figure 4.4 Normalized absorption spectra of TPA-PH (a), TPA-PHA (b) and TPA-PFA (c) in different polar solvents.

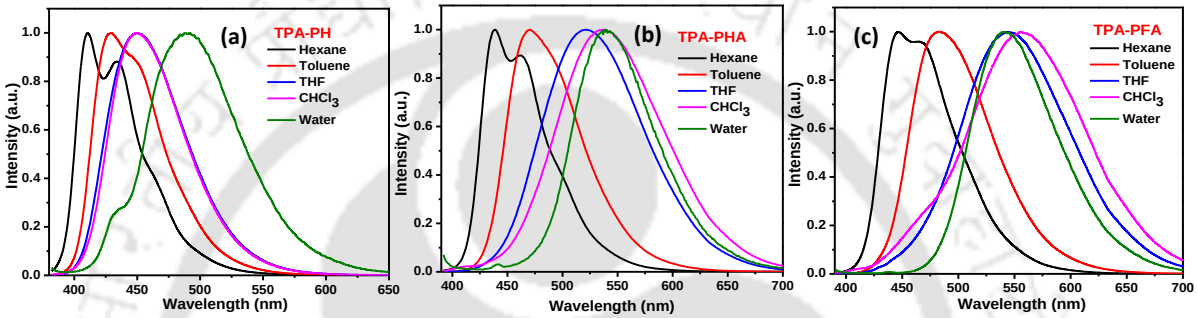

Figure 4.5 Normalized PL spectra of TPA-PH (a), TPA-PHA (b) and TPA-PFA (c) in different polar solvents.

Table 4.1 Optical and electrochemical characterization of chromophores and dyes

S.No	compound	λ_{max}	Molar extinction Coefficient at higher wavelength (M^{-1} Cm^{-1})	HOMO (eV)	LUMO (eV)	Band gap	$\Phi_{Solvent}$ (EtOH)	Φ_{Water}
1	**TPA-PH**	300 nm, 370 nm	7,698	-5.15	-2.22	2.93	75.8	23.50
2	**TPA-PHA**	305 nm, 390 nm	19,831	-5.15	-2.39	2.76	50.0	88.32
3	**TPA-PFA**	307 nm, 392 nm	41,252	-5.17	-2.43	2.74	56.36	82.13
5	**Dye-1**	307 nm, 383 nm	10,664	-5.61	-2.78	2.83	–	–
6	**Dye2**	297 nm, 377 nm	16,976	-5.71	-2.86	2.85	–	–

fluorine substitution on phenyl containing chromophore. But, the emission peak of TPA-PH, TPA-PHA and TPA-PFA are 410 nm, 438 nm and 446 nm in hexane whereas 490 nm, 539 nm and 541 nm in water respectively. When polarity increases from hexane to water, emission peak of 80 nm, 101 nm and 95 nm are red-shifted for TPA-PH, TPA-PHA and TPA-PFA, respectively. The three chromophores have high emission value (λ_{max}), but less emission intensity in polar solvent such as water.

The absorption maximum wavelength of dye-1 was 307 nm, 383 nm, for dye-2 it was 297 nm, 377 nm and its corresponding molar extinction coefficients 12,054 $M^{-1}cm^{-1}$, 10,664 $M^{-1}cm^{-1}$ for dye-1 and 16,664 $M^{-1}cm^{-1}$, 16,976 $M^{-1}cm^{-1}$ for dye-2. The weak charge transfer occurring from D to A due to the "rod" like structure of dyes exhibits strong aggregation in liquid state. Dye-1 and dye-2 shows an emission maximum in liquid state (in $CHCl_3$) at 522 nm and 483 nm. Comparatively phenyl spacer dyes and fluorine substituted phenyl spacer dyes showed blue-shift in absorption and emission spectra due to the meta-fluorine inductive effect.[20]

4.2.3 AIEE Properties of chromophores:

To investigate the AIEE attributes of TPA-PH, TPA-PHA and TPA-PFA, spectrometric verification tests were performed in various fractions of ethanol/water mixtures. Water was used as a poor solvent for the three compounds with ethanol. While the water fraction (f_w) increases from 0 to 99%, the absorption and PL spectra changes. Each time the concentration of the solution was kept 1×10^{-5} $mol.L^{-1}$.

Figure 4.6 (1a, 2a and 3a) shows the absorption spectra of TPA-PH, TPA-PHA and TPA-PFA, respectively in various fractions of ethanol/water mixture. Similarly, figure 4.6 (1b), (2b) and (3b) are PL spectra of TPA-PH, TPA-PHA and TPA-PFA, respectively in various ratios of ethanol/water mixtures. Figure 4.6 (1a) and (1b) explains that compound TPA-PH is not affected even if f_w increases up to 99%, indicating that TPA-PH is "AIEE-inactive" (ACQ property). The absorption spectra [Fig.4.6 (2a)] of TPA-PHA were slightly affected, even if f_w increases up to 30%. When the water fraction (f_w) is further increased to 40%, the absorption spectrum is red-shifted from 382 nm to 398 nm. At the same time the absorption intensity dramatically decreases. It explains that molecule begins to aggregate at this composition of solvent. The emission spectra of TPA-PHA as shown in the Fig. 4.6 (2b) demonstrates the AIEE property in the $EtOH/H_2O$ mixtures. With increase of f_w from 0% to 30%, the PL intensity is gradually increased but not shifted. When the f_w increases above 30% and up to 70% the emission peak is red shifted

from 470 nm to 529 nm, and the peak intensity also suddenly rises above f_w 40%. At this stage the compound begins to aggregate and hydrophobic environment is created resulting in strong ICT in the excited state. This increase in PL intensity can be attributed to the AIEE effect. Further increase in the f_w (above 70%) slightly decreases then stabilizes at 531 nm. Since there is no obvious aggregates are observed, this change was mainly due to the increase of solvent polarity.

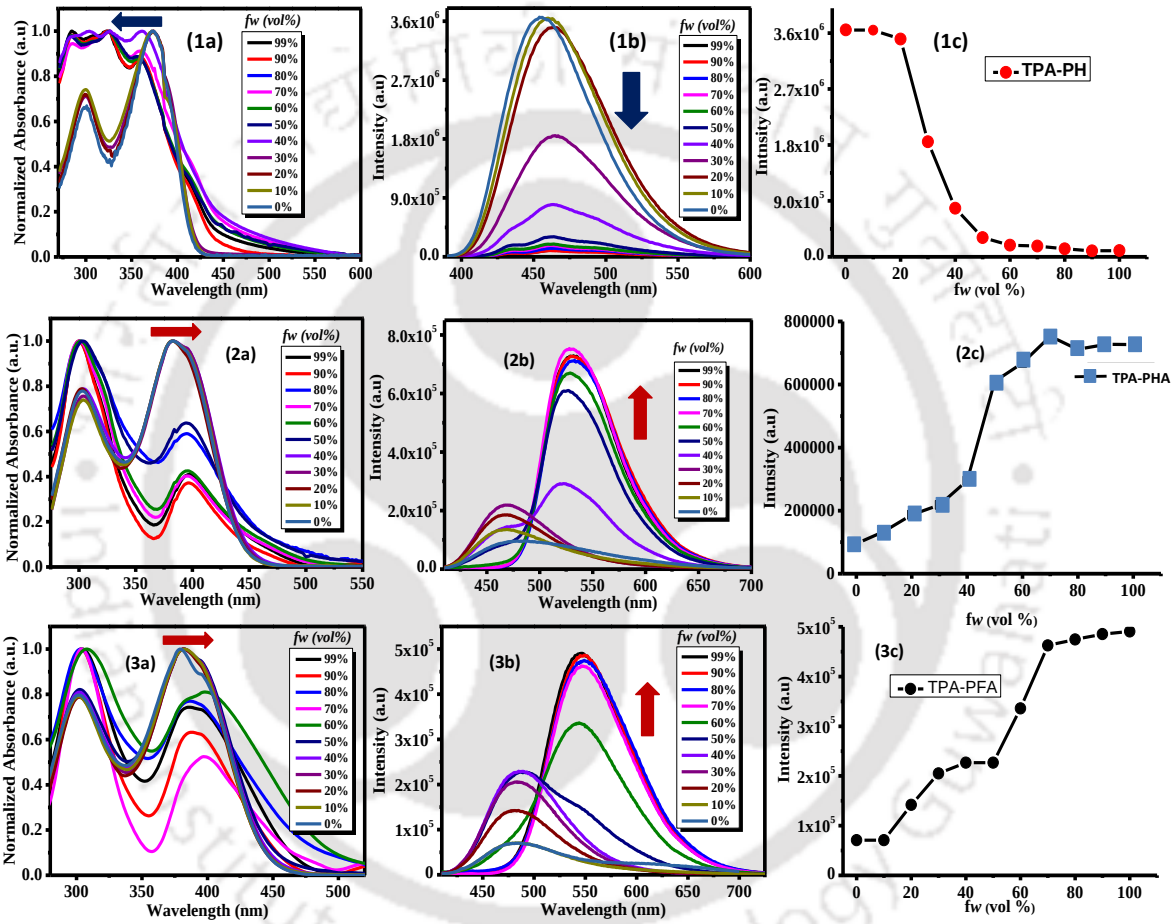

Figure 4.6 Various chromophores TPA-PH, TPA-PHA and TPA-PFA absorption (1a, 2a and 3a) and emission spectra (1b, 2b, and 3b) recorded in 0-99% fraction of ethanol/water mixtures and then maintained the concentration of solution 1×10^{-5} M.

Similarly, to detect the optical behavior of the aggregation process of TPA-PFA chromophore, we added different amounts of water fraction (f_w) (from 0% to increases up to 99%) to ethanol solution, and then monitored the absorption and PL changes. Fig. 4.6 3a, 3b explain the AIEE property of absorption and emission spectra in aqueous mixtures. However, up to 50% of dilute ethanol solution, we could not get any changes in

absorption and emission spectra. With gradual addition of water to ethanol solution, at f_w = ≥ 60% the absorption spectrum is red-shifted from 379 nm to 397 nm, and at the same time the ICT peak intensity was dramatically decreased. In PL spectra, f_w increases from pure ethanol to ethnol/water mixture up to 50%, yet we could not observe any peak shift, but addition of water increased the peak intensity. When the water fraction (f_w) is further increased to 50%, the PL spectrum is red-shifted from 487 nm to 542 nm. Similar enhancement can be observed in the behavior of TPA-PHA chromophore at f_w = ≥ 50%.

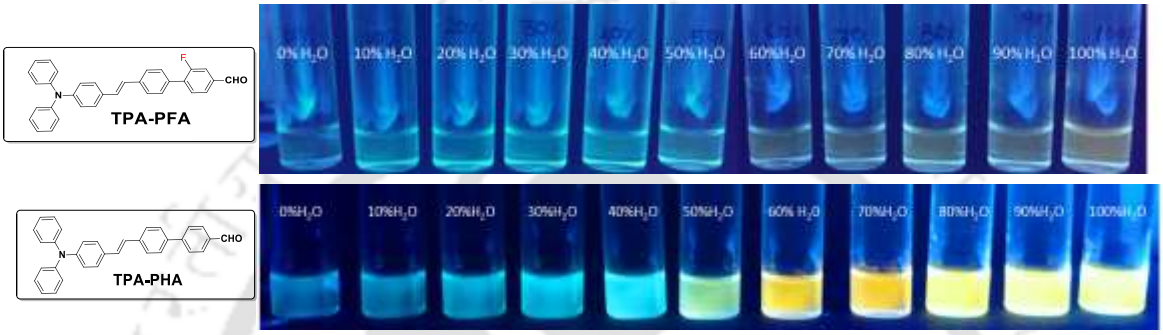

Figure 4.7 Fluorescence photographs of TPA-PH, TPA-PFA chromophores in 0-99% fraction of ethanol/water mixtures.

4.2.4 FE-SEM analysis:

From, FE-SEM analysis (Figure 4.8), TPA-PH and TPA-PFA exhibits opposite properties. In solid state TPA-PHA exhibits "Nano rods", but TPA-PFA exhibits "Nano particles" in water: ethanol (9:1 v/v) at concentration 1 × 10^{-5} M, resulting in higher PL intensity than TPA-PFA [Fig. 4.6 (2b) and (3b)].

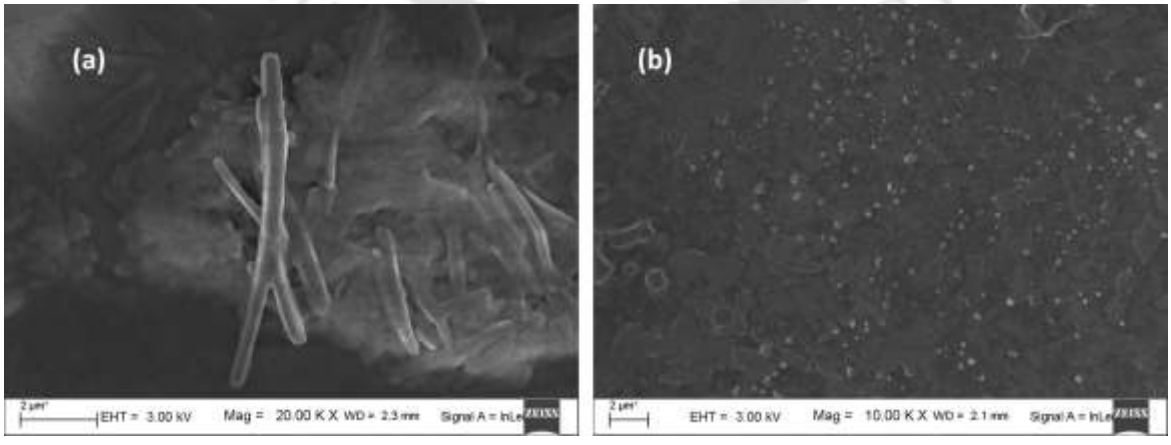

Figure 4.8 (a) FE-SEM images of TPA-PHA and (b) TPA-PFA Nano-aggregates prepared in water:ethanol (9:1 v/v) at concentration 1 × 10^{-5} M.

4.2.5 Electrochemical properties

We also investigated the electrochemical behaviors of triphenylamine substituted styrene derivatives by cyclic voltammetry (CV). Fig. 4.9 (a) shows the cyclic voltammetry diagrams of TPA-PH, TPA-PHA and TPA-PFA. Similarly, Fig. 4.9 (b) shows the CV diagram of dyes and relevant data are summarized in Table. 4.1. Electrochemical properties for all chromophores and dye derivatives were investigated by using 0.1 M tetrabutyl ammonium hexaflurophosphate ($TBAF_6$) as a supporting electrolyte in dry CH_3CN solvent and ferrocene/ferrocenium (Fc/Fc^+) redox couples used as external standard. According to the redox potential of Fc/Fc^+ standards the HOMO energy levels were estimated from the onset potential of the first oxidation peak.

The estimated HOMO levels were calculated according to $E_{HOMO} = -(E_{ox} - E_{1/2(ferrocene)}) + 4.8$ eV formula. The HOMO energy level was found to be -5.15 eV for TPA-PH, -5.15 eV for TPA-PHA, -5.17 eV for TPA-PFA, -5.61 eV for dye-1 and -5.71 eV for dye-2, respectively. Chromophores TPA-PH, TPA-PHA and TPA-PFA exhibits two quasi-reversible oxidation peaks due to the monocation and dication formation of triphenylamine unit. The cyclic voltammetry clearly shows that the conversion of TPA-PH into TPA-PHA (Phenyl to Phenyl substitution) compound does not affect the first oxidation peak (cathodic peak) and does not change the HOMO level. The dyes HOMO energy levels are more negative than the redox potential of I^-/I_3^- (-5.1 eV), indicating that the oxidized dye can regenerate effectively.

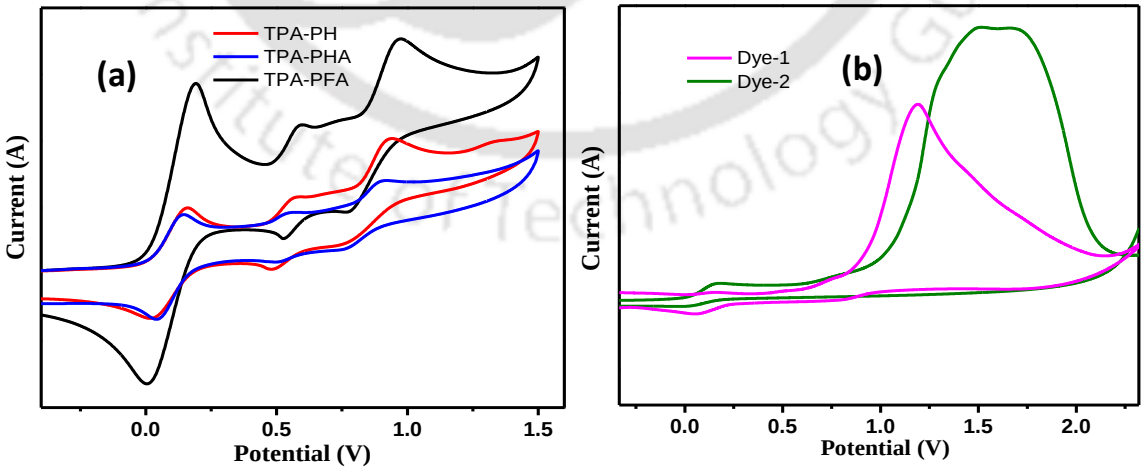

Figure 4.9 (a) Cyclic voltammograms corresponding to the oxidation of TPA-PH, TPA-PHA, and TPA-PFA Chromophores. (b) CV corresponding to the oxidation of organic dyes in 0.1 M $TBAF_6/CH_3CN$.

The LUMO level of chromophores and dyes were calculated from the $E_{LUMO}= E_{0\text{-}0}$ - E_{HOMO} formula, which are -2.22 eV, -2.39 eV and -2.44 eV of TPA-PH, TPA-PHA and TPA-PFA respectively. The calculated LUMO energy level of TPA-PFA (-2.39 eV) was lower than that of TPA-PHA (-2.44 eV) due to the strong accepting ability of the substituted fluorine atom. The calculated LUMO level of dye-1 (-2.81 eV), dye-2 (-2.88 eV) values are higher than the conduction band (CB) of the TiO_2 electrode. These LUMO energy levels of dyes are suitable driving force for electron injection from oxidized dye to CB of TiO_2 surface.

4.2.6 Theoretical molecular orbital calculations:

The frontier molecular orbitals of chromophores and D-π-A based dyes were studied using density functional theory (DFT) calculations (shown in Fig. 4.10**)** done by TD-DFT/CAM-B3LYP/6-31G(d,p) basis set. The HOMO levels of the dyes are mainly located on the donor segment, having, triphenylamine unit and strongly diffused into phenyl unit. The LUMO levels are mainly located on aldehyde containing phenyl unit and diffused into substituted phenyl unit. The transitions at longer wavelength are due to the ICT processes with the major contribution of HOMO to the LUMO orbitals, while the remaining transitions are due to the π−π* transitions of the chromophores and dyes. The corresponding data are summarized in Table 4.2.

4.3 Device fabrication

The TiO_2 colloid for liquid-state DSSCs was prepared according to the literature.[20] Substrates are fluorine-doped tin oxide conducting glass (FTO) which is first cleaned with mild detergent, rinsed with distilled water for several times and subsequently with ethanol in an ultrasonic bath, finally dried under air stream. For fabricating the device, ~15 nm thick TiO_2 (buffer) compact layer was spin-coated on the pre-cleaned FTO glass, then sintered at 450 °C. Subsequently, 12μm-thickness mesoporous TiO_2 anatase compact layer were deposited by doctor blade techniques. The TiO_2 electrodes were heated at 450 °C for 20 min. After sintering, when the temperature cooled to about 65 °C, the electrodes were immersed in a dye bath containing 10^{-5} M dyes (dye 1 and 2) in ethanol/dichloromethane solvents and left overnight. The films were then rinsed in ethanol to remove excess dye. Devices were assembled, using a 20μm thick thermoplastic Surlyn frame, with a platinized (50 mM H_2PtCl_6 solution in Iso-propyl alcohol, IPA) counter electrode. An electrolyte solution was then introduced through the hole predrilled in the counter electrode, and the holes were covered with a glass coverslip. The liquid

electrolyte employed was a solution of 0.5M LiI, 0.05M I_2 and 0.5M TBP (4-tert-butyl pyridine) in 3-methoxy propeonitrile.

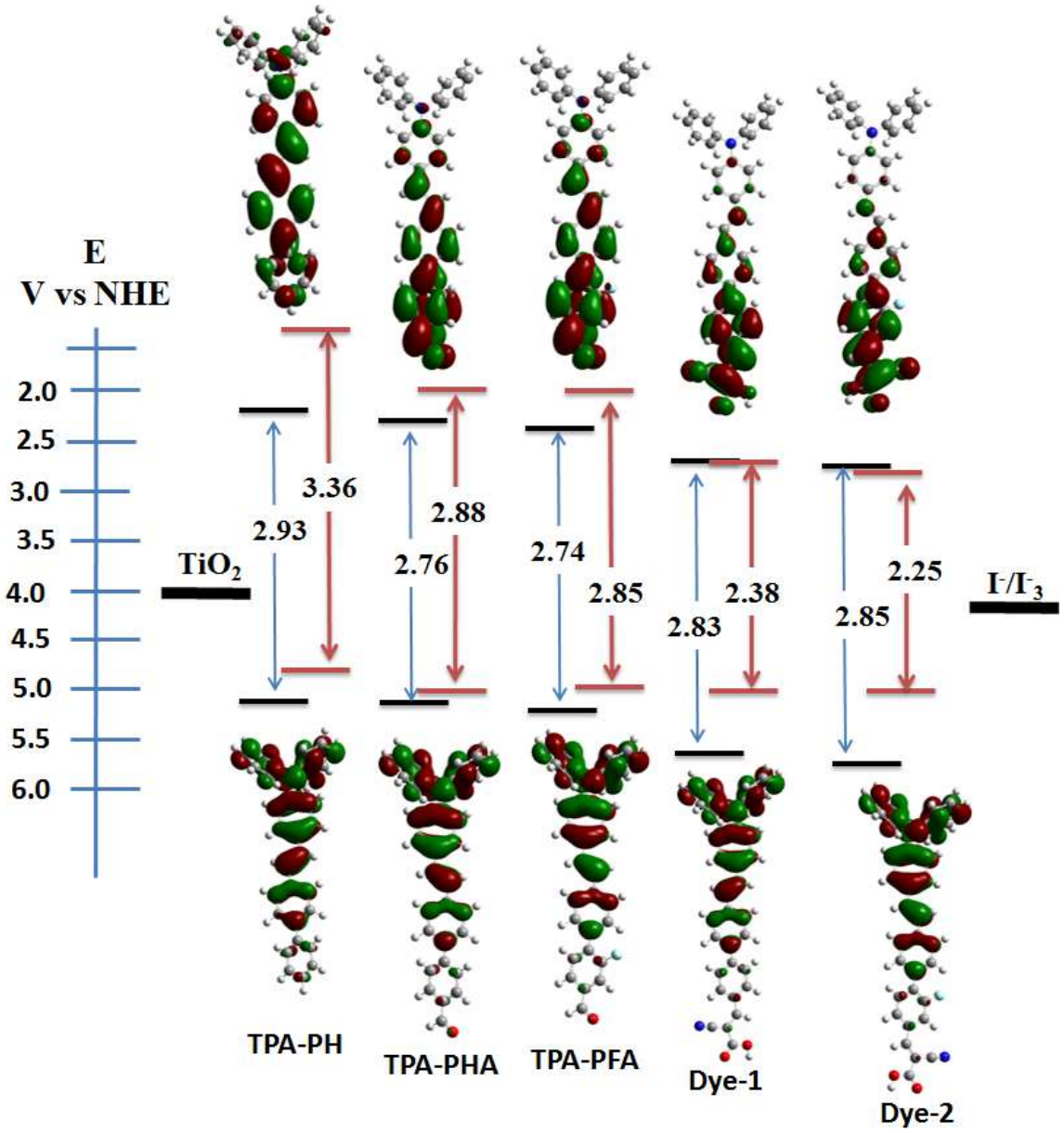

Fig. 4.10 Calculated energy levels and electronic distribution of frontier molecular orbital of various chromophores and dye molecules.

Table 4.2 Computed selected transition energies wavelengths, oscillator strengths (*f*), and their orbital contribution for the chrmophores and dyes using TD-DFT, CAM-B3LYP/6-31G (d,p) basis set.

Dye	λ/nm	*f*	Wavefunctions
TPA-PH	274	0.2526	H ⟶ L +3 (57%), H ⟶ L +2 (22%)
	348	1.7429	H ⟶ L (85%)
TPA-PHA	300	0.4142	H ⟶ L+1 (84%)
	326	0.1182	H-1 ⟶ L (95%)
	360	0.2551	H ⟶ L (97%)
TPA-PFA	266	0.2040	H ⟶ L+1 (20%)
	272	0.2413	H ⟶ L+3 (81%)
	360	1.8881	H ⟶ L (60%), H ⟶ L+1 (24%)
Dye-1	271	0.2384	H ⟶ L+4 (81%)
	296	0.4859	H ⟶ L (42%) H-1 ⟶ L (21%)
	382	2.1711	H ⟶ L (52%), H ⟶ L+1 (23%)
Dye-2	271	0.2407	H ⟶ L+4 (81%)
	303	0.5612	H ⟶ L (38%) H-1 ⟶ L (28%)
	389	2.0235	H ⟶ L (55%), H ⟶ L+1 (21%)

4.4 Photovoltaic performance of TPA-PHA and TPA-PFA

Table 4.3 conclude that aldehyde anchoring group has weak interaction with TiO_2 film, compared to other (i.e. –COOH, -SO_3H, etc) acceptor group. [21]

Table 4.3 Amount of dye loading on TiO_2 surfaces

Dyes	Dye loading ($mol^{-1}.cm^{-1}$)*
TPA-PHA	**0.4×10^{-7}**
TPA-PFA	**0.7×10^{-7}**
Dye -1	**2.0×10^{-6}**
Dye-2	**1.9×10^{-6}**

**Amount of dye loading (before and after sensitization on TiO_2 surface calculated) calculated by UV-vis spectroscopy*

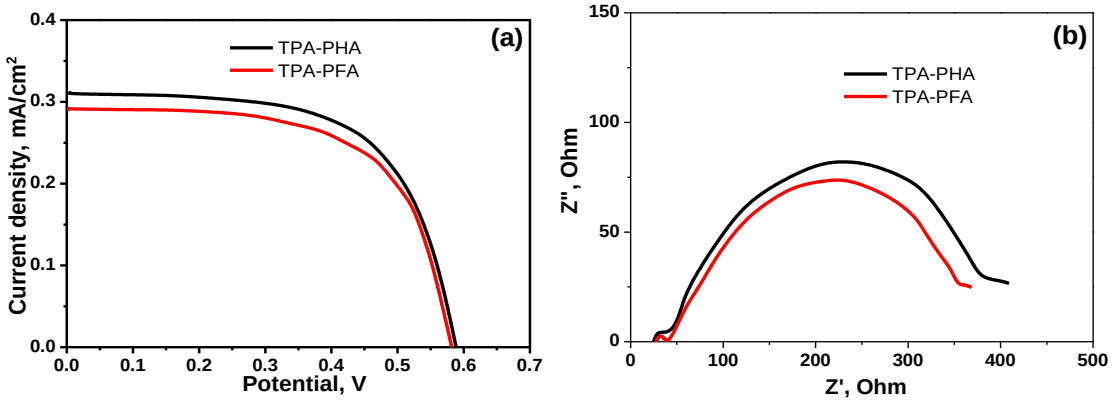

Figure 4.11 (a) *J–V* curve, (b) EIS curves of DSSCs based on TPA-PHA and TPA-PFA

Fig. 4.11 (a) presents the photovoltaic performance of the DSSCs was measured at 100 mW cm^{-2} under simulated AM 1.5G solar light conditions. TPA-PHA and TPA-PFA chromophores based photovoltaic devices gave a J_{sc}, V_{oc}, FF and PCE quite comparable and lower then dye 1 and 2. (The photovoltaic performance parameters are collected in Table 4.4). It is worth mentioning here that the maximum adsorption amount of dyes adsorbed on TiO_2 for dye 1 and 2 is twice times as much as that of chromophores (TPA-PHA and TPA-PFA). The high adsorption ability of dyes (dye 1 and 2) relative to chromophores is attributed to the formation of bi-dentate bridging linkage between the -COOH group of dye 1 and 2, the Bronsted acid site on the TiO_2 surface.

Table 4.4 DSSC performance parameters of TPA-PHA and TPA-PFA

Dye	J_{sc} (mA/cm²)[a]	V_{oc} (V) [a]	FF (%)[a]	η (%)[a]	R_{pt} (Ω)[b]	R_{rec} (Ω) [b]	CPR-P [b]
TPA-PHA	0.39 (± 0.2)	0.58 (± 0.02)	53 (± 0.2)	0.25 (± 0.05)	25.0	155	0.56
TPA-PFA	0.29 (± 0.2)	0.58 (± 0.01)	52 (±0.2)	0.20 (± 0.02)	26.6	142	0.56

[a]performances of DSSCs were measured with 0.25 cm^2 working area (measurement were performed under AM 1.5, 1 Sun irradiation). [b]Values estimated by fitting Nyquist plot, J_{sc}: short-circuit current, V_{oc}: open circuit voltage, FF**:** fill factor and η%: power conversion efficiency.

Fig. 4.11(b) compares the impedance spectra for TPA-PHA and TPA-PFA chromophore sensitized cells measured in the dark under a forward bias of -0.65 V with a frequency

range of 0.01 Hz to 10^5 KHz, respectively. The curves are fitted by the circuit, obtained parameters (R_{ct}, R_{rec} and CPE-P) are given in Table 4.4. The electron lifetime values derived from curve fitting of both sensitizers are 0.152 ms (TPA-PHA) and 0.148 ms (TPA-PFA), it is quite lower then dye 1 (0.235 ms) and dye 2 (0.221 ms). The longer electron lifetime indicates more effective suppression of the back reaction of the injected electron with triiodide in the electrolyte.

4.5 Photovoltaic performance of dyes

The DSSC cell efficiency (η) of TPA-PHA and TPA-PFA had 0.25 (± 0.05) and 0.20 (± 0.02), respectively. Due to the poor dye loading capacity and formation of strong π-stacked aggregation between the chromophores on TiO_2 surface, electron-injection capacity from dyes to conduction band of TiO_2 tends to reduce, owing to intermolecular energy transfer (excited-state quenching) between chromophores.[22] After successful substitution of cyanoacetic acid to chromophores, the cell performance was enhanced for dyes (dye-1, dye-2). Without using any co-absorbents and additives the power conversion efficiency (PCE, η) of Dye-1 and Dye-2 exhibits 2.1% and 1.9% respectively. This moiety not only improves the efficiency, but is also beneficial to tune the molecular energy levels and improves the dye loading capacity.

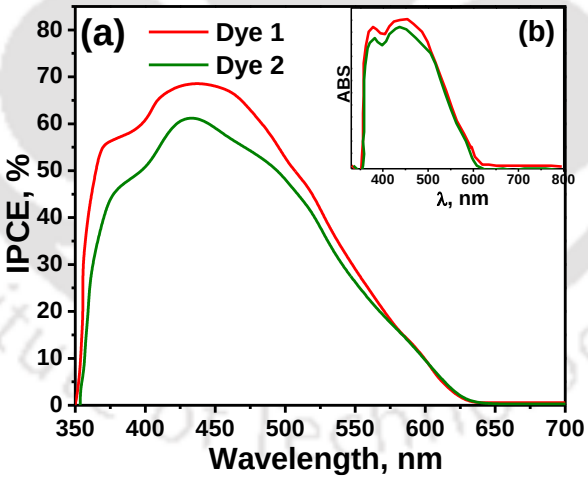

Figure 4.12 (a) Photocurrent action spectra of dye 1 and 2, (b) Electronic absorption spectra of dye-1 and dye-2 sensitized TiO_2 thin film surface.

The monochromatic incident photon to collected electron conversion efficiencies (IPCEs) against wavelength were measured as shown in **Fig. 4.12(a)**. Apart from a comparable summit of IPCE of ~68%, the onset wavelengths of photocurrent response are stepwise blue shifted from dye 1 to dye 2. The IPCE, defined as the number of electrons generated

by light in the outer circuit divided by the number of incident photons, was determined by the following equation.[23]

$$IPCE\ (\%) = {100 \times 1240 \times I_{sc}(mA\ cm^{-2})}\Big/{\lambda(nm) \times P_{in}(mW\ cm^{-2})}$$

Where, I_{sc} is the short-circuit photocurrent generated by the incident light and λ is the wavelength of this light with intensity P_{in}. The dye 1 and 2 efficiently converts visible light to photocurrent in the region from 350-650 nm. It is important to note that the IPCE spectrum reveals blue-shifted bands compared to absorption spectral (on TiO_2 thin film) peaks shown in Fig. 4.12 (b). It appears to be a common phenomenon for such types of most organic dyes, which has been ascribed to the de-protonation of carboxylic acid, as well as to the formation of H-aggregation on the semiconductor surface.[24-26]

Table 4.5 Summary of the current-voltage (*J*-*V*) characteristics and EIS parameters of the dye 1 and 2.

Dye	J_{sc} **(mA/cm^2)**[a]	V_{oc} **(V)**[a]	**FF (%)**[a]	η **(%)**[a]	R_{pt} **(Ω)**[b]	R_{rec} **(Ω)**[b]	**CPR-P**[b]
Dye 1	5.05 (± 0.4)	0.677 (± 0.05)	61 (± 0.2)	2.1 (±0.1)	27.0	175	0.58
Dye 2	4.68 (± 0.3)	0.700 (± 0.04)	59 (± 0.2)	1.9 (±0.2)	27.6	163	0.57

[a]performances of DSSCs were measured with 0.25 cm^2 working area (measurement were performed under AM 1.5, 1 Sun irradiation). [b]Values estimated by fitting Nyquist plot, J_{sc}: short-circuit current, V_{oc}: open circuit voltage, FF**:** fill factor and η%: power conversion efficiency.

Fig. 4.13 presents the photocurrent density–voltage (*J*-*V*) of these two DSSCs measured at the simulated AM 1.5G conditions, and the photovoltaic parameters were shown in Table 4.5**.** It can be seen that dye 1 is the basic structure, and dye 2 the structural modification on *m*-fluorine substitution, of phenylene spacer, have been selected to examine the substituent effects on the photovoltaic performance of DSSCs. In Table 4.5, the short-circuit photocurrent (J_{sc}) was gradually decreased from 5.05 mA/cm^2 (η = 2.1%) with dye 1 and 4.68 mA/cm^2 (η = 1.9%) with dye 2, respectively. These changes in J_{sc} are

mainly attributed to the extended wavelength range of light absorption that was confirmed by the IPCE spectra.

Electrochemical impedance spectroscopy (EIS) was performed to study the charge transfer processes in DSSCs. The Nyquist curves of photovoltaic devices based on two sensitizers are shown in Fig. 4.13 (a), three semicircles were observed in the Nyquist plots. The higher frequency from 10^3 to 10^5 Hz (smaller), lower mid frequency from 1 to 10^2 Hz (larger semicircles) and last low frequency 0.01H to 1Hz in the Nyquist plots corresponds to the charge transfer at the Pt-counter electrode/ I^-/I_3^- electrolyte interface, the TiO_2/sensitizer/electrolyte interface and diffusion process of I^-/I_3^- in the electrolytes respectively. Small circles were almost similar in all the sensitizers due to the use of similar Pt-counter electrode and I^-/I_3^- electrolyte. The curves are fitted for the circuit shown in [Inset Fig. 4.14 (a)] and obtained parameters (R_{ct}, R_{rec} and CPE-P) are given in Table 4.5.

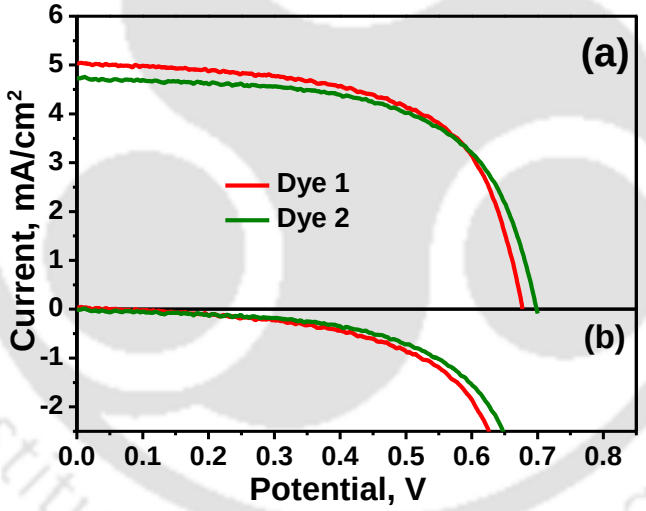

Figure 4.13 Photocurrent density vs voltage (*J-V*) curves of DSSCs using dye 1 and 2 as sensitizers (a) under irradiation of AM 1.5G simulated solar light (100 mW cm^{-2}) and (b) dark condition in the presence of I^-/I_3^- redox mediator in MNP.

These DSSCs show similar series resistances (R_{pt}), of about 27.0-27.6 Ω, due to the same I^-/I_3^- electrolyte and electrode in both materials and surface area. The interfacial charge recombination reaction of electrons with I_3^- can be described by a charge recombination resistance (R_{rec}). As shown in Table 4.5 and Figure 4.14, a major intermediate semicircle for each dye 1 and 2 can be observed in the EIS Nyquist plot, which is related to the

charge transfer resistance on the TiO_2/dye/electrolyte interface (R_{rec}). EIS results reveals that the electron transport property of dye 1 based device is slightly enhanced, which has been reflected by middle arc (lower frequency shift) and gives R_{rec} as higher than dye 2 based devices.

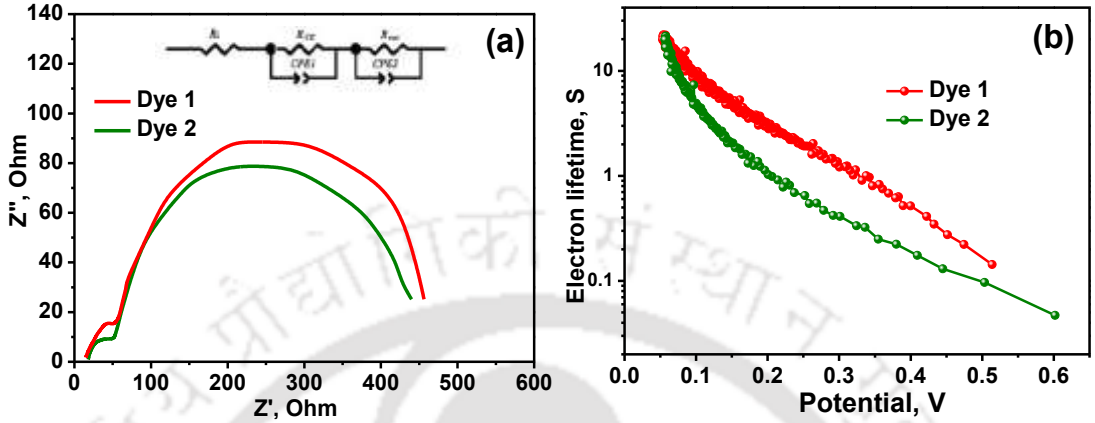

Figure 4.14 (a) Nyquist plots of the DSSCs fabricated by dye 1 and dye 2 sensitizers (Inset show equivalent circuit model) and (b) OCVD spectra for dye 1 and 2, plots of photovoltaic devices electron lifetime (τ_n) as a function of open circuit voltage, V_{oc}.

The OCVD (Open-circuit voltage decay) is a technique to monitoring the decay of photovoltaic V_{oc} after turning off the illumination in a steady state and the suppressed charge recombination at the FTO-electrolytes interface can also be confirmed by this technique. Fig. 4.14 (b) shows electron life time (τ) calculated from the OCVD curves, from following equation.[27]

$$\tau_n = \frac{K_B T}{e}\left(\frac{dV_{oc}}{dt}\right)^{-1}$$

Where, "*e"* is the positive elementary charge, (dV_{oc}/dt) the rate of change of V_{oc} and K_BT is the thermal energy. The photovoltaic decay rate is directly related to electron lifetime τ_e, because as the illumination of the photovoltaic devices at the OCP is interrupted, excess electrons are diminished through recombination. Fig. 4.14 (b) curves linear its charge recombination reaction has indicated 1st order dependence on the electron concentration of TiO_2 photoanode.[23] The dye 1 shows much longer electron life times compared to dye 2 device, these result conclusion above device two factor affected such as faster electron transportation and lower recombination rate.

4.6 Experimental Section

Materials and methods

All reactions were performed under argon atmosphere and appropriate THF, CH_3CN, EtOH etc., solvents were distilled from drying agents prior to use. The starting material (*E*)-4-(4-bromostyryl)-*N*,*N*-diphenylanilinewere prepared according to the published references.[28] Compound "TPA-PH, TPA-PHA, and TPA-PFA" was synthesized by Suzuki-coupling reaction and dye-1, dye-2 was prepared by Knoevenagel condensation method.

4.6.1 General synthesis procedures for TPA-PH, TPA-PHA and TPA-PFA

In a clean 50 ml RB flack compound A (1 mmol), phenyl boronic acid/4-formylphenyl boronic acid/2-fluoro-4-formylphenyl boronic acid (1.5 mmol), aliquat 2-3 drops and 2 M potassium carbonate were dispersed into the mixture of THF:H_2O (2:1) solvent. Finally, in the presence of argon condition $Pd(PPh_3)_4$ were added. After that the reaction was performed 80 °C for 12 h under "Ar" condition. The reaction mixture was poured into water extracted with chloroform. The organic layer washed dried over anhydrous sodium sulphate. The solvent was removed with roto evaporator and the residue was purified by silica gel column.

4.6.2 General synthesis procedures for Dye-1 and Dye-2

In two-neck RB Compound B or C (1.10 mmol), cyanoacetic acid (1.50 mmol) was dissolved into mixture of CH_3CN and $CHCl_3$ (1:1) solvent. In the presence of Argon condition catalytic amount of piperidine was added, and the reaction was carried out 80 °C for 8 h. After cooling, the reaction mixture was extracted with $CHCl_3$. The organic layer is washed and dried over anhydrous sodium sulphate, and the solvent was removed with roto evaporator and the residue was purified by silica gel column.

[4-(2-Biphenyl-4-yl-vinyl)-phenyl]-diphenyl-amine (TPA-PH):

Analytical TLC on silica gel, 1:4 ethyl acetate/hexane white solid; 82% yield, ^{1}H NMR (600 MHz, $CDCl_3$) δ 7.69-7.66 (m, 3H), 7.63-7.60 (m, 2H), 7.59-7.55 (m, 4H), 7.49-7.48 (d, 1H), 7.47 (s, 1H), 7.46-7.43 (m, 2H), 7.41-7.40 (d, 2H), 7.36-7.33 (t, 1H), 7.28-7.25 (m, 5H), 7.13-7.11(d, 3H), 7.09-7.07 (d, 2H), 7.06-7.02 (m, 3H); ^{13}C NMR (150 MHz, $CDCl_3$) δ 147.76, 132.36, 132.29, 132.20, 129.50, 129.01, 128.78, 128.70, 128.46, 127.59, 127.54, 127.47, 127.10, 126.93, 126.73, 124.73, 123.79, 123.27.

(*E*)-4'-(4-(diphenylamino)styryl)-[1,1'-biphenyl]-4-carbaldehyde (TPA-PHA):

Analytical TLC on silica gel, 1:4 ethyl acetate/hexane light green solid; 85% yield, ^{1}H NMR (600 MHz, $CDCl_3$) δ 10.05 (s, 1H), 7.96 (d, J = 12 Hz, 1H), 7.78 (d, J = 6 Hz, 2H),7.65 (d, J = 12 Hz ,2H), 7.60 (d, J = 6 Hz, 2H), 7.42 (d, J = 6 Hz, 2H), 7.29-7.26 (dd, 4H), 7.14 (d, J = 6 Hz, 4H), 7.05 (t, J = 6.8 Hz, 4H); ^{13}C NMR (150 MHz, $CDCl_3$) δ 192.01, 147.82, 147.64, 146.79, 138.37, 138.18,135.29, 131.29, 130.49, 129.50, 129.26, 127.76, 127.67, 127.48, 127.08, 126.20, 124.79, 123.56, 123.36; HRMS (ESI) m/z: $[M+H]^+$ calcd for $C_{33}H_{25}NO$ 452.2014, found 452.2002.

(*E*)-4'-(4-(diphenylamino)styryl)-2-fluoro-[1,1'-biphenyl]-4-carbaldehyde(TPA-PFA):

Analytical TLC on silica gel, 1:4 ethyl acetate/hexane light green solid; 85% yield, ^{1}H NMR (600 MHz, $CDCl_3$) δ 10.01 (s, 1H), 7.86-7.65 (m, 2H), 7.42 (dd, 2H),7.27 (t, 4H), 7.17-7.12 (m, 5H), 7.08-7.01 (m, 5H) ;^{13}C NMR (150 MHz, $CDCl_3$) δ 161.31, 147.68, 147.46, 138.20, 136.93, 134.85, 133.10, 131.15, 131.12, 131.04, 129.38, 129.32, 127.52, 126.51, 126.09, 126.00, 124.62, 123.37, 123.18, 116.56, 116.33 HRMS (ESI) m/z: $[M+H]^+$ calcd for $C_{33}H_{24}FNO$ 470.1920, found 470.1919.

(*E*)-2-cyano-3-(4'-((*E*)-4-(diphenylamino)styryl)-[1,1'-biphenyl]-4-yl)acrylic acid (Dye-1):

Analytical TLC on silica gel, 1:4 ethyl acetate/hexane light green solid; 85% yield, ^{1}H NMR (600 MHz, $CDCl_3$) δ 8.02 (s, 1H), 8.84 (d, 2H), 7.68 (d, 3H), 7.60 (d, 2H), 7.52 (d, 2H), 7.31(m, 5H), 7.17 (d, 1H), 7.04 (d, 6H), 6.95 (d, 2H); ^{13}C NMR (150 MHz, $CDCl_3$) δ 146.92, 146.42, 137.50, 134.18, 132.87, 131.07, 130.89, 130.15, 129.55, 129.11, 128.82, 127.75, 126.51, 126.18, 126.02, 124.20, 123.31, 122.86, 118.52, 116.69, 116.53; HRMS (ESI) m/z: $[M+H]^+$ calcd for $C_{36}H_{26}N_2O_2$ 519.2073, found 519.2077.

(*E*)-2-cyano-3-(4'-((*E*)-4-(diphenylamino)styryl)-2-fluoro-[1,1'-biphenyl]-4-yl)acrylic acid (Dye-2):

Analytical TLC on silica gel, 1:4 ethyl acetate/hexane light green solid; 85% yield, ^{1}H NMR (600 MHz, $CDCl_3$) δ 8.14 (s, 1H), 8.00 (d, 2H), 7.7 (d, 2H), 7.62-7.55 (dd, 4H), 7.40 (d, 2H), 7.17(d, 2H), 7.25 (d, 2H), 7.11 (d, 4H), 7.05 (d, 4H); ^{13}C NMR (150 MHz, $CDCl_3$) δ 147.54, 147.46, 143.67, 138.40, 137.63, 136.65, 136.01, 131.58, 131.21, 130.78, 129.27, 128.81, 127.43, 127.30, 127.14, 126.84, 126.15, 124.54, 123.42, 123.10, 117.44; HRMS (ESI) m/z: $[M+H]^+$ calcd for $C_{36}H_{25}N_2O_2F$ 537.1978, found 537.1999.

4.7 Crystal Data

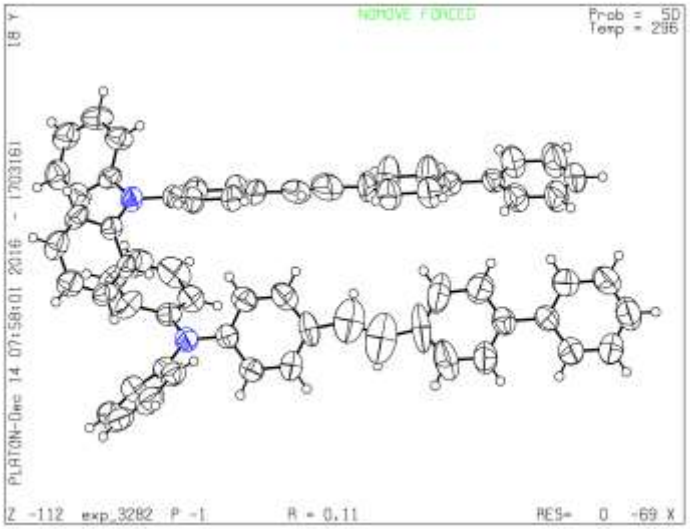

Figure 4.15 ORTEP diagram of (*E*)-4-(2-([1,1'-biphenyl]-4-yl)vinyl)-N,N-diphenyl-aniline

Table 4.6 Crystallographic parameters of (*E*)-4-(2-([1,1'-biphenyl]-4-yl)vinyl)-*N*,*N*-diphenylaniline

Compound	NPh3-Ph2
Sum Formula	$C_{32}H_{25}N$
CCDC NO	1522685
Formula. wt.	423.53
Crystal system	Triclinic
Space group	P -1
a (A°)	10.3348(14)
b (A°)	10.6780(15)
C(A°)	24.291(3)
α(°)	82.824(12)
β(°)	80.865(12)
γ(°)	63.255(14)
V/ A3	2359.2(6)
Z	4
Density/Mgm^{-3}	1.201
Abs. Coeff/mm^{-1}	0.070
F(0 0 0)	1000
Total no. of reflections	14278
Reflections, $I > 2\sigma(I)$	0.0421>*0.1113*
Max. 2θ/°	3.59 to 20.31°
Ranges (h, k, l)	-12 ≤ h ≤ 12, -12 ≤ k ≤ 10, -28 ≤ l ≤ 27

Complete to 2θ (%)	0.917
Goof (*F2*)	1.140
R indices [*I* >= *2σ(I)*]	0.1096
R indices (all data)	0.2372

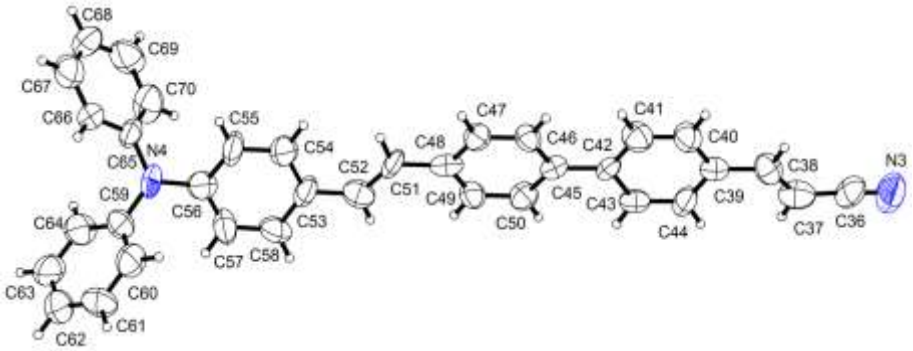

Figure 4.16 ORTEP diagram of (*E*)-3-(4'-((*E*)-4-(diphenylamino)styryl)-[1,1'-biphenyl]-4-yl)acrylonitrile

Table 4.7 Crystallographic parameters of (*E*)-3-(4'-((*E*)-4-(diphenylamino)styryl)-[1,1'-biphenyl]-4-yl)acrylonitrile

Compound	NPh3-Ph2-CN
Sum Formula	$C_{35}H_{26}N_2$
CCDC NO	1416063
Formula. wt.	949.16
Crystal system	Triclinic
Space group	P -1
a (A°)	9.5617(12)
b (A°)	11.6648(15)
C(A°)	24.400(3)
α(°)	88.063(9)
β(°)	89.343(9)
γ(°)	74.841(9)
V/ A3	2625.3(6)
Z	2
Density/Mgm^{-3}	1.201
Abs. Coeff/mm^{-1}	0.070
F(0 0 0)	1000
Total no. of reflections	8480
Max. 2θ/°	0.83 to 25°
Ranges (h, k, l)	-11 ≤ h ≤ 11, -13 ≤ k ≤ 13, -29 ≤ l ≤ 26
Complete to 2θ (%)	0.917
Data/ Restraints/Parameters	8480/0/667

Goof (*F2*)	1.140
R indices [*I* >= *2σ(I)*]	0.0796
R indices (all data)	0.1060

4.8 Summary

In conclusion, a series of D-π-A based triphenylamine derivatives have been designed and synthesized. The two AIEE chromophores (after substitution of cyanoacrylic acid) were successfully applied in DSSC application for the first time. Their optical and electrochemical properties are explained by experimental and theoretical studies. TPA-PH exhibits ACQ property due to the strong π-π interaction of phenyl units, remaining TPA-PHA, TPA-PFA chromophores exhibits AIEE property due to multiple intermolecular interactions to aldehyde group such as C-H$^{\cdots}$π and C-H$^{\cdots}$O and TPA-PHA exhibit Nano rods, TPA-PFA exhibits nanoparticles in aggregated state (ethanol-water mixture) which are confirmed by FESEM images. The organic dyes, while they had been absorbed onto the surface of nanocrystalline anatase TiO_2, showed 2.1 and 1.9% quantum efficiencies in DSSCs. Certain structural features were found to be related to the performance of devices, adding a fluorine substituted at the *m*-position on phenelyne spacer of dye 2 which in turn slightly reduces the performance of solar cells.

4.9 References

1. Wu, W. B.; Tang, R. L.; Li. Q. Q.; Li. Z. *Chem. Soc. Rev*. **2015**, ***44***, 3997-4022.
2. Liu, J. J.; Cheng, Y. X.; Xie, Z. Y.; Geng, Y. H.; Wang, L. X.; Jing, X. B.; Wang, F. S. *Adv. Mater*. **2008**, *20*, 1357-1362.
3. Uoyama, H.; Goushi, K.; Shizu, K.; Nomura. H.; Adachi, C. *Nature* **2012**, *492*, 234-238.
4. Friend, R. H.; Gymer, R. W.; Holmes, A. B.; Burroughes, J. H.; Marks, R. N.; Taliani, C.; Bradley, D. D. C.; Dos Santos, D. A.; Bredas, J. L.; Logdlund, M.; Salaneck, W. R. *Nature* **1999**, *397*, 121-128.
5. Farinola, G. M.; Ragni, R. *Chem. Soc. Rev*. **2011**, *40*, 3467-3482.
6. Gompper, R.; Wagner, H. U. *Angew. Chem. Int. Edit*. **1988**, *27*, 1437-1455.
7. Zhelev, Z.; Ohba, H.; Bakalova, R. *J. Am. Chem. Soc*. **2006**, *128*, 6324-6325.
8. Bakalova, R.; Zhelev, Z.; Aoki, I.; Ohba, H.; Imai, Y.; Kanno, I. *Anal. Chem*. **2006**, *78*, 5925-5932.

9. Luo, J. D.; Xie, Z. L.; Lam, J. W. Y.; Cheng, L.; Chen, H. Y.; Qiu, C. F.; Kwok, H. S.; Zhan, X. W.; Liu, Y. Q.; Zhu, D. B.; Tang, B. Z. *Chem. Commun*. **2001**, 1740-1741.
10. Mei, J.; Leung, N. L. C.; Kwok, R. T. K.; Lam, J. W. Y.; Tang, B. Z. *Chem. Rev*. **2015**, *115*, 11718-11940.
11. Gao, B. R.; Wang, H. Y. Hao, Y. W.; Fu, L. M.; Fang, H. H.; Jiang, Y.; Wang, L.; Chen, Q. D.; Xia, H.; Pan, L. Y.; Ma, Y. G.; Sun, H. B. *J. Phys. Chem. B* **2010**, *114*, 128-134.
12. Zhang, Y. J.; Sun, J. W.; Bian, G. F.; Chen, Y. Y.; Ouyang, M.; Hu, B.; Zhang, C. *Photoch. Photobio. Sci*. **2012**, *11*, 1414-1421.
13. Liu, Y.; Tao, X. T.; Wang, F. Z.; Dang, X. N.; Zou, D. C.; Ren, Y.; Jiang, M. H. *J. Phys. Chem. C* **2008**, *112*, 3975-3981.
14. Li, H. Y.; Chi, Z. G.; Zhang, X. Q.; Xu, B. J.; Liu, S. W.; Zhang, Y.; Xu, J. R. *Chem. Commun*. **2011**, *47*, 11273-11275.
15. Jiang, Y. H.; Wang, Y. C.; Hua, J. L.; Tang, J.; Li, B.; Qian, S. X.; Tian, H. *Chem. Commun*. **2010**, *46*, 4689-4691.
16. Ding, A. X.; Hao, H. J. Gao, Y. G. Shi, Y. D.; Tang, Q.; Lu, Z. L. *J. Mater. Chem. C* **2016**, *4*, 5379-5389.
17. Yang, W.; Li, C.; Zhang, M.; Zhou, W.; Xue, R.; Liu, H.; Li, Y. *Phys. Chem. Chem. Phys*. **2016**, *18*, 28052-28060.
18. Ouyang, M.; Zhan, L.; Lv, X.; Cao, F.; Li, W.; Zhang, Y.; Wang, K.; Zhang, C. *RSC. Adv*. **2016**, *6*, 1188-1193.
19. Liang, Z.-Q.; Wang, X.-M.; Dai, G.-L.; Ye, C.-Q.; Zhou. Y.-Y.; Tao, X.-T. *New J. Chem*. **2015**, 39, 8874-8880.
20. Raju, T. B.; Vaghasiya, J. V.; Afroz, M. A.; Soni, S. S.; Iyer, P. K. *Organic Electronics* **2016**, *39*, 371-379.
21. Zhang, L.; Cole. J. M. *ACS Appl. Mater. Inter.* **2015**, *7*, 3427–3455.
22. Ooyama. Y.; Harima, Y. *ChemPhysChem* **2012**, *13*, 4032 – 4080.
23. Kalyanasundaram, K. EPFL Press: Lausanne, Switzerland, 2010.
24. Nazeeruddin, M. K.; Pechy, P.; Renouard, T.; Zakeeruddin, S. M.; Humphry-Baker, R.; Comte, P.; Liska, P.; Cevey, L.; Costa, E.; Shklover, V.; Spiccia, L.; Deacon, G. B.; Bignozzi, C. A.; Grätzel, M. *J. Am. Chem. Soc.* **2001**, *123*, 1613-1624.

25. Kim, S.; Choi, H.; Kim, D.; Song, K.; Kang, S. O.; Ko, J. *Tetrahedron* **2007**, *63*, 9206-9212.
26. Yang, C. J.; Chang, Y. J.; Watanabe, M.; Hon, Y. S.; Chow, T. J. *J. Mater. Chem.* **2012**, *22*, 4040-4049.
27. Soni, S. S.; Fadadu, K. B.; Vaghasiya, J. V.; Solanki, B. G.; Sonigara, K. K.; Singh, A.; Das, D.; Iyer, P. K. *J. Mater. Chem. A* **2015**, *3*, 21664-21671.
28. Hwang, S.; Lee, J. H.; Park, C.; Lee, H.; Kim, C.; Park, C.; Lee, M. H.; Lee, W.; Park, J.; Kim, K.; Park, N. G.; Kim, C. *Chem. Commun*. **2007**, 4887-4889.

Appendix

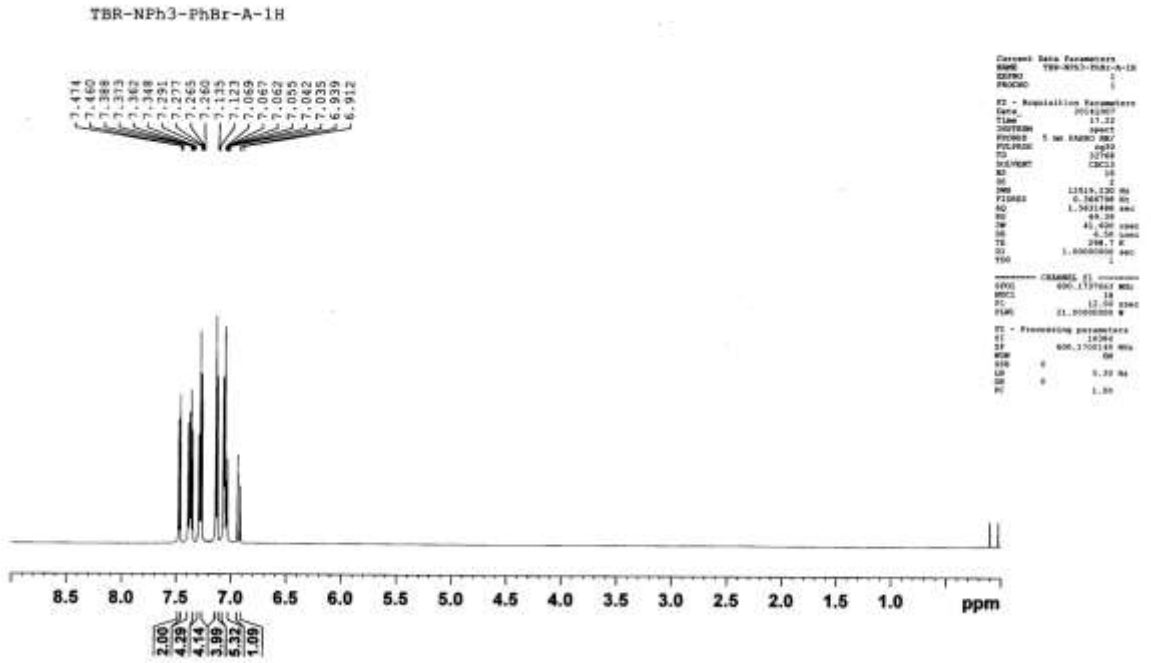

^{1}H-NMR spectrum of (*E*)-4-(4-bromostyryl)-*N*,*N*-diphenylaniline

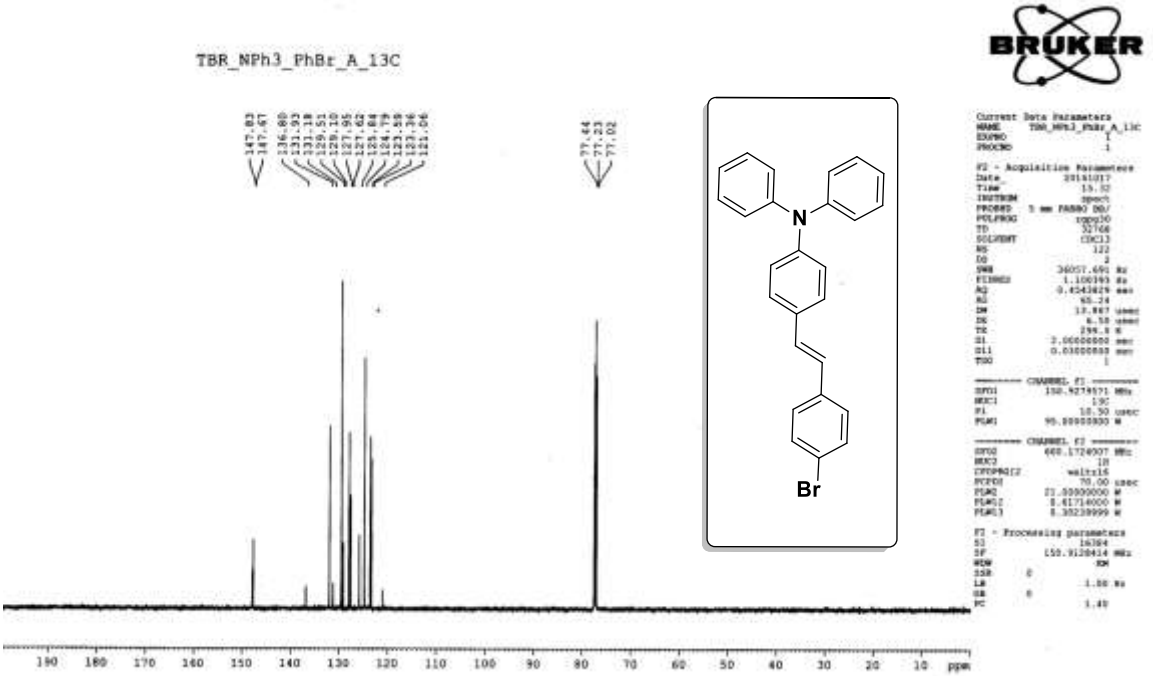

^{13}C-NMR spectrum of (*E*)-4-(4-bromostyryl)-N,N-diphenylaniline

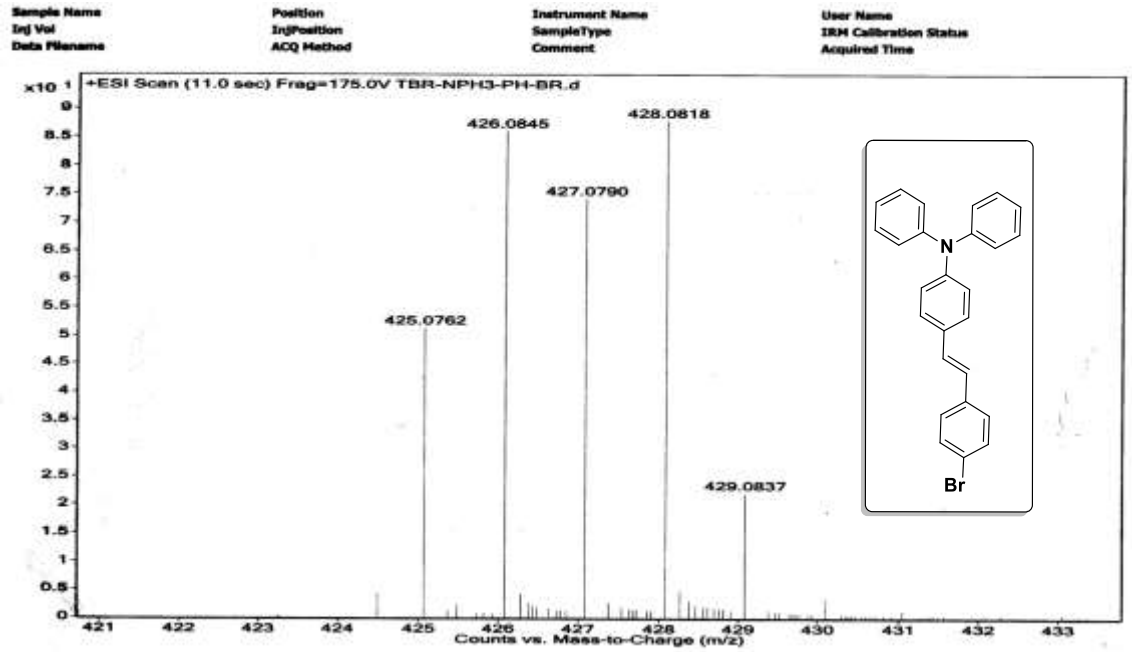

ESI-MS spectrum of (*E*)-4-(4-bromostyryl)-*N*,*N*-diphenylaniline

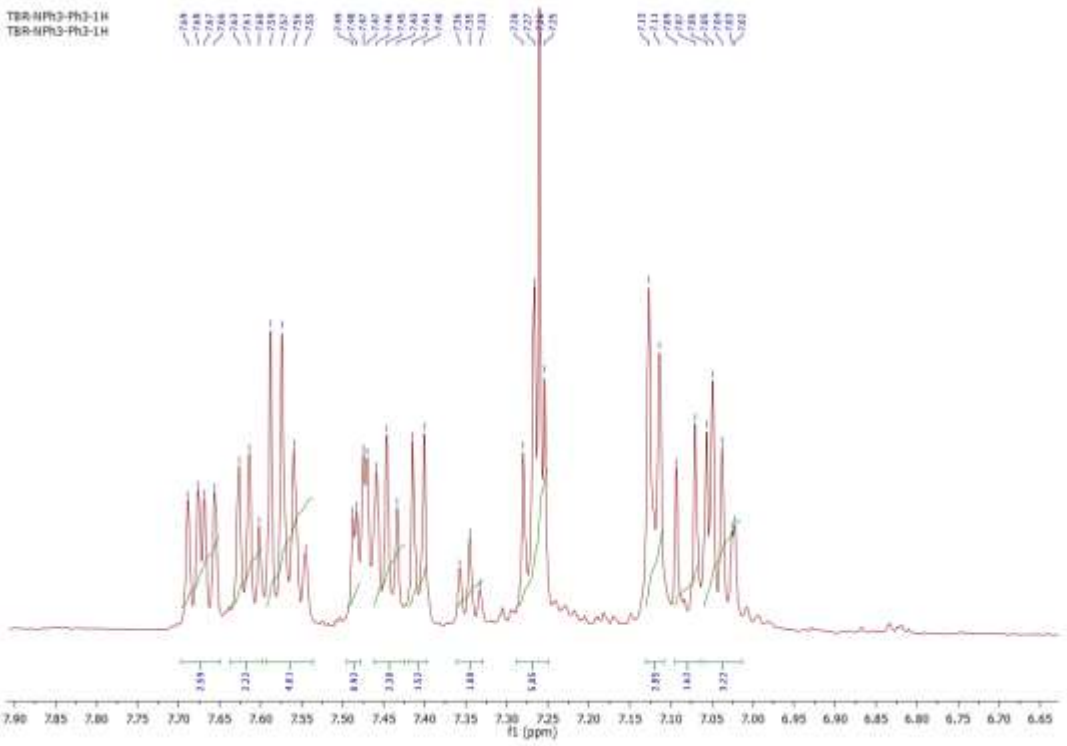

^{1}H-NMR spectrum of [4-(2-Biphenyl-4-yl-vinyl)-phenyl]-diphenyl-amine

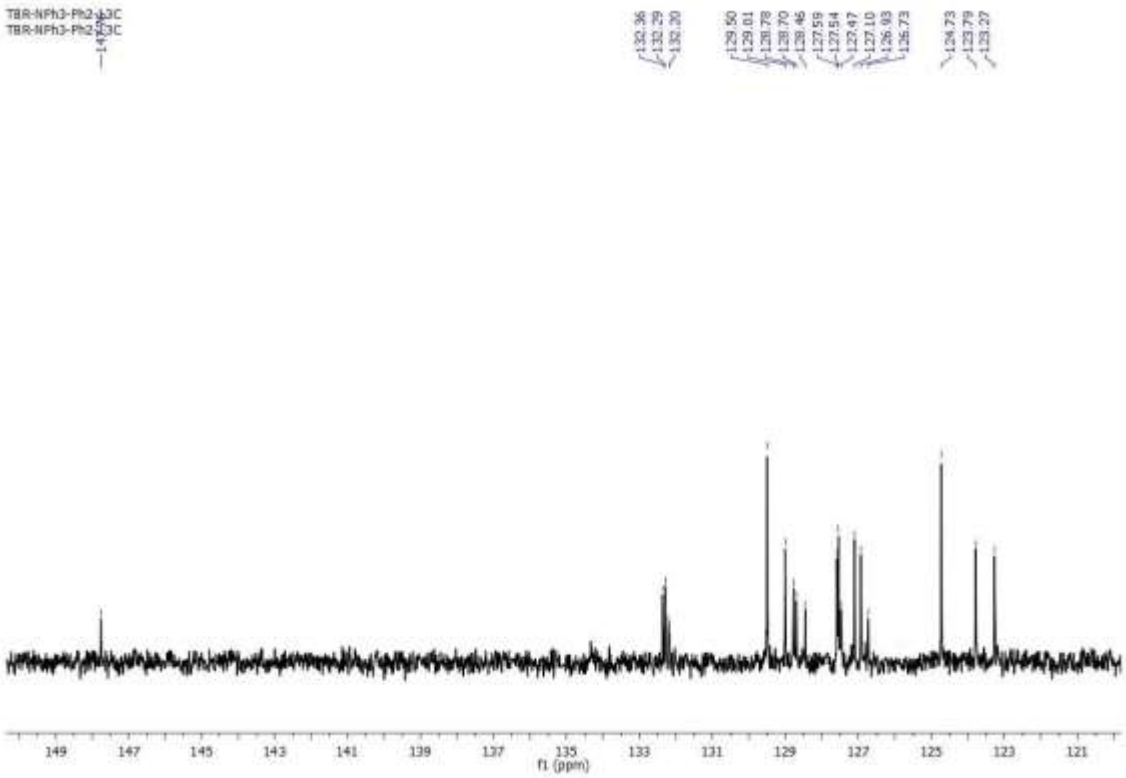

^{13}C-NMR spectrum of (*E*)-4-(2-([1,1'-biphenyl]-4-yl)vinyl)-*N*,*N*-diphenylaniline

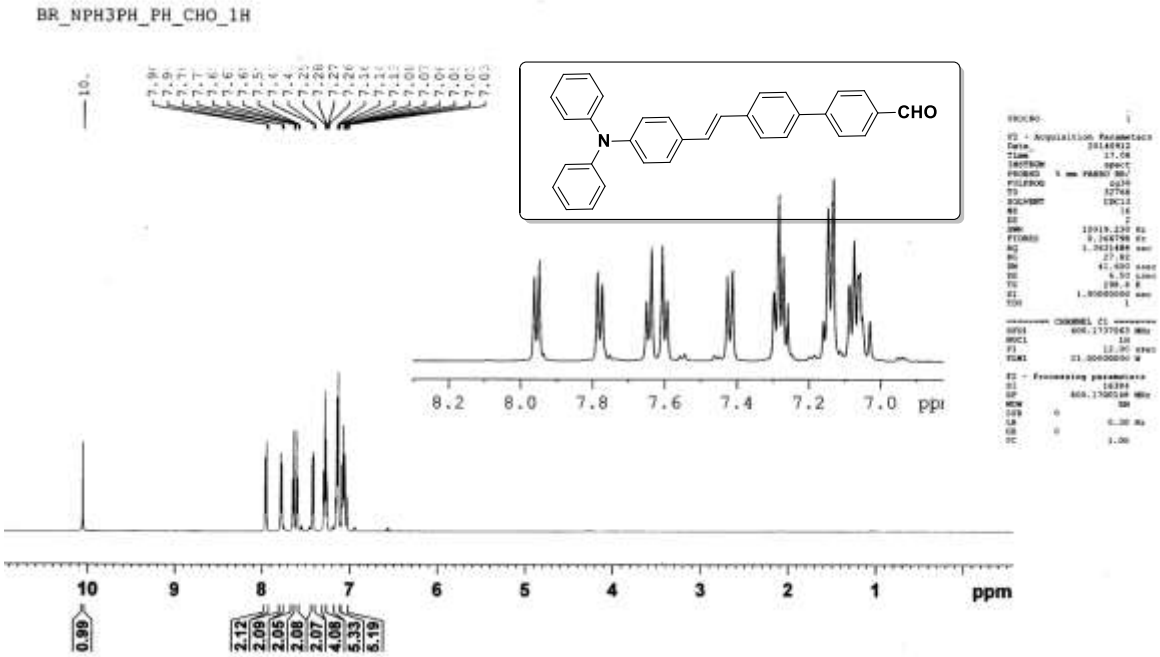

^{1}H-NMR spectrum of (*E*)-4'-(4-(diphenylamino)styryl)-[1,1'-biphenyl]-4-carbaldehyde

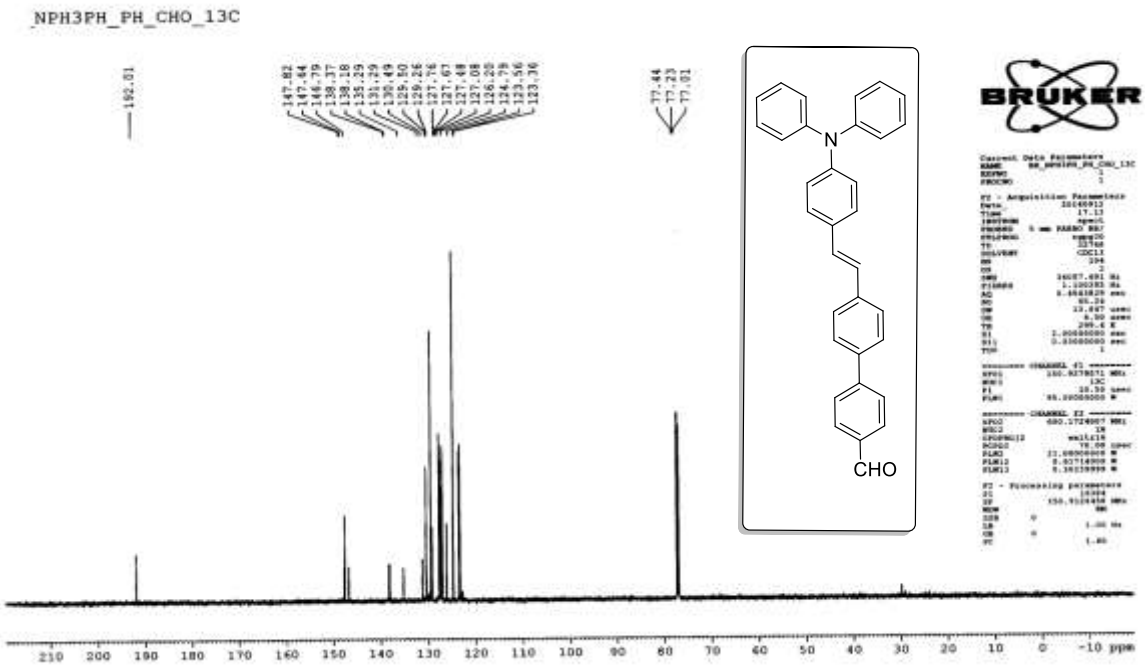

^{13}C-NMR spectrum of (*E*)-4'-(4-(diphenylamino)styryl)-[1,1'-biphenyl]-4-carbaldehyde

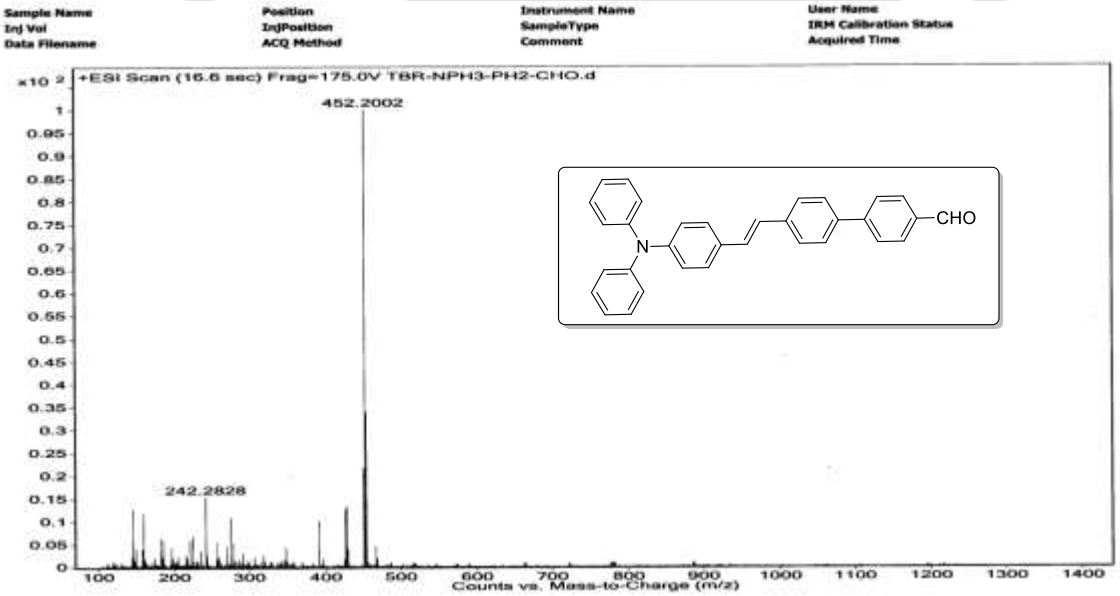

ESI-MS spectrum of (*E*)-4'-(4-(diphenylamino)styryl)-[1,1'-biphenyl]-4-carbaldehyde

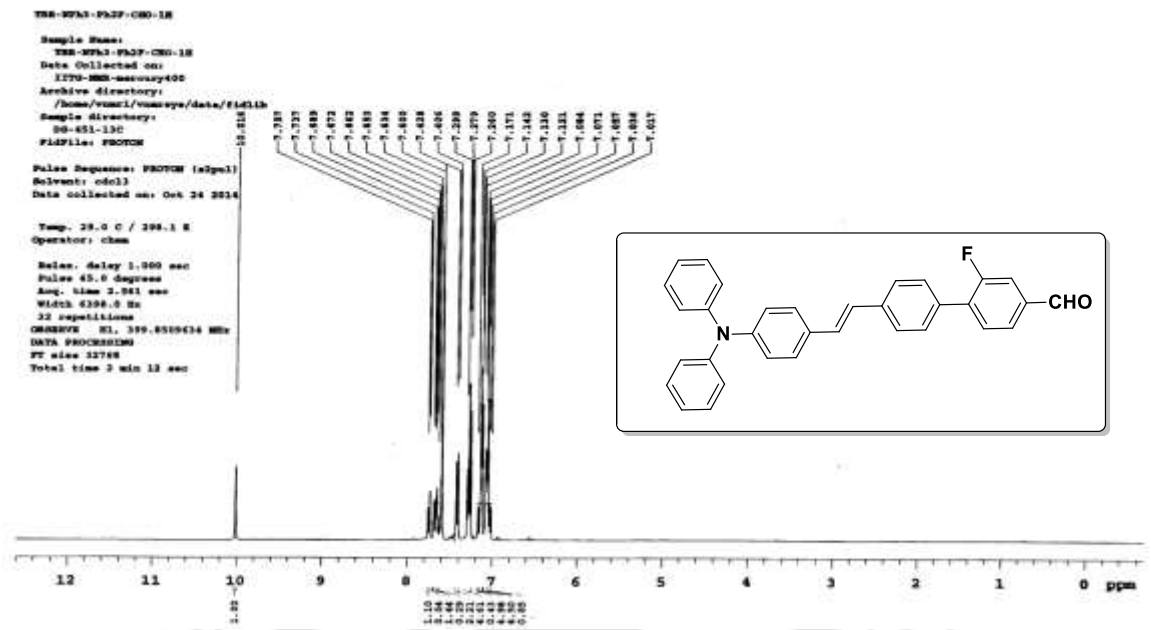

^{1}H-NMR spectrum of (*E*)-4'-(4-(diphenylamino)styryl)-2-fluoro-[1,1'-biphenyl]-4-carbaldehyde

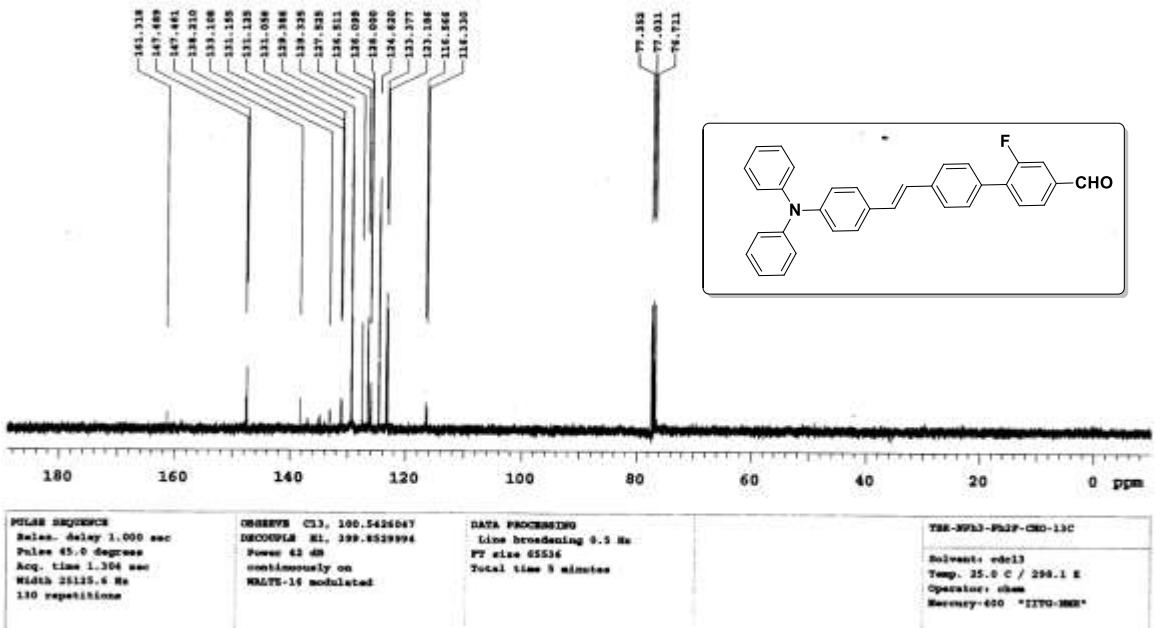

^{13}C-NMR spectrum of (*E*)-4'-(4-(diphenylamino)styryl)-2-fluoro-[1,1'-biphenyl]-4-carbaldehyde

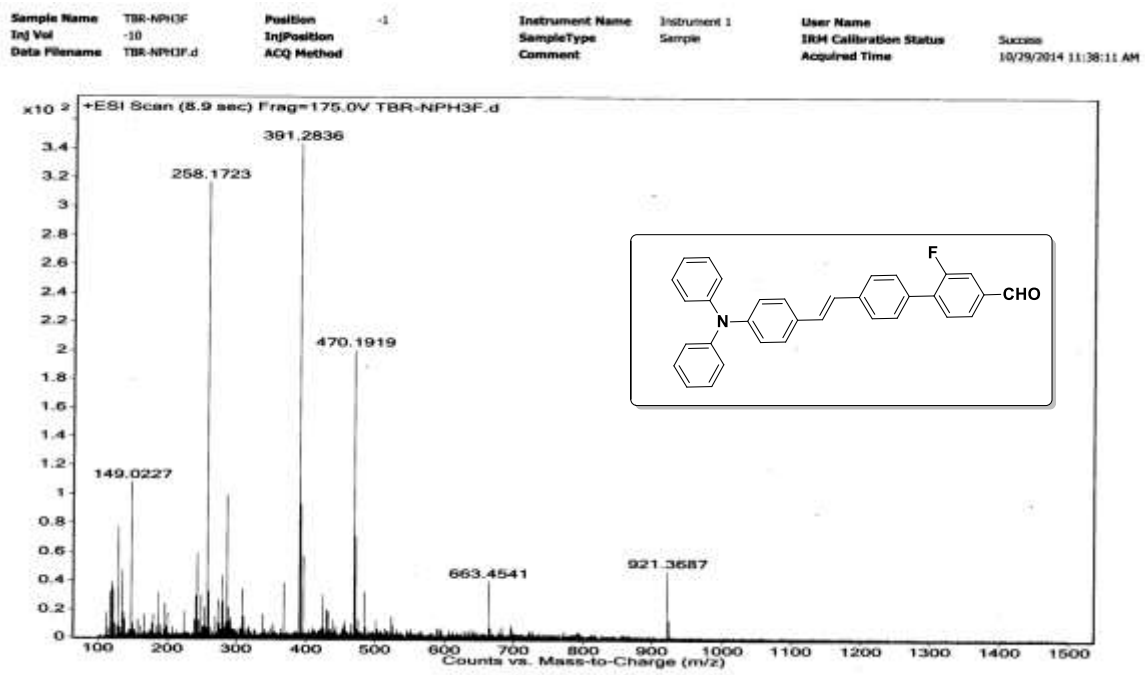

ESI-MS spectrum of (*E*)-4'-(4-(diphenylamino)styryl)-2-fluoro-[1,1'-biphenyl]-4-carbaldehyde

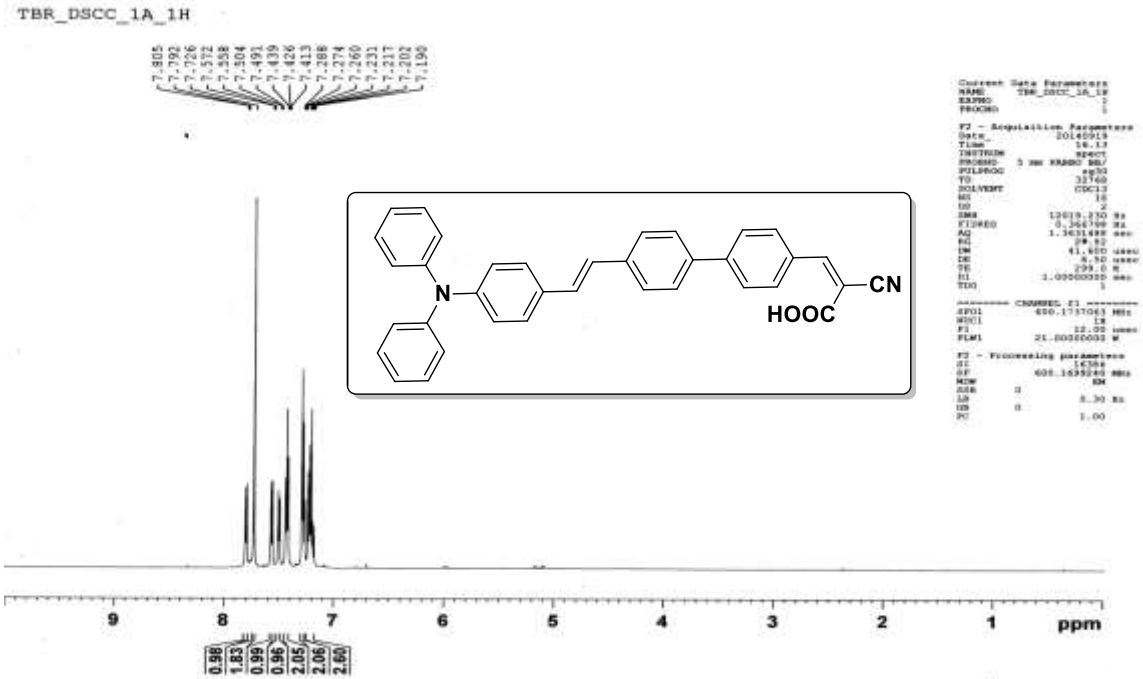

^{1}H-NMR spectrum of (*Z*)-2-cyano-3-(4'-((*E*)-4-diphenylamino) styryl)-[1,1'-biphenyl]-4-yl)acrylic acid

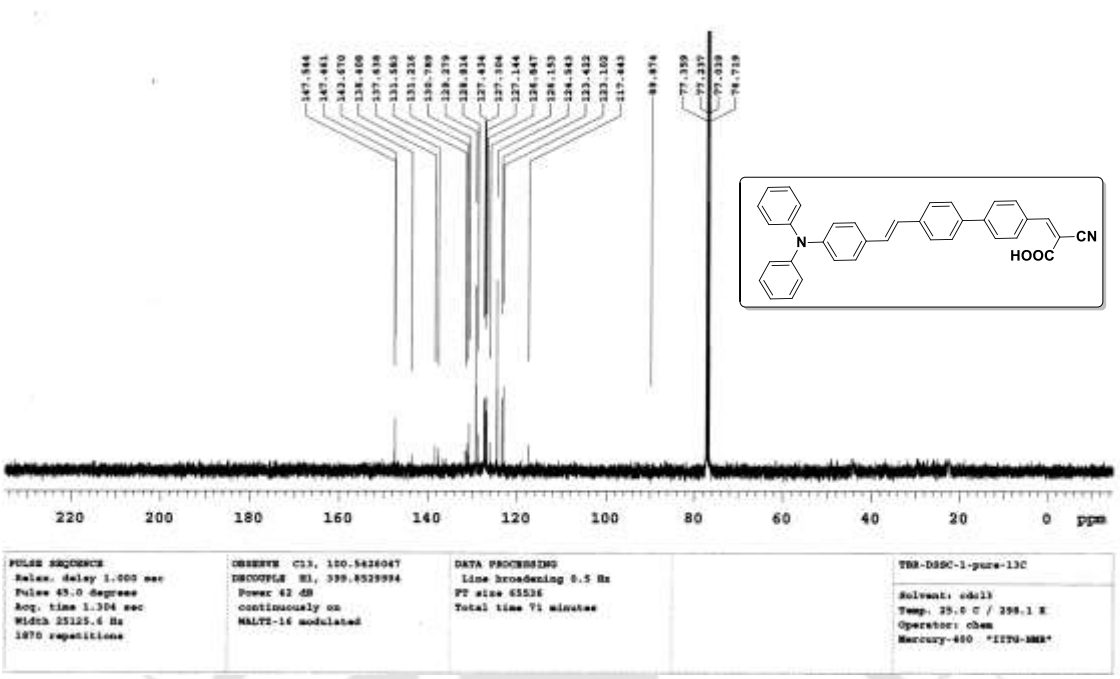

^{13}C NMR spectrum of (*Z*)-2-cyano-3-(4'-((*E*)-4-diphenylamino)styryl)-[1,1'-biphenyl]-4-yl)acrylic acid

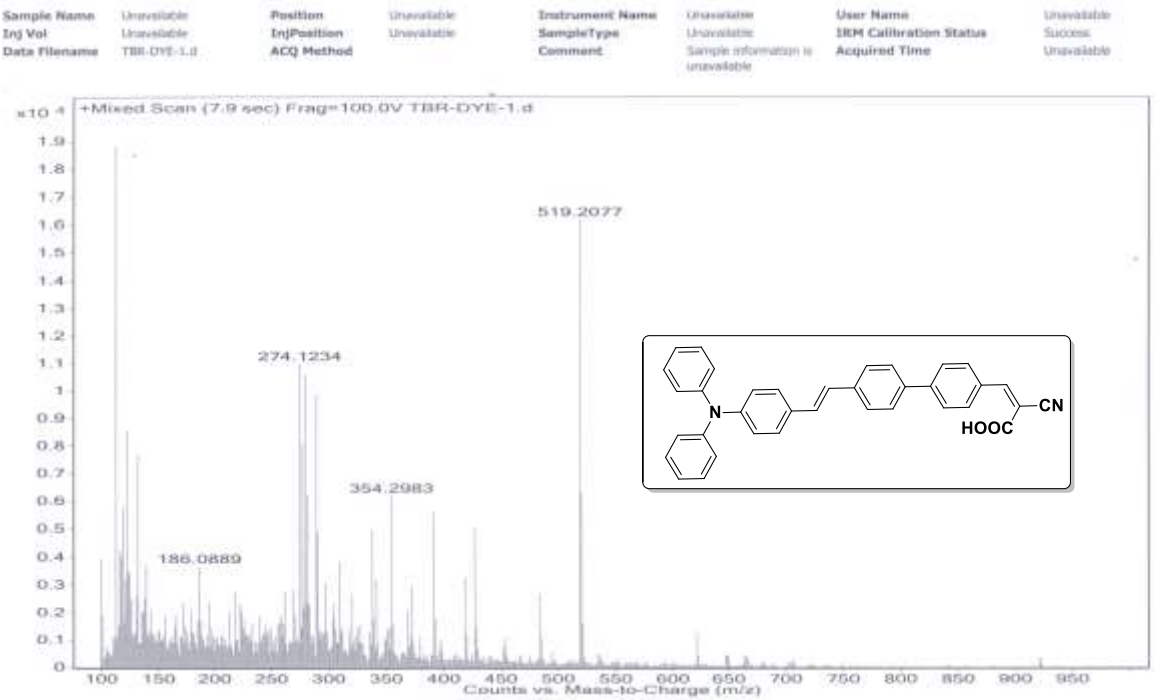

ESI-MS spectrum of (*Z*)-2-cyano-3-(4'-((*E*)-4-diphenylamino)styryl)-[1,1'-biphenyl]-4-yl)acrylic acid

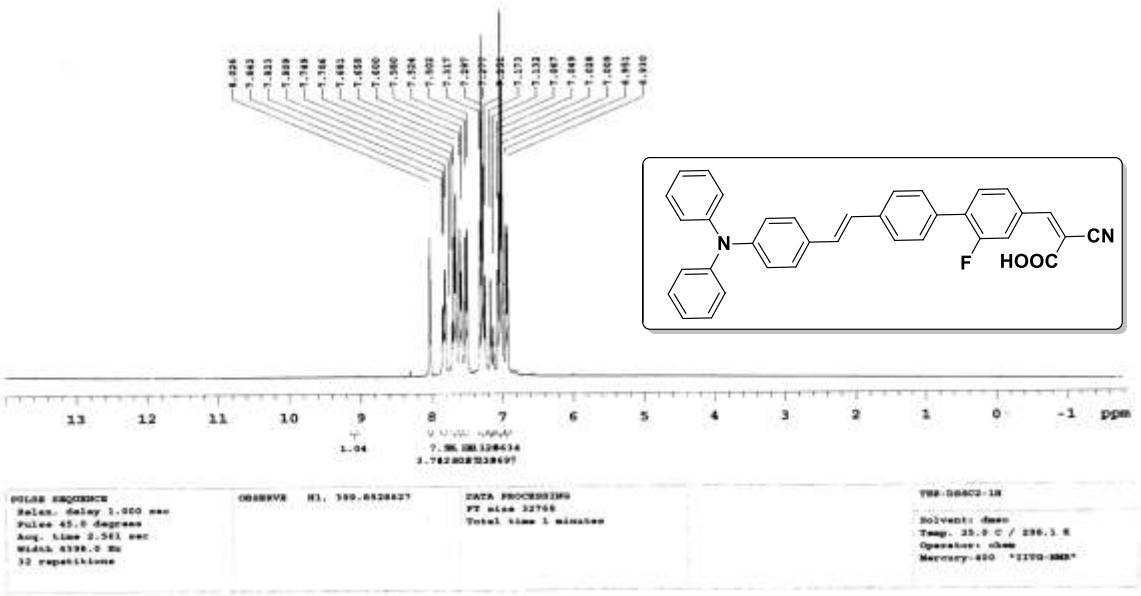

^{1}H NMR spectrum of (*Z*)-2-cyano-3-(4'-((*E*)-4-diphenylamino)styryl)-2-fluoro-[1,1'-biphenyl]-4-yl)acrylic acid

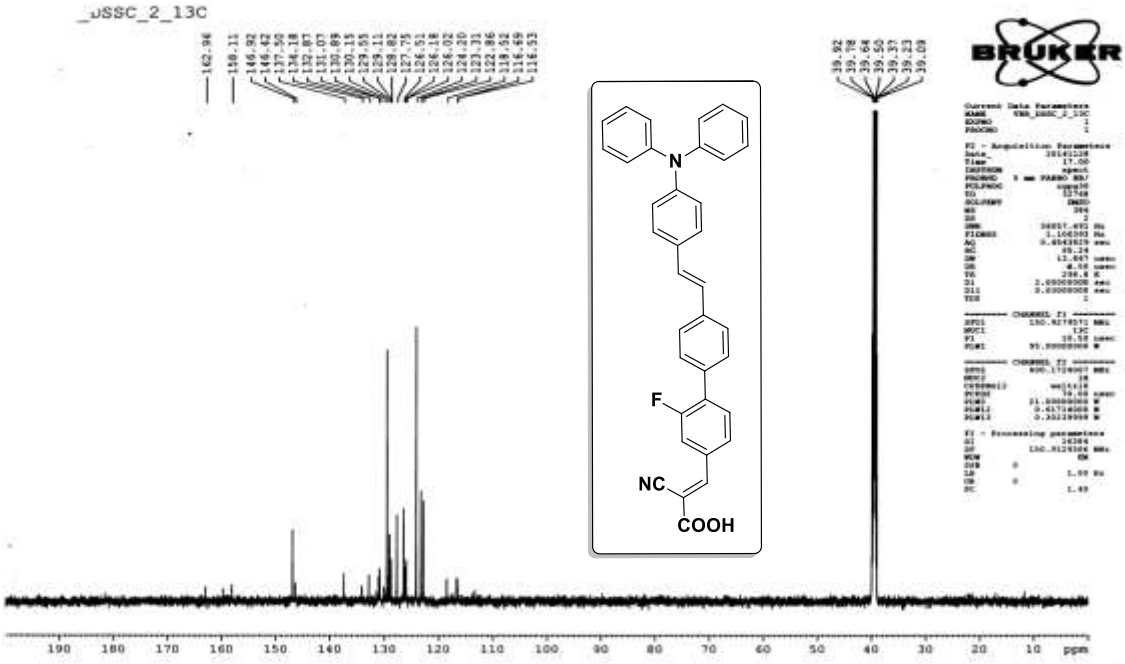

^{13}C NMR spectrum of (*Z*)-2-cyano-3-(4'-((*E*)-4-diphenylamino)styryl)-2-fluoro-[1,1'-biphenyl]-4-yl)acrylic acid

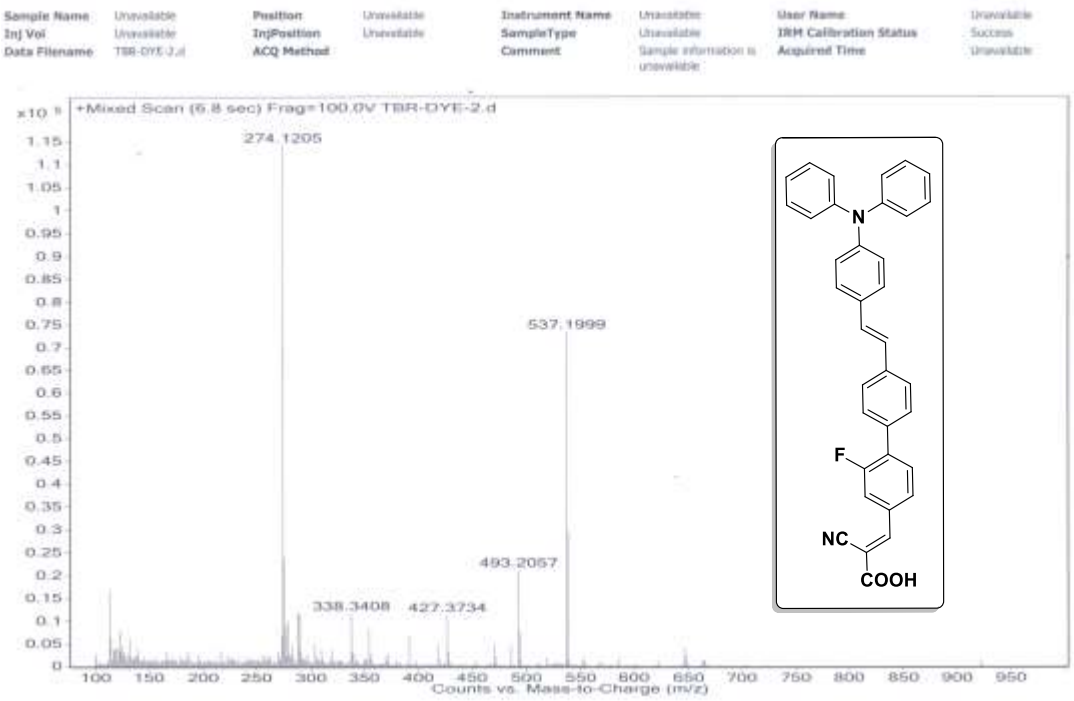

ESI-MS spectrum of (*Z*)-2-cyano-3-(4'-((*E*)-4-diphenylamino)styryl)-2-fluoro-[1,1'-biphenyl]-4-yl)acrylicacid

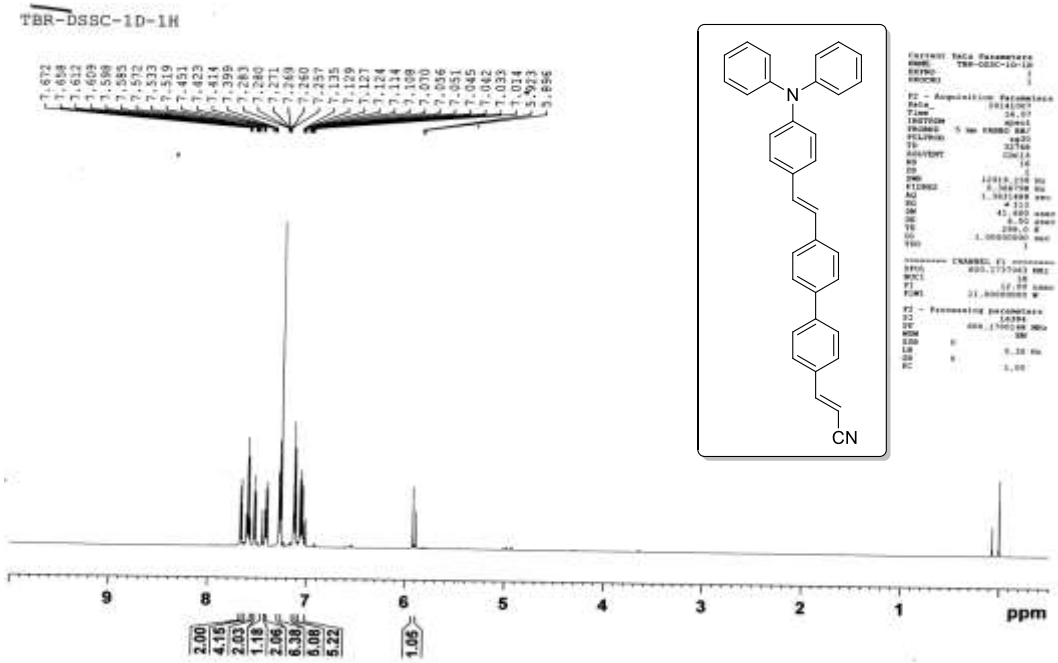

^{1}H NMR spectrum of (*E*)-3-(4'-((*E*)-4-(diphenylamino)styryl)-[1,1'-biphenyl]-4-yl)acrylonitrile

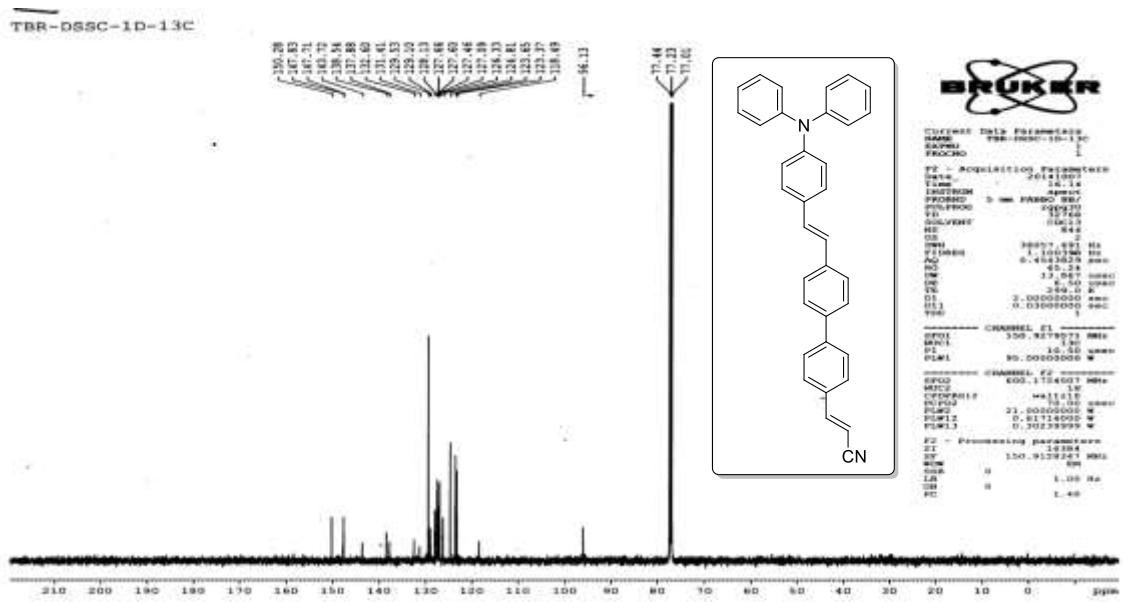

^{13}C NMR spectrum of (*E*)-3-(4'-((*E*)-4-(diphenylamino)styryl)-[1,1'-biphenyl]-4-yl)acrylonitrile

CHAPTER-5

Influence of 3, 4-di substituted thiophene derivative π-extended dyes and its effect on dye-sensitized solar cells

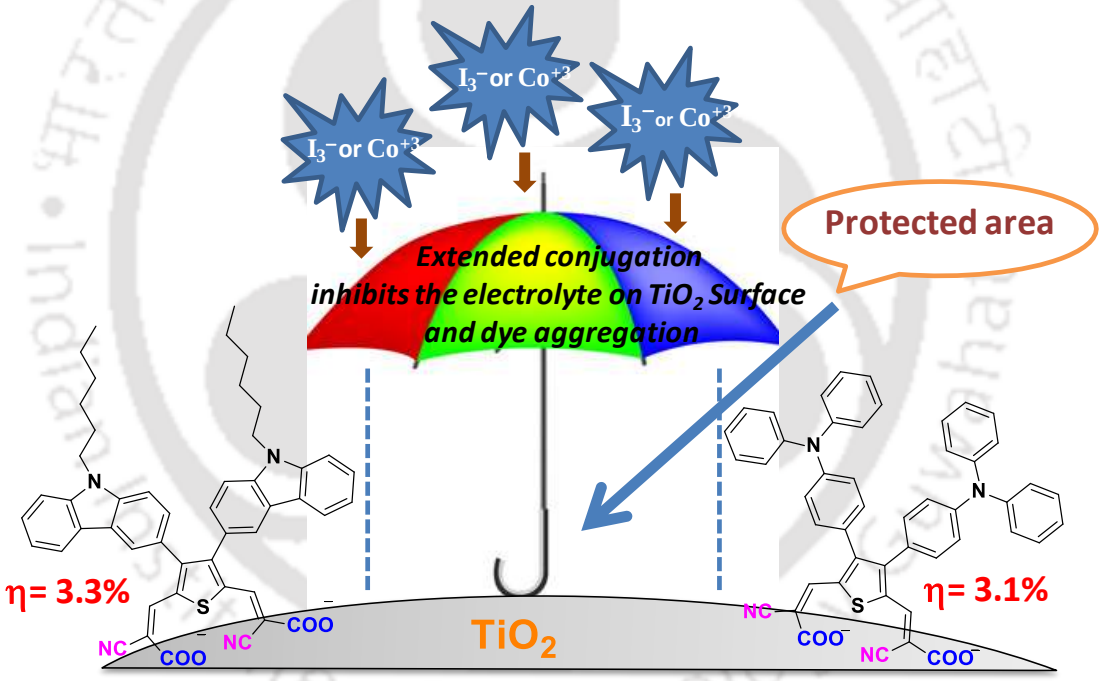

(*manuscript communicated*)

Abstract

The design and synthesis of two novel thiophene 3,4-di substituted organic dyes with double acceptor at 2,5-position frame work, as photosensitizers for the dye sensitized solar cell application are reported. In this work, the influence of carbazole and triphenylamine units substitution at 3,4-position of thiophene based dyes were studied. These planar and three-dimension structure of donors were found to effectively inhibit the I^-/I_3^- and Co^{+2}/Co^{+3} electrolyte on TiO_2 surface. The results show that varying the donor position in dyes also effectively works for DSSC application, but does not broaden the absorption peak in visible region of Cz-Th-Dye and NPh3-Th-Dye due to the blocking of electron delocalization at 2,5-positions by acceptor units. With two twisted donors at 3,4-position in Cz-Th-Dye, NPh3-Th-Dye the dye aggregation and charge recombination retarded. The optical, electrochemical, density functional theory and TRPL studies were used to estimate the photovoltaic properties of the dyes. Without using any additives Cz-Th dye and NPh3-Th dye in presence of Co^{+2}/Co^{+3} redox shuttle resulted in an overall power conversion efficiency (PCE) of 3.3% and 3.1% respectively. By replacing one acceptor with any other donor, these thiophene moiety effectively worked as a new π-spacer in DSSC application.

5.1 Introduction

Since 1991 scientific community have paid considerable attention on dye sensitized solar cells (DSSCs),[1] because compared to conventional silicon based solar cells these had low cost, easy fabrication process and good efficiency among other prominent features. In the past two decades, tremendous research efforts have been devoted to design and synthesize various new π- spacers, anchors and photosensitizers (D-π-A, D-D-π-A, D-A-π-A etc.,).[2-5] Many researchers have focused on developing metal-free organic sensitizers due to the many advantages like facile synthesis and purification, low cost, convenience of customized molecular design, high molar absorption coefficients, with introduction of substituents on chromophore, which easily tunes photophysical and electrochemical properties and lower environmental impact.[6-8] In most of the D-π-A dyes typically cyano-acrylic acid was used as a acceptor because carboxyl group functionality allows a strong binding to the photoanode layer,[9] ultimately the current research is devoted to choose a suitable π-spacer and donor moiety to increase the DSSC performance.[10-15] To get good results with organic dyes, the electrons can be effectively delocalised through the overlapping of "p-orbitals" that facilitates the effective charge transfer from D to A in the molecule.[16,17] The suitable electronic structure, such as HOMO, LUMO, and HOMO-LUMO band gap also plays a crucial role in DSSC to improve the solar energy to electricity conversion efficiency.[5] The layer thickness of TiO_2,[18] choosing of suitable electrolyte,[19] chemical structure of the photosensitizer (dye) and the morphology of the TiO_2 surface (Dye/TiO_2 interface) also plays an important role to increase efficiency of DSSC.[16] If the electrolyte ions penetrate the dye layer, the recombination rate in between TiO_2 and electrolyte will increase resulting in decrease of the open-circuit voltage (V_{oc}) significantly.[20] To prevent the direct contact between the TiO_2 and electrolyte, and π-stacked aggregation between the dye molecules, we could introduce bulky groups or long alkyl chains at donor side or on π-spacer, that prevents electrolyte ions to penetrate the dye layer, results in longer electron lifetime in DSSC.[21,22]

Herein, two new dye molecules viz. Cz-Th-dye, NPh3-Th-dye which contains carbazole and triphenylamine donor groups substituted on thiophene unit at 3,4-position were designed and synthesized (Scheme 5.1).

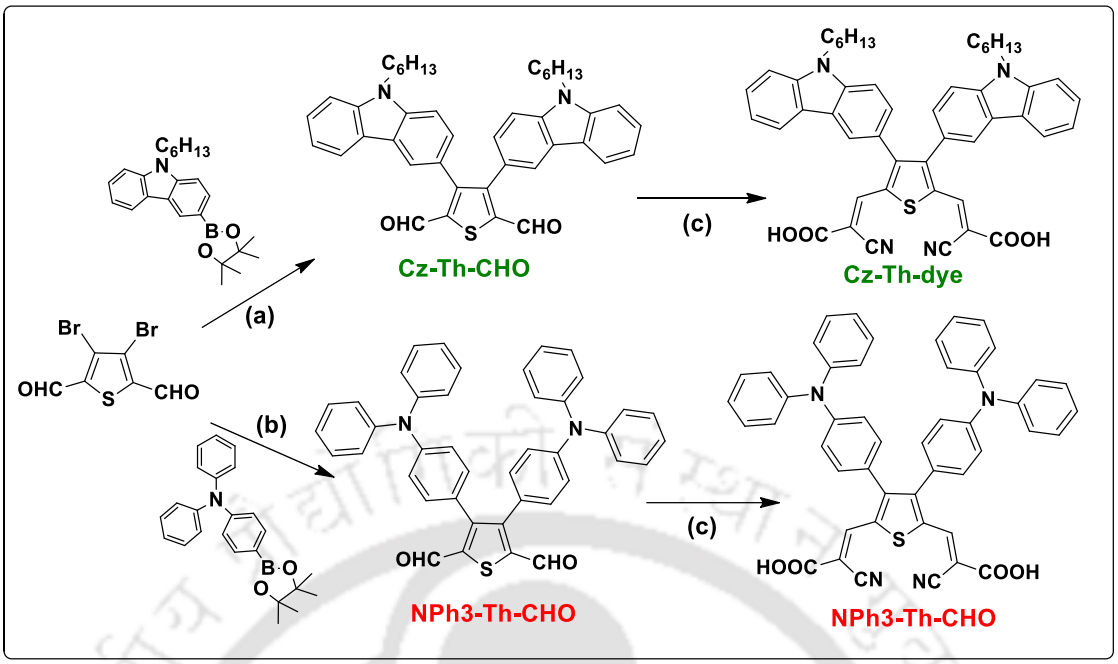

Scheme 5.1 Synthetic route of organic sensitizers (a) 9-hexyl-9*H*-carbazole-3-boronic acid pinacol ester, THF:H_2O=2:1, K_2CO_3, Aliquat, $Pd(PPh_3)_4$, 85 °C, 12 h. (b) 4-(Diphenylamino)phenylboronic acid pinacol ester, THF:H_2O=2:1, K_2CO_3, Aliquat, $Pd(PPh_3)_4$, 85 °C, 12 h (ii) Cyanoacetic acid, Piperidine, CH_3CN, 85 °C, 8 h.

The three critical processes that determine the photovoltaic performance of the dye sensitized solar cell are: (i) intramolecular charge transfer (ICT) characteristics, (ii) anti-aggregation (iii) prevent the electrolyte ions on TiO_2 surface. From the view point of a chemist, to get good efficiency in DSSC, the effective charge transfer must occur from D to A in Donor-(thiophene/furane/pyrrole)-A dyes, when donor units are substituted at α-position.[12,25] Very few scientific groups have reported the 2,3-disubstituted thiophene based organic dyes,[26] however, they have focused on the donor and also extension of π-bridge since their optical and electrochemical properties can be effectively tuned by the chemical structure.[17] To the best of our knowledge, we report the effect of 3,4-di substituted thiophene based dyes used in DSSC to study the effect of donor units at β-position of thiophene dye for the first time. In future, by replacing one acceptor with any other donor, these thiophene moiety dyes will also be utilized as a new π-spacer in DSSC application.

In the present work, we report the substitution of donor units at β-position on thiophene unit, like Cz-Th dye and NPh3-Th dyes, exhibiting mild charge transfer band appearing in

the visible region of absorption spectra is reported. This spectrum confirms very less charge transfer (ICT) occurring from D to A. While, compared to NPh3-Th dye, the Cz-Th dye have long alkyl chains and Planar structure of carbazole moiety better prevent the electrolyte on TiO_2 surface. In presence of Co^{+2}/Co^{+3} redox shuttle Cz-Th dye exhibit η = 3.2 ± (0.18) (J_{sc}= 6.30 mA cm^{-2}, V_{oc}= 0.69 V, *FF*=70%), similarly NPh3-Th dye exhibit η = 2.9 ± (0.20) (J_{sc}= 5.99 mA cm^{-2}, V_{oc}= 0.69 V, FF=69%). However, in presence of I^-/I_3^- redox couples Cz-Th dye showed η = 2.6 ± (0.12) (J_{sc}= 5.50 mA cm^{-2}, V_{oc}= 0.64 V, FF=67%), similarly NPh3-Th dye exhibits η = 2.4 ± (0.14) (J_{sc}= 5.28 mA cm^{-2}, V_{oc}= 0.64 V, FF=69%), due to the smaller size of iodine redox shuttle that easily penetrates on photoanode surface. These novel dyes are characterized by NMR (^{1}H NMR, ^{13}C NMR), mass spectrometry (ESI) and the corresponding optical, electrochemical and photovoltaic properties are also presented and discussed elaborately. The optimized geometry calculations of D-π-A dyes were ascertained by DFT calculation by using TD-DFT, CAM-B3LYP/631G(d,p) basis set.

Table 5.1 Optical, electrochemical and life time properties of dyes.

Dye	**Solution λ_{max} [nm]*a)***	**Film λ_{max} [nm]*b)***	**ε_{max}/M^{-1} cm^{-1}**	**HOMO [eV]*c)***	**LUMO [eV]*c)***	**τ (ns)**
Cz-Th	244, 274, 299, 393	487	15,000	5.42	2.88	1.07, 2.05
NPh3-Th	243, 307	401	33,000	5.37	3.20	1.14, 2.82

*a)*Maximum absorption wavelength of dyes in chloroform solution; *b)*Maximum absorption wavelength of dyes that were absorbed onto the TiO_2 films; *c)*onset potentials from CV measurements of thin films in 0.1 M Bu_4NPF_6 / CH_3CN solution, estimated from E_{HOMO} = -{(E_{on}^{ox}-$E_{1/2(ferrocene)}$) + 4.8} eV and E_{LUMO} = Estimated band gap by using onset of UV (TiO_2 film) – E_{HOMO}.

5.2 Result and discussion

5.2.1 Optical Properties

The UV-Visible absorption spectra of the sensitizers in chloroform solution and absorbed dye on TiO_2 film are shown in Figure 5.1. The corresponding properties for the sensitizers are summarized in Table 1. From the spectra, it is seen that Cz-Th dye exhibits multiple

bands in the range of 240-550 nm. The lower wavelength region absorption peaks at 240-360 nm is ascribed to a localized aromatic π-π* transition of conjugated system,

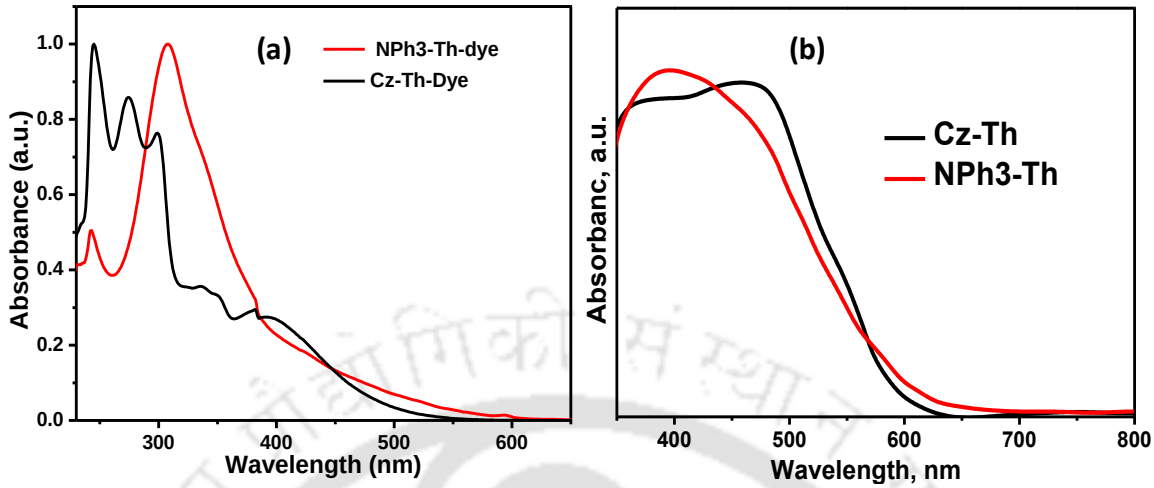

Figure 5.1 (a) Normalized absorption spectra of sensitizers recorded in chloroform solution, (b) on nanocrystaline TiO_2 film.

while the peak at a range of 360-550 nm is mainly attributed to an intramolecular charge transfer (ICT) transition from carbazole donor to cyanoacrylic acid acceptor. In Cz-Th dye, the intensity of the ICT peak has lesser intensity, due to the poor electron delocalization at 3,4- position of thiophene unit. While, NPh3-Th dye exhibits two major prominent bands in the range of 240-600 nm, the first peak (λ_{max}) at 243 nm, and second peak (λ_{max}) at 307 nm were ascertained. These lower wavelength peaks are due to the localized aromatic π-π* transition. The triphenylamine substituted NPh3-Th dye exhibit molar extinction coefficient (ε) = 33,000 $M^{-1}cm^{-1}$ at 307 nm, similarly Cz-Th exhibits molar extinction coefficient (ε) = 15,000 $M^{-1}cm^{-1}$ at 393 nm.

5.2.2 Electrochemical studies and TRPL studies:

The electrochemical properties of sensitizers were studied by cyclic voltammetry with 0.1M tetra n-butylammonium hexafluorophosphate ($TBAPF_6$) in acetonitrile solution. The first oxidation potential peaks corresponding to HOMO level of the dyes are shown in Figure 5.2 (a), and relevant data compiled in Table 5.1. The oxidation peaks indicate the removal of an electron from the donor moiety. HOMO energy levels were estimated from onset oxidation potential according to an empirical formula $E_{HOMO} = [-(E_{onset} - E_{onset(FC/FC+ vs. Ag/AgCl))} - 4.8]$ eV equation. LUMO levels were determined by the onset of the absorption spectra (E_g), $E_g=E_{HOMO}-E_{LUMO}$.

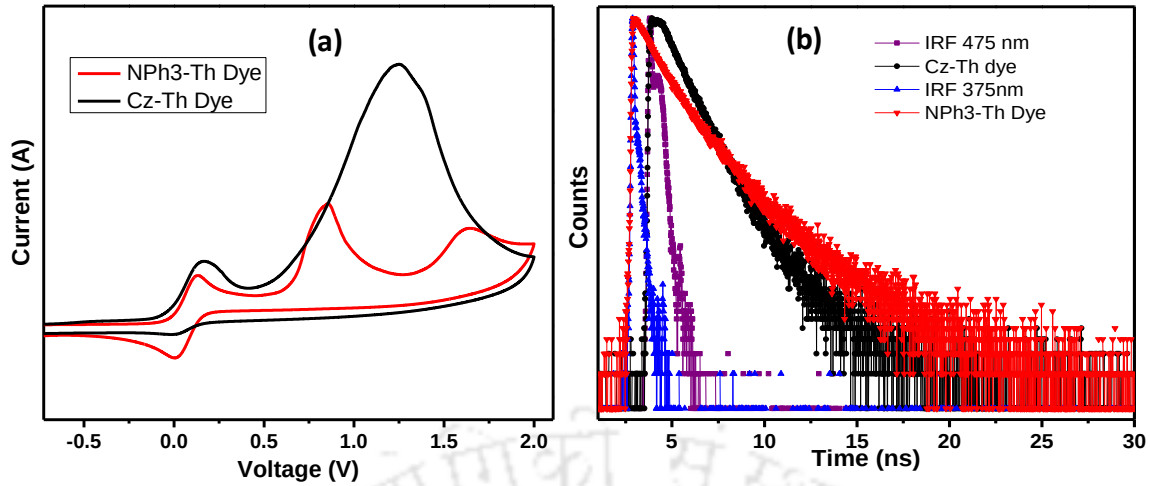

Figure 5.2 (a) Cyclic voltammograms of sensitizers recorded in 0.1M $TBAPF_6$ in acetonitrile solution, (b) Time-resolved photoluminescence (TRPL) spectra of sensitizers recorded in $CHCl_3$ solution, with respect to their fitting curves.

Experimentally evaluated LUMO level of dyes is shown in Table 5.1, Figure 5.2 (c). Cz-Th dye has deep HOMO level of -5.42 eV, compared to NPh3-Th dye at -5.37 eV, and these HOMO levels are feasible for dye regeneration in the presence of I^-/I_3^- and Co^{+2}/Co^{+3} redox electrolyte system due to the more positive oxidation potential of sensitizers compared with that of the I^-/I_3^- redox potential (-4.5 eV vs NHE) and Co^{+2}/Co^{+3} redox potential (-5.1 eV vs NHE). While, compared to the Cz-Th dye, NPh3-Th dyes have more sufficient driving force for electron injection from oxidized dye to CB of nanocrystaline TiO_2 surface.

Time-resolved photoluminescence (TRPL) measurements were carried out in $CHCl_3$ solution. Cz-Th dyes and NPh3-Th dyes were applied with pulse excitation at 475 nm and 375 nm, respectively [Fig. 5.2 (b)]. The corresponding data are summarized in Table 5.1.

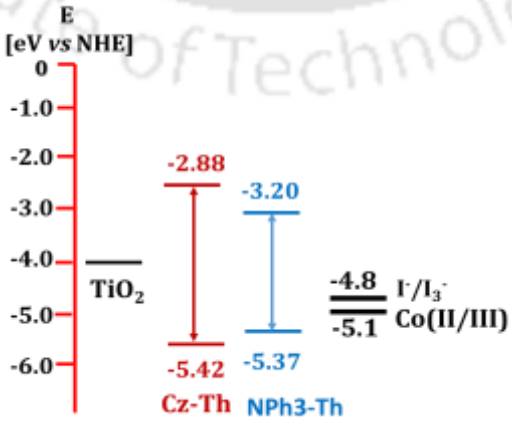

Figure 5.2 (c) Energy level diagram of organic dyes calculated by cyclic voltammetry.

5.2.3 Theoretical molecular orbital calculations:

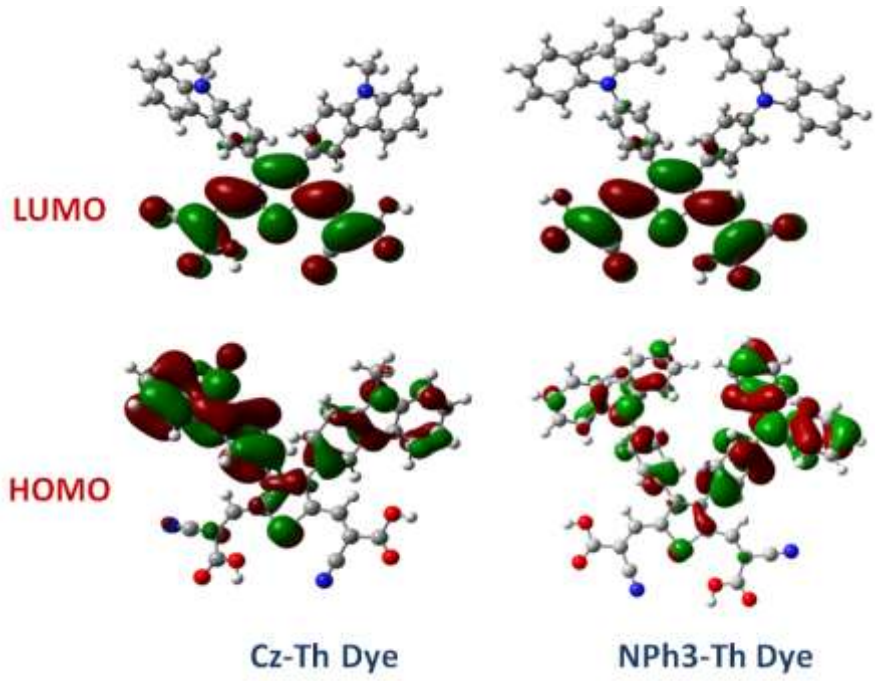

Figure 5.3 Schematic representation of electronic distributions observed in frontier orbitals of the dyes using TD-DFT/B3LYP/6-31G(d,p) basis set.

To obtain insight into the difference in photovoltaic performances of the dyes having different donors with same spacer and acceptors, the optimized structure of dyes and its frontier orbital electronic structures, geometries were identified using Density functional theory (DFT) calculations in Gaussian 09 program at TD-DFT, B3LYP/631G(d,p) basis sets. The optimized geometries of dyes are shown in **Figure 5.3** and calculated transition energies wavelengths, Oscillator Strengths (*f*), and orbital contribution for the dyes using TD-DFT, CAM-B3LYP/6-31G(d,p) basis set are shown in Table 5.2. In Cz-Th and NPh3-Th dyes HOMO levels are mainly located on donor segment having carbazole and triphenyl amine unit. However, in Cz-Th dye HOMO levels are strongly diffused in thiophene-π-bridge and mild on acceptor unit, resulting in better intramolecular charge transfer (ICT) from donor to acceptor therefore giving maximum PCE and ICT peak that were observed in Figure 5.2 (a) whereas, in NPh3-Th dye the HOMO levels are mildly distributed on thiophene π-spacer resulting in poor PCE and the ICT peak disappeared in Figure 5.1(a).

The LUMO level electron density is mainly located on the cyanoacrylic acid acceptor and thiophene unit in Cz-Th and NPh_3-Th dye. In these dyes the HOMO and LUMO levels are well separated, which is an advantage for charge migration from donor to acceptor in photo excitation state of dyes.

Table 5.2 Computed selected Transition Energies Wavelengths, Oscillator Strengths (*f*), and Their Orbital Contribution for the Dyes Using TD-DFT, CAM-B3LYP/6-31G(d,p) basis set.

Dye	λ/nm	*f*	Wavefunctions
Cz-Th Dye	371	0.1182	H-1 → L (63%)
	336	0.1938	H-2 → L (46%)
	317	0.1496	H-5 → L (42%), H-2 → L (34%)
	295	0.1224	H-1 → L+1 (29%)
NPh3-Th Dye	443	0.1182	H → L (95%)
	350	0.1791	H-1 → L (68%)
	291	0.2001	H → L+3 (42%)
	286	0.5087	H-1 → L+1 (75%)

5.3 Fabrication of DSSC

The DSSCs were fabricated following a literature procedure.[27] In brief, FTO glasses were cleaned with acetone, ethanol, and then deionized water in an ultrasonic water bath and dried in air. Scotch tape was employed as a spacer to control the film thickness and to provide uncoated areas for electrical contact. TiO_2 paste was spread over the spacer between the scotch tape on the FTO glass substrate using the doctor blade technique. The TiO_2 coating was then dried in air at 20 °C for 10 min and sintered at 450 °C in air to remove any organic matter. The thickness of the TiO_2 photoanode film was about 12µm and its area was 0.25 cm^2. After cooling, the TiO_2 electrodes were immersed into 0.3 mM dyes solution for 24 h. A Pt counter electrode was prepared by H_2PtCl_6 solution spreading by spin coating technique and sintered at 450 °C, 2 h. DSSCs were fabricated using the sandwich type configuration of a TiO_2 photoanode and Pt-counter electrode. To complete the device, the electrolyte was injected into the space between the cell's anode and

cathode through a hole drilled on the counter electrode. The I^-/I_3^- electrolyte was obtained by mixing 0.5M1-Butyl-3-methylimidazolium iodide (BIMI), 0.05M I_2, 0.5M TBP, 0.5M guanidiumthiocynate (GSCN) in 3-methoxy propionitrile. The cobalt (II/III) were prepared using 0.2M $[Co(bpy)_3]^{2+}$, 0.02M $[Co(bpy)_3]^{3+}$, 0.1M $LiClO_4$, 0.5M TBP in acetonitrile.[28]

5.4 Photovoltaic Result and Discussions

5.4.1 IPCE spectra

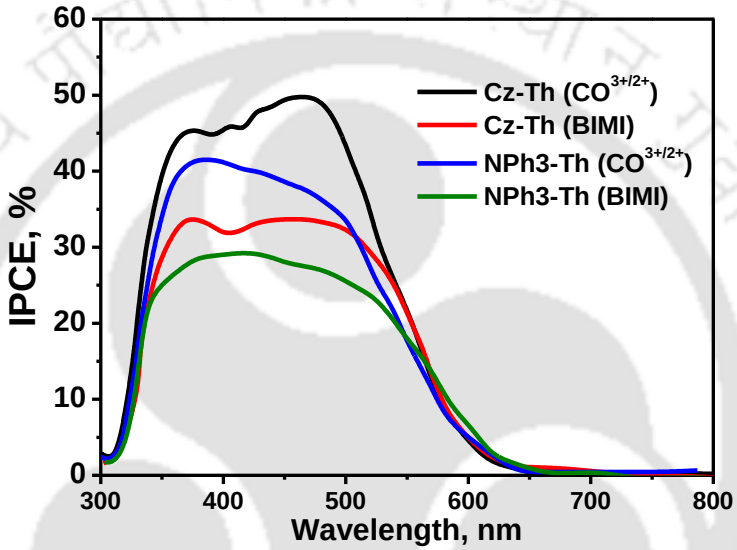

Figure 5.4 IPCE action spectra for DSSC cells fabricated using dyes (Cz-Th and NPh3-Th) and electrolytes (Co(II/III) and I^-/I_3^-) under AM 1.5, 100mW.cm^{-2} solar irradiation.

The incident monochromatic photon-to-current conversion efficiency (IPCE) spectra of the Cz-Th and NPh3-Th dyes based device with $[Co(bpy)_3]^{2+/3+}$ and I^-/I_3^- electrolytes redox couples are shown in Figure 5.4 IPCEs were systematically enhanced with the use of the $[Co(bpy)_3]^{2+/3+}$ instead of I^-/I_3^-electrolyte. The $[Co(bpy)_3]^{2+/3+}$ electrolyte based device using the Cz-Th dye exceeds 50% in the spectral region ranging from 350 nm to 540 nm and I^-/I_3^- redox couples based device reaches a 35% at 540 nm. In comparison, the IPCE spectra of NPh3-Th dye exhibits significantly lower values than that of Cz-Th, showing IPCEs of 42% in $[Co(bpy)_3]^{2+/3+}$ and 29% in I^-/I_3^-, which correlates well with the absorption behaviors.

5.4.2 Photocurrent-voltage (*J-V*) properties of dyes

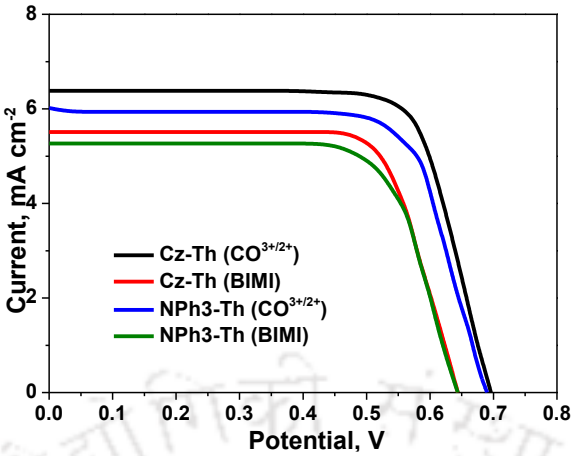

Figure 5.5 *J-V* curves of the DSSCs employing the Cz-Th and NPh3-Th dyes under 100 mW.cm^{-2} light illumination.

Table 5.3 Summary of the photovoltaic parameters of the DSSCs with respect to Different sensitizers and redox electrolytes.

Dye	Electrolytes	J_{sc} (mA cm^{-2})	V_{oc} (V)	*ff* (%)	PCE (%)
Cz-Th	**Co $^{(III)/(II)}$**	6.30 ± (0.4)	0.696 ± (0.05)	70 ± (1.1)	3.2 ± (0.18)
	I^-/I_3^-	5.50 ± (0.1)	0.643 ± (0.03)	67 ± (0.6)	2.6 ± (0.12)
NPh3-Th	**Co $^{(III)/(II)}$**	5.99 ± (0.4)	0.690 ± (0.04)	69 ± (1.2)	2.9 ± (0.20)
	I^-/I_3^-	5.28 ± (0.2)	0.640 ± (0.02)	69 ± (1.1)	2.4 ± (0.14)

Performances of DSSCs were measured with 0.25 cm^2 working area (measurement were performed under AM 1.5, one Sun irradiation). J_{sc}: short-circuit current, V_{oc}: open circuit voltage, FF: fill factor and η%: power conversion efficiency.

Fig. 5.5 shows the current density voltage (*J*−*V*) characteristics of the DSSCs under standard global AM 1.5G, 100 mW.cm^{-2} solar irradiation. The photovoltaic parameters including short circuit photocurrent density (J_{sc}), open-circuit voltage (V_{oc}), fill factor (FF), and the photocurrent conversion efficiency (PCE) are summarized in **Table 5.3**.

The cobalt (II/III) electrolyte based device parameters J_{sc}, V_{oc}, and FF values are 6.30 mA cm^{-2}, 0.696 V, and 70 %, respectively, for the Cz-Th dye and 5.99 mA cm^{-2}, 0.690 V, and 69 %, respectively, for the NPh3-Th dye, yielding rather PCE values of 3.2% and 2.9%, respectively. Under the same conditions, I^-/I_3^- electrolyte based device on Cz-Th dye

shows PCE of 2.6% with relatively lower J_{sc} (5.50 mA cm^{-2}) and V_{oc} (0.643 V) and NPh3-Th dye PCE of 2.4% with J_{sc} (5.28 mA cm^{-2}) and V_{oc} (0.640 V).

As per the *J-V* data, $[Co(bpy)_3]^{2+/3+}$ based DSSCs systematically displayed higher J_{sc} and V_{oc} than I^-/I_3^- electrolyte, $[Co(bpy)_3]^{2+/3+}$ based electrolyte has lower redox potential compared with I^-/I_3^-.[29] [Figure 5.2 (c)] The variation in J_{sc} and V_{oc} forCz-Th and NPh3-Th dyes can be explained by the inferior dye-loading (molar coefficient) for both dyes that generated a larger number of voids on the TiO_2 surface. Accordingly, the I^-/I_3^- has higher redox potential (compare to $Co^{2+/3+}$) and much smaller size which can penetrate much deeper into the dye layer compared to that of $Co^{2+/3+}$ electrolyte, giving much greater charge recombination and the greater difference in PCE. In addition, the Cz-Th dye has long alkyl chain that suppresses the dye aggregation on the TiO_2 photoanode surface, thereby it shows higher V_{oc} compared to NPh3-Th dye.

5.4.3 Electrochemical Impedance Spectroscopy (EIS)

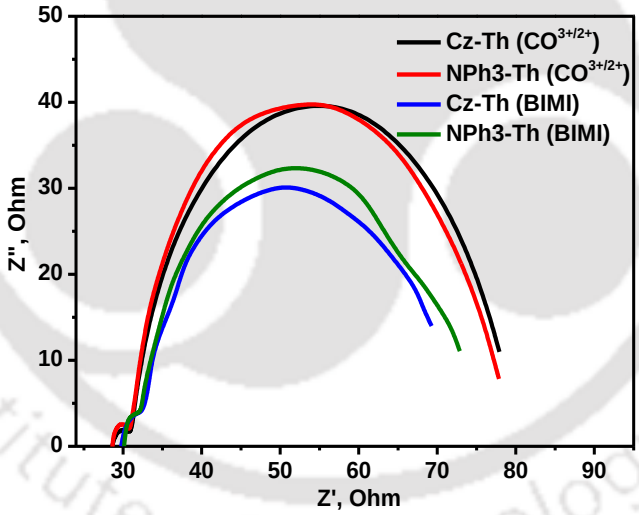

Figure 5.6 Electrochemical Impedance Spectroscopy (EIS) measurements of DSSC based on dyes Cz-Th and NPh3-Th recorded in dark at 0.65 V DC bias

To further characterize the electron transport and recombination effect on photovoltaic performance for the Cz-Th and NPh3-Th dyes with the different geometric structure orientations, we measured the EIS under dark conditions at a forward bias of 0.65 V (Fig. 5.6). The charge transfer resistance, R_{ct} and recombination rate, R_{rec} values at the TiO_2/dye/electrolyte interface corresponding to the second semicircle of the Nyquist plot fitting parameter are shown in Table 5.4.

Table 5.4 DSSC parameters R_{ct}, R_{rec}, τ_n and J_o extracted from EIS measurements

ESI Parameters	Cz-Th		NPh3-Th	
	Co $^{(III)/(II)}$	I^-/I_3^-	Co $^{(III)/(II)}$	I^-/I_3^-
R_{ct} (Ω)	28.5	30.1	28.6	30.2
R_{rec} (Ω)	128.0	96.0	124.0	95.0
CPE-P (%)	62	61	63	61
τ_e (ms)	1.73	1.02	1.54	0.98
J_o(nA cm^{-2})	0.74	0.42	0.70	0.39

From the EIS results, The R_{ct} at counter electrode is quite comparable in both devices but little difference is observed in the R_{rec}. Recombination resistance of the Cz-Th dye based device is higher than that of NPh3-Th devices suggesting that the Cz-Th device performs with higher PCE. The electron lifetime (τ_n) of Cz-Th device can also be higher than NPh3-Th, while a shift of high-frequency.

5.4.4 Electron lifetime (τ_e)

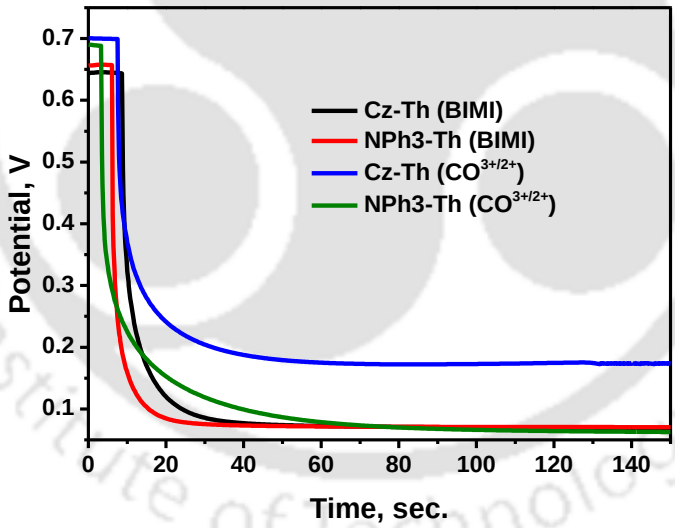

Figure 5.7 Open circuit voltage decay (OCVD) curves of the DSSCs based on the Cz-Th and NPh3-Th dyes

The electron recombination kinetics in Cz-Th and NPh3-Th dyes based devices was investigated by an open circuit voltage decay (OCVD) measurement.[30] This measurement was conducted by obtaining a steady state V_{oc} value for the DSSC under 100 mW.cm^{-2} light illumination, and then the decay of the V_{oc} was monitored after the illumination was stopped.

The transient V_{oc} as a function of time with the absence of incident light was investigated. When the solar light illumination of the device is switched off under a steady voltage, the V_{oc}, which is related to the electron lifetime, will decay sharply because of the electron recombination. **Fig. 5.7** shows that the decay rate of the V_{oc} with NPh3-Th and it is much slower than that of Cz-Th. This indicates that Cz-Th device can effectively inhibit the back recombination reaction between electrons in the CB of TiO_2 and oxidative species and suggests a large reduced recombination rate in the DSSCs.

5.4.5 Tafel Polarization:

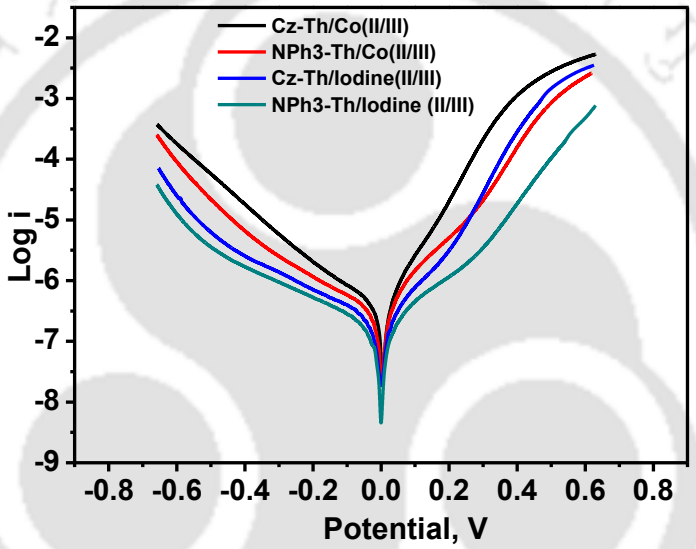

Figure 5.8 Tafel polarization curves for dyes showing the intensities of dark current (Tafel data were recorded in dark and fitted by using corr-view software)

Tafel polarization experiment was carried out by using Solartron FRA (Electrcochemical workstation) interface. The devices were swept with DC potential varying from -0.62 to 0.62 at a scan rate of 20 mV/sec in dark and fitted by using Corrview software (Scribners Associates Inc.). This technique, which shows the kinetics of the reaction in the electrolyte component of the dye solar cell under dark conditions (Figure 5.8).[31,32]

Tafel analysis takes insight into the interfacial charge transfer properties for electrolyte (I^-/I_3^- or $Co^{(II/III)}$) redox couple on the TiO_2 surface. The well-known Butler-Volmer equation (plot graph *log i* Vs potential) which gives the rates of β_c and β_a (cathodic and anodic) reactions in the semiconductor/Electrolyte interface.

$$j = -j_o[exp\frac{\alpha_c nF}{RT}(E - E_{eq}) - exp\frac{\alpha_a nF}{RT}(E - E_{eq})]$$

Where,

j_o = The exchange current density, E_{eq} is the equilibrium potential of electrolytes redox couple system.

Intersection point of the Tafel curves gives exchange current density (j_o) which is directly related to the recombination reactions occurring in the DSSC (Shown in Table 5.4).

5.5 Experimental section

5.5.1 General Synthesis procedure of Cz-Th-CHO or NPh3-Th-CHO:

$Pd(PPh_3)_4$ (20 mol%), 2M K_2CO_3 aqueous solutions (6 ml) were added to a solution of boronic ester derivative (0.25 mmol) and 3,4-dibromothiophene-2,5-dicarbaldehyde (0.2 mmol) in THF (12 ml) under argon condition. The mixture was heated to 85 °C for 12 h. After cooling the mixture to room temperature, evaporate the THF solution under reduced pressure. The extracted compound was wash with chloroform and brine solution. Finally extracted chloroform was dried with anhydrous $MgSO_4$. The product was purified by column chromatography (silica gel, ethyl acetate-hexane 1:2 as eluent).

5.5.2 General synthetic procedure of Dyes:

A mixture of Cz-Th-CHO/NPh3-Th-CHO (0.2 mmol) and cyanoacetic acid (0.3 mmol) were dissolved in acetonitrile and chloroform (1:1) solution. Finally, piperidine (0.02 mmol) was added to the solution in presence of argon atmosphere and then the solution was refluxed for 12 h. After cooling, the solution was removed by rota vapor at reduced pressure. Extracted compound was washed with chloroform and 0.1M aqueous HCl solution of . Then the organic layer was dried with Na_2SO_4. The product was purified by column chromatography (silica gel, ethyl acetate-hexane 1:2 as eluent). The product was obtained as an orange solid.

3,4-Bis-(9-hexyl-9*H*-carbazol-3-yl)-thiophene-2,5-dicarbaldehyde (Cz-Th-CHO):

Yield=75%, ^{1}H NMR (400 MHz, $CDCl_3$): δ (ppm) 9.91 (s, 1H), 8.01-8.02 (d, 3H), 7.99 (s, 1H), 7.49 (t, 2H), 7.40-7.42 (d, 2H), 7.22-7.25 (m, 4H), 7.13-7.15 (d, 2H), 4.23 (t, 2H), 1.82 (t, 2H), 1.36-1.26 (m, 6H), 0.90-0.83 (m, 3H). ^{13}C NMR (100 MHz, $CDCl_3$): δ (ppm) 186.61, 152.65, 143.81, 141.04, 140.41, 128.16, 126.44, 123.44, 123.25, 122.88, 122.55, 120.57, 119.66, 110.19, 109.26, 108.76, 43.59, 31.40, 30.14, 26.76, 22.36, 14.28. HRMS (ESI) m/z: $[M+H]^+$ calcd for $C_{42}H_{43}N_2O_2S$ 639.3045, found 639.3064.

3-[5-(2-Carboxy-2-cyano-vinyl)-3,4-bis-(9-hexyl-9H-carbazol-3-yl)-thiophen-2-yl]-2-cyano-acrylic acid (Cz-Th-Dye):

Yield=70%, ^{1}H NMR (400 MHz, $CDCl_3$): ^{1}H NMR (400MHz, $CDCl_3$): δ (ppm) 9.43 (s, 4H), 8.17 (s, 1H), 7.92-7.94 (d, 1H), 7.85 (s, 1H), 7.41 (t, 1H), 7.33-7.34 (d, 1H), 7.11-7.15 (m, 2H), 7.00-6.98 (d, 1H) 4.16 (t, 2H), 1.77 -0.80 (m, 11H).^{13}C NMR (100 MHz, $CDCl_3$): δ (ppm) 168.21, 167.09, 150.68, 142.57, 140.75, 140.07, 136.16, 128.52, 126.05, 124.65, 123.15, 122.74, 120.61, 119.17, 117.67, 109.47, 108.93, 108.54, 44.44, 31.63, 29.03, 27.45, 22.69, 14.14. HRMS (ESI) m/z: $[M+Na]^+$ calcd for $C_{48}H_{44}N_4O_4S$ 795.2981, found 795.2960.

3,4-Bis-(4-diphenylamino-phenyl)-thiophene-2,5-dicarbaldehyde (NPh3-Th-CHO):

Yield=65%, ^{1}H NMR (400 MHz, $CDCl_3$): δ (ppm) 9.91 (s, 1H), 7.30 (t, 2H), 7.08-7.15 (m, 6H), 7.01-7.04 (m, 6H). ^{13}C NMR (100 MHz, $CDCl_3$): δ (ppm) 185.74, 147.12, 131.59, 129.65, 125.33, 124.00, 122.83, 121.53. HRMS (ESI) m/z: $[M+H]^+$ calcd for $C_{42}H_{41}N_2O_2S$ 627.2106, found 627.2118.

3-[5-(2-Carboxy-2-cyano-vinyl)-3,4-bis-(4-diphenylamino-phenyl)-thiophen-2-yl]-2-cyano-acrylic acid (NPh3-Th-Dye):

Yield=75%, ^{1}H NMR (400 MHz, $CDCl_3$): δ (ppm) 8.16 (s, 1H), 6.78-7.29 (m, 15H). ^{13}C NMR (100 MHz, $CDCl_3$): δ (ppm) 147.69, 147.40, 147.29, 139.51, 131.88, 129.81, 129.62, 129.52, 125.24, 124.80, 123.69, 123.32, 122.84, 119.30, 114.28 HRMS (ESI) m/z: $[M-2]^+$ calcd for $C_{48}H_{30}N_4O_4S$ 758.1988, found 758.3262.

5.6 Summary

In conclusion, a series of new thiophene 3,4-π-conjugated metal-free organic dyes, comprising carbazole, triphenylamine moieties as the electron donor, cyanoacrylic acid as the electron acceptor/anchoring groups and thiophene as the conjugated bridge were synthesized and applied in DSSC. But, these dyes do not show broad absorption peak in visible region due to the blocking of electron delocalization at 2,5-positions by acceptor units. In this work donor moieties at 3,4-position of thiophene unit successfully prevent the dye aggregation and charge recombination on TiO_2 surface. The ICT peak of Cz-Th dye in absorption spectra causes very high PCE which are explained by optimized geometry calculations were ascertained by DFT calculation by using B3LYP/631G(d,p) basis set. The photovoltaic results of Cz-Th and NPh3-Th dye exhibits higher PCE and the longest electron lifetime in Cobalt (II/III) electrolyte compared with I^-/I_3^- electrolyte.

Both the dyes prevent Cobalt (II/III) electrolyte from reaching the TiO_2 surface due to steric hindrance, thus causing the recombination reaction. On the other hand, Cz-Th dye attracted the Cobalt (II/III) electrolyte to the TiO_2 surface, increasing the recombination rate. However, the Cz-Th dye exhibits higher visible range light absorption and shows the highest J_{sc} (6.30 mA cm^{-2}) and PCE (3.2%). These DSSC results were supported by studying the decay curve of V_{oc}, impedance spectrum, and electron lifetime measurements.

5.7 References:

1. O'regan, B.; Grätzel, M. *Nature* **1991,** *353*, 737-740.
2. Wang, Y.; Zheng, Z. W.; Li, T. Y.; Robertson, N.; Xiang, H. D.; Wu, W. J.; Hua, J. L.; Zhu, W. H.; Tian, H. *ACS. Appl. Mater. Inter.* **2016,** *8*, 31016-31024.
3. Hao, Y.; Saygili, Y.; Cong, J. Y.; Eriksson, A.; Yang, W. X.; Zhang, J. B.; Polanski, E.; Nonomura, K.; Zakeeruddin, S. M.; Gratzel, M.; Hagfeldt, A.; Boschloo, G. *ACS. Appl. Mater. Inter.* **2016,** *8*, 32797-32804.
4. Wu, Y. Z.; Zhu, W. H.; Zakeeruddin, S. M.; Gratzel, M. *ACS. Appl. Mater. Inter.* **2015,** *7*, 9307-9318.
5. Ahmad, S.; Guillen, E.; Kavan, L.; Gratzel, M.; Nazeeruddin, M. K. *Energ. Environ. Sci.* **2013,** *6*, 3439-3466.
6. Chen, W. C.; Kong, F. T.; Li, Z. Q.; Pan, J. H.; Liu, X. P.; Guo, F. L.; Zhou, L.; Huang, Y.; Yu, T.; Dai, S. Y. *ACS. Appl. Mater. Inter.* **2016,** *8*, 19410-19417.
7. Higashino, T.; Kawamoto, K.; Sugiura, K.; Fujimori, Y.; Tsuji, Y.; Kurotobi, K.; Ito, S.; Imahori, H. *ACS. Appl. Mater. Inter.* **2016,** *8*, 15379-15390.
8. Mathew, S.; Yella, A.; Gao, P.; Humphry-Baker, R.; Curchod, B. F. E.; Ashari-Astani, N.; Tavernelli, I.; Rothlisberger, U.; Nazeeruddin, M. K.; Grätzel, M. *Nat. Chem.* **2014,** *6*, 242-247.
9. Zhang, L.; Cole, J. M. *ACS. Appl. Mater. Inter.* **2015,** *7*, 3427-3455.
10. Chou, S. H.; Tsai, C. H.; Wu, C. C.; Kumar, D.; Wong, K. T. *Chem-Eur. J.* **2014,** *20*, 16574-16582.
11. Paramasivarn, M.; Chitumalla, R. K.; Singh, S. P.; Islam, A.; Han, L. Y.; Rao, V.; Bhanuprakash, K. *J. Phys. Chem. C* **2015,** *119*, 17053-17064.
12. Jia, H. L.; Ju, X. H.; Zhang, M. D.; Ju, Z. M.; Zheng, H. G. *Phys. Chem. Chem. Phys.* **2015,** *17*, 16334-16340.

13. Wang, X. X.; Guo, L.; Xia, P. F.; Zheng, F.; Wong, M. S.; Zhu, Z. T. *J. Mater. Chem. A* **2013,** *1*, 13328-13336.
14. Chang, Y. J.; Watanabe, M.; Chou, P. T.; Chow, T. J. *Chem. Commun.* **2012,** *48*, 726-728.
15. Chen, J. H.; Tsai, C. H.; Wang, S. A.; Lin, Y. Y.; Huang, T. W.; Chiu, S. F.; Wu, C. C.; Wong, K. T. *J. Org. Chem.* **2011,** *76*, 8977-8985.
16. Raju, T. B.; Vaghasiya, J. V.; Afroz, M. A.; Soni, S. S.; Iyer, P. K. *Org. Electron.* **2016,** *39*, 371-379.
17. Thomas, K. R. J.; Hsu, Y. C.; Lin, J. T.; Lee, K. M.; Ho, K. C.; Lai, C. H.; Cheng, Y. M.; Chou, P. T. *Chem. Mater.* **2008,** *20*, 1830-1840.
18. Raju, T. B.; Vaghasiya, J. V.; Afroz, M. A.; Soni, S. S.; Iyer, P. K. *Phys. Chem. Chem. Phys.* **2016,** *18*, 28485-28491.
19. Wu, J. H.; Lan, Z.; Lin, J. M.; Huang, M. L.; Huang, Y. F.; Fan, L. Q.; Luo, G. G. *Chem. Rev.* **2015,** *115*, 2136-2173.
20. Zheng, J. X.; Zhang, K.; Fang, Y. Y.; Zuo, Y. X.; Duan, Y. D.; Zhuo, Z. Q.; Chen, X. M.; Yang, W. L.; Lin, Y.; Wong, M. S.; Pan, F. *ACS. Appl. Mater. Inter.* **2015,** *7*, 25341-25351.
21. Murakami, T. N.; Koumura, N.; Yoshida, E.; Funaki, T.; Takano, S.; Kimura, M.; Mori, S. *Langmuir* **2016,** *32*, 1178-1183.
22. Ogawa, J.; Agrawal, S.; Koumura, N.; Mori, S. *J. Phys. Chem. C* **2016,** *120*, 3612-3618.
23. Zhou, N. J.; Prabakaran, K.; Lee, B.; Chang, S. H.; Harutyunyan, B.; Guo, P. J.; Butler, M. R.; Timalsina, A.; Bedzyk, M. J.; Ratner, M. A.; Vegiraju, S.; Yau, S.; Wu, C. G.; Chang, R. P. H.; Facchetti, A.; Chen, M. C.; Marks, T. J. *J. Am. Chem. Soc.* **2015,** *137*, 4414-4423.
24. Shi, J.; Chai, Z. F.; Zhong, C.; Wu, W. J.; Hua, J. L.; Dong, Y. Q.; Qin, J. G.; Li, Q. Q.; Li, Z. *Dyes Pigments* **2012,** *95*, 244-251.
25. Li, H. Y.; Hou, Y. Q.; Yang, Y. Z.; Tang, R. L.; Chen, J. N.; Wang, H.; Han, H. W.; Peng, T. Y.; Li, Q. Q.; Li, Z. *ACS. Appl. Mater. Inter.* **2013,** *5*, 12469-12477.
26. Zhang, F.; Luo, Y. H.; Song, J. S.; Guo, X. Z.; Liu, W. L.; Ma, C. P.; Huang, Y.; Ge, M. F.; Bo, Z. S.; Meng, Q. B. *Dyes Pigments* **2009,** *81*, 224-230.
27. Fadadu, K. B.; Vaghasiya, J. V.; Choudhury, S.; Soni, S. S. *J. Renew. Sustain. Ener.* **2015,** *7*. 023114.

28. Soni, S. S.; Fadadu, K. B.; Vaghasiya, J. V.; Solanki, B. G.; Sonigara, K. K.; Singh, A.; Das, D.; Iyer, P. K. *J. Mater. Chem. A* **2015,** *3*, 21664-21671.
29. Fan, J. D.; Hao, Y.; Cabot, A.; Johansson, E. M. J.; Boschloo, G.; Hagfeldt, A. *ACS. Appl. Mater. Inter.* **2013,** *5*, 1902-1906.
30. Li, T. L.; Lee, Y. L.; Teng, H. *Energ. Environ. Sci.* **2012,** *5*, 5315-5324.
31. Petra J. Cameron and Laurence M. Peter. *J. Phys. Chem. B* **2005,** *109*, 930-936.
32. Rohit L. Vekariya, Keval K. Sonigara, Kishan B. Fadadu, Jayraj V. Vaghasiya, and Saurabh S. Soni. *ACS Omega* **2016**, *1*, 14−18.

Appendix

.

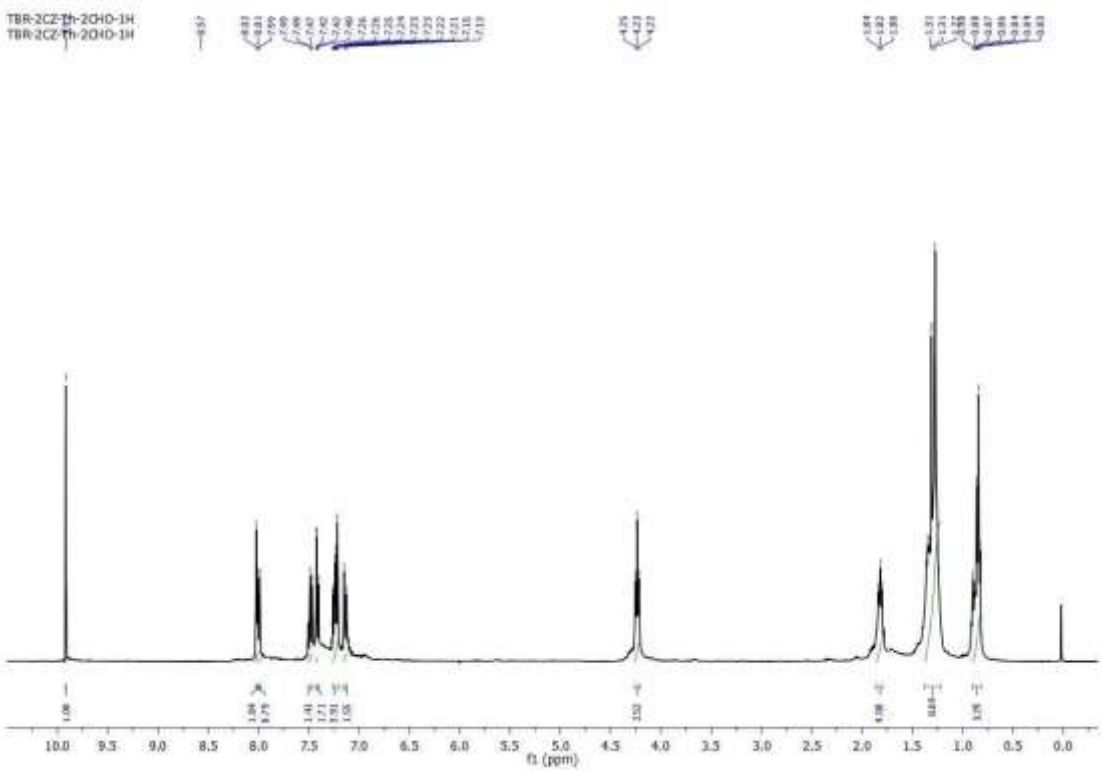

^{1}H-NMR spectrum of 3,4-bis(9-hexyl-9*H*-carbazol-3-yl)thiophene-2,5-dicarbaldehyde

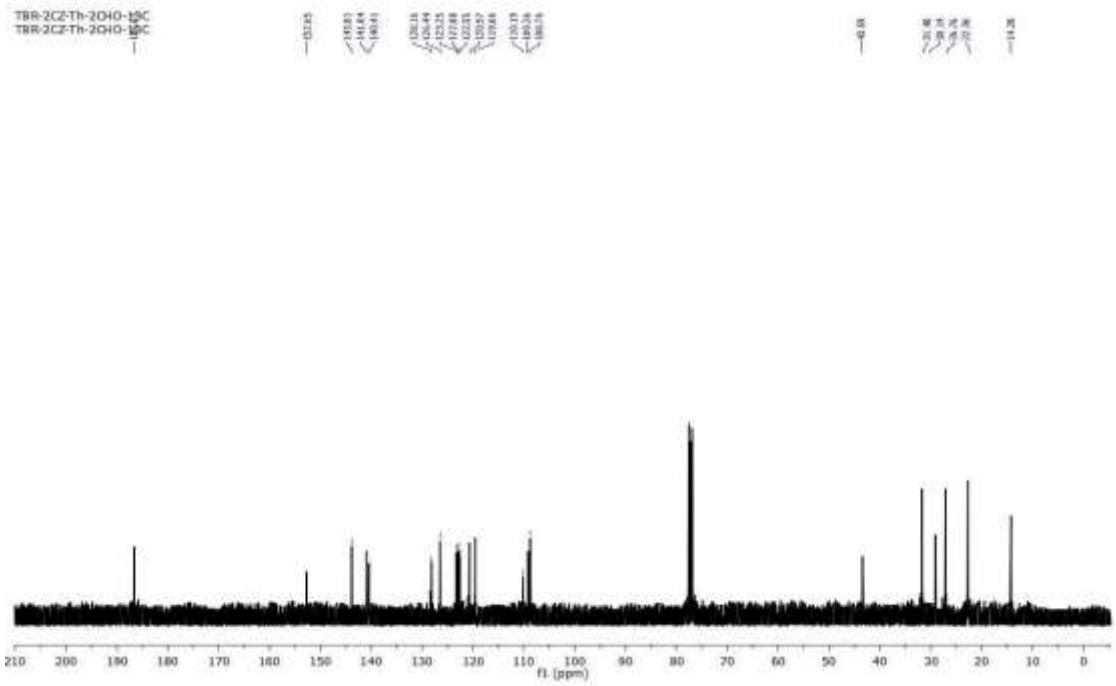

^{13}C-NMR spectrum of 3,4-bis(9-hexyl-9*H*-carbazol-3-yl)thiophene-2,5-dicarbaldehyde

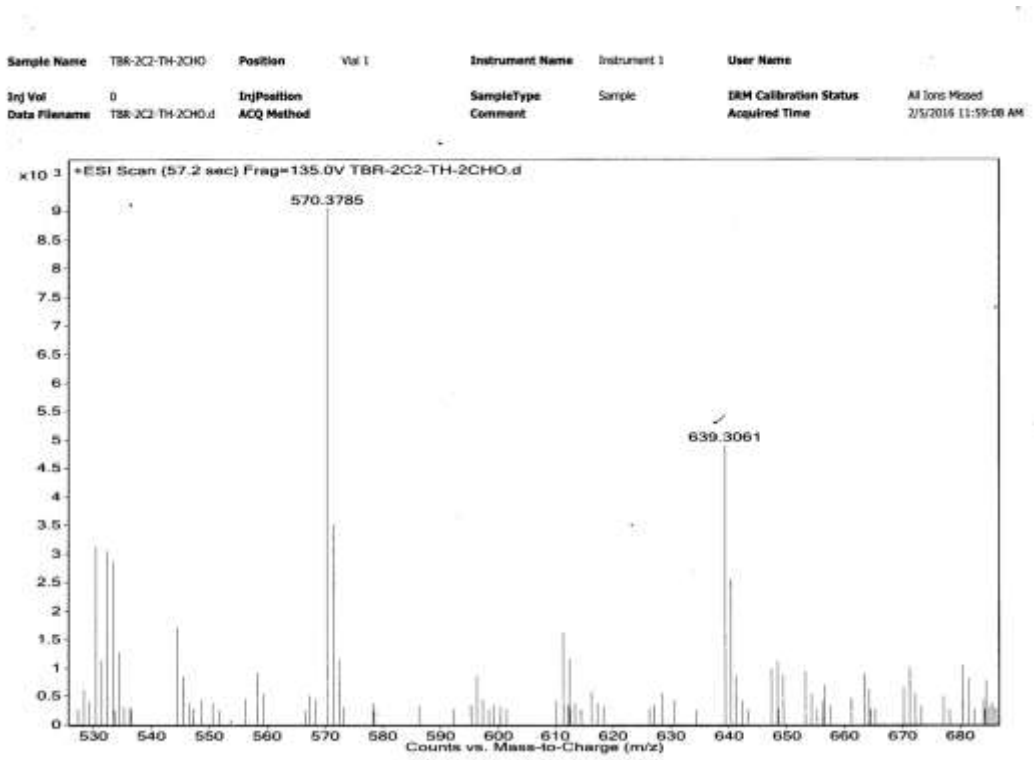

ESI-MS spectrum of 3,4-bis(9-hexyl-9*H*-carbazol-3-yl)thiophene-2,5-dicarbaldehyde

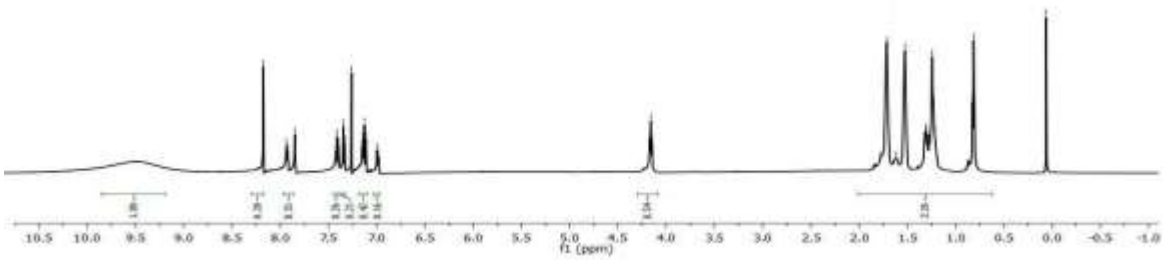

^{1}H-NMR spectrum of 3,4-bis(9-hexyl-9*H*-carbazol-3-yl)thiophene-2,5-dicarbaldehyde

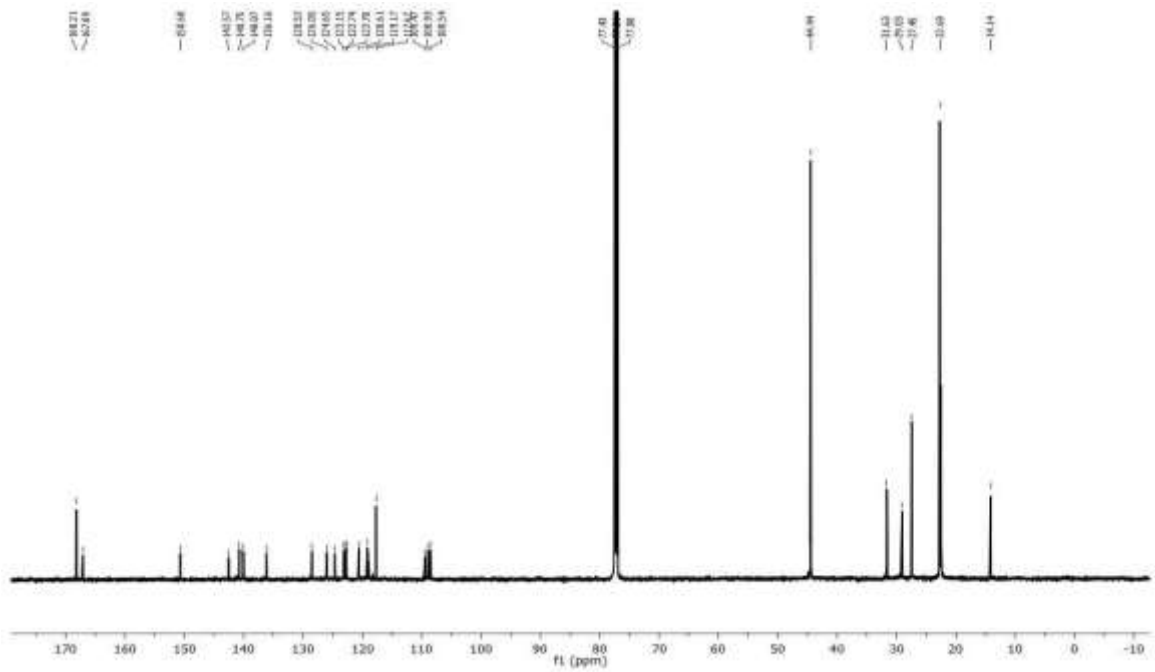

^{13}C-NMR spectrum of 3,4-bis(9-hexyl-9*H*-carbazol-3-yl)thiophene-2,5-dicarbaldehyde

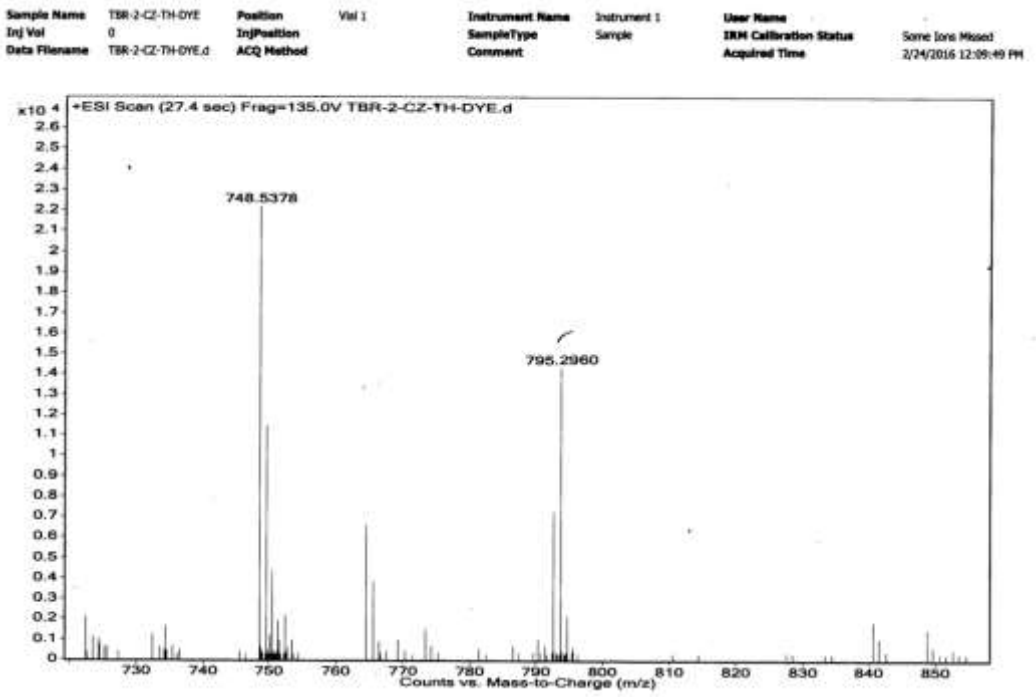

ESI-MS spectrum of 3,4-bis(9-hexyl-9*H*-carbazol-3-yl)thiophene -2,5-dicarbaldehyde

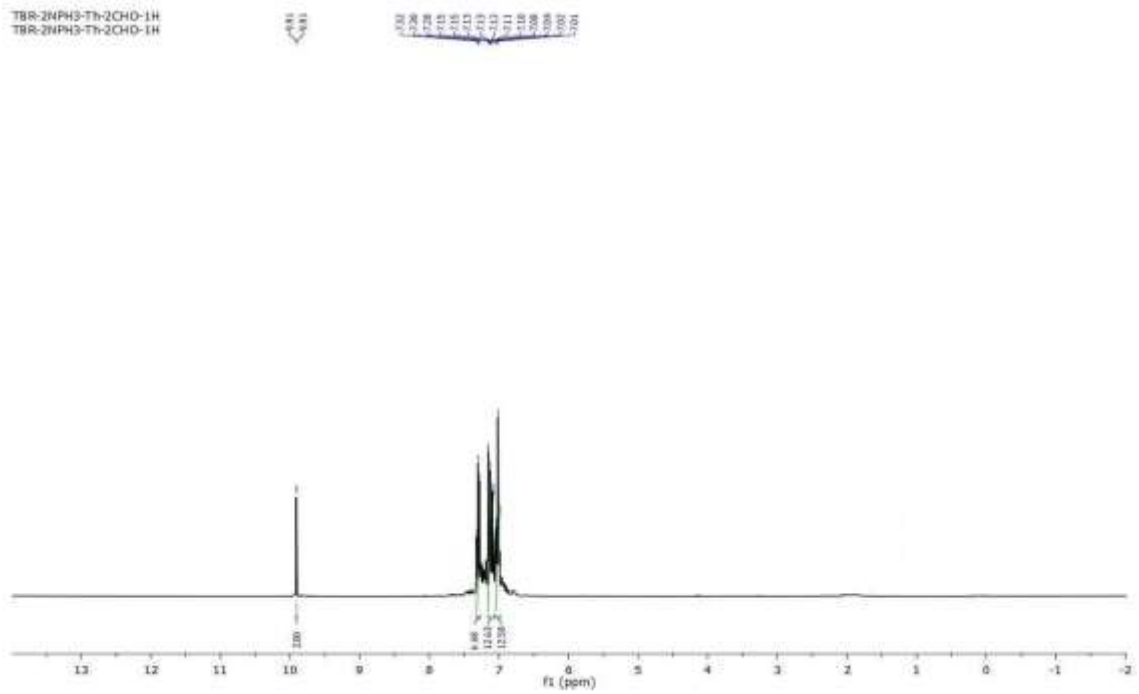

^{1}H-NMR spectrum of 3,4-bis(4-(diphenylamino)phenyl) thiophene-2,5-dicarbaldehyde

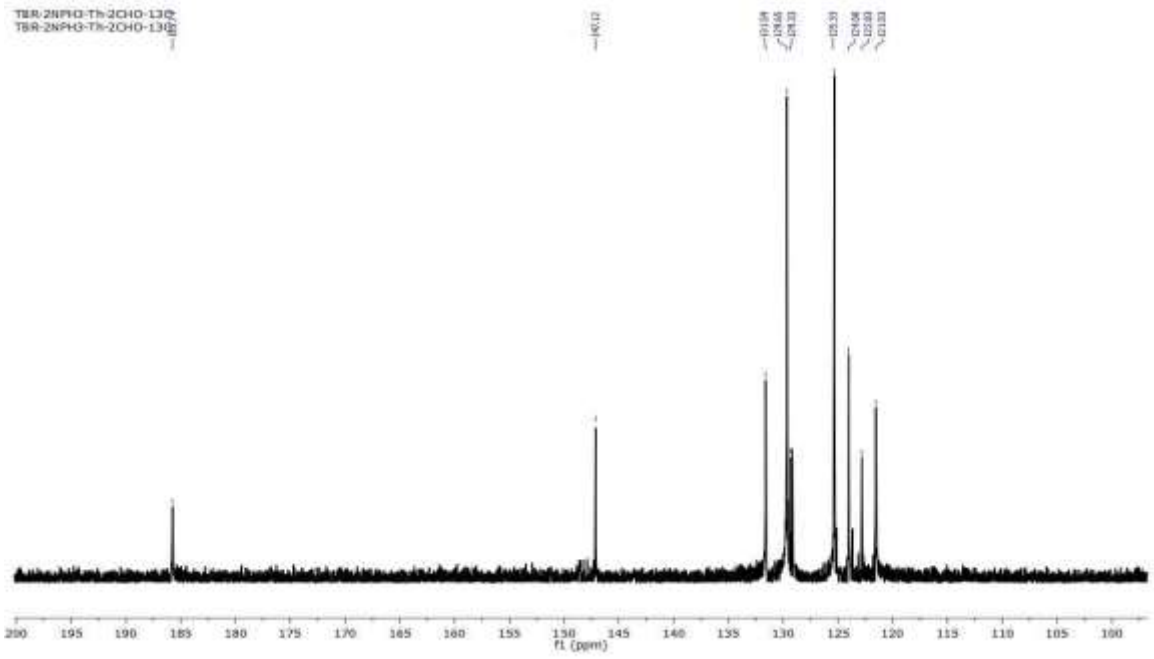

^{13}C-NMR spectrum of 3,4-bis(4-(diphenylamino)phenyl)thiophene-2,5-dicarbaldehyde

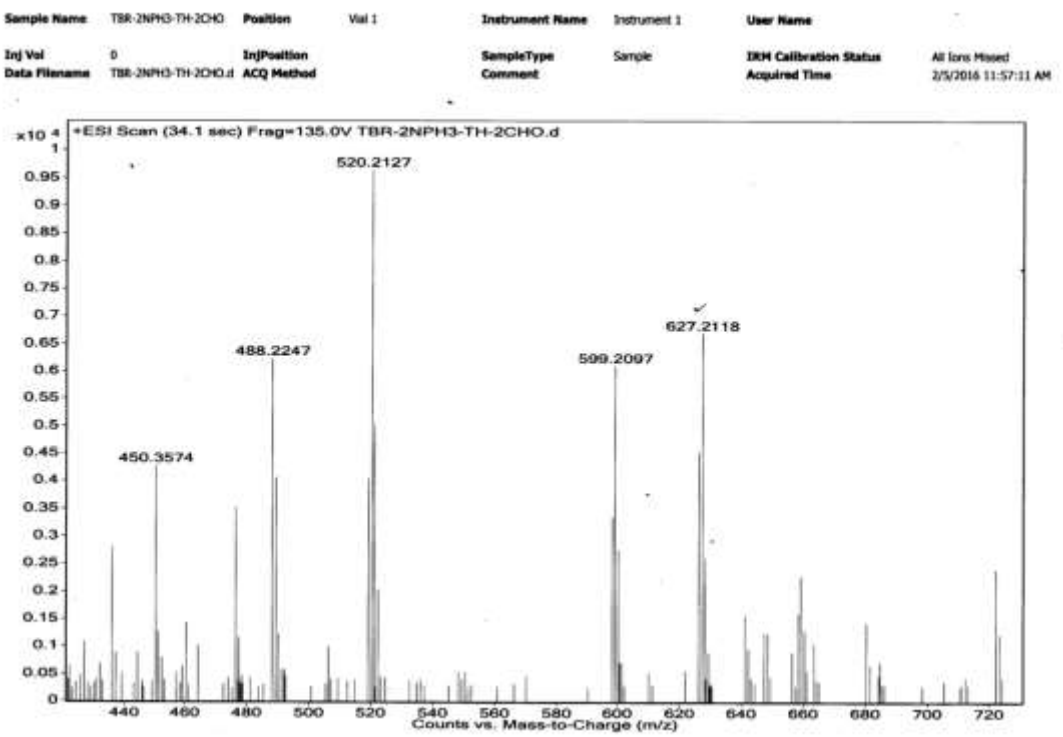

ESI-MS spectrum of 3,4-bis(4-(diphenylamino)phenyl) thiophene-2,5-dicarbaldehyde

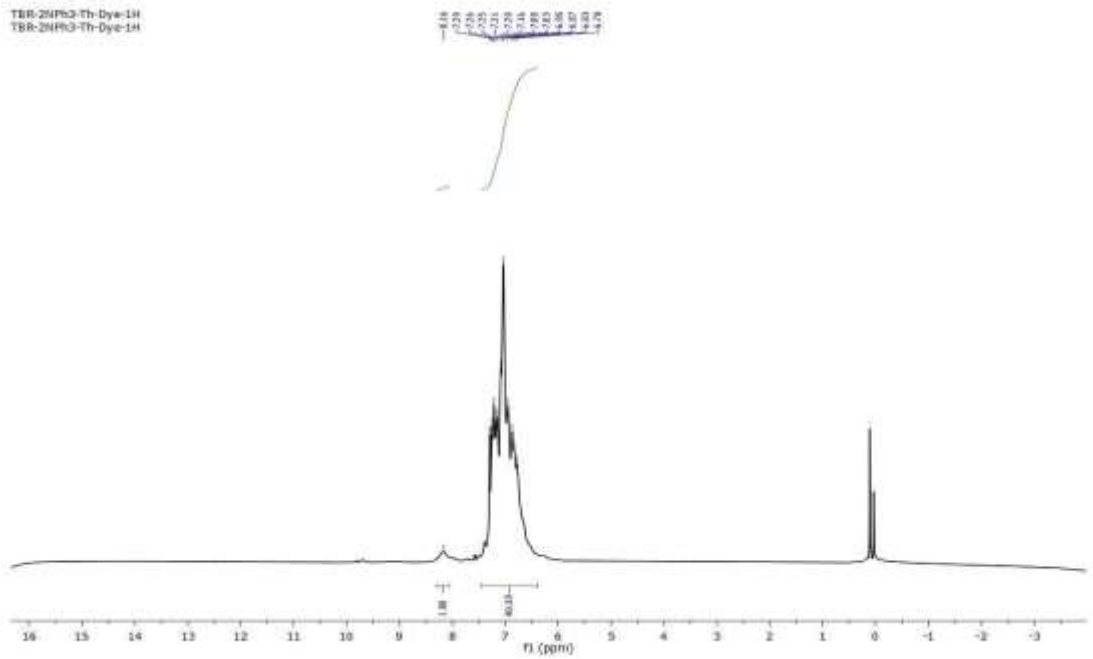

^{1}H-NMR spectrum of (2*E*,2′*E*)-3,3'-(3,4-bis(4-(diphenylamino) phenyl) thiophene-2,5-diyl)bis(2-cyanoacrylic acid)

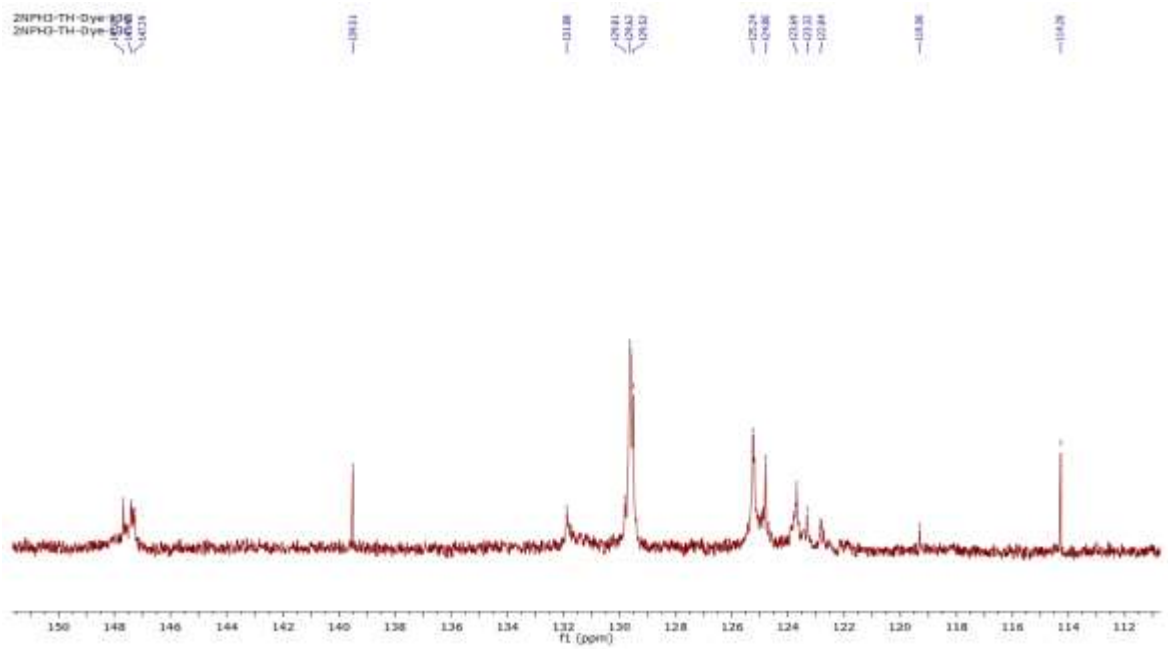

^{13}C-NMR spectrum of (2*E*,2′*E*)-3,3'-(3,4-bis(4-(diphenylamino) phenyl) thiophene-2,5-diyl)bis(2-cyanoacrylic acid)

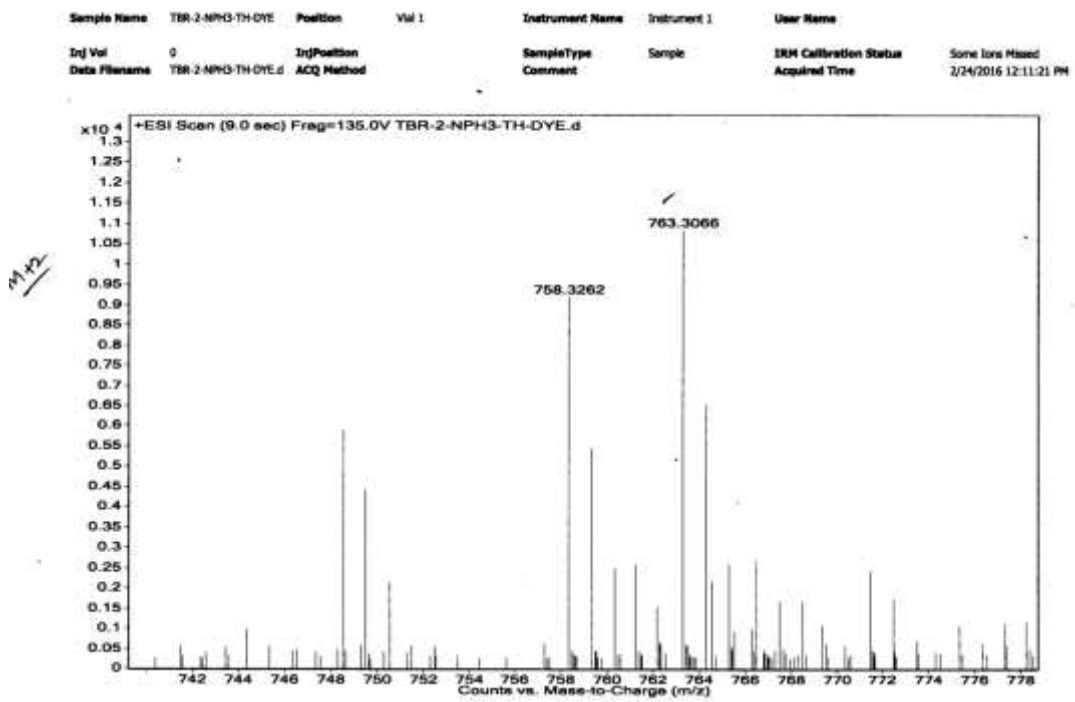

ESI-MS spectrum of (2*E*,2′*E*)-3,3'-(3,4-bis(4-diphenylamino) phenyl)thiophene-2,5-diyl)bis(2-cyanoacrylic acid)

CHAPTER-6

Highly efficient and facile alkylation of 4*H* Cyclopenta-[2,1-b:3,4-b']dithiophene in water

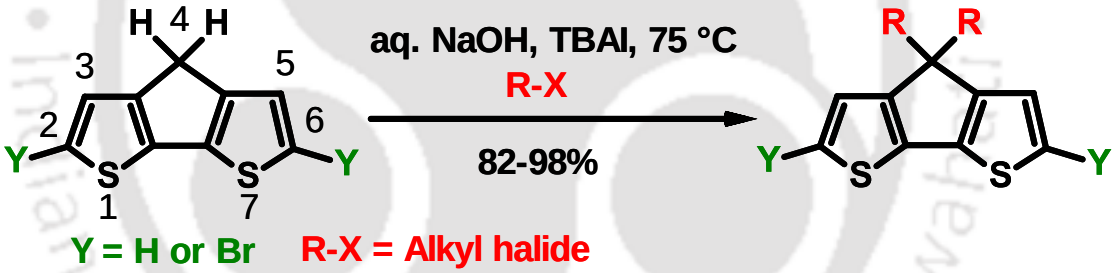

RSC Adv., **2014**, *4*, 37738-37745.

Abstract

In this chapter, a new and highly convenient method to perform alkylation of 4*H*-cyclopenta-[2,1-b:3,4-b']dithiophene (CPDT) in aqueous conditions is reported. This method was also extended to successfully perform alkylation of 2,6-dibromo-4*H*-cyclopenta-[2,1-b:3,4-b']dithiophene for the first time. This facile method has several advantages such as the exclusive use of water instead of high boiling toxic solvents, simple separation of the defect free dialkylated CPDT product and the use of mild reaction conditions. Despite using mild reagents and reaction conditions very high yields of up to 98% pure dialkylated CPDT products are obtained much more readily by this method in less time than literature procedures.

6.1 Introduction

Organic electronic devices based on heterocyclic compounds, especially, thiophene derivatives have gained huge popularity over the past few decades due to their tunable structure as well as excellent photophysical, electrochemical, thermal and solution processable parameters.[1–17] These materials enable a wide variety of functionalization and low cost, light weight fabrication processes on large-area substrates along with mechanical fexibility.[18] Fused bithiophenes such as, 4*H*-cyclopenta-[2,1-b:3,4-b']dithiophene (CPDT) are structural analogs of fluorene molecule, and the "two biphenyl rings" in fluorene molecule conjoined with a methylene carbon bridge are replaced by "two thiophene rings". CPDT, which consists of rigidly planar bithiophene units with a sp^3-hybridized methylene bridge allows functionalization at the 4-position resulting in higher solubility and enhancing the processing ability in the resulting polymer. 4,4'-dialkyl CPDT, regarded as a fused-ring analogue of 3-alkyl thiophene and structural analogue of dialkyl fluorene, possesses several advantages over both these systems.[8] In π-conjugated (semi) conducting copolymer systems, the 4,4'-dialkyl CPDT based oligomers and polymers having electron rich (donor) moieties, copolymerized with electron poor (acceptor) moieties, are known to have tunable and narrow band gaps.[3,4]

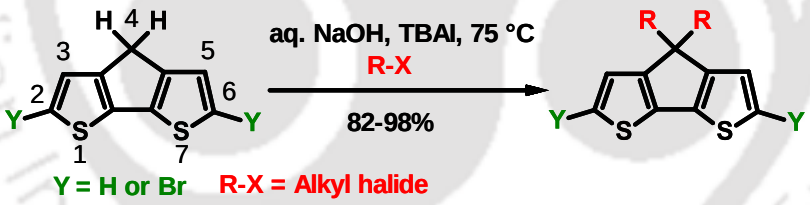

Scheme 6.1 General synthetic scheme for synthesis of 4,4'-dialkylation of CPDT derivatives

Various synthetic methods have been utilized in the past to substitute the 4,4'-position of CPDT (Scheme. 6.1) by linear and branched alkyl chains to enhance their solubility and processability. These include mainly symmetrically,[7–12] asymmetrically, [14] in-plane,[15] and substituted C-4 alkylation reactions of CPDT. Few reports on the symmetrically substituted CPDT and their application in optoelectronic devices have also been demonstrated with superior device characteristics compared to polythiophenes.[3,4,16] It was observed that all these prior methods utilized high boiling organic solvents such as DMF, DMSO, toluene, *etc*. to perform the dialkylation of CPDT.[8–10,12] These reactions were

reported to be air and water sensitive, harsh conditions such as hazardous and strong acids or strong bases were applied and in few cases metal catalysts were used to obtain the desired dialkylated products.[7–14] The first dialkylation of 4*H*-cyclopenta-[2,1-b:3,4-b']dithiophene reported in 1994, used lithiation method to obtain the dialkylated CPDT product with 35–47% yields.[7] Further improvements in the above method by using KOH in DMSO with catalytic amount of KI, NaI or KF resulted in 65–85% yields.[8–10] The use of NaH in DMF with KI was also reported to give desired dialkylated CPDT product with 57% yield.[11] The dialkylation of CPDT using aq. KOH and TBAI in toluene as a solvent gave 62% yield.[12] These dialkylated CPDT yields could be improved up to 95% in the presence of KOH and KI in DMSO.[13] The two step synthesis of dialkylated CPDT from 3-bromo-2,2'-bithophene by using n-BuLi and H_2SO_4 having 70% yields has also been reported.[14] These developments over the years are proof of the enormous interest that CPDT molecule has generated. Despite the growing importance of these CPDT derivatives in numerous interdisciplinary applications, it is observed that all the synthetic routes use high boiling solvents, hazardous chemicals and adverse reaction conditions that are, in several cases, also air and water sensitive and are too expensive for practical purposes. Moreover, the formation of 4-alkyl-4*H*-cyclopenta-[2,1-b:3,4-b']dithiophene as the major impurity are very common by these methods.[8] The formation of these mono-substituted product even in small amounts are detrimental for unwanted impurity formation during device operation with the end result of oxidized product during exposure to oxygenated environment or during device fabrication or even when exposed to light.[16] Hence, these unfavorable synthetic routes having several drawbacks such as the use of expensive as well as harsh reagents along with high boiling solvents also require additional separation steps which make them less viable, incur higher costs of reactions, need additional precautions and special conditions for making defect-free dialkylated products. This encouraged us to investigate a simple route for synthesizing the dialkylated CPDT.

6.2 Results and discussion

The development of new organic materials for optoelectronic device application relies on the improvement in the existing functionalization routes on the widely used aromatic and heterocyclic compounds. Bithiophene units have more planarity or less rigidity compared to biphenyl units.[3] In order to achieve superior polymer solubility and processability parameters, the fluorene and CPDT units with sp^3-hybridized carbon at the methylene

bridge position are functionalized. Here, a facile, solvent free and high yielding method for the dialkylation of CPDT and 2,6- dibromo CPDT has been reported. To the best of our knowledge, there are no reports for the dialkylation reaction of 2,6-dibromo substituted CPDT (Scheme 6.1, Y= Br). In our initial attempts 50% aq. NaOH, TBAI, 1-bromo octane, CPDT were used for dialkylation in atmospheric conditions, but resulted in formation of a mixture of unwanted products in major amounts. The same reaction again started with careful degassing of the reaction mixture comprising three freeze–thaw cycles. Stirring the reaction at room temperature (35–40 °C) for extended time did not give desired dialkylated CPDT which prompted to slowly raise the temperature. During the course of 5 minutes the color of the reaction mixture changed into greenish black at 75 °C, however, no starting material was observed in the reaction mixture after 3 h. This modification in the reaction conditions resulted in the development of highly successful dialkylation reaction of CPDT without the use of any organic solvents, metal catalyst, inert gases, strong acids, and high pressure/temperature, yet 82–96% (Table 6.1) isolated yield of the desired product 4,4'-dialkyl CPDT could be achieved with a variety of alkyl halides including chloro alkanes.

Before addition of the alkyl halide, the reaction mixture was thoroughly degassed by performing three freeze–thaw degassing repetitions, as mentioned above, to ensure the complete removal of oxygen. The reaction conditions were also optimized for appropriate base and their concentration. Diverse phase transfer catalysts and their quantities, the reaction temperature and time were also optimized by attempting dialkylation reactions with different alkyl halides. The reaction of CPDT with linear and branched alkyl chains having chloroalkyl, bromoalkyl and iodoalkyl chains were attempted under similar reaction conditions. To perform dialkylation of CPDT, bromo alkanes are the most preferred substrates due to their better reactivity and lower costs compared to chloro-alkanes and iodo-alkanes. We report seven different types of bromo alkanes, which include linear alkyl chain, branched chain and dibromo substituted alkyl chain derivatives (Table 6.1). Among these substrates, the highest yield of up to 96% was obtained for the alkylation of CPDT with 1-bromooctane (Table 6.1, entry 1b).

The optimized reaction conditions (Table 6.1) of CPDT were also extended to perform the dialkylation of 2,6-dibromo CPDT. It was observed that the dialkylation of 2,6-dibromo CPDT with the alkyl halide substrates examined here required very less time to form the desired dialkylated product and nearly all the reactions conformed that this

dibromo CPDT had been completely reacted within an hour of the reaction (except with chloro halides) (Table 6.1, entry 1k and 1t). Due to the presence of the two electron withdrawing bromide groups on CPDT the reactivity of this substrate was higher compared to the unsubstituted CPDT. The highest yield of 98% in the case of 2,6-dibromo CPDT was also obtained on reacting with 1-bromooctane (Table 6.1, entry 1l). In the Table 6.1, right columns, the reaction time and the isolated yield of the dialkylation reaction products obtained with 2,6-dibromo CPDT has been summarized. All the pure dialkylated products were extensively characterized by ^{1}H NMR, ^{13}C NMR, and high resolution mass spectroscopy (HRMS).

Table 6.1 Yields obtained for alkylation of CPDT, alkylation of 2,6-dibromo CPDT with various alkyl halides in aqueous NaOH, TBAI as PTC at 75 °C.

Alkyl halide (R-X)	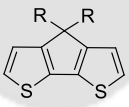 Entry	Time (min)	Isolated yield (%)	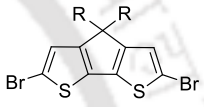 Entry	Time (min)	Isolated yield (%)
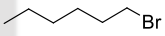	**1a**	150	94	**1k**	45	96
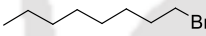	**1b**	150	96	**1l**	45	98
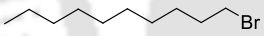	**1c**	150	90	**1m**	45	92
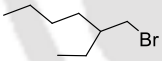	**1d**	150	88	**1n**	45	91
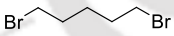	**1e**	180	82	**1o**	45	83
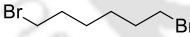	**1f**	180	92	**1p**	45	94
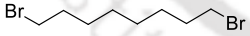	**1g**	180	90	**1q**	45	91
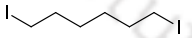	**1h**	180	90	**1r**	45	92
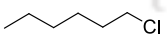	**1i**	240	82	**1s**	105	84
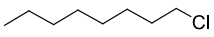	**1j**	240	84	**1t**	105	85

Compared to all other dialkylation reactions of CPDT with dibromo alkanes, 1,5-dibromo alkane gives lesser yields of 82% was observed. This is due to the formation of an unexpected by product occurring due to the attack of both the terminal bromine of this 1,5-dibromo pentane alkyl chain at the 4,4'- position of CPDT[14,17] as well as 2,6-dibromo CPDT, which gets converted via ring cyclization into a stable six-member ring. The

byproduct 2,6-dibromo spiro[4,5] ([2,1-b:3,4-b']dithieno)decane product (Fig. 6.1) was well characterized by ^{1}H and ^{13}C NMR, M.P. as well as single crystal X-ray crystallography analysis.

All the dialkylation reactions with CPDT as well as 2,6-dibromo CPDT were successfully done in 50% aq. NaOH without the use of any additional organic solvents (Table 6.1). Further, dialkylation of CPDT and 2,6-dibromo CPDT in the presence of various bases such as KOH, K_2CO_3, Na_2CO_3 and potassium acetate were also attempted with 1-bromooctane and TBAI (Table 6.2). It was observed that the dialkylated CPDT yields obtained with aq. KOH were nearly identical (Table 6.2 entry 2b) to those obtained with aq. NaOH. Dialkylation reactions performed in the absence of base with CPDT and 2,6-dibromo CPDT did not give any product (Table 6.2 entry 2f).

Table 6.2 Comparative reactivity study of CPDT and 2, 6-dibromo CPDT alkylation with 1-bromooctane in presence of different types of bases at 75 °C

	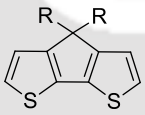			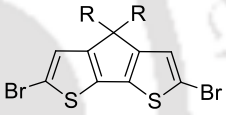		
Type of base	Entry	Time (min)	Isolated yield (%)	Entry	Time (min)	Isolated yield (%)
NaOH	**2a**	150	96	**2g**	45	98
KOH	**2b**	150	95	**2h**	45	96
K_2CO_3	**2c**	360	35	**2i**	180	40
Na_2CO_3	**2d**	420	30	**2j**	180	30
CH_3COOK	**2e**	720	—	**2k**	360	—
Without base	**2f**	1440	—	**2l**	720	—

This indicates that choosing an appropriate base is crucial for obtaining high dialkylation yields in shorter time. We have also optimized the quantity of aq. NaOH required for these reactions by reducing and increasing the quantity under identical reaction parameters (Table 6.3). It was observed that on decreasing the quantity of base from 50% (w/w in water) to 40%, 30%, 20% and 10%, there was a significant drop in the desired dialkylated product to 80%, 65%, 48% and 40% under similar reaction conditions (Table

6.3 entry 3a to 3e). Further, increasing the quantity of base above 50% did not alter the reaction yield or reduce the time of reaction (Table 6.3 entry 3f). Hence, all the reactions were performed in 50% aq. NaOH.

The effect of different type of bases on the dialkylated product yield with 2,6-dibromo CPDT as well as the quantity of NaOH are presented in Tables 6.2 and 6.3. The reaction time and isolated yield summarized in these two tables confirm that 50% aq. NaOH solution is appropriate for these dialkylation reaction with both CPDT as well as 2,6-dibromo CPDT.

Table 6.3 Comparative reactivity study of CPDT and 2,6-dibromo CPDT alkylation with 1-bromooctane in presence of different quantities of aqueous NaOH at 75 °C.

	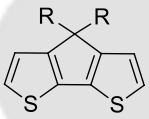			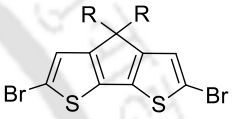		
Quantity of base	Entry	Time (min)	Isolated yield (%)	Entry	Time (min)	Isolated yield (%)
10 %	**3a**	420	40	**3g**	240	45
20 %	**3b**	420	48	**3h**	240	55
30 %	**3c**	360	65	**3i**	180	70
40 %	**3d**	300	80	**3j**	180	85
50 %	**3e**	150	96	**3k**	45	98
60 %	**3f**	150	96	**3l**	45	98

The quantity and type of PTC also had a significant influence in obtaining the dialkylated products with these two CPDT derivatives in high yields. It was observed that the highest yield of 96% and 98% dialkylated CPDT and dialkylated 2,6-dibromo CPDT products were obtained with TBAI (Table 6.4 entry 4a, 4h) in 50% aq. NaOH in 240 min and 80 min respectively. However, the dialkylated CPDT product yields obtained with tetrabutylammonium chloride (TBAC) and tetrabutylammonium fluoride (TBAF) were reduced to 70–75% and 60–65% respectively (Table 6.4 entry 4c, 4d, 4j and 4k) with the reaction taking up to 120–420 min to complete. The use of anionic and neutral surfactants

such as SDS, and 15-crown-5 gave negligible to poor yields (15–40%) under similar reaction conditions (Table 6.4 entry 4e, 4f, 4k and 4m). The dialkylation reaction with both CPDT as well as 2,6-dibromo CPDT did not proceed when performed in the absence of phase transfer catalyst (Table 6.4 entry 4g) indicating the vital role of phase transfer catalyst in this reaction.

A general trend observed in these reactions indicated that the iodide containing PTC were most efficient compared to bromide, chloride and fluoride. The use of 15-crown-5 and SDS gave very less product yields requiring extended reaction time whereas reactions performed in the absence of PTC did not yield any dialkylated CPDT products.

Table 6.4 Comparative Reactivity Study of CPDT and 2,6-dibromo CPDT alkylation with 1-Bromooctane in presence of different types of PTCs in aqueous NaOH at 75 °C.

	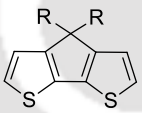			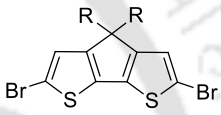		
Phase-transfer catalyst (PTC)	Entry	Time (min)	Isolated yield (%)	Entry	Time (min)	Isolated yield (%)
TBAI	**4a**	150	96	**4h**	45	98
TBAB	**4b**	240	92	**4i**	80	92
TBAC	**4c**	360	70	**4j**	120	75
TBAF	**4d**	420	60	**4k**	180	65
15-crown-5	**4e**	540	35	**4l**	240	40
Sodium dodecyl sulfate (SDS)	**4f**	420	15	**4m**	180	15
without PTC	**4g**	720	—	**4n**	360	—

After establishing that TBAI is the most suitable PTC for the dialkylation of CPDT and 2,6-dibromo CPDT, we investigated the accurate quantity that would be required for the best product yields.

For optimization of the quantity of PTC, different mol% of TBAI was utilized in these reactions. The Table 6.5 depicts that 20 mol% of TBAI was sufficient for the successful dialkylation of CPDT reactions. On adding 2.5 mol% of TBAI resulted in the formation of dialkylated CPDT and dialkylated 2,6-dibromo CPDT in 55–60% yields (Table 6.5

entry 5a) in (480 minutes) 8 hours. Increasing the quantity of TBAI to 5 mol% and 7.5 mol% helped in enhancing the yields up to 80%, however, (480 minutes) 8 hours were required to achieve this yield (Table 6.5 entry 5b and 5c). A significant drop in reaction time as well as increase in the dialkylated product yields with both CPDT as well as 2,6-dibromo CPDT was achieved on increasing the quantity of TBAI up to 10 mol%. On further increasing the TBAI quantity to 20 mol% gave the maximum yield of 96–98% within 150 min (Table 6.5 entry 5e and 5l). Adding greater than 20 mol% of TBAI did not enhance the yields of desired product or reduce the reaction time (Table 6.5 entry 5e, 5f, 5g, 5l, 5m, and 5n).

Table 6.5 Comparative Reactivity Study of CPDT and 2,6-dibromo CPDT alkylation with 1-Bromooctane in presence of different quantities of TBAI at 75 °C.

Different quantities of TBAI	Entry	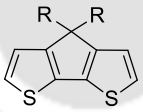 Time (min)	Isolated yield (%)	Entry	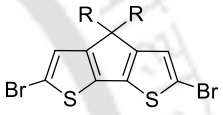 Time (min)	Isolated yield (%)
2.5 mol%	**5a**	480	55	**5h**	240	60
5 mol%	**5b**	480	70	**5i**	240	75
7.5 mol%	**5c**	480	78	**5j**	240	80
10 mol%	**5d**	240	92	**5k**	120	95
20 mol%	**5e**	150	96	**5l**	45	98
50 mol%	**5f**	150	96	**5m**	45	98
100 mol%	**5g**	150	96	**5n**	45	98

6.3 Experimental section

6.3.1 General procedure followed for the dialkylation of 4*H*-Cyclopenta [2,1-b:3,4-b']dithiophene (CPDT).

CPDT (0.2 g, 1.12 mmol), freshly prepared 50% aq. NaOH, and phase transfer catalyst tetrabutylammonium iodide (0.08 g, 20 mol%) were added into a round bottom flask. The flask was degassed thrice by applying freeze-thaw cycles to remove trace amounts of oxygen completely, followed by alkyl halide (2.8 mmol) addition via syringe (degassed)

and the mixture heated at 75 °C continuously for 150-240 min. The reaction mixture was cooled to room temperature and extracted with ethyl acetate. The organic layer was washed with water and dried over anhydrous sodium sulphate. The solvent was removed under vacuum, and the crude was purified via column chromatography over silica/ hexane.

6.3.2 General procedure followed for the dialkylation of 2,6-dibromo-4*H*-Cyclopenta [2,1-b:3,4-b']dithiophene (Br-CPDT)

2,6-dibromo-4*H*-Cyclopenta [2,1-b:3,4-b']dithiophene (Br-CPDT) (0.2 g, 0.5951 mmol), freshly prepared 50% aq. NaOH, and phase transfer catalyst tetrabutylammonium iodide (0.04 g, 20 mol%) were added into a round bottom flask. The flask was degassed thrice by applying freeze-thaw cycles to remove trace amounts of oxygen completely, followed by alkyl halide (1.48 mmol) addition via syringe (degassed) and the mixture heated at 75 °C continuously for 45-105 min. The reaction mixture was cooled to room temperature and extracted with ethyl acetate. The organic layer was washed with water and dried over anhydrous sodium sulphate. The solvent was removed under vacuum, and the crude was purified via column chromatography over silica / hexane.

4,4'-Dihexyl-4*H*-cyclopenta[2,1-b:3,4-b']dithiophene (entry 1a).[7,9]

Yield: 94% as a light yellow color liquid. ^{1}H NMR (600 MHz, $CDCl_3$): δ 7.10(d, 2H), 6.92(d, 2H), 1.84(m, 4H), 1.22(m, 4H), 1.14(m, 8H), 0.88(m, 10H); ^{13}C NMR (100 MHz, $CDCl_3$): δ 158.32, 137.01, 124.61, 121.83, 53.44, 37.97, 31.85, 29.92, 24.70, 22.89, 14.35; HRMS (ESI): m/z $[M+H]^+$calcd for $C_{21}H_{30}S_2$ 347.1867, found 347.1877.

4,4'-Dioctyl-4*H*-cyclopenta[2,1-b:3,4-b']dithiophene (entry 1b).[8]

Yield: 96% as a light yellow color liquid. ^{1}H NMR (600 MHz, $CDCl_3$): δ 7.13 (d, J= 4.8 Hz, 2H), 6.90(d, J= 5.4 Hz, 2H), 1.81(m, 4H), 1.34(m, 20H), 1.15(m, 4H), 0.84(t, 6H); ^{13}C NMR (100 MHz, $CDCl_3$): δ 158.20, 136.72, 124.76, 121.82, 53.43, 37.97, 33.70, 30.62, 29.94, 29.61, 28.630, 24.64, 14.38; HRMS (ESI): m/z $[M+H]^+$calcd for $C_{25}H_{38}S_2$ 403.2493, found 403.2497.

4,4'-Bisdecyl-4*H*-cyclopenta[2,1-b:3,4-b']dithiophene (entry 1c).

Yield: 90% as a light yellow color liquid. ^{1}H NMR (600 MHz, $CDCl_3$): δ 7.14(d, J= 4.8 Hz, 2H), 6.92(d, J= 5.4 Hz, 2H), 1.87(m, 4H), 1.38(m, 4H), 1.32(m, 28H), 0.96(m, 6H); ^{13}C NMR (150 MHz, $CDCl_3$): δ 158.30,136.63, 124.57, 121.81, 53.43, 45.32, 39.24, 33.79, 30.23, 29.91, 28.98, 27.46, 25.14, 22.63, 14.57; HRMS (ESI): m/z $[M+H]^+$calcd for $C_{29}H_{46}S_2$ 459.3119, found 459.3119.

4,4'-Bis(2-ethylhexyl)-4*H*-cyclopenta[2,1-b:3,4-b']dithiophene (entry 1d).[3m]

Yield: 88% as a light yellow color liquid. ^{1}H NMR (600 MHz, $CDCl_3$): δ 7.11(d, J= 4.8 Hz, 2H), 6.93(d, J= 5.4 Hz, 2H), 1.89(m, 4H), 0.99(m, 18H), 0.77(t, 6H), 0.61(t, 6H); ^{13}C NMR (150 MHz, $CDCl_3$): δ 157.83, 137.01, 124.16, 122.55, 53.44, 43.45, 35.21, 34.35, 29.04, 27.48, 23.05, 14.33, 11.08; HRMS (ESI): m/z $[M+H]^+$calcd for $C_{25}H_{38}S_2$ 403.2493, found 403.2493.

4,4'-Bis-(5-bromopentyl)-4*H*-cyclopenta[2,1-b:3,4-b']dithiophene (entry 1e).

Yield: 82% as a light yellow color liquid. ^{1}H NMR (600 MHz, $CDCl_3$): δ 7.14(d, J= 4.8 Hz, 2H), 6.89(d, J=5.4 Hz, 2H), 3.25(t, J=13.8 Hz, 4H), 1.85(m, 4H), 1.68(t, J= 13.2 Hz 4H), 1.26(m, 4H), 0.90(m, 4H); ^{13}C NMR (150 MHz, $CDCl_3$): δ 157.62, 136.93, 125.06, 121.57, 53.22, 37.92, 34.04, 32.72, 29.11, 23.81; HRMS (ESI): m/z $[M+H]^+$calcd for $C_{19}H_{24}Br_2S_2$ 476.9744, found 476.9752.

4,4'-Bis-(6-bromohexyl)-4*H*-cyclopenta[2,1-b:3,4-b']dithiophene (entry 1f).[12]

Yield: 92% as a light yellow color liquid. ^{1}H NMR (600 MHz, $CDCl_3$): δ 7.16(d, J=4.8 Hz, 2H), 6.92(d, J= 4.8 Hz, 2H), 3.32(t, J=6.6 Hz, 4H), 1.83(m, 4H), 1.73(t, J=7.8 Hz, 4H), 1.29(m, 4H), 1.15(m, 4H), 0.93(m, 4H); ^{13}C NMR (150 MHz, $CDCl_3$): δ 157.85, 136.73, 124.83, 121.65, 53.24, 37.84, 34.12, 32.81, 29.85, 28.03, 24.29; HRMS (ESI): m/z $[M+H]^+$calcd for $C_{21}H_{28}Br_2S_2$ 505.0057, found 505.0056.

4,4'-Bis-(8-bromoctyl)-4*H*-cyclopenta[2,1-b:3,4-b']dithiophene (entry 1g).

Yield: 90% as a light yellow color liquid. ^{1}H NMR (600 MHz, $CDCl_3$): δ 7.15(d, J= 4.8 Hz, 2H), 6.92(d, J= 4.2 Hz, 2H), 3.36(t, J= 6.6 Hz, 4H), 1.82(m, 8H), 1.33(m, 4H), 1.15(m, 12H), 0.92(m, 4H).^{13}C NMR (150 MHz, $CDCl_3$): δ 158.15, 136.69, 124.70, 121.77, 53.39, 37.93, 34.21, 32.94, 30.01, 29.30, 28.80, 28.24, 24.59; HRMS (ESI): m/z $[M+H]^+$calcd for $C_{25}H_{36}Br_2S_2$ 561.0683, found 561.0687.

4,4'-Bis-(6-iodohexyl)-4*H*-cyclopenta[2,1-b:3,4-b']dithiophene (entry 1h).

Yield: 90% as a light yellow color liquid. ^{1}H NMR (600 MHz, $CDCl_3$): δ 7.16(d, J= 4.2 Hz, 2H), 6.92(d, J= 4.8 Hz, 2H), 3.10(t, J= 7.2 Hz, 4H), 1.82(m, 4H), 1.68(m, 4H), 1.28(m, 4H), 1.15(m, 4H), 0.85(m, 4H); ^{13}C NMR (150 MHz, $CDCl_3$): δ 154.36, 137.65, 124.53, 122.66, 44.36, 33.47, 31.85, 30.99, 28.70, 27.24, 7.22; HRMS (ESI): m/z $[M+H]^+$calcd for $C_{21}H_{28}I_2S_2$ 598.9800, found 599.0084.

2,6-Dibromo-4,4'-dihexyl-4*H*-cyclopenta[2,1-b:3,4-b']dithiophene (entry 1k).

Yield: 96% as a light yellow color liquid. ^{1}H NMR (600 MHz, $CDCl_3$): δ 6.94(s, 2H), 1.78(m, 4H), 1.27(m, 16H), 0.92(m, 6H); ^{13}C NMR (150 MHz, $CDCl_3$): δ 156.13, 136.51,

124.77, 111.31, 55.23, 37.79, 31.79, 29.92, 24.63, 22.84, 14.34; HRMS (ESI): m/z $[M+H]^+$calcd for $C_{21}H_{28}Br_2S_2$ 505.0057, found 505.0054.

2,6-Dibromo-4,4'-dioctyl-4*H*-cyclopenta[2,1-b:3,4-b']dithiophene (entry 1l).[8]

Yield: 98% as a light yellow color liquid. ^{1}H NMR (600 MHz, $CDCl_3$): δ 6.93(s, 2H), 1.72(m, 4H), 1.23(m, 20H), 1.11(m, 4H), 0.85(m, 6H); ^{13}C NMR (150 MHz, $CDCl_3$): 156.16, 136.50, 124.79, 111.27, 55.24, 37.74, 31.99, 30.17, 29.90, 29.49, 24.61, 22.90, 14.29; HRMS (ESI): m/z $[M+H]^+$calcd for $C_{25}H_{36}Br_2S_2$ 561.0683, found 561.0668.

2,6-Dibromo-4,4'-didecyl-4*H*-cyclopenta[2,1-b:3,4-b']dithiophene (entry 1m).

Yield: 92% as a light yellow color liquid. ^{1}H NMR (600 MHz, $CDCl_3$): δ 6.93 (s, 2H), 1.77(m, 4H), 1.26(m, 32H), 0.86(m, 6H); ^{13}C NMR (150 MHz, $CDCl_3$): δ 156.17, 136.52, 124.80, 111.30, 55.25, 37.76, 32.15, 30.16, 29.93, 29.89, 29.76, 29.56, 24.65, 22.90, 14.34; HRMS (ESI): m/z $[M+H]^+$calcd for $C_{29}H_{44}Br_2S_2$ 617.1309, found 617.1309.

2,6-Dibromo-4,4'-bis(2-ethylhexyl)-4*H*-cyclopenta[2,1-b:3,4-b']dithiophene (entry 1n).[3m]

Yield: 0.303 g (91%) as a light yellow color liquid. ^{1}H NMR (600 MHz, $CDCl_3$): δ 6.93(s, 2H), 1.81(m, 4H), 1.32(m, 18H), 0.86(t, 12H).^{13}C NMR (150 MHz, $CDCl_3$): δ 155.67, 136.87, 125.33, 111.048, 55.13, 43.29, 35.35, 29.89, 28.78, 23.62, 14.69, 11.28; HRMS (ESI): m/z $[M+H]^+$calcd for $C_{25}H_{36}Br_2S_2$ 561.0683, found 561.0668.

2,6-Dibromo-4,4'-bis(5-bromopentyl)-4*H*-cyclopenta[2,1-b:3,4-b']dithiophene (entry 1o).

Yield: 83% as a light yellow color liquid. ^{1}H NMR (600 MHz, $CDCl_3$): δ 6.89(s, 2H), 3.27(t, J= 6.6 Hz, 4H), 1.78(m, 4H), 1.70(t, J= 6.6 Hz, 4H), 1.25(m, 4H), 0.88(m, 4H); ^{13}C NMR (150 MHz, $CDCl_3$): δ 155.46, 136.75, 124.52, 111.74, 54.96, 37.74, 33.97, 32.67, 28.65, 23.79; HRMS (ESI): m/z $[M+H]^+$calcd for $C_{19}H_{22}Br_4S_2$ 634.7934, found 634.7934.

2,6-Dibromo-4,4'-bis(6-bromohexyl)-4*H*-cyclopenta[2,1-b:3,4-b']dithiophene (entry 1p).[12]

Yield: 94 %.as a light yellow color liquid. ^{1}H NMR (600 MHz, $CDCl_3$): δ 6.92(s, 2H), 3.34(t, J= 10.2 Hz, 4H), 1.77(m, 8H), 1.29(m, 4H), 1.15(m, 4H), 0.90(m, 4H); ^{13}C NMR (100 MHz, $CDCl_3$): δ 155.73, 136.65, 124.62, 111.55, 55.06, 37.74, 34.14, 32.87, 29.22, 28.08, 24.41; HRMS (ESI): m/z $[M+H]^+$calcd for $C_{21}H_{26}Br_4S_2$ 662.8247, found 662.8272.

2,6-Dibromo-4,4'-bis(8-bromooctyl)-4*H*-cyclopenta[2,1-b:3,4-b']dithiophene (entry 1q).

Yield: 91% as a light yellow color liquid. ^{1}H NMR (600 MHz, $CDCl_3$): δ 6.92(s, 2H), 3.34(t, J= 8 Hz, 4H), 1.77(m, 8H), 1.29(m, 4H), 1.15(m, 4H), 0.90(m, 4H); ^{13}C NMR (100 MHz, $CDCl_3$): δ 152.06, 137.570, 125.32, 112.21, 55.98, 38.20, 33.68, 30.61, 30.07, 29.43, 28.66, 28.58, 24.06; HRMS (ESI): m/z $[M+H]^+$calcd for $C_{25}H_{34}Br_4S_2$ 718.8873, found 718.8872.

2,6-Dibromo-4,4'-bis(6-iodohexyl)-4H-cyclopenta[2,1-b:3,4-b']dithiophene (entry 1r).

Yield: 92% as a light yellow color liquid. ^{1}H NMR (600 MHz, $CDCl_3$): δ 6.97(s, 2H), 3.13(t, J= 6.6 Hz 4H), 1.78(m, 4H), 1.69(m, 4H), 1.29(m, 4H), 1.17(m, 4H), 0.92(m, 4H); ^{13}C NMR (150 MHz, $CDCl_3$): δ 155.73, 136.65, 124.63, 111.57, 55.06, 37.74, 33.66, 30.38, 28.98, 24.38, 7.36; HRMS (ESI): m/z $[M+H]^+$calcd for $C_{21}H_{26}Br_2I_2S_2$ 756.7990, found 756.7992.

X-ray crystallographic analysis of 2,6-Dibromo spiro[4,5]([2,1-b; 3,4-b']dithieno) decane:

Single crystals of 2,6-Dibromo spiro[4,5]([2,1-b; 3,4-b']dithieno) decane were grown from $CHCl_3$ / hexane mixture. CCDC-1005162, the crystal parameters are available in the ESI. ^{1}H NMR (400 MHz, $CDCl_3$): δ 7.13(s, 2H), 1.76-1.63(m, 10H); ^{13}C NMR (100 MHz, $CDCl_3$): δ 157.39, 135.86, 126.00, 110.95, 51.76, 42.05, 25.58, 22.92; M. P. 84 °C.

6.4 Crystal Data

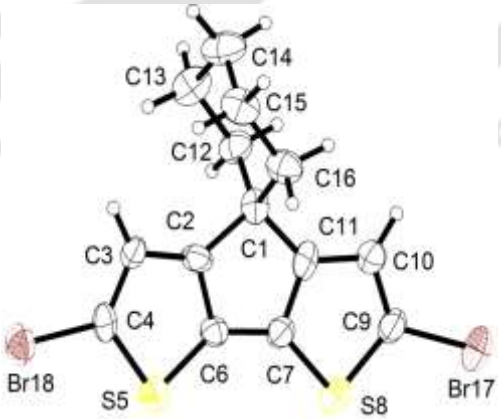

Figure 6.1 ORTEP diagram of 2,6-Dibromo spiro[4,5] ([2,1-b; 3,4-b']dithieno)decane

Table 6.6 Crystal data and structure refinement for TBr-Brcpdb-C5br at 296 K Crystallographic parameters of 2,6-dibromo spiro[4,5] ([2,1-b; 3,4-b']dithieno)decane

Compound	TBr-Brcpdb-C5br
Formula	$C_{14}H_{12}Br_2S_2$
CCDC No	1005162
Formula. wt.	404.18
Crystal system	Monoclinic
Space group	P 21/c
a (A°)	6.5657(4)
b (A°)	15.4051(8)
C(A°)	14.3212(7)
α(°)	90
β(°)	100.183(5)
γ(°)	90
V/ A^3	1425.71(14)
Z	4
Density/Mgm^{-3}	1.883
Abs. Co eff/mm^{-1}	5.957
F(000)	792
Total no. of reflections	5206
Reflections, $I > 2\sigma(I)$	1578
Max. 2θ/°	6.02 to 57.2°
Ranges (h, k, l)	$-7 \leq h \leq 7$, $-16 \leq k \leq 18$, $-16 \leq l \leq 17$
Complete to 2θ (%)	1.00
Data/ Restraints/Parameters	2507/0/163
Goof (*F2*)	1.026
R indices [$I >= \sigma(I)$]	0.0631
R indices (all data)	0.1046

6.5 Summary

We developed a facile and highly economical methodology for the dialkylation of 4*H* cyclopenta-[2,1-b:3,4-b']dithiophene. This reaction avoided the use of any organic solvents, metal catalysts and no additional inert gases were applied while performing these reactions, yet high yield of up to 96% dialkylated CPDT were obtained. Furthermore, this methodology could also be extended, for the first time, to perform dialkylation of 2,6-dibromo CPDT under similar mild conditions. The yields of dialkylated product with 2,6-dibromo CPDT were even higher and required very less time to complete as compared to unsubstituted CPDT. 50% aqueous NaOH and 20 mol%

TBAI as phase transfer catalyst were found to be the most optimum to obtain the desired products. Dialkylation using even chloro alkanes, bromo and dibromo alkanes, and diiodo alkanes gave high yields with both CPDT and 2,6-dibromo CPDT. Importantly, these reactions work best in the absence of oxygen, whereas presence of water has virtually no effect on the reaction, thereby facilitating the reaction in aqueous medium. This simple methodology will facilitate the development and expansion of this environmentally friendly reaction and these fused thiophene derivatives in various interdisciplinary applications.

6.6 References

1. Beaujuge, P. M.; Pisula, W.; Tsao, H. N.; Ellinger, S.; Müllen, K.; Reynolds, J. R. *J. Am. Chem. Soc.* **2009**, *131*, 7514-7515.
2. Wanwong, S.; Poe, A.; Balaji, G.; Thayumanavan, S. *Org. Biomol. Chem*. **2014**, *12*, 2474-2478.
3. Zhang, Z.–G.; Wang, J. Z.; *J. Mater. Chem*. **2012**, *22*, 4178-4187.
4. Tsao, H. N.; Cho, D. M.; Park, I.; Hansen, M. R.; Mavrinskiy, A.; Yoon, D. Y.; Graf, R.; Pisula, W.; Spiess, H. W.; Müllen, K. *J. Am. Chem. Soc*. **2011**, *133*, 2605-2612.
5. Zotti, G.; Vercelli, B.; Berlin, A. *Chem. Mater*. **2008**, *20*, 397-412.
6. Kostyanovsky, V. A.; Susarova, D. K.; Adam, G. Lyubovskaya, R. N.; Troshin, P. A. *Mendeleev Commun*. **2013**, *23*, 26-28.
7. Zotti, G.; Schiavon, G.; Berlin, A.; Fontana, G.; Pagani, G. *Macromolecules* **1994**, *27*, 1938-1942.
8. Coppo, P.; Cupertino, D. C.; Yeates, S. G.; Turner, M. L. *Macromolecules* **2003**, *36*, 2705-2711.
9. Song, H.-Y.; Tong, H.; Xie, Z.-Y.; Wang, L.-X.; Wang, F.-S.; *Chin. J. Polym. Sci.* **2013**, *31*, 1117-1126.
10. Coffin, R. C.; Peet, J.; Rogers, J.; Bazan, G. C. *Nat. Chem*. **2009**, *1*, 657-661.
11. Wu, C.-G.; Ho, M.-H.; Tsai, P.-F. U.S. Pat. Appl. Publ., 20110040055.
12. Henson, Z. B.; Zhang, Y.; Nguyen, T.–Q.; Seo, J. H.; Bazan, G. C. *J. Am. Chem. Soc*. **2013**, *135*, 4163-4166.
13. Gao, P.; Cho, D.; Yang, X. Y.; Enkelmann, V.; Baumgarten, M.; Müllen, K. *Chem. Eur. J*. **2010**, *16*, 5119-5128.

14. Van Mierloo, S.; Adriaensens, P. J.; Maes, W.; Lutsen, L.; Cleij, T. J.; Botek, E.; Champagne, B.; Vanderzande, D. J. *J. Org. Chem*. **2010**, *75*, 7202-7209.
15. Bünnagel, T. W.; Galbrecht, F.; Scherf, U. *Macromolecules* **2006**, *39*, 8870-8872.
16. Marin, L.; Penxten, H.; Van Mierloo, S.; Carleer, R.; Lutsen, L.; Vanderzande, D.; Maes, W.; *J. Polym. Sci. Polym. Chem*. **2013**, *51*, 4912-4922.
17. Benincori, T.; Consonni, V.; Gramatica, P.; Pilati, T.; Rizzo, S.; Sannicolo, F.; Todeschini, R.; Zotti, G. *Chem. Mater*. **2001**, *13*, 1665-1673.
18. Mahajan, A.; Francis, L. F.; Frisbie, C. D.; *ACS Appl. Mater. Inter*. **2014**, *6*, 1306-1312.

Appendix

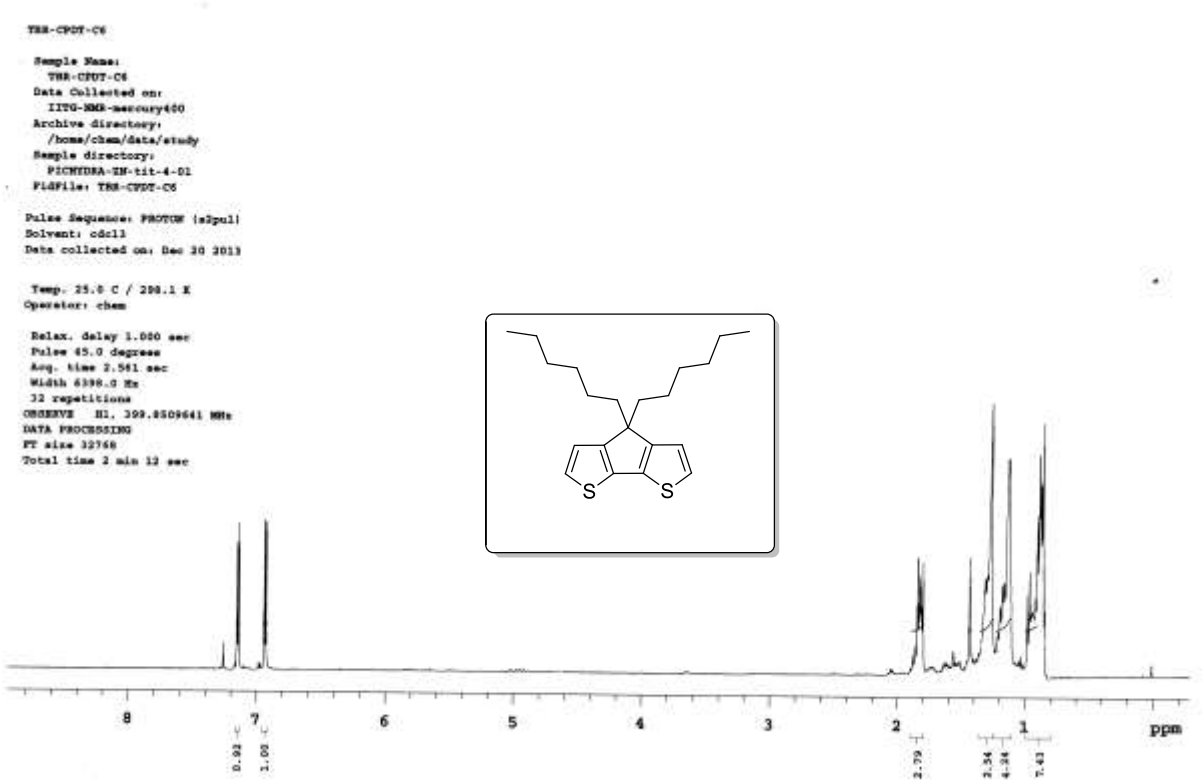

^{1}H-NMR spectrum of 4,4'-Dihexyl-4*H*-cyclopenta[2,1-b:3,4-b']dithiophene (entry 1a)

.

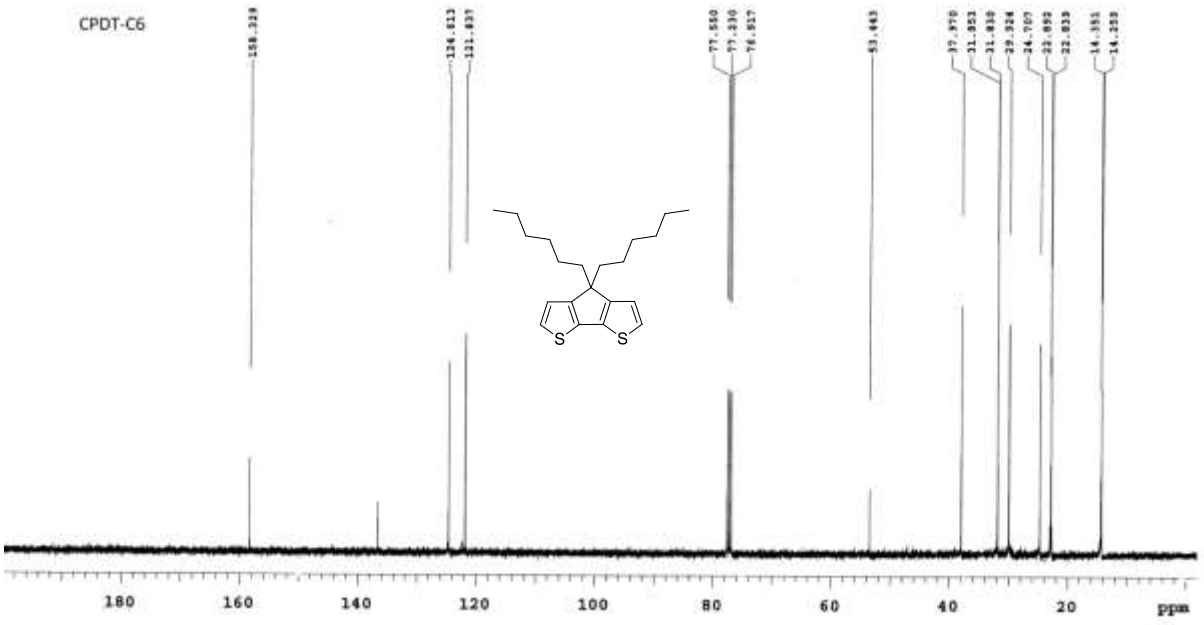

^{13}C-NMR spectrum of 4,4'-Dihexyl-4*H*-cyclopenta[2,1-b:3,4-b']dithiophene (entry 1a).

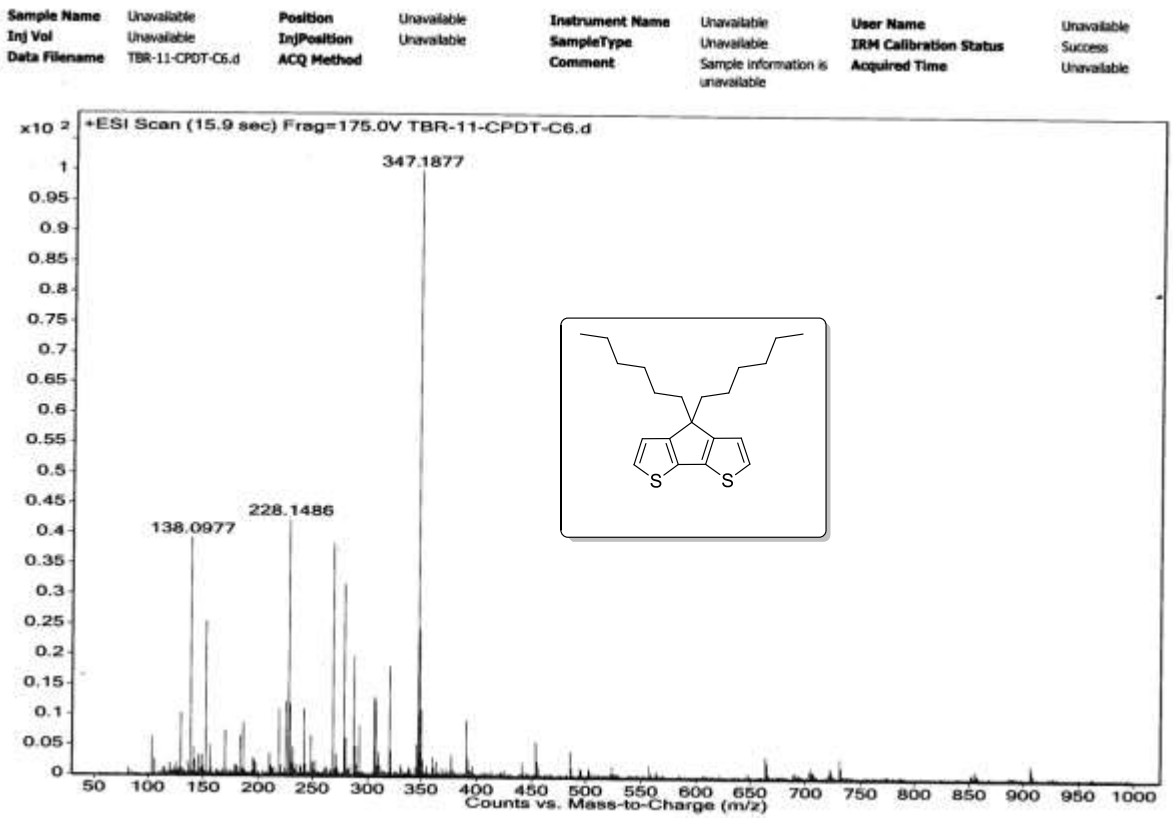

ESI-MS spectrum of 4,4'-Dihexyl-4*H*-cyclopenta[2,1-b:3,4-b']dithiophene (entry 1a).

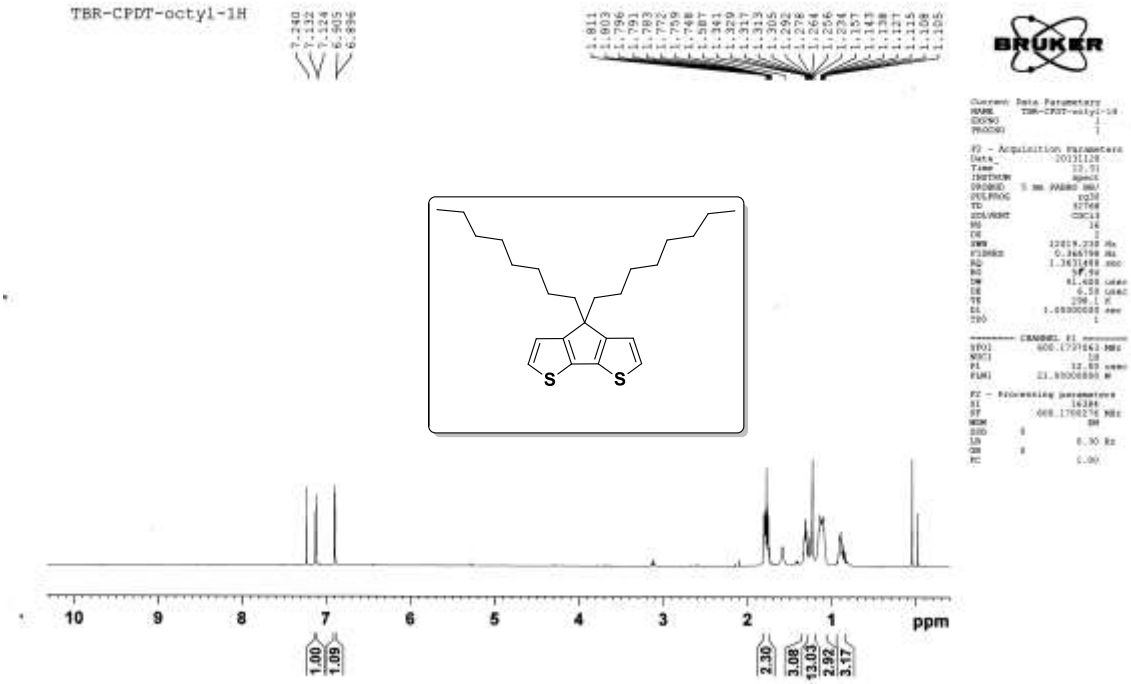

^{1}H-NMR spectrum of 4,4'-Dioctyl-4*H*-cyclopenta[2,1-b:3,4-b']dithiophene (entry 1b).

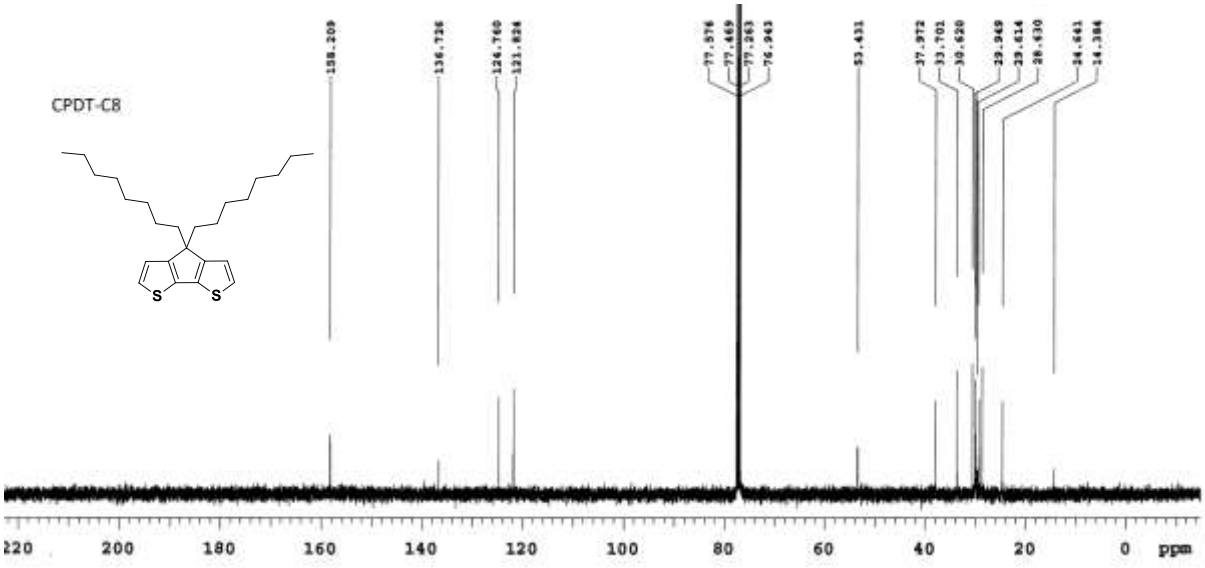

^{13}C NMR spectrum of 4,4'-Dioctyl-4*H*-cyclopenta[2,1-b:3,4-b']dithiophene (entry 1b)

.

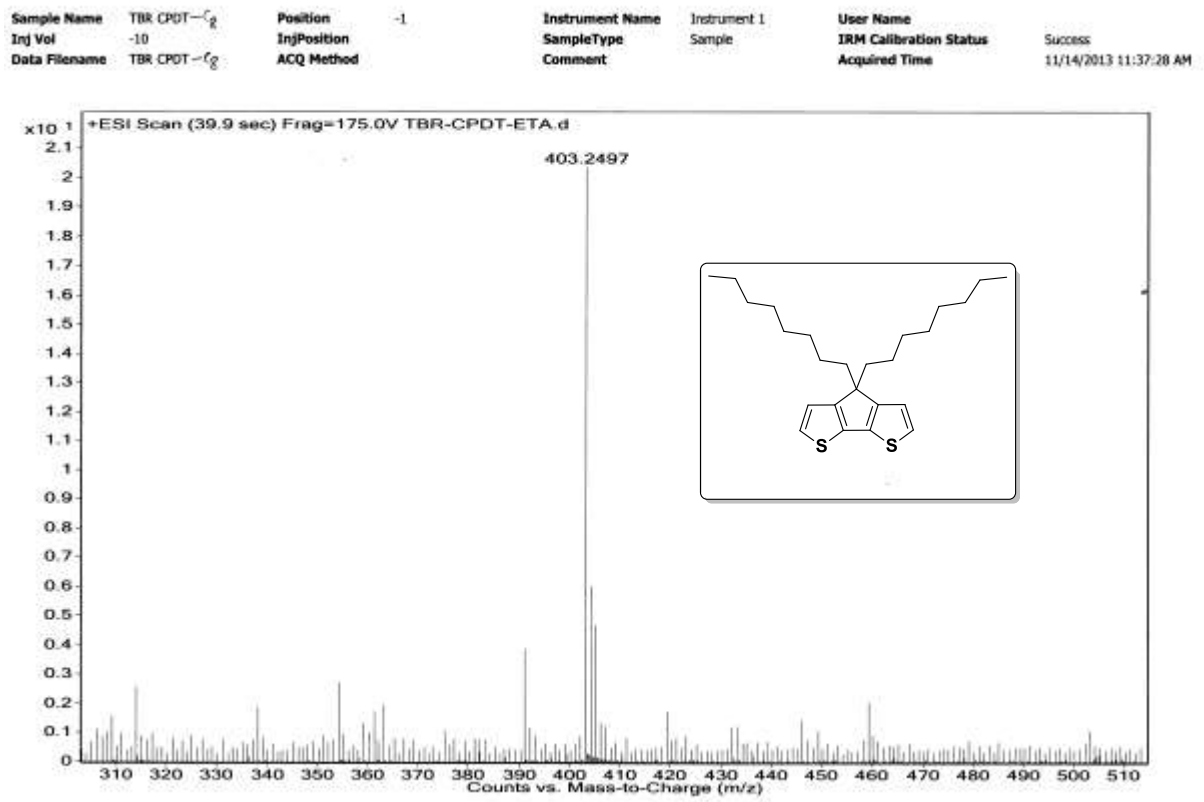

ESI-MS spectrum of 4,4'-Dioctyl-4*H*-cyclopenta[2,1-b:3,4-b']dithiophene (entry 1b).

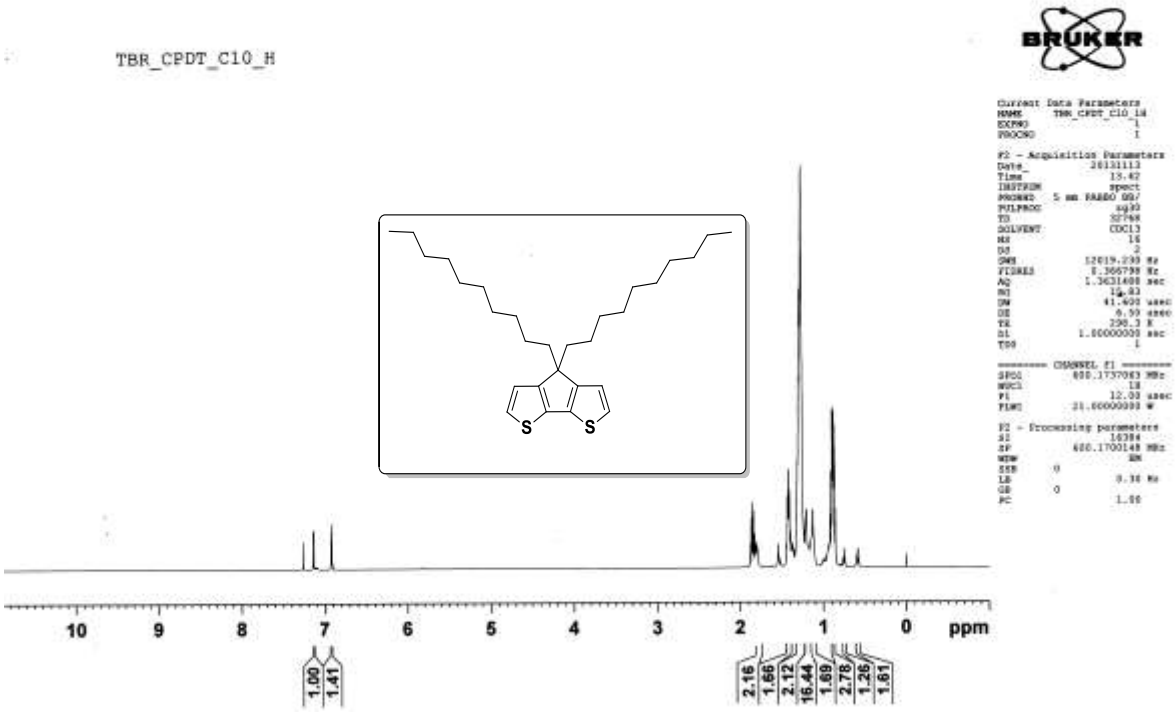

^{1}H-NMR spectrum of 4,4'-Bisdecyl-4*H*-cyclopenta[2,1-b:3,4-b']dithiophene (entry 1c).

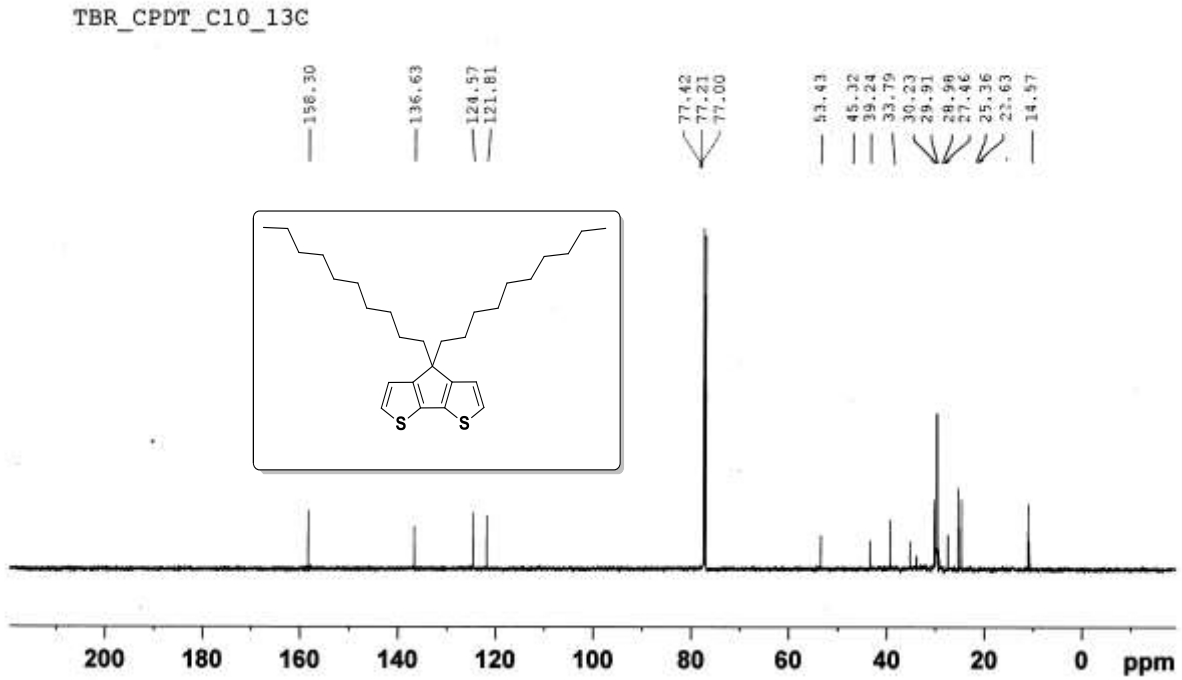

^{13}C NMR spectrum of 4,4'-Bisdecyl-4*H*-cyclopenta[2,1-b:3,4-b']dithiophene (entry 1c).

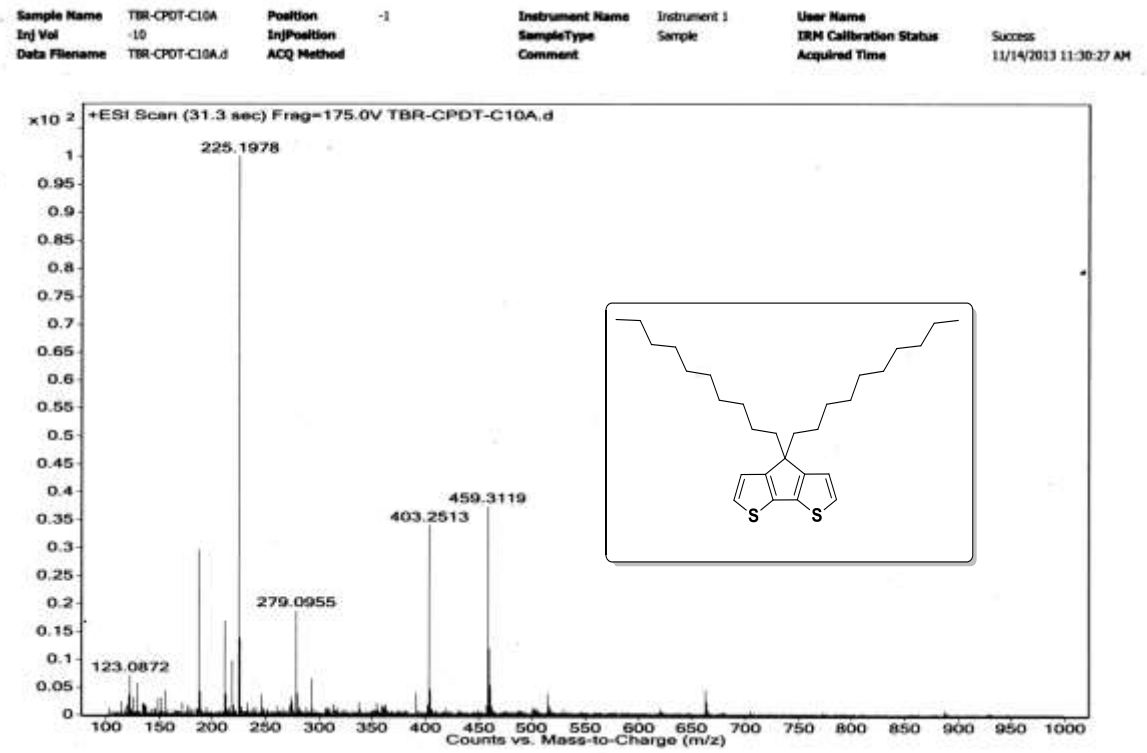

ESI-MS spectrum of 4,4'-Bisdecyl-4*H*-cyclopenta[2,1-b:3,4-b']dithiophene (entry 1c).

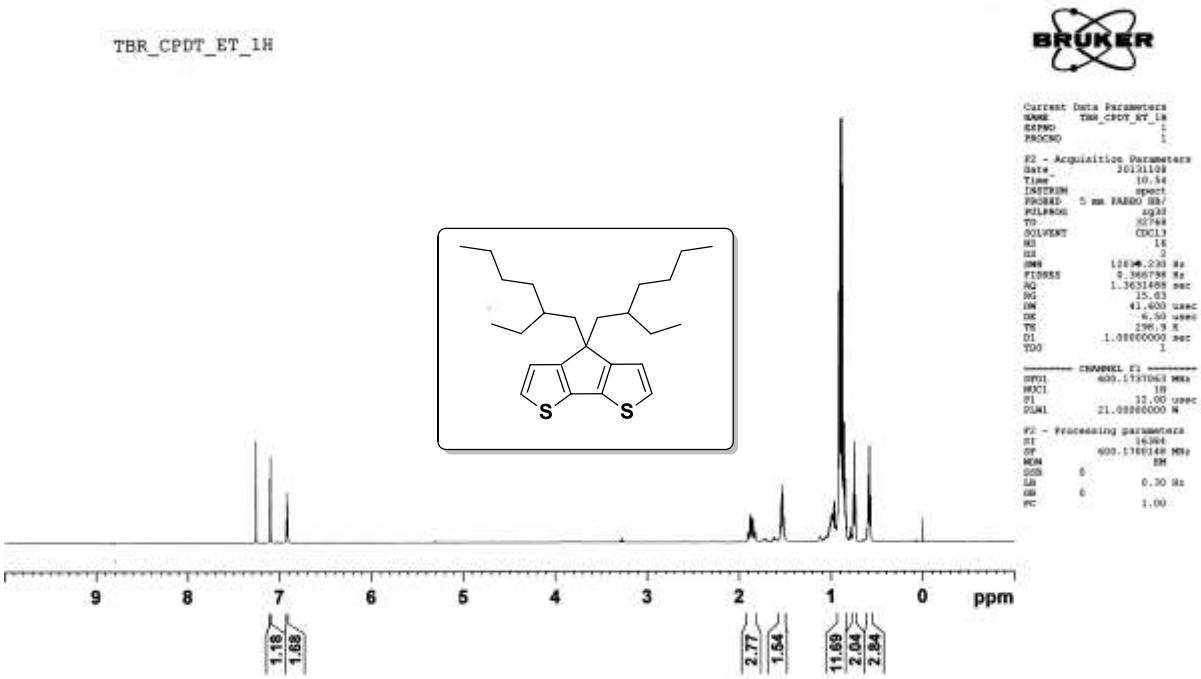

^{1}H-NMR spectrum of 4,4'-Bis(2-ethylhexyl)-4*H*-cyclopenta[2,1-b:3,4-b']dithiophene (entry 1d).

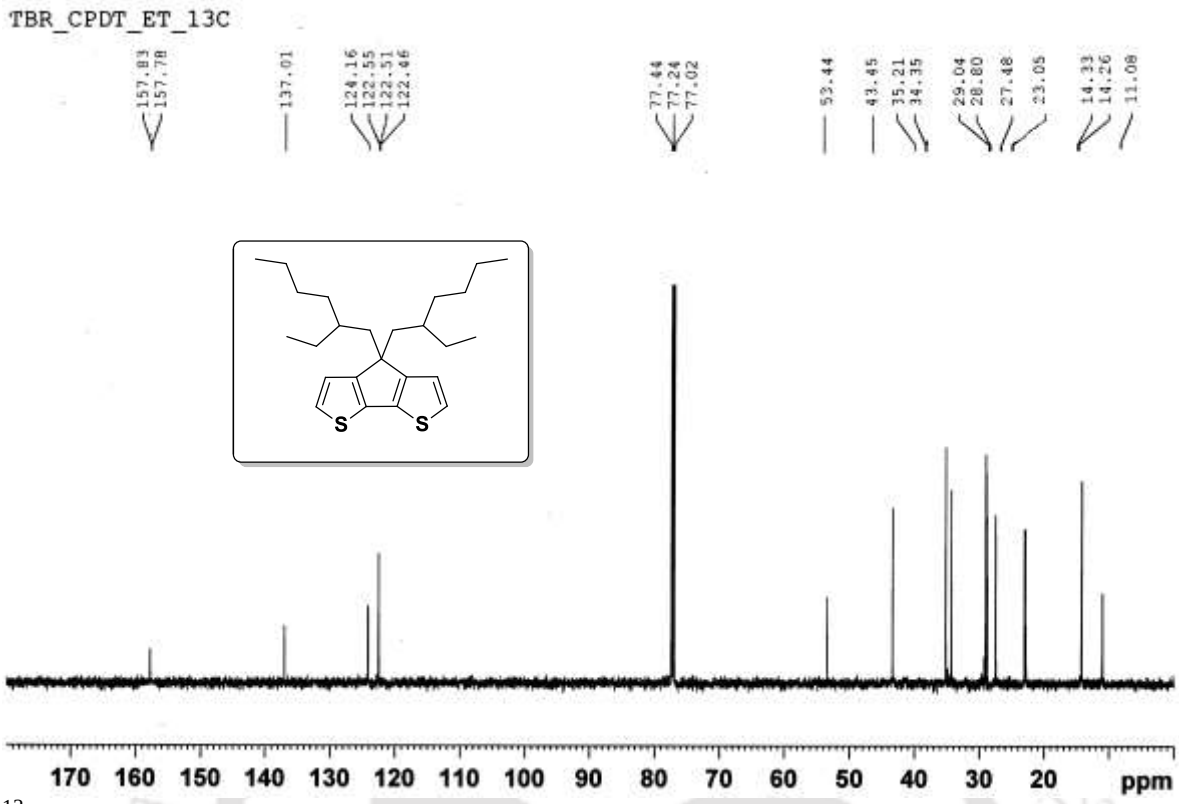

^{13}C NMR spectrum of 4,4'-Bis(2-ethylhexyl)-4*H*-cyclopenta[2,1-b:3,4-b']dithiophene (entry 1d).

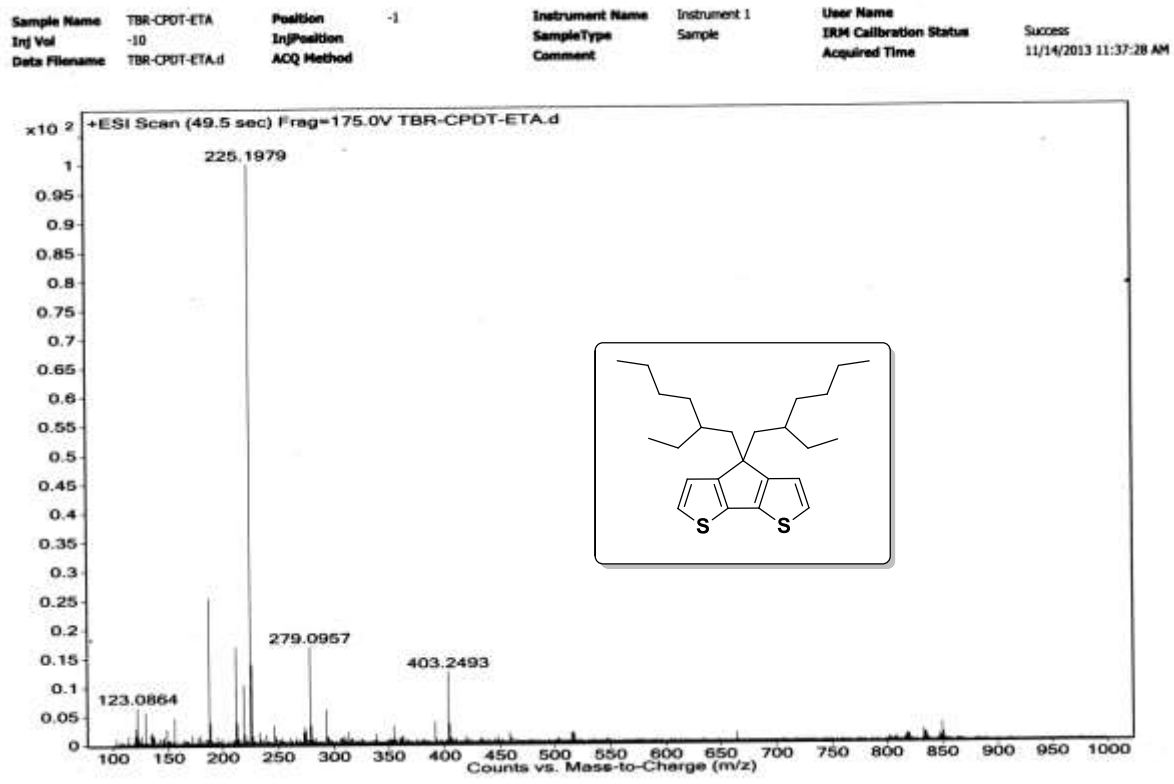

ESI-MS spectrum of 4,4'-Bis(2-ethylhexyl)-4*H*-cyclopenta[2,1-b:3,4-b']dithiophene (entry 1d).

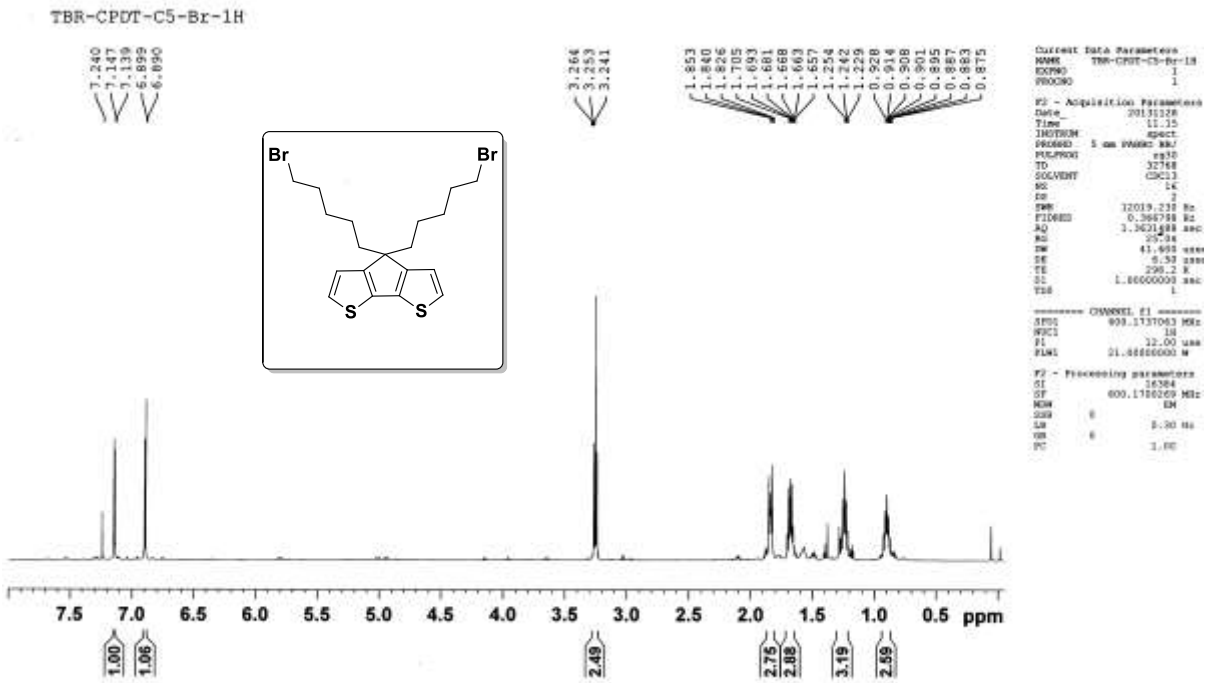

^{1}H-NMR spectrum of 4,4'-Bis-(5-bromopentyl)-4*H*-cyclopenta[2,1-b:3,4-b']dithiophene (entry 1e).

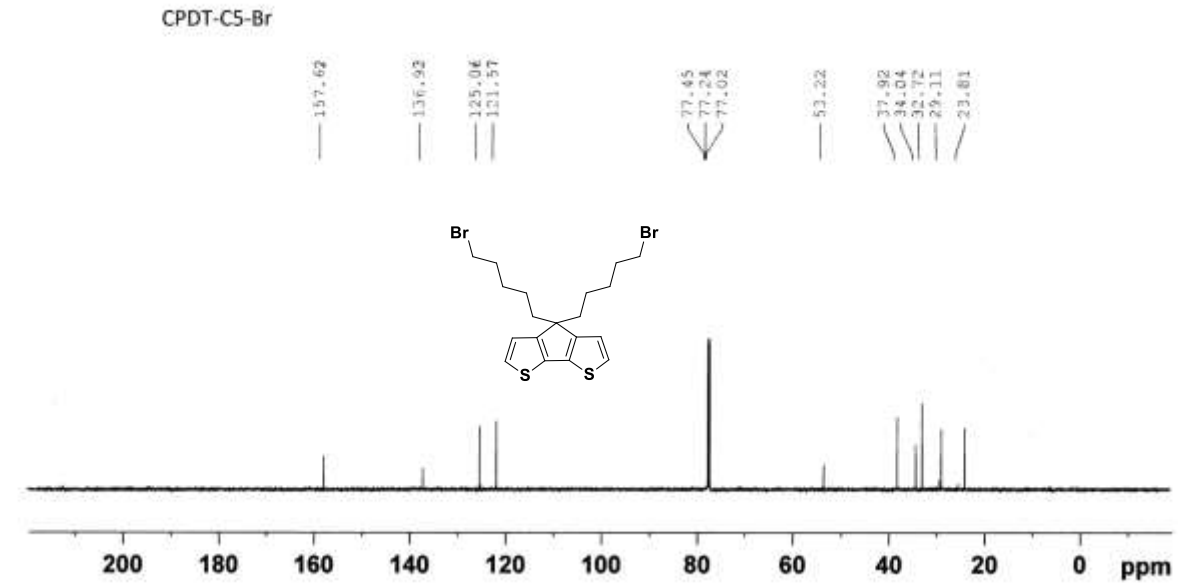

^{13}C NMR spectrum of 4,4'-Bis-(5-bromopentyl)-4*H*-cyclopenta[2,1-b:3,4-b']dithiophene (entry 1e).

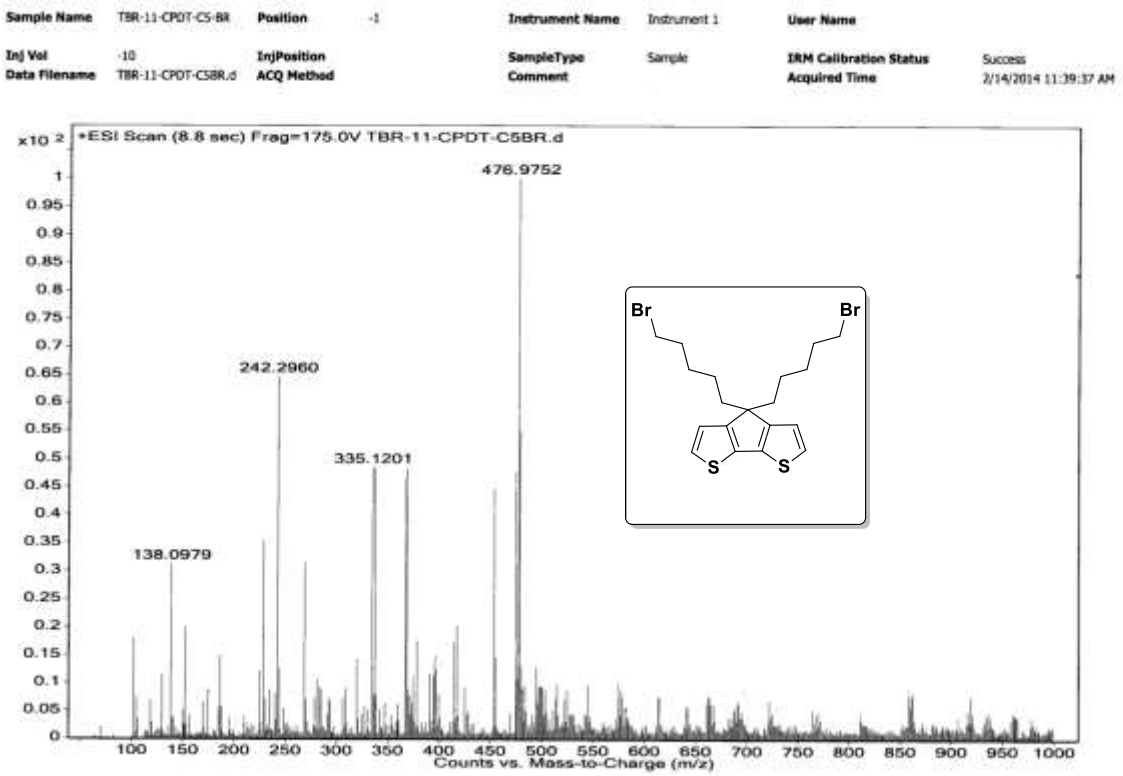

ESI-MS spectrum of 4,4'-Bis-(5-bromopentyl)-4*H*-cyclopenta[2,1-b:3,4-b']dithiophene (entry 1e).

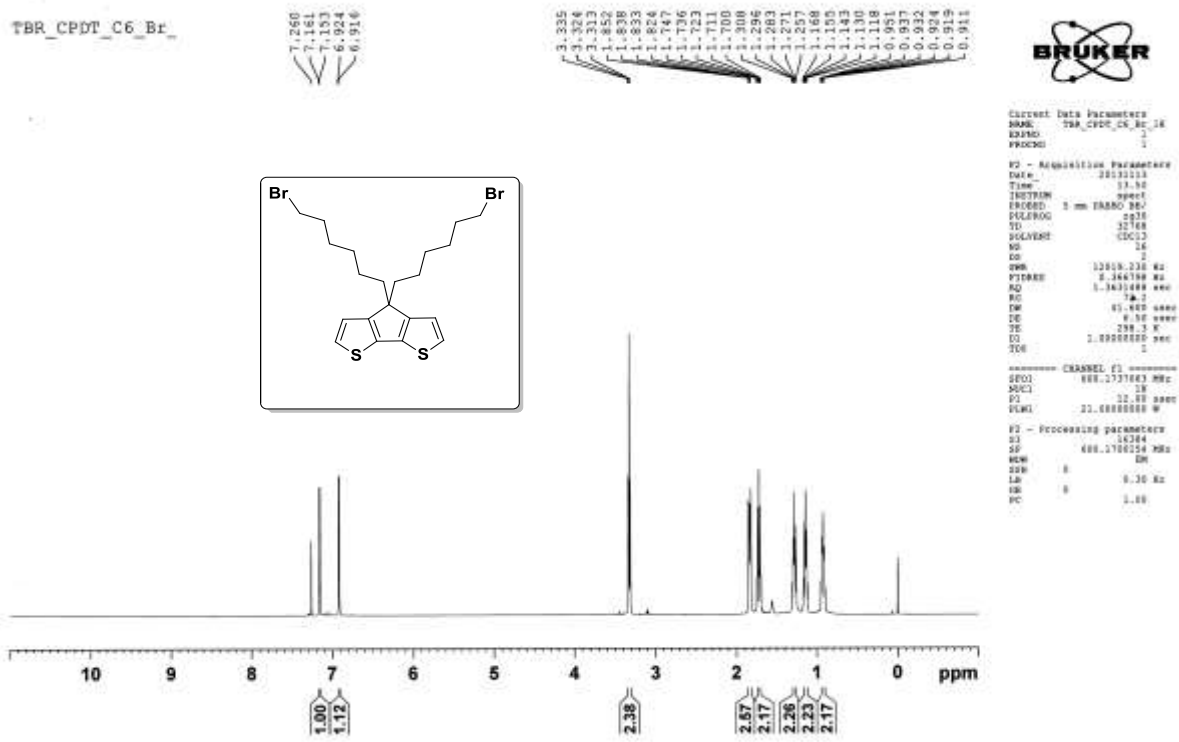

^{1}H NMR spectrum of 4,4'-Bis-(6-bromohexyl)-4*H*-cyclopenta[2,1-b:3,4-b']dithiophene (entry 1f).

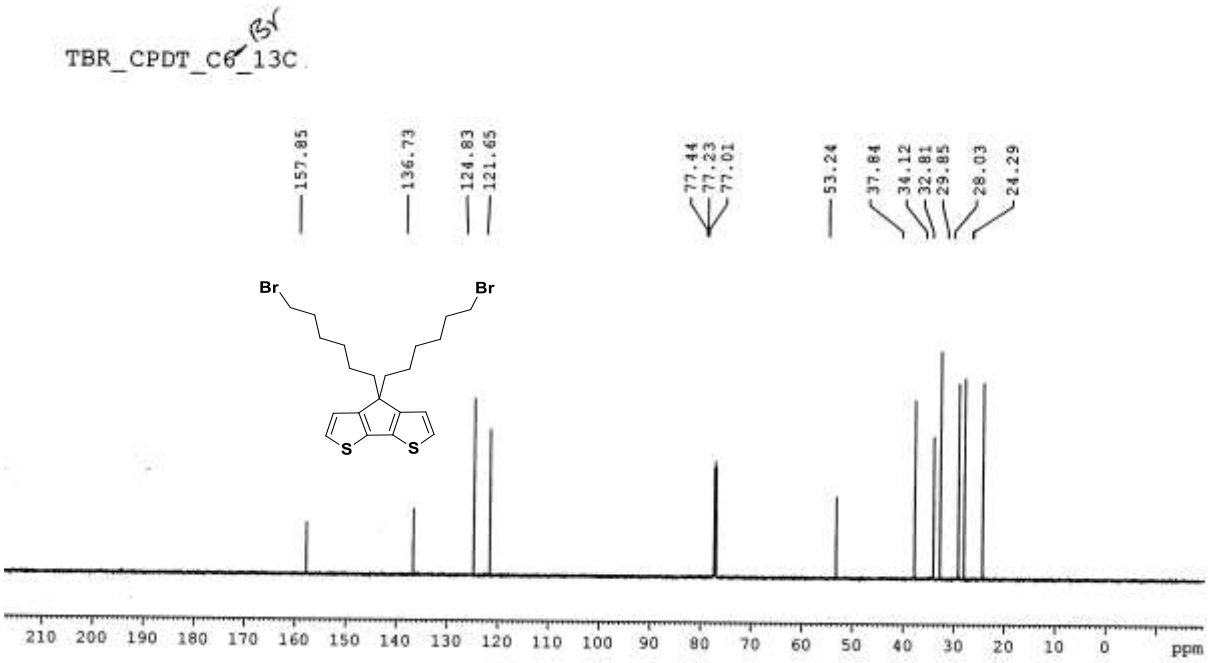

^{13}C NMR spectrum of 4,4'-Bis-(6-bromohexyl)-4*H*-cyclopenta[2,1-b:3,4-b']dithiophene (entry 1f).

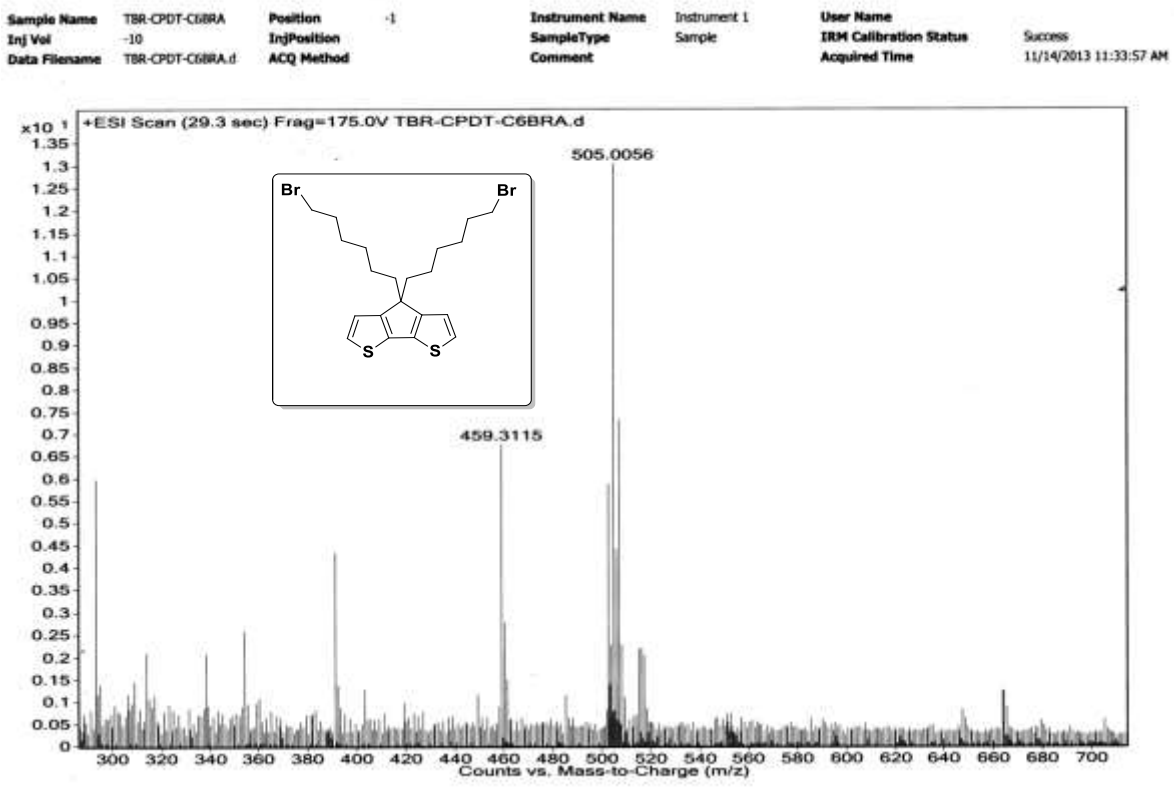

ESI-MS spectrum of 4,4'-Bis-(6-bromohexyl)-4*H*-cyclopenta[2,1-b:3,4-b']dithiophene (entry 1f).

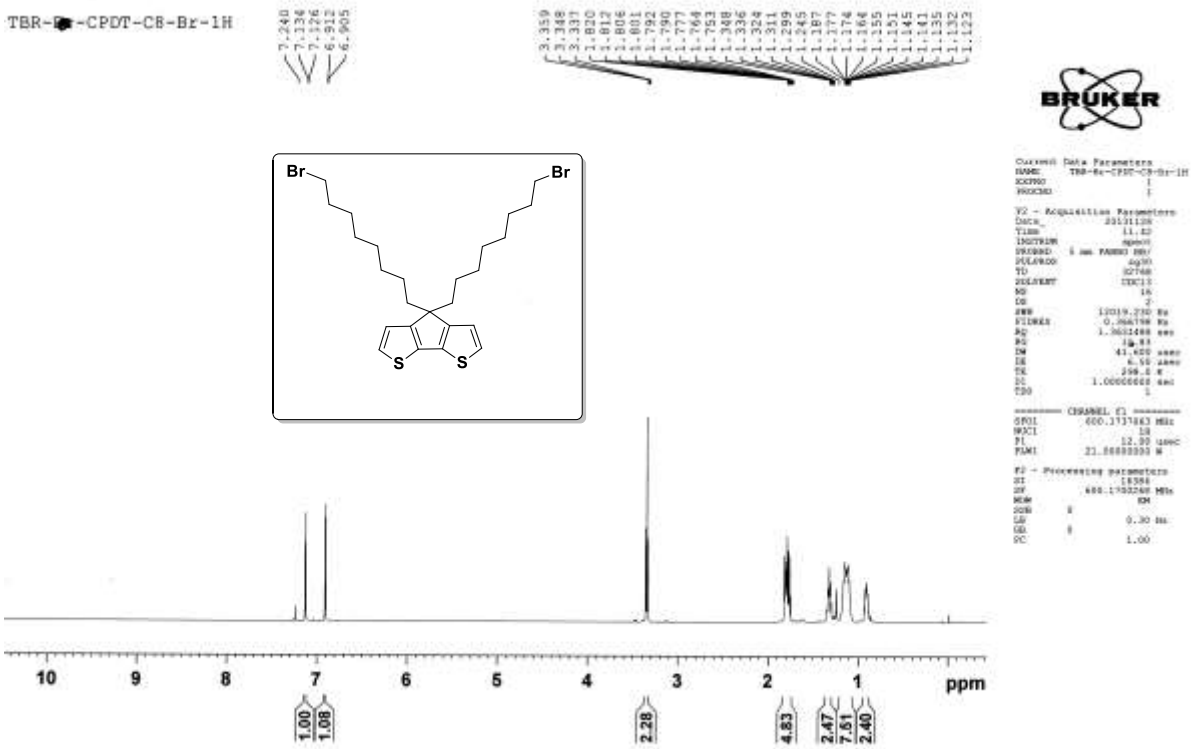

^{1}H NMR spectrum of 4,4'-Bis-(8-bromoctyl)-4*H*-cyclopenta[2,1-b:3,4-b']dithiophene (entry 1g).

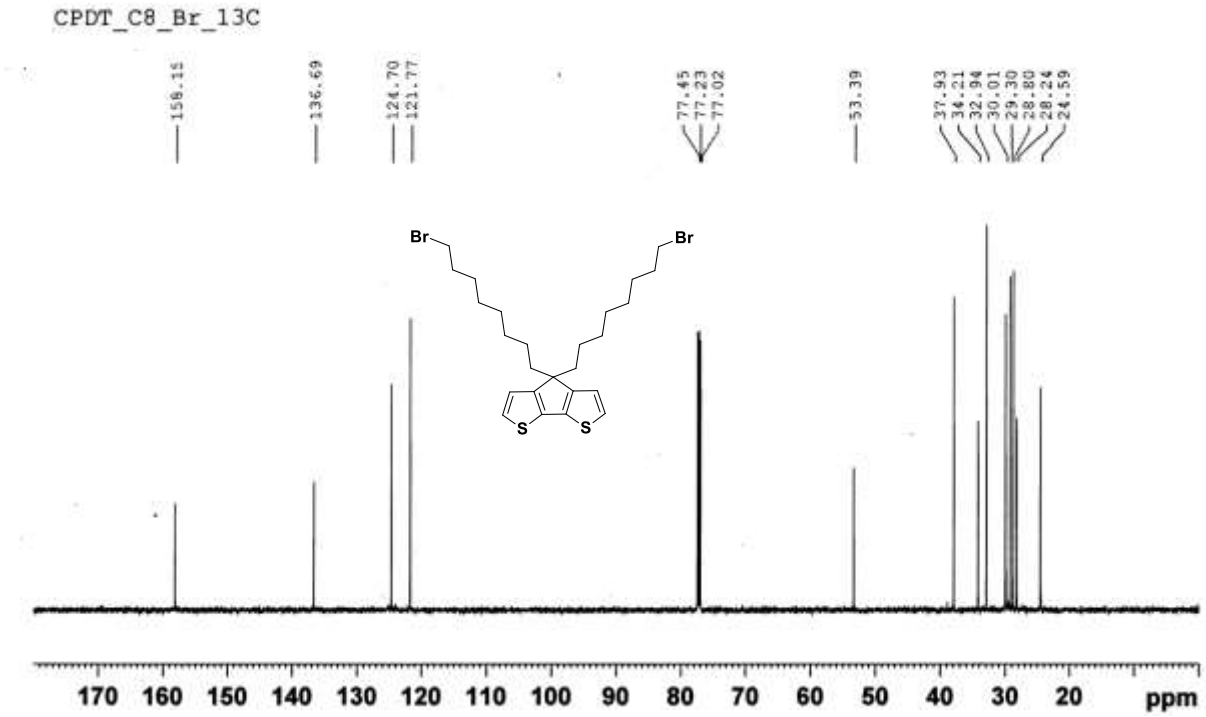

^{13}C NMR spectrum of 4,4'-Bis-(8-bromoctyl)-4*H*-cyclopenta[2,1-b:3,4-b']dithiophene (entry 1g).

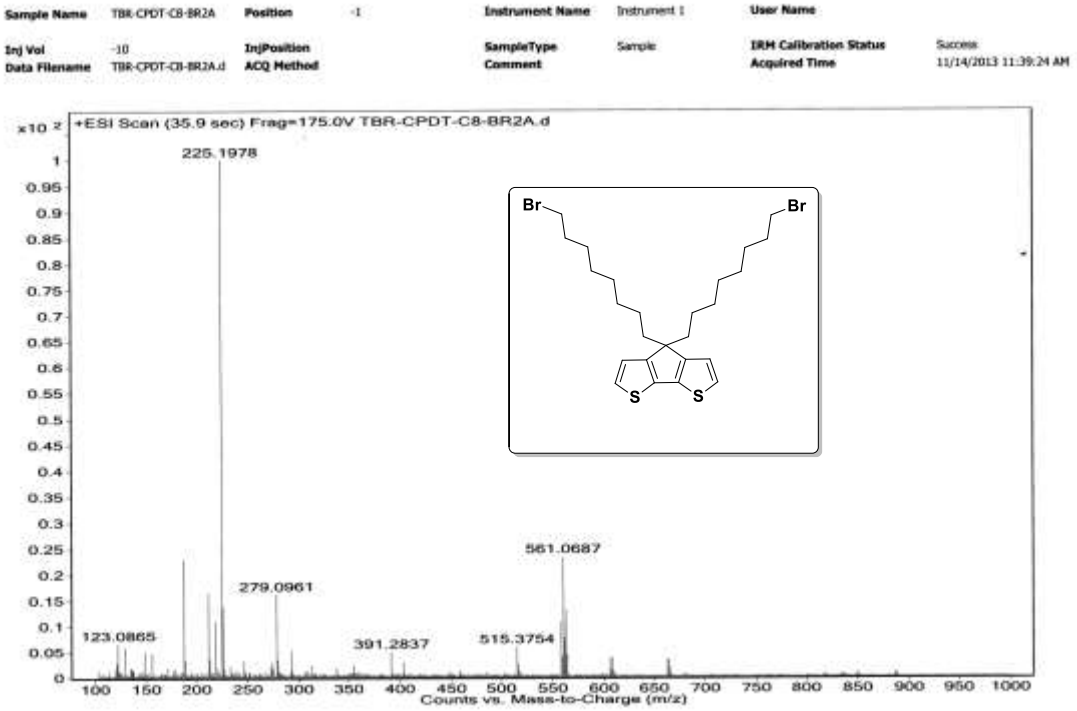

ESI-MS Spectrum of 4,4'-Bis-(8-bromoctyl)-4*H*-cyclopenta[2,1-b:3,4-b']dithiophene (entry 1g).

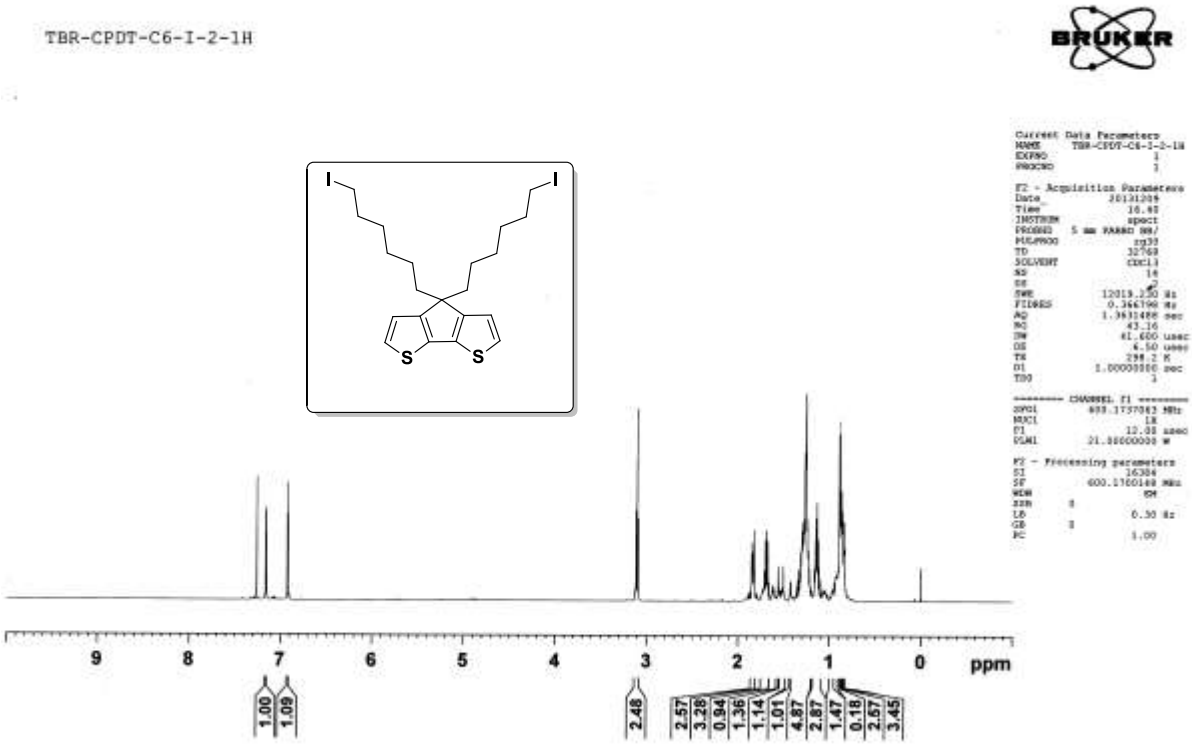

^{1}H NMR spectrum of 4,4'-Bis-(6-iodohexyl)-4*H*-cyclopenta[2,1-b:3,4-b']dithiophene (entry 1h).

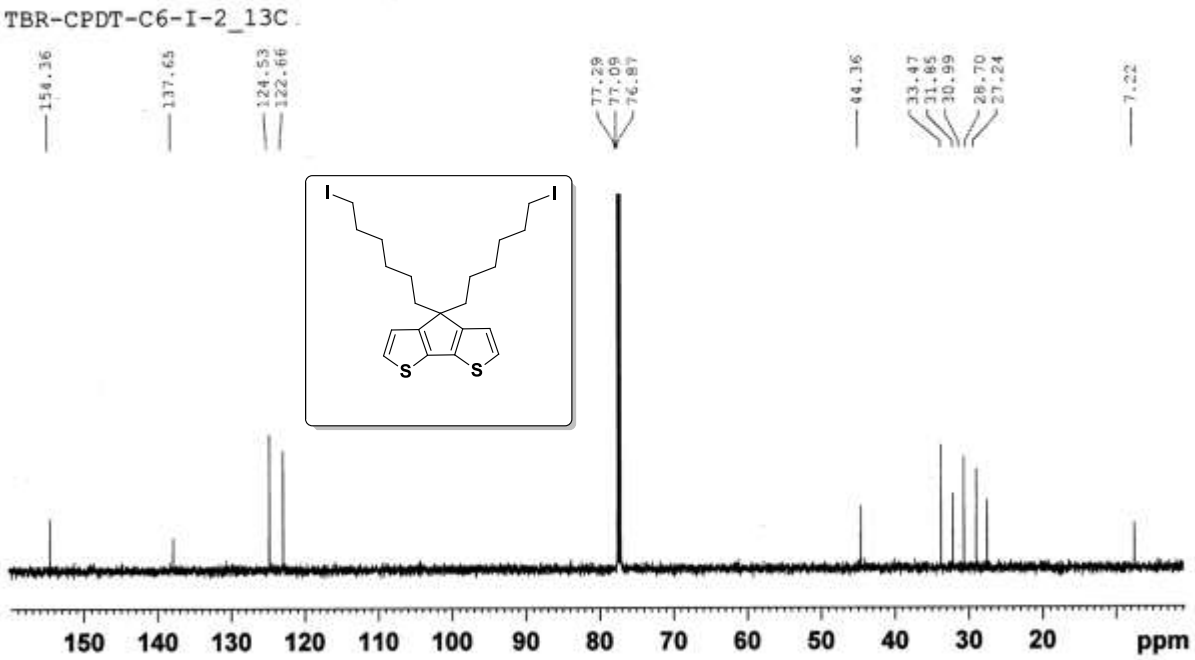

^{13}C NMR spectrum of 4,4'-Bis-(6-iodohexyl)-4*H*-cyclopenta[2,1-b:3,4-b']dithiophene (entry 1h).

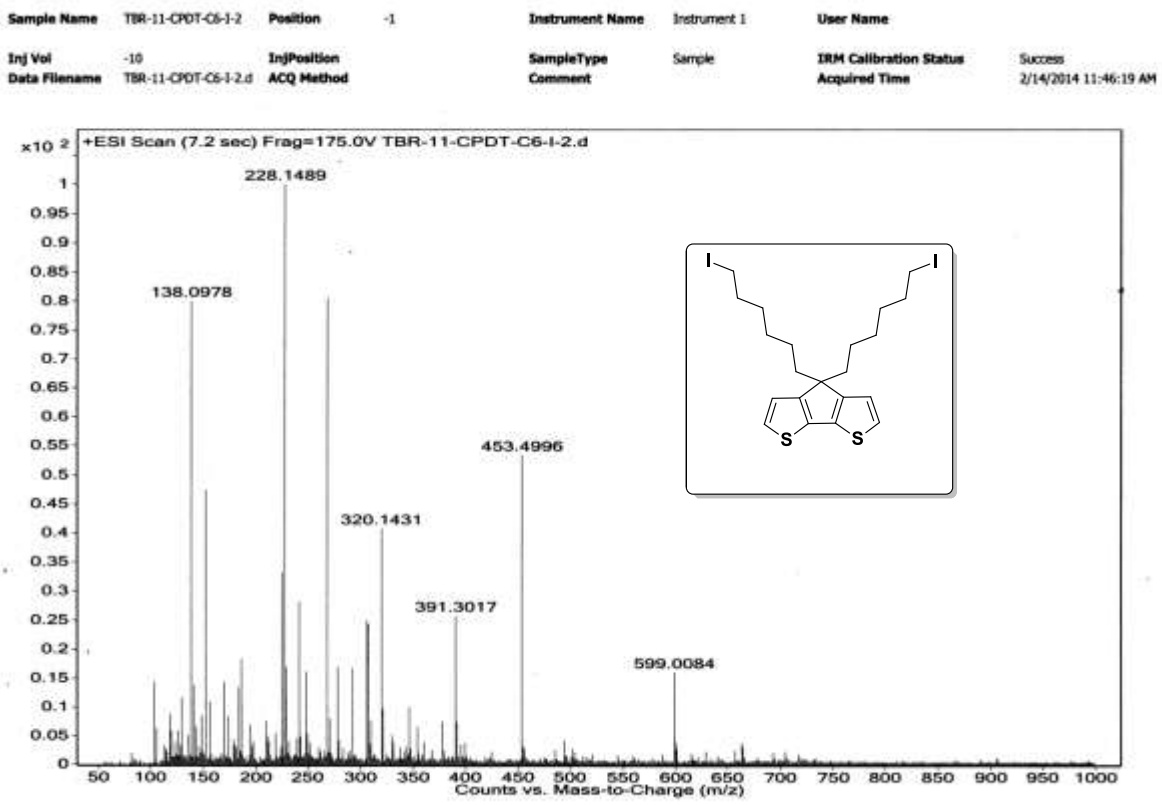

ESI-MS spectrum of spectrum of 4,4'-Bis-(6-iodohexyl)-4*H*-cyclopenta [2,1-b:3,4-b']dithiophene (entry 1h).

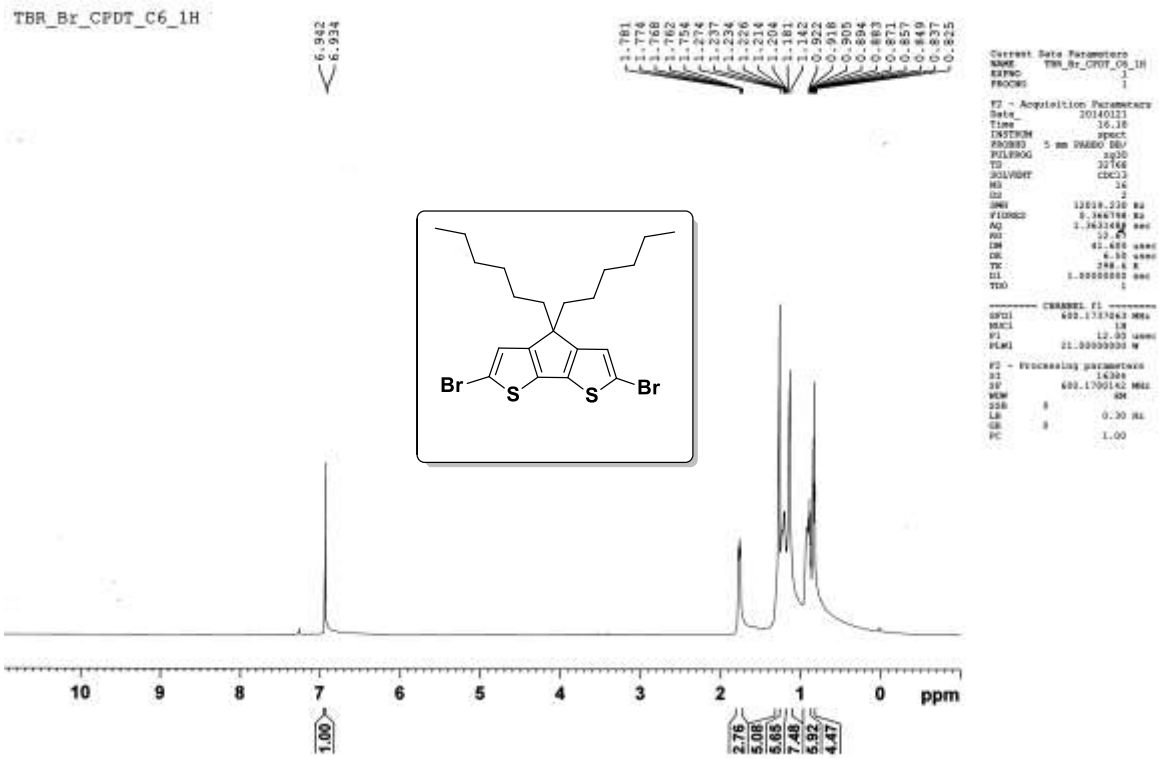

^{1}H NMR spectrum of 2,6-Dibromo-4,4'-dihexyl-4*H*-cyclopenta[2,1-b:3,4-b']dithiophene (entry 1k).

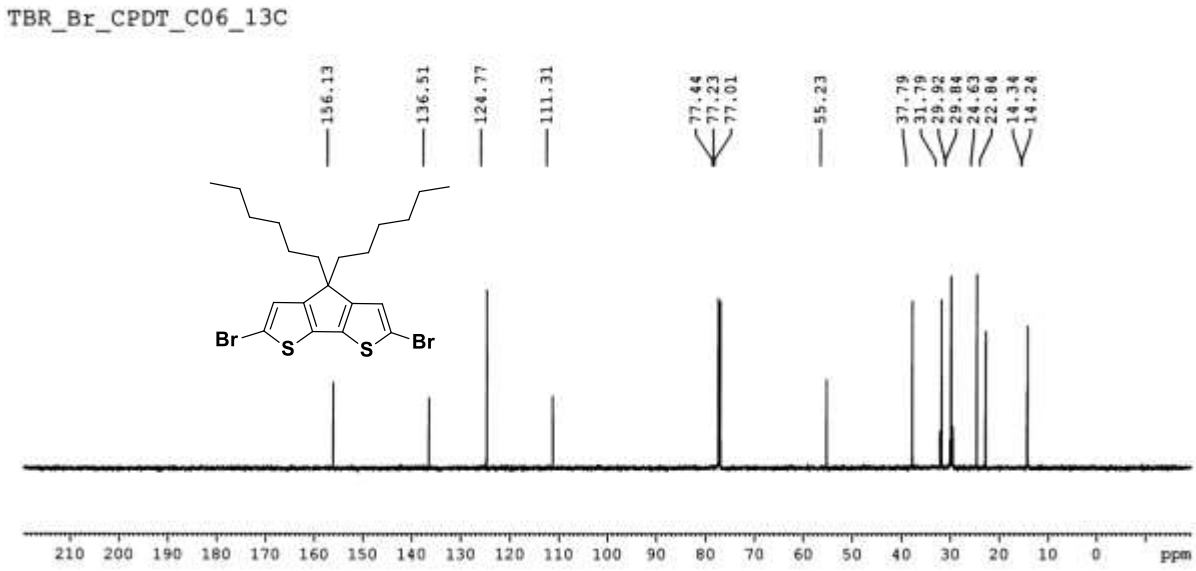

^{13}C NMR spectrum of 2,6-Dibromo-4,4'-dihexyl-4*H*-cyclopenta[2,1-b:3,4-b']dithiophene (entry 1k).

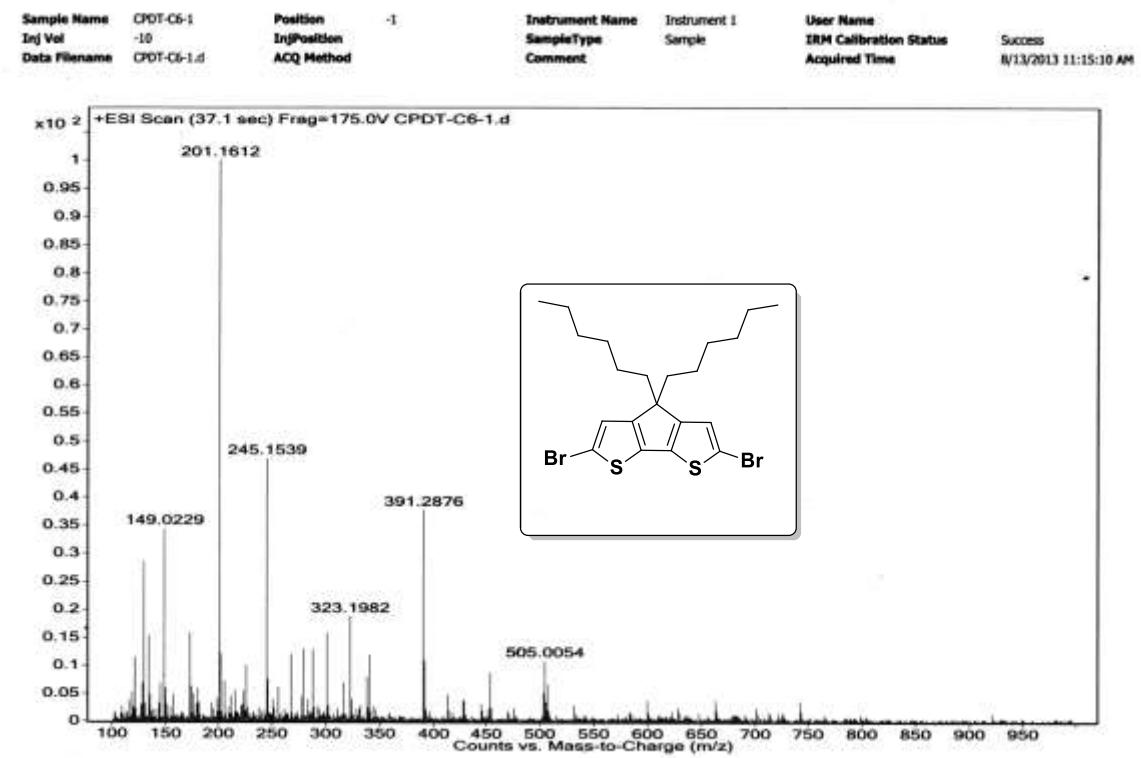

ESI-MS spectrum of 2,6-Dibromo-4,4'-dihexyl-4*H*-cyclopenta[2,1-b:3,4-b']dithiophene (entry 1k).

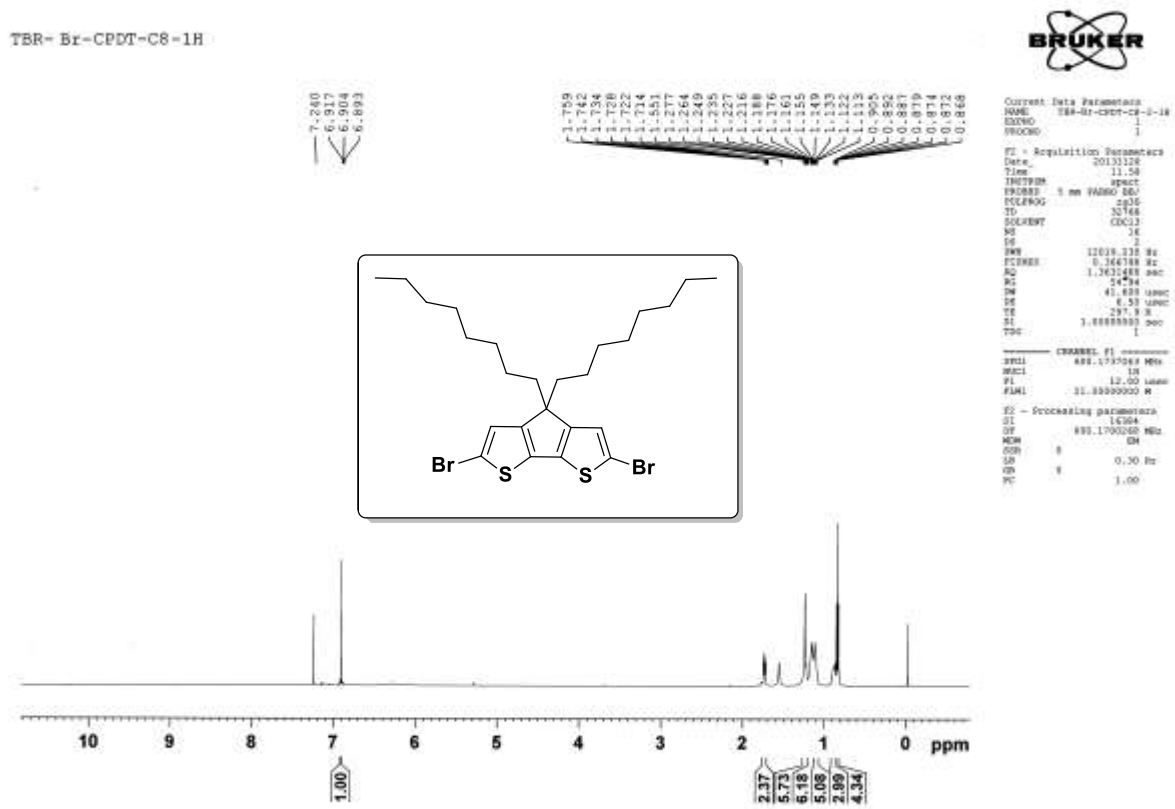

^{1}H NMR spectrum of 2,6-Dibromo-4,4'-dioctyl-4*H*-cyclopenta[2,1-b:3,4-b']dithiophene (entry 1l).

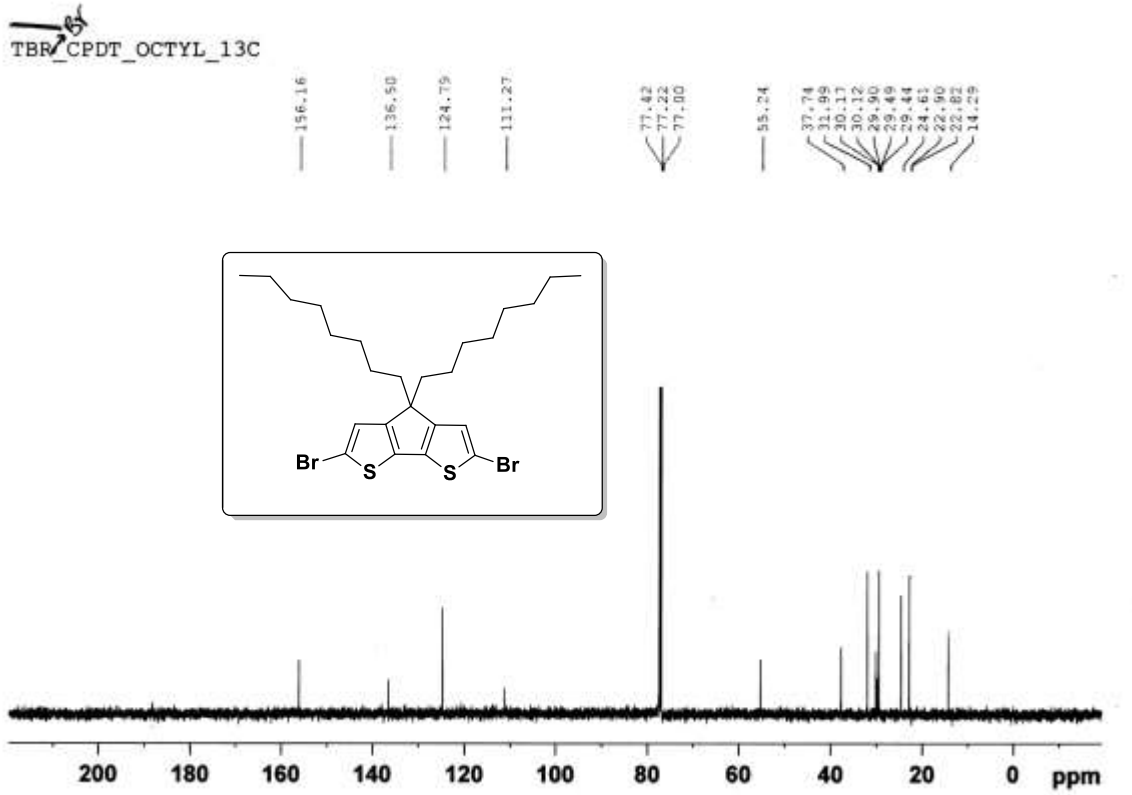

^{13}C NMR spectrum of 2,6-Dibromo-4,4'-dioctyl-4*H*-cyclopenta[2,1-b:3,4-b']dithiophene (entry 1l).

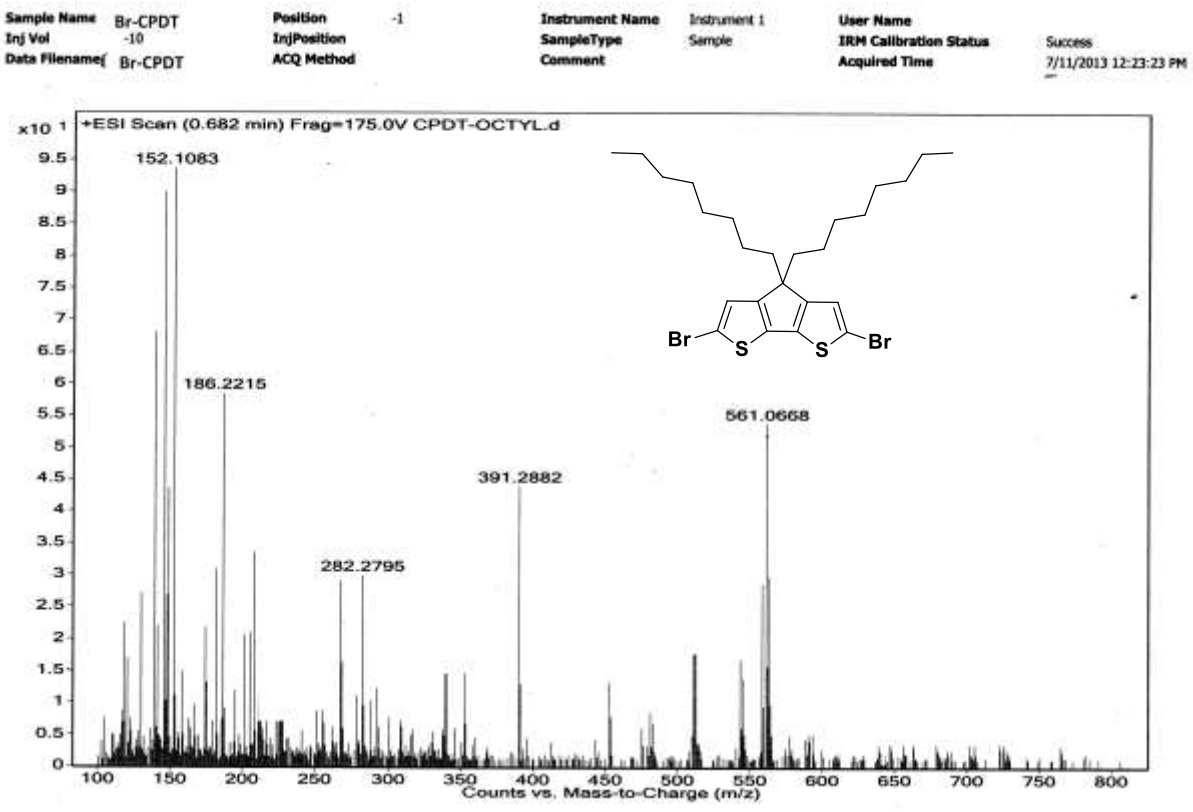

ESI-MS spectrum of 2,6-Dibromo-4,4'-dioctyl-4*H*-cyclopenta[2,1-b:3,4-b']dithiophene (entry 1l).

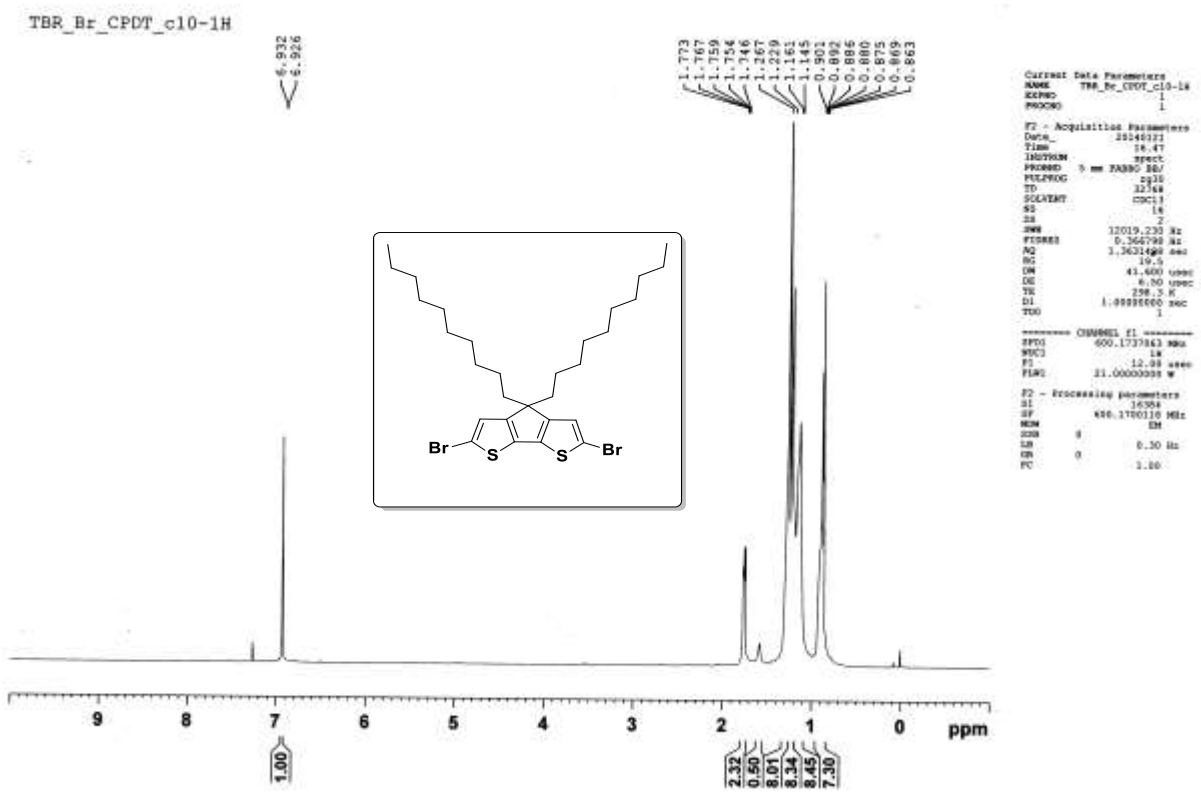

^{1}H NMR spectrum of 2,6-Dibromo-4,4'-didecyl-4*H*-cyclopenta[2,1-b:3,4-b']dithiophene (entry 1m).

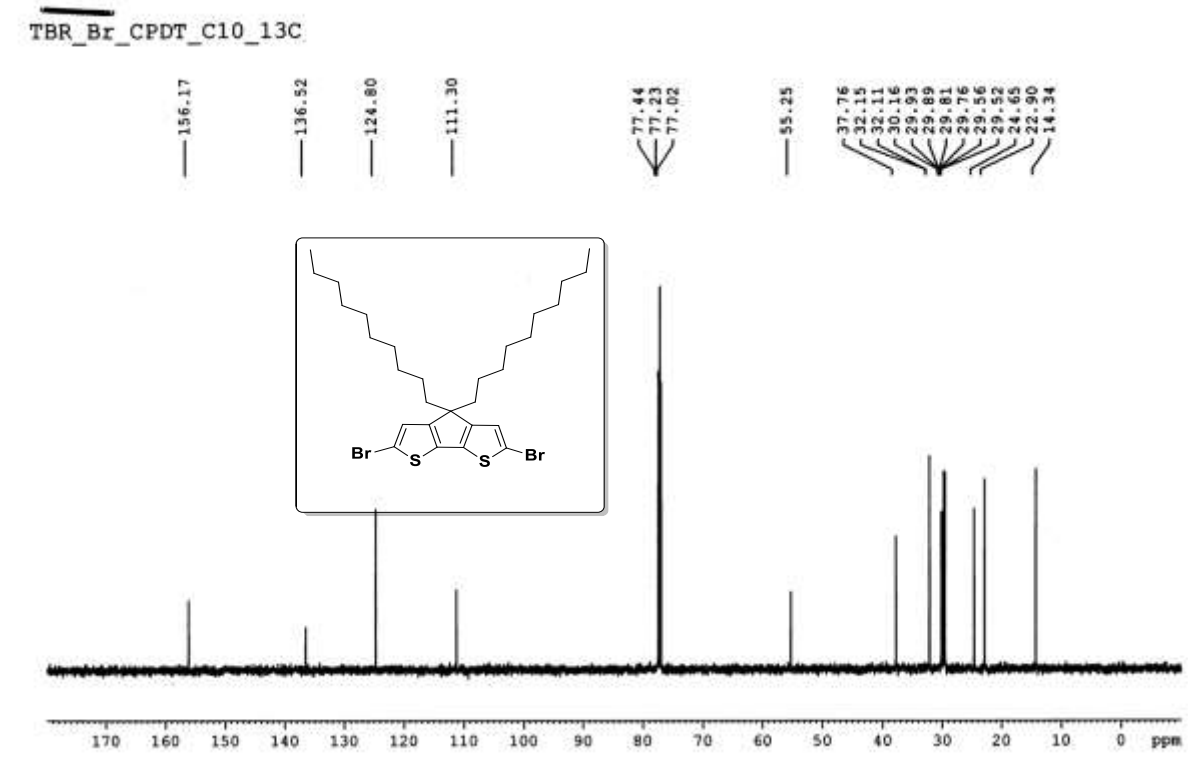

^{13}C NMR 2,6-Dibromo-4,4'-bisdecyl-4*H*-cyclopenta[2,1-b:3,4-b']dithiophene (entry 1m).

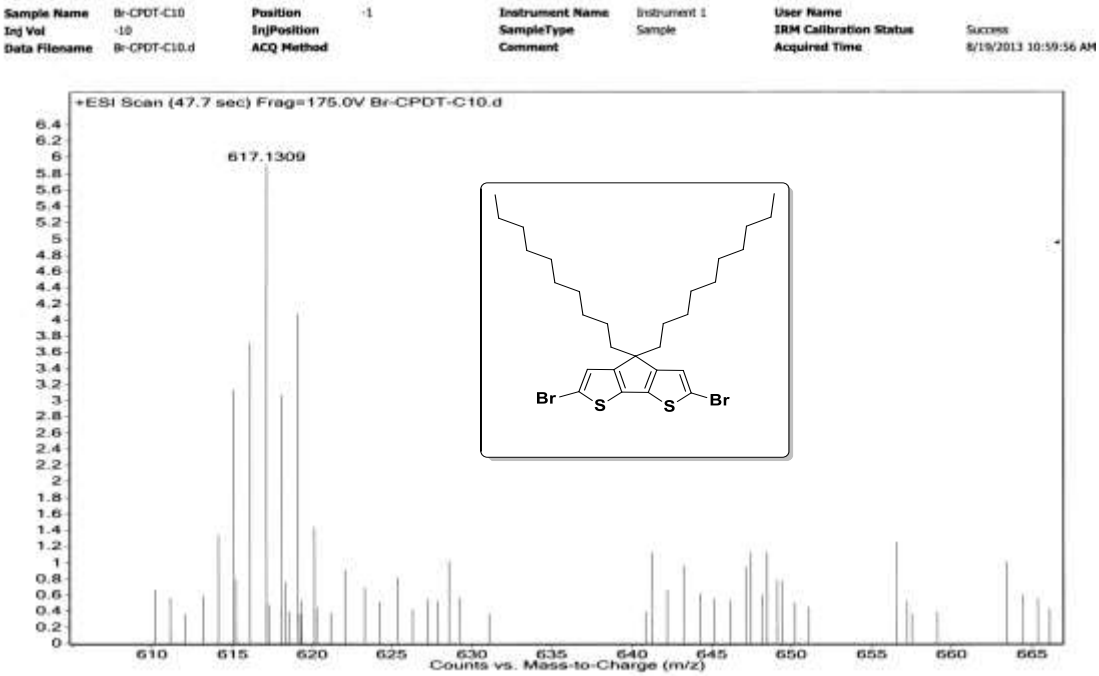

ESI-MS spectrum of 2,6-Dibromo-4,4'-bisdecyl-4*H*-cyclopenta[2,1-b:3,4-b']dithiophene (entry 1m).

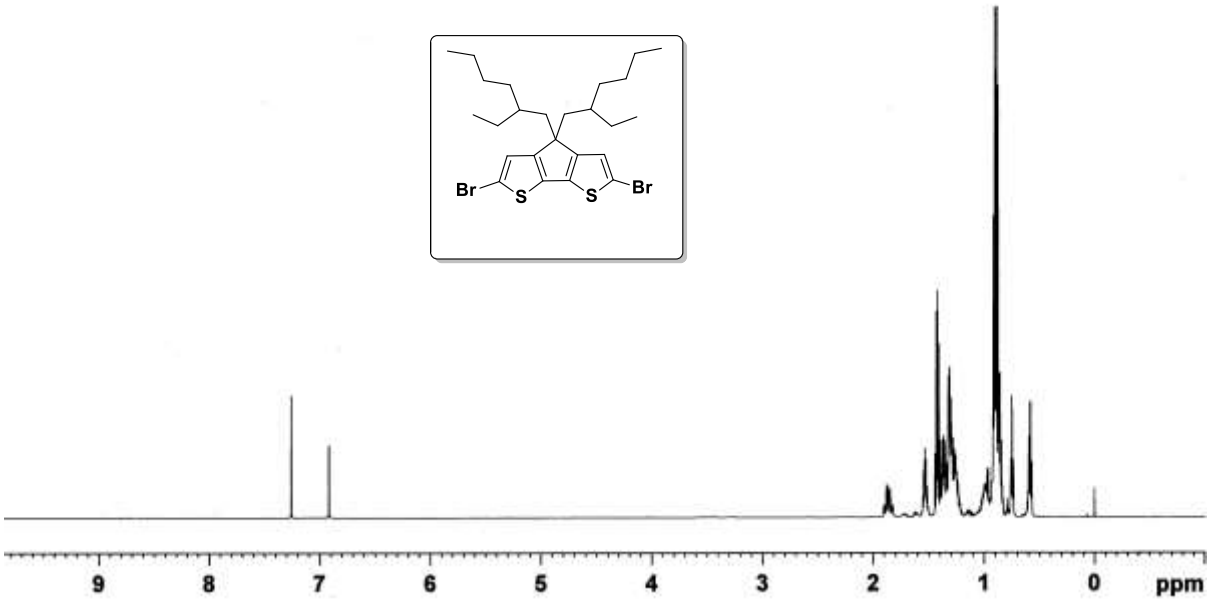

^{1}H NMR spectrum of 2,6-Dibromo-4,4'-bis(2-ethylhexyl)-4*H*-cyclopenta[2,1-b:3,4-b']dithiophene (entry 1n).

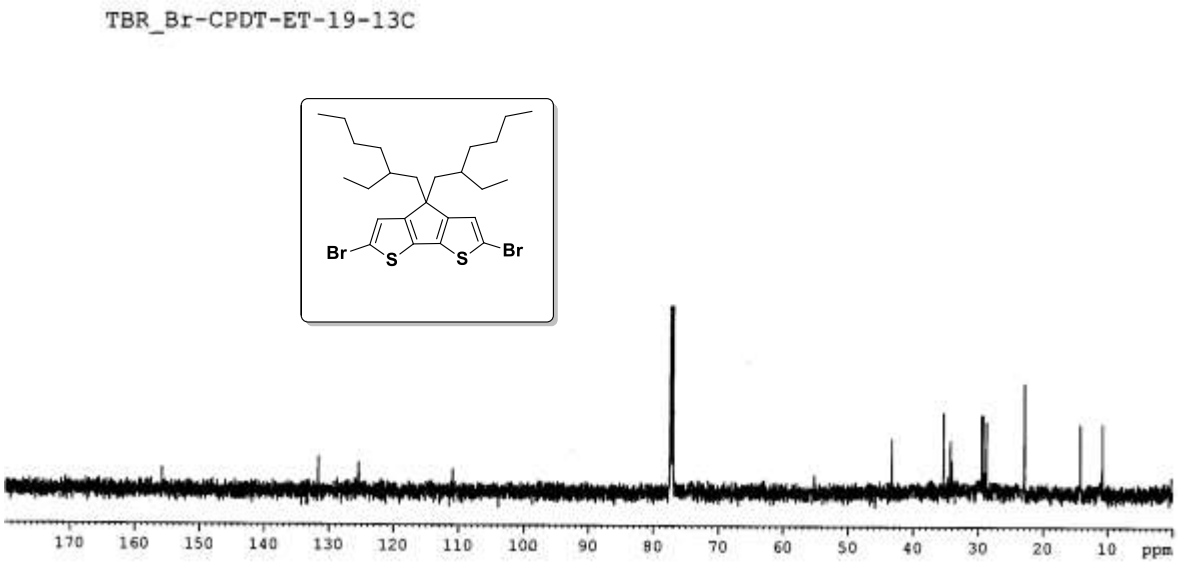

^{13}C NMR spectrum of 2,6-Dibromo-4,4'-bis(2-ethylhexyl)-4*H*-cyclopenta[2,1-b:3,4-b']dithiophene (entry 1n).

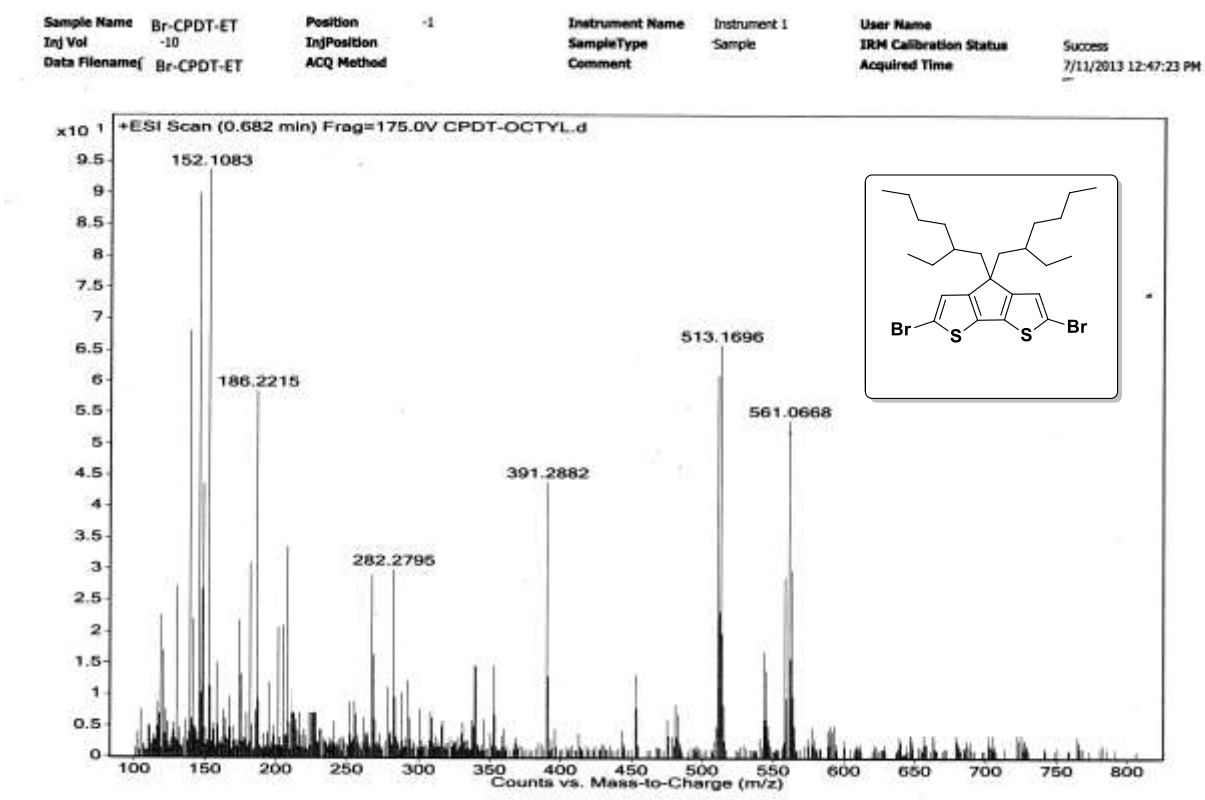

ESI-MS spectrum of 2,6-Dibromo-4,4'-bis(2-ethylhexyl)-4*H*-cyclopenta[2,1-b:3,4-b']dithiophene (entry 1n).

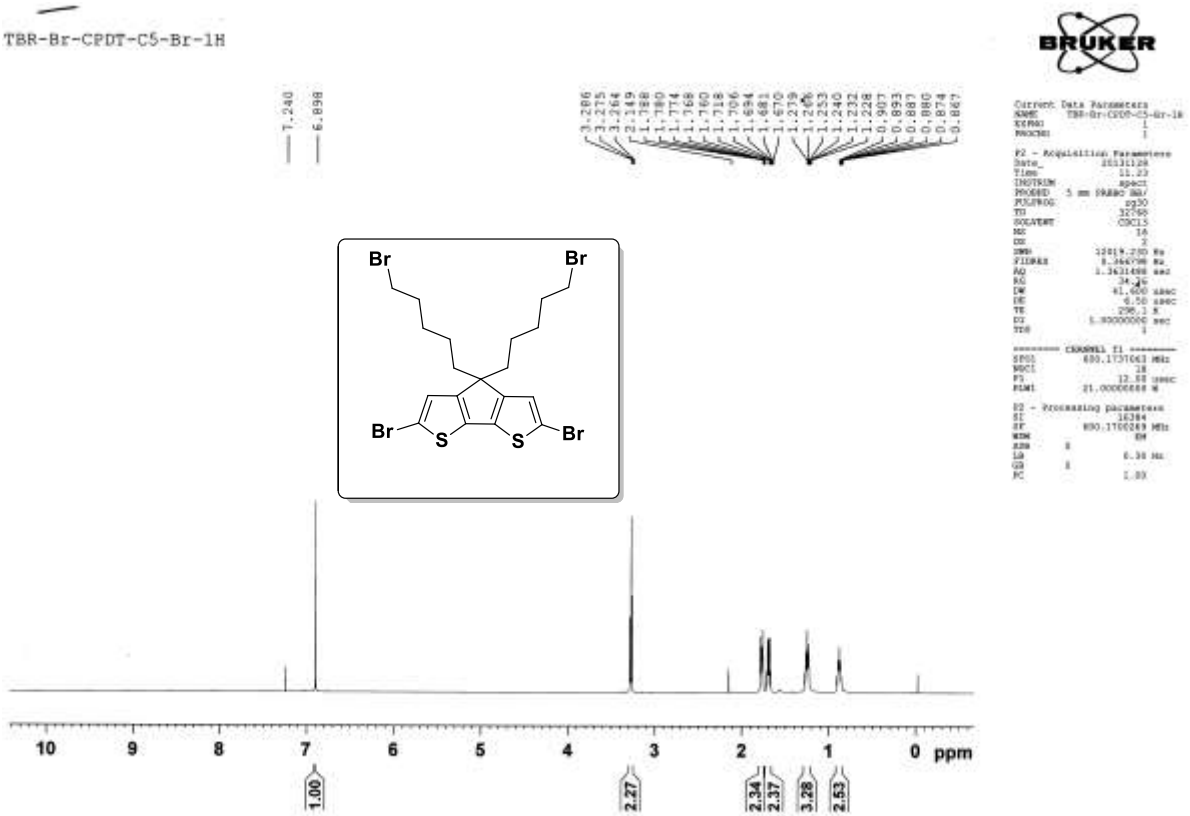

^{1}H NMR spectrum of 2,6-Dibromo-4,4'-bis(5-bromopentyl)-4*H*-cyclopenta[2,1-b:3,4-b']dithiophene (entry 1o).

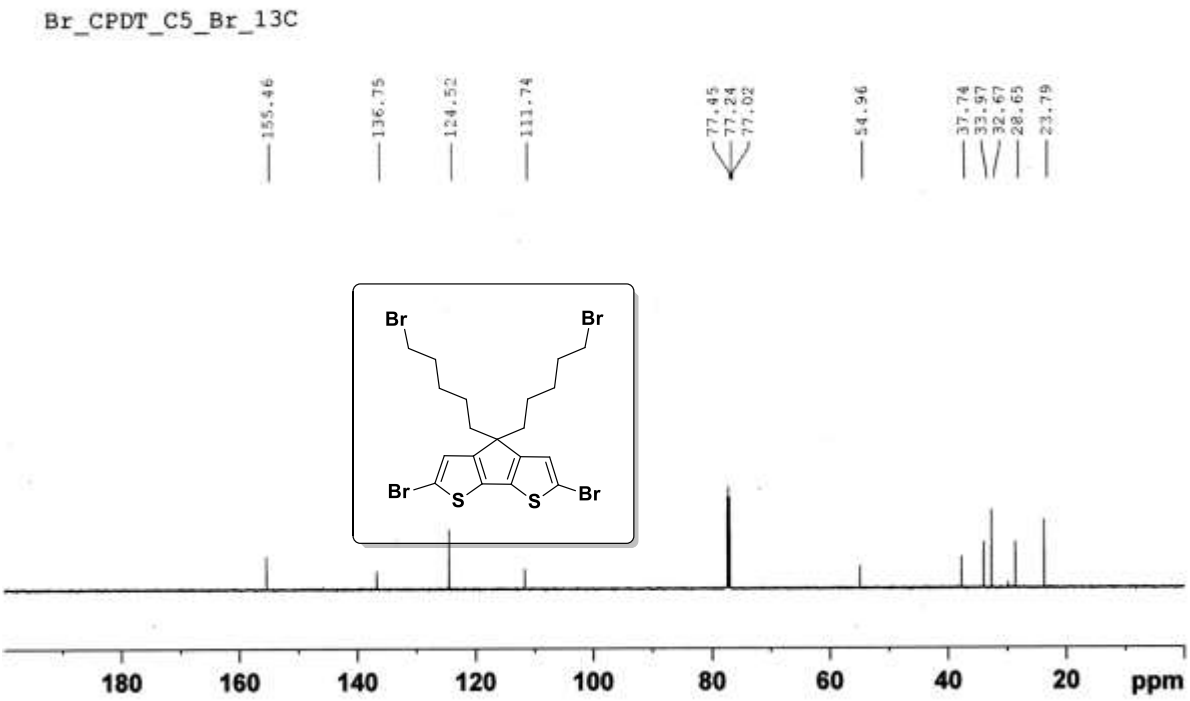

^{13}C NMR spectrum of 2,6-Dibromo-4,4'-bis(5-bromopentyl)-4*H*-cyclopenta[2,1-b:3,4-b']dithiophene (entry 1o).

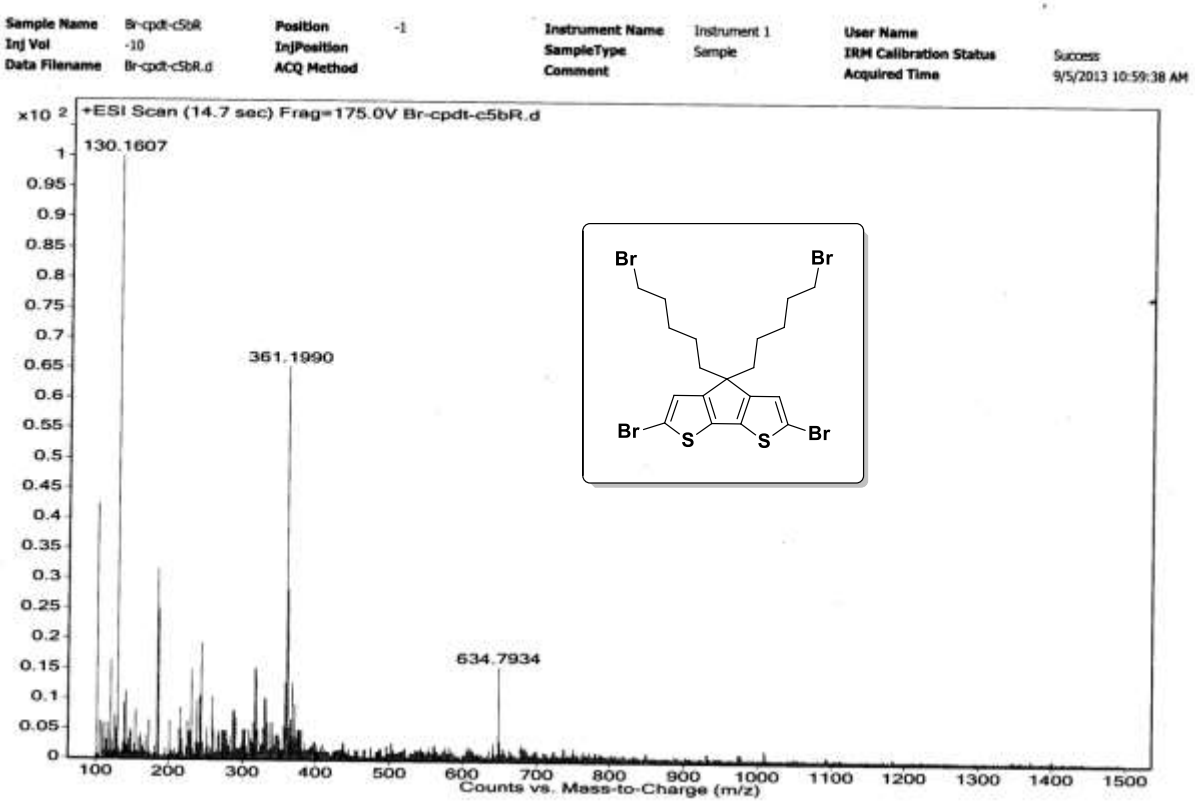

ESI-MS Spectrum of spectrum of 2,6-Dibromo-4,4'-bis(5-bromopentyl)-4*H*-cyclopenta[2,1-b:3,4-b']dithiophene (entry 1o).

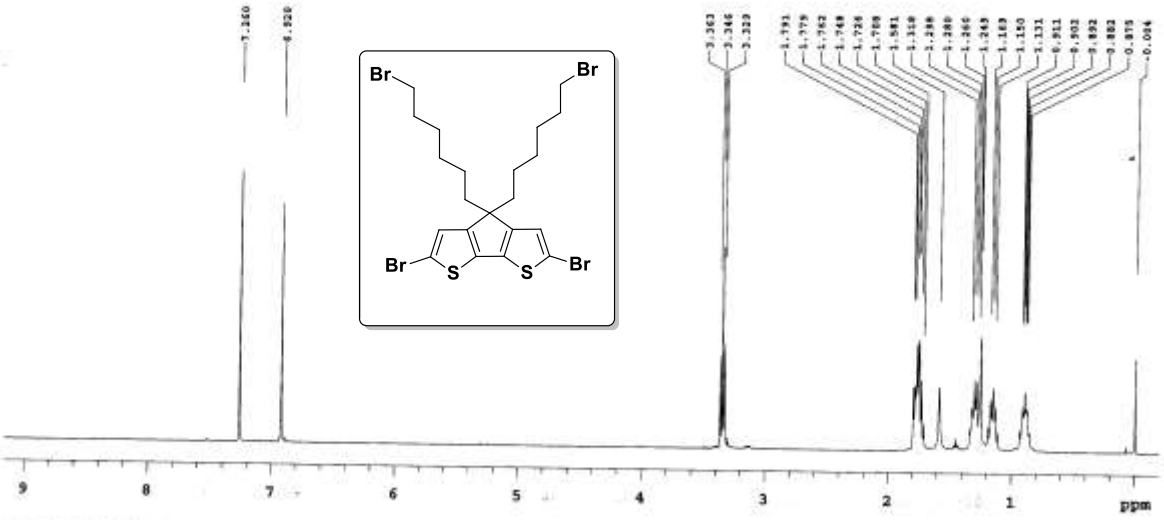

^{1}H NMR spectrum of 2,6-Dibromo-4,4'-bis(6-bromohexyl)-4*H*-cyclopenta[2,1-b:3,4-b']dithiophene (entry 1p).

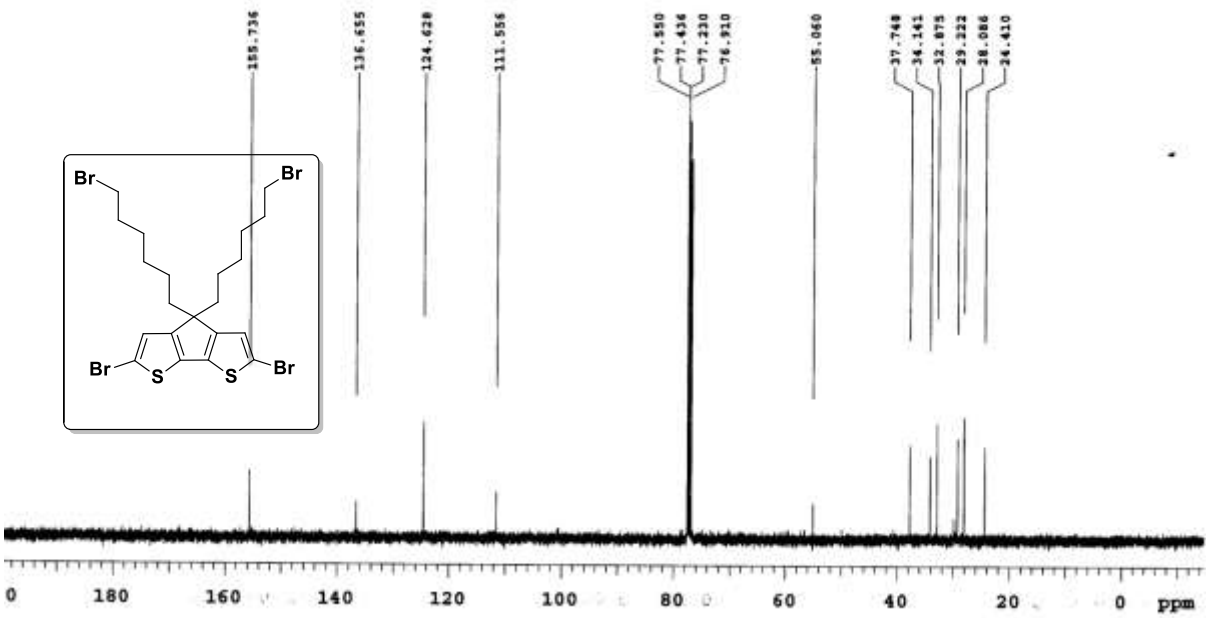

^{13}C NMR spectrum of 2,6-Dibromo-4,4'-bis(6-bromohexyl)-4*H*-cyclopenta[2,1-b:3,4-b']dithiophene (entry 1p).

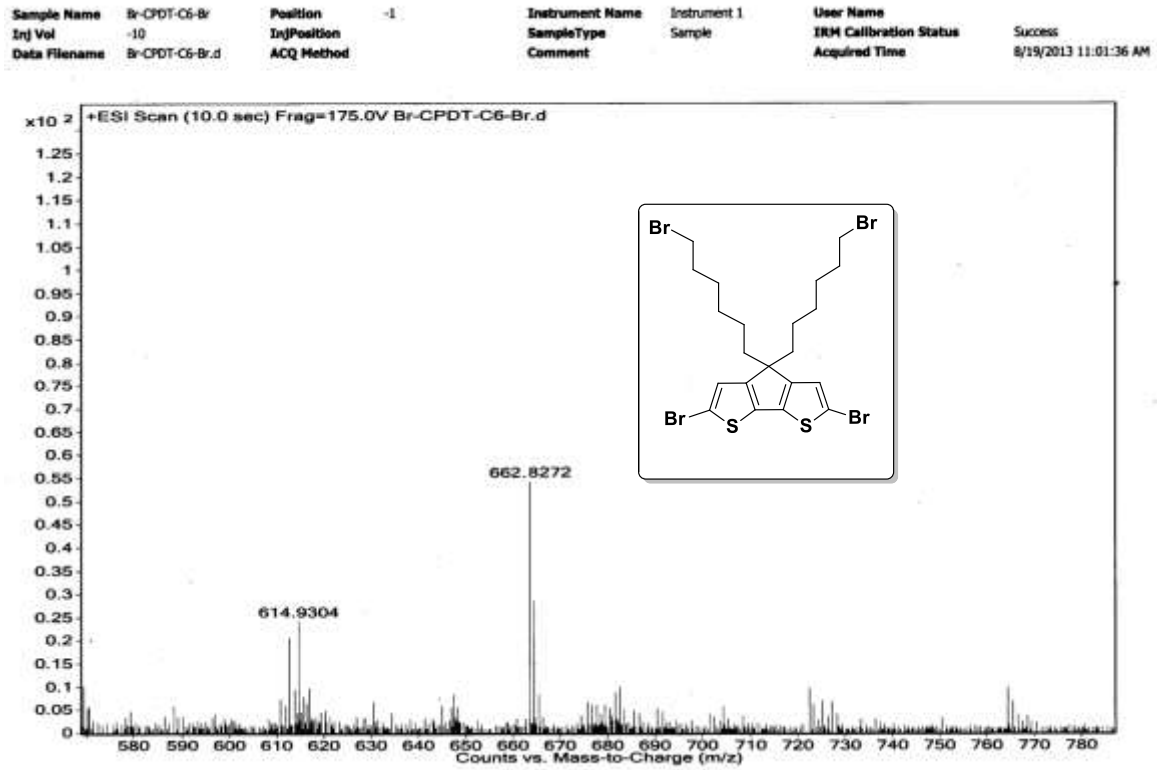

ESI-MS spectrum of 2,6-Dibromo-4,4'-bis(6-bromohexyl)-4*H*-cyclopenta[2,1-b:3,4-b']dithiophene (entry 1p).

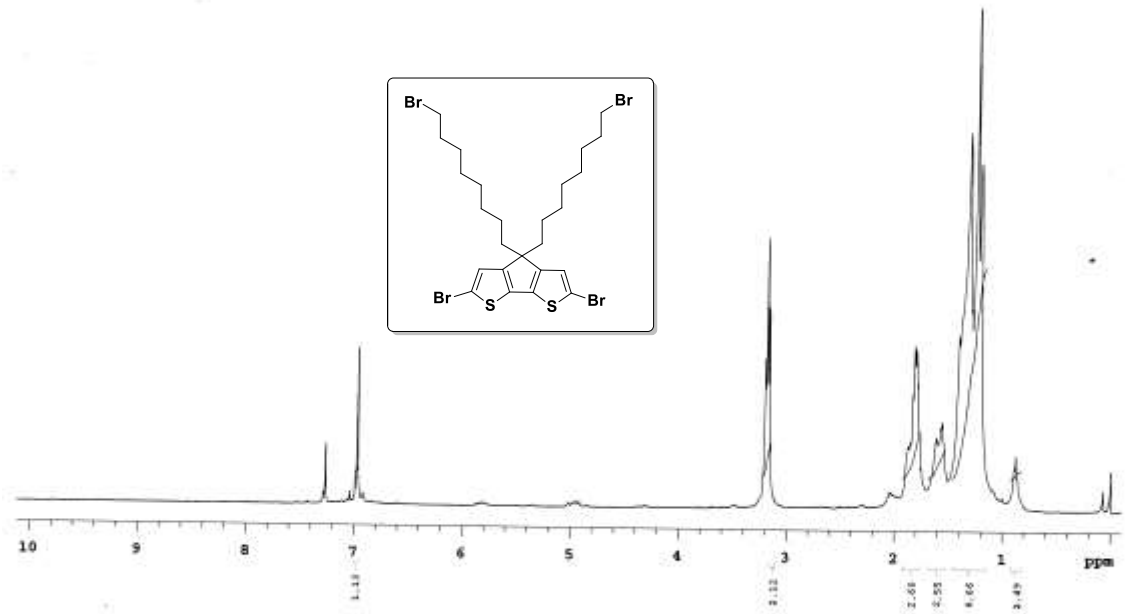

^{1}H NMR spectrum of 2,6-Dibromo-4,4'-bis(8-bromooctyl)-4*H*-cyclopenta[2,1-b:3,4-b']dithiophene (entry 1q).

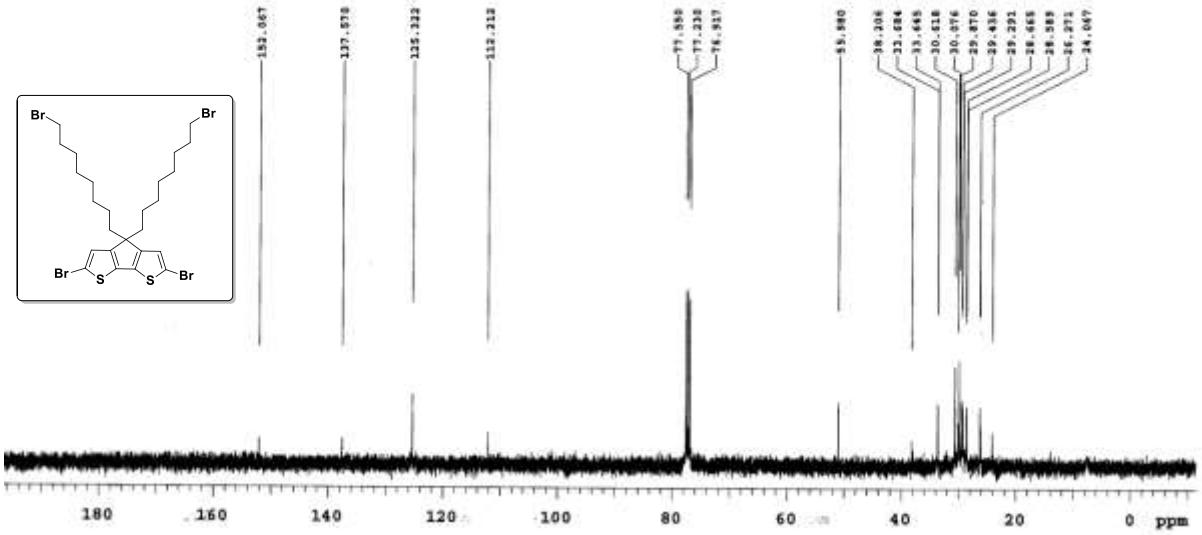

^{13}C NMR spectrum of 2,6-Dibromo-4,4'-bis(8-bromooctyl)-4*H*-cyclopenta[2,1-b:3,4-b']dithiophene (entry 1q).

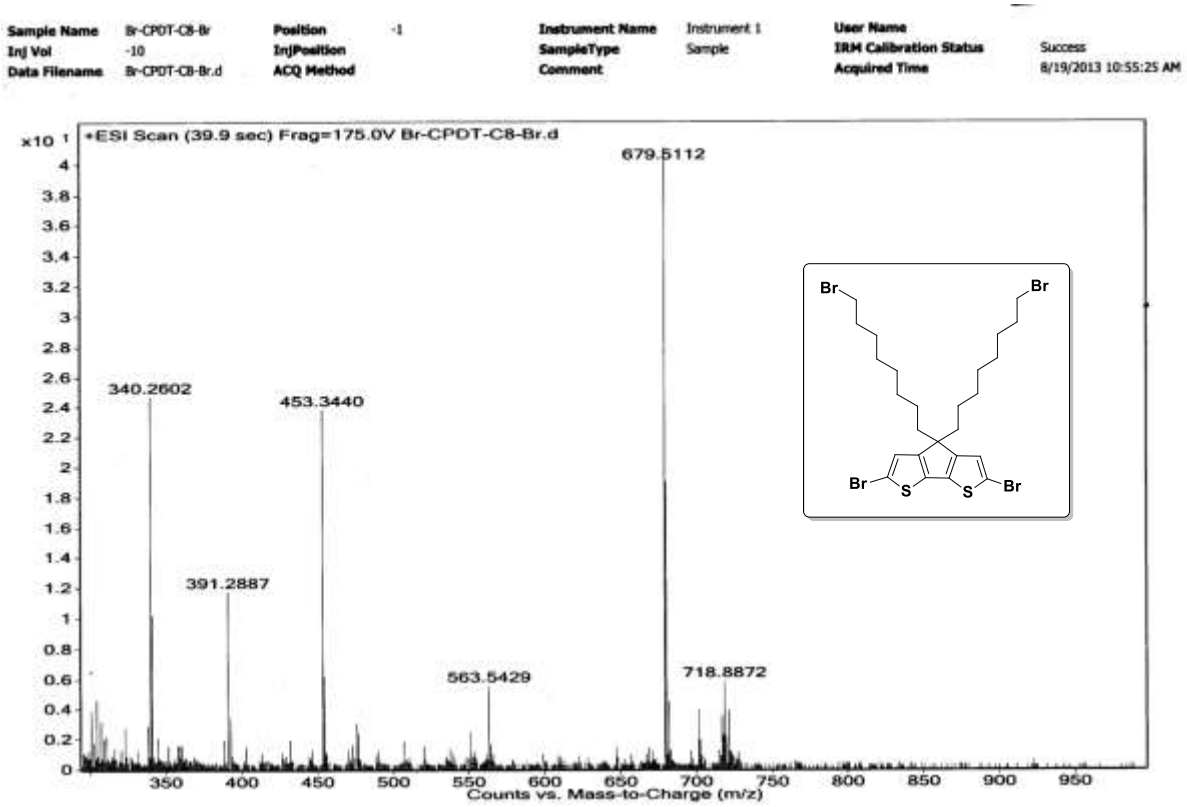

ESI-MS spectrum of 2,6-Dibromo-4,4'-bis(8-bromooctyl)-4*H*-cyclopenta[2,1-b:3,4-b']dithiophene (entry 1q).

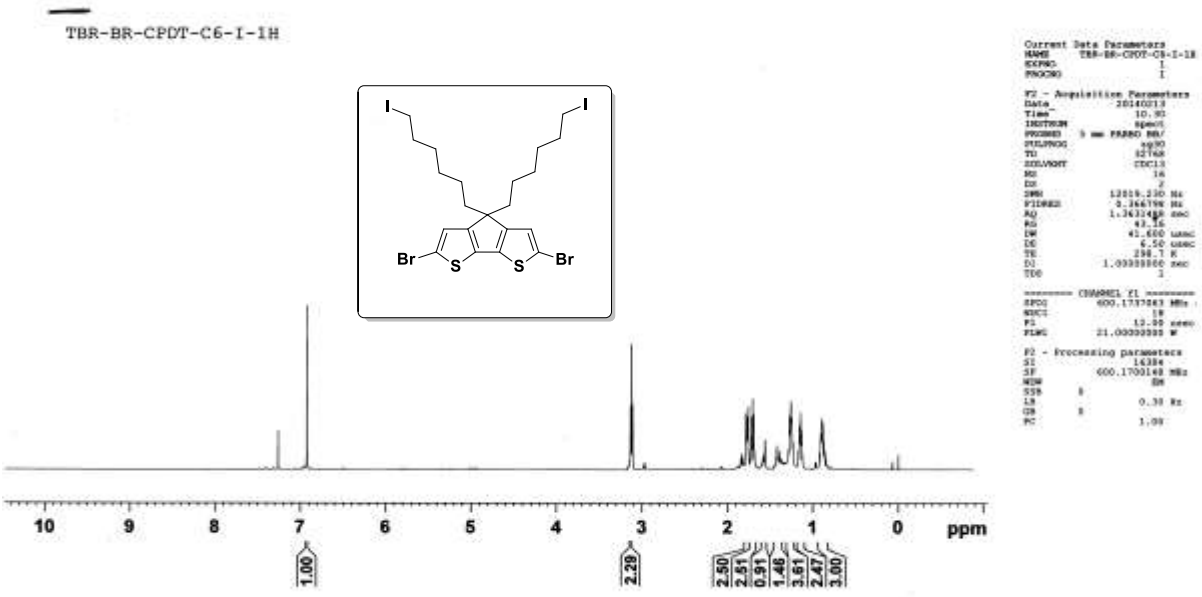

^{1}H NMR spectrum of 2,6-Dibromo-4,4'-bis(6-iodohexyl)-4*H*-cyclopenta[2,1-b:3,4-b']dithiophene (entry 1r).

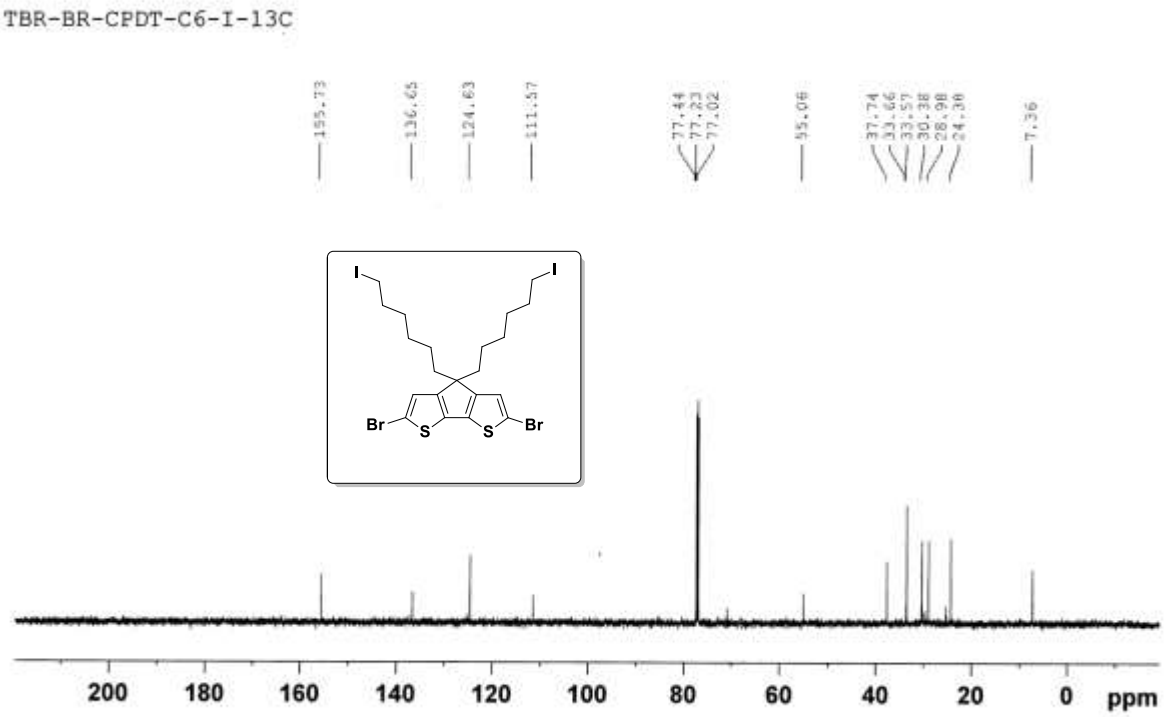

^{13}C NMR spectrum of 2,6-Dibromo-4,4'-bis(6-iodohexyl)-4*H*-cyclopenta[2,1-b:3,4-b']dithiophene (entry 1r).

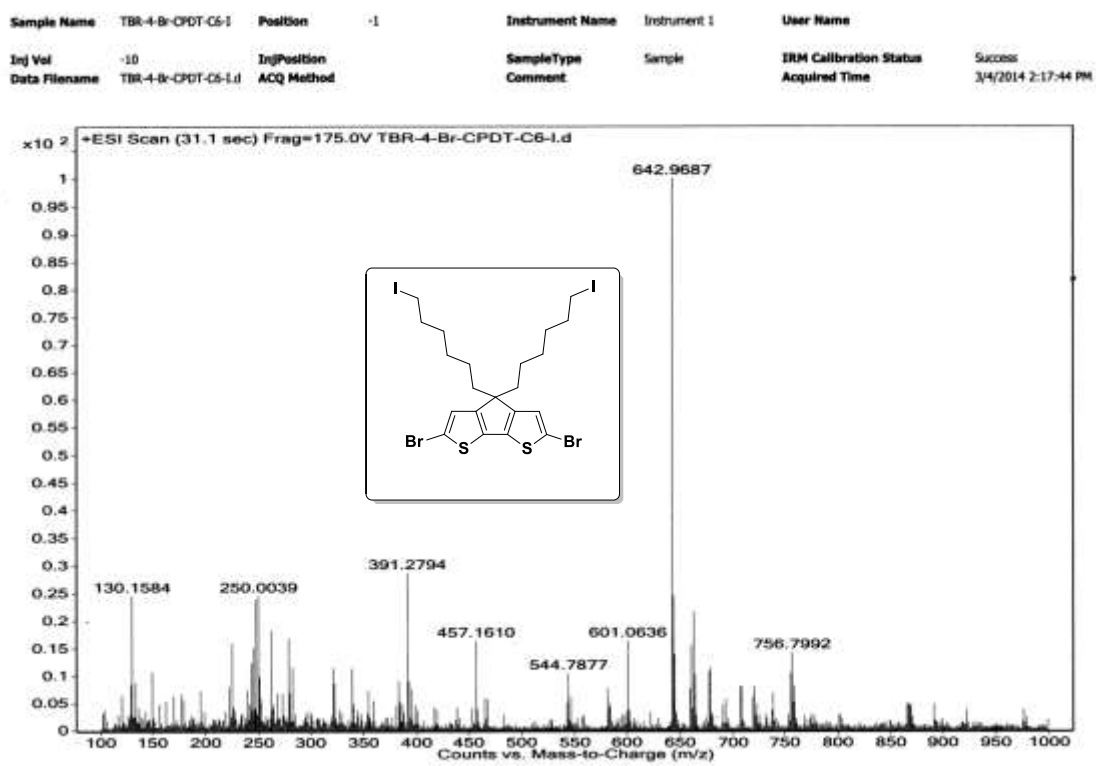

ESI-MS spectrum of 2,6-Dibromo-4,4'-bis(6-iodohexyl)-4*H*-cyclopenta[2,1-b:3,4-b']dithiophene (entry 1r).

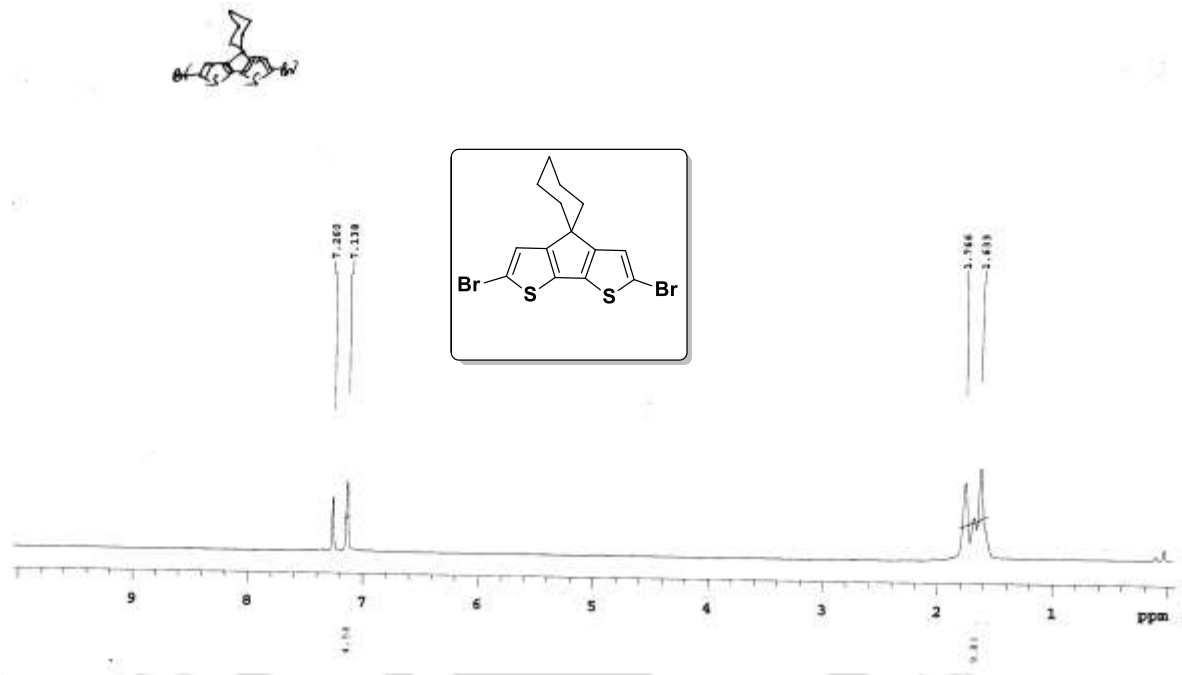

^{1}H NMR spectrum of 2,6-Dibromo spiro[4,5] ([2,1-b; 3,4-b']dithieno)decane.

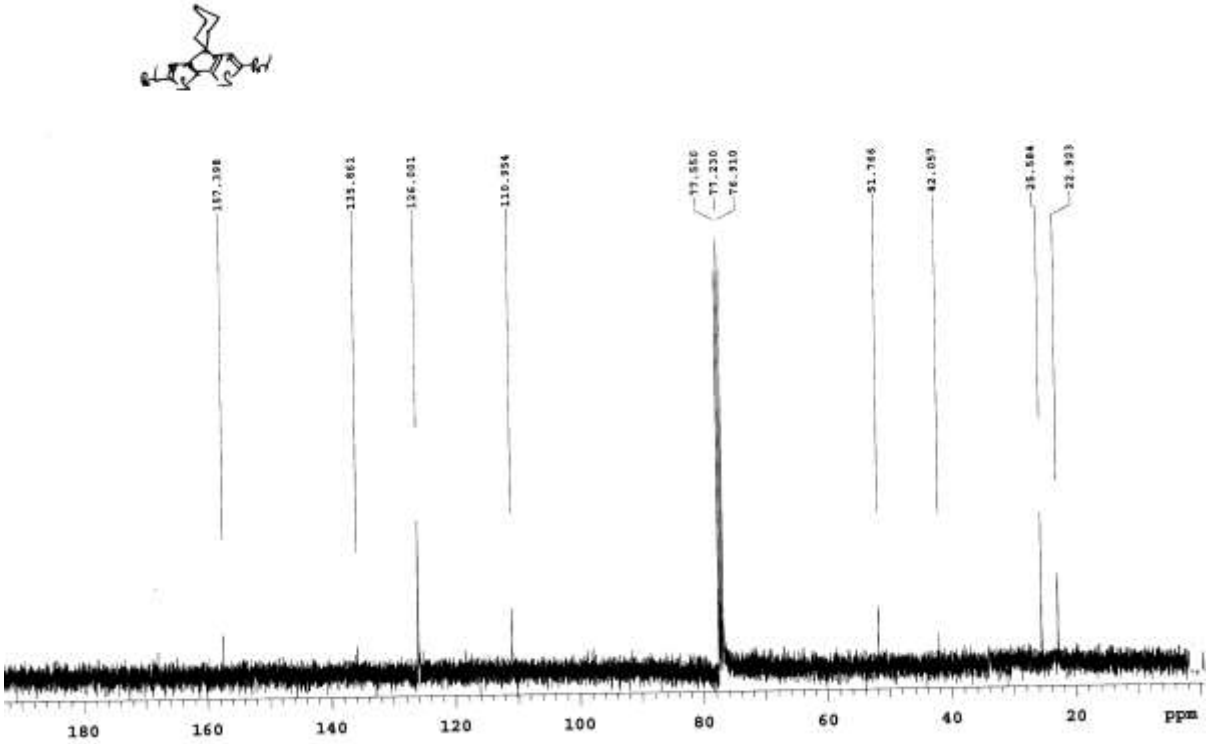

^{13}C NMR spectrum of 2,6-Dibromo spiro[4,5] ([2,1-b; 3,4-b']dithieno)decane.

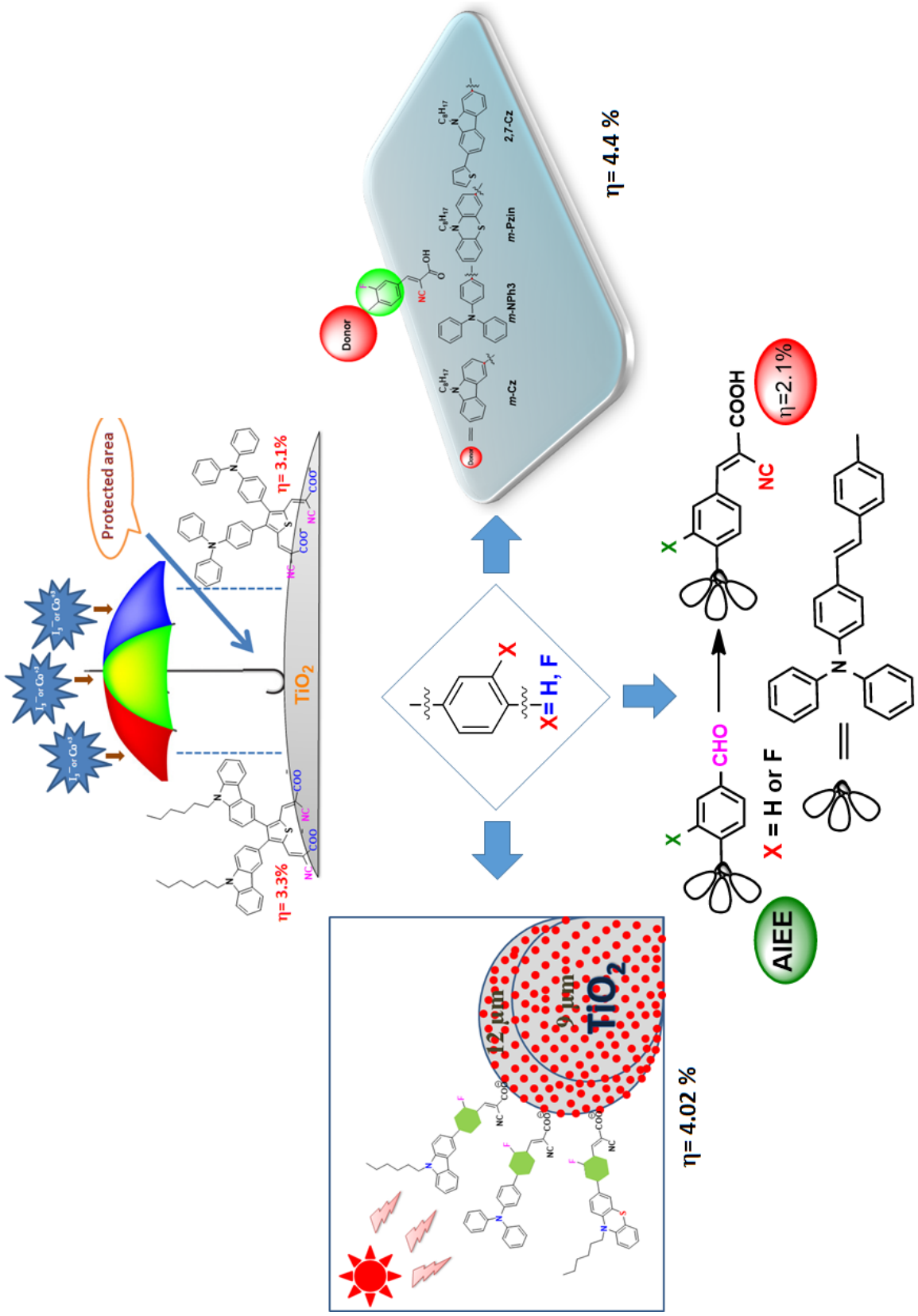
η= 4.4 %
Donor
2,7-Cz
m-Pzin
m-NPh3
m-Cz
Protected area
η= 3.1%
η= 3.3%
TiO2
X
X= H, F
COOH
NC
η=2.1%
CHO
X = H or F
AIEE
12 μm
9 μm
TiO2
η= 4.02 %

Published Papers

1. **Telugu Bhim Raju,** P. Gopikrishna, Parameswar K. Iyer "Highly efficient and facile alkylation of 4*H*-Cyclopenta [2,1-b:3,4-b']dithiophene in water." *RSC. Adv.* **2014**, *4*, 37738-37745.
2. **Telugu Bhim Raju,** Jayraj V. Vaghasiya, Mohammad Adil Afroz, Saurabh S. Soni, Parameswar Krishnan Iyer "Design, synthesis and DSSC performance of *o*-fluorine substituted phenylene spacer sensitizers: Effect of TiO_2 thickness variation" *Phys. Chem. Chem. Phys.* **2016**,*18*, 28485-28491.
3. **Telugu Bhim Raju,** Jayraj V. Vaghasiya, Mohammad Adil Afroz, Saurabh S. Soni, Parameswar Krishnan Iyer "Influence of *m*-fluorine substituted phenylene spacer dyes in dye-sensitized solar cells" *Org. Electron.* **2016,** *39*, 371-379.

Under Review

1. **Telugu Bhim Raju,** P. Gopikrishna, Jayraj V. Vaghasiya, Saurabh S. Soni, Parameswar Krishnan Iyer "Effect The solvatochromism and aggregation-induced enhanced emission of triphenylamine substituted styrene derivatives and its application in dye sensitized solar cells".
2. **Telugu Bhim Raju,** Jayraj V. Vaghasiya, Mohammad Adil Afroz, Saurabh S. Soni, Parameswar Krishnan Iyer "Influence of 3, 4-disubstituted thiophene derivative π-extended dyes and its effect on dye-sensitized solar cells"

Patent (Indian patent applied)

"METHODS AND COMPOSITIONS TO PREPARE 4,4-DIALKYL-4*H* CYCLOPENTA [2,1-b:3,4-b'] DITHIOPHENE DERIVATIVES" thereof. P. K. Iyer, **T. Bhim Raju**, P. Gopikrishna, Patent filed through DST, TIFAC. (January 2014).

Conferences

1. "2nd International Conference on Advanced Nanomaterials and Nanotechnology (ICANN-2011)" held at IIT Guwahati, Guwahati, India during Dec 8-10, 2011.
2. "3rd International Conference on Advanced Nanomaterials and Nanotechnology (ICANN-2013)" held at IIT Guwahati, Guwahati, India during Dec 1-3, 2013.
3. "Hands on training and attended ELED & ESPV International Conference on Energy efficient LED Lighting and Solar Photovoltaic systems, 27-29 March, 2014, IIT Kanpur, India.
4. "INUP Hands on training and work shop" held in Center for Nanotechnology and Nano Science, IISc Bangalore, India during 24 June - 3 July 2014.
5. "Advances in Polymer science and Technology" (APST-2015) held at IASST Guwahati, Guwahati, India during March 13, 2015. (**Best Poster**).

6. "4th International Conference on Advanced Nanomaterials and Nanotechnology (ICANN-2015)" held at IIT Guwahati, Guwahati, India during Dec 8-10, 2015.
7. "Advanced Nano materials and Nanotechnology (Nanos-2015) conducted by GITAM University, India during Dec 17-20, 2015.
8. "National Conference on Material Research Society of India (MRSI-2016)" on 5th February, 2016 organized by CSIR-Jorhat, India.